Understanding the Molecular Basis of the Strength Differences in Skins Used in Leather Manufacture

A dissertation presented in partial fulfillment of the requirements for the degree of

Doctor of Philosophy

at Massey University, Palmerston North

New Zealand

RAFEA MUSTAFA NAFFA

2017

1 Dedication

To my mother

To Haifa, Lilian and Maya

for giving me the confidence and love to keep going

and not give up

2 Acknowledgements

I would like to thank my supervisor Gillian Norris for her guidance and advice throughout the project, help with skin preparation when time was at a premium, and their unfailing optimism. Thank you for encouraging me to follow and develop my own ideas, and to make contact, and discuss my work, with experts in different fields. Also thanks to my co-supervisors Richard Haverkamp and Meekyung Ahn for their support.

I would like to thank Trevor Loo for his help and advice throughout my studies, particularly for his assistance with the mass spectrometry. My PhD study would not have been possible without Geoff Holmes who has kindly provided me with all skin samples used in this study. I would also like to thank Richard Edmonds, Dylan Ball and Catherine Maidment from Leather and Shoe Research Association of New Zealand (LASRA®) for their help in skin sample collection and analyses, and David Harding, (Institute of Fundamental Sciences at Massey University, (IFS)), for his help with the HPLC, and for making his laboratory available to me to carry out the chemical procedures that were part of this project.

A big thank you to Bridget Ingham, Callaghan Innovation, Wellington, New Zealand for her help with both the SAXS data collection and analyses.

Thanks also to Matthew Savoian, Jordan Tylor and Niki Minards of the Manawatu Microscopy and Imaging Centre, Steve Glasgow (Massey Institute of Food Science and Technology) for his help with using the Instron instrument, and Bob Stewart (Institute of Agriculture and Environment) for the help with the polarizing light microscope, Pat Edwards (IFS) for his help with NMR analyses.

My special gratitude goes to Ihsan Shehadi who was the inspiration for me to pursue my PhD studies abroad. I will always remember the memories we shared together

I gratefully acknowledge the financial support of the Ministry of Business, Innovation and Employment (MBIE®) through a grant to LASRA (MBX801), the Institute of Fundamental Sciences at Massey University and the New Zealand Synchrotron Group Ltd. for access to the SAXS/WAXS beamline at the Australian Synchrotron.

3 Abstract

Although skin structure and its physical properties have been extensively studied, little research has been devoted to understanding the links between them. A comprehensive study of the molecular components of four animal skins commonly used to manufacture shoes, clothing and furniture was therefore undertaken in order to attempt to identify a common indicator of skin strength. The molecular architecture of the protein components of each skin was analysed using polarising, confocal and transmission-electron microscopy (TEM), small angle X-ray scattering (SAXS) and amino-acid and cross-link analysis; glycosaminoglycans were quantified and visualised using TEM; and, for the sake of completeness, total carbohydrate and lipid content were measured using a colorimetric assay and thin layer chromatography respectively. Differences in these properties were then related to different physical characteristics of each skin.

The results showed that an individual mechanical property of skin such as tensile strength is complex and related to different combinations of molecular properties. For example, deer and cow skins are the strongest of the skins examined, however they derive their strength from different combinations of molecular properties. Cow skin collagen fibrils have the largest diameter, but deer skin fibrils have the smallest. On the other hand, the fibrils in deer skin frequently change direction, and have a “wavy” or crimped appearance in contrast to the fibrils in cow skin which are aligned in two main directions approximately 60 and 90 degrees apart, differences that are also reflected in the types and amount of their collagen crosslinks. Deer skin fibrils contain a higher proportion of trivalent crosslinks while cow skin fibrils contain a higher proportion of tetravalent links. For the two weaker skins, goat skin fibrils are more crimped than those of sheep skin, but both fibrils have diameters intermediate between those of cow- and deer skins and have lower mature to immature crosslink ratio. In deer skin, glycosaminoglycans are observed by TEM to link fibrils in

regular arrays and are present in higher concentrations than in cow, sheep and goat skins. This study showed the relationship between the molecular structure of skin and its mechanical functions is complex, arising from different combinations of molecular features rather than just one.

4 Table of Contents

5 List of Figures

6 List of Tables

7 LIST OF PUBLICATIONS/CONFERENCES

1. **Naffa, R.,** Holmes, G., Ahn, M., Harding, D., & Norris, G. (2016). Liquid chromatography-electrospray ionization mass spectrometry for the simultaneous quantitation of collagen and elastin crosslinks. *Journal of Chromatography A*, 1478, 60-67.
2. **Rafea Naffa,** Meekyung Ahn, Richard Haverkamp and Gillian Norris. "Understanding the Molecular Basis of the Strength Differences in Skins Used in Leather Manufacture Part Three: Quantitation of Crosslinks", oral talk presented at the 68th Annual Leather and Shoe Research Association (LASRA®) Conference, 17th August 2017, Queenstown, New Zealand.
3. **Rafea Naffa** and Gillian Norris. "Rapid Simultaneous Quantitation of Mature Collagen Crosslinks by Silica Hydride Column and Liquid Chromatography-Mass Spectrometry (LC-MS) without derivatization", oral talk presented at Australian and New Zealand Society for Mass Spectrometry Conference, Adelaide, Australia, (15-20) July, 2017.
4. **Rafea Naffa**, Meekyung Ahn and Gillian Norris. "Analysis of natural crosslinks by liquid chromatography mass spectrometry using a silica hydride column", oral talk presented at the Proceedings of World Congress on Chromatography, Amsterdam, Netherlands, (21-23) September, 2016.
5. **Rafea Naffa,** Meekyung Ahn, Richard Haverkamp and Gillian Norris. "Understanding the Molecular Basis of the Strength Differences in Skins Used in Leather Manufacture Part Three: Quantitation of Crosslinks", oral talk presented at the 67th Annual Leather and Shoe Research Association (LASRA®) Conference, 27th July 2016, Wellington, New Zealand.
6. **Rafea Naffa,** Meekyung Ahn, Richard Haverkamp and Gillian Norris. "The Isolation and Characterization of Natural Crosslinks in Animal skins by Liquid Chromatography and Electrospray Ionization-Mass Spectrometry Detection", poster presented at the 21st Annual Lorne Proteomics Symposium", Lorne, Victoria, Australia, (4-7) February, 2016.
7. **Rafea Naffa,** Meekyung Ahn, Richard Haverkamp and Gillian Norris. "Understanding the Molecular Basis of the Strength Differences in Skins Used in Leather Manufacture Part Two: Analysis of Glycosaminoglycans, elastin, carbohydrates and lipids", oral talk presented at the 66th Annual Leather and Shoe Research Association (LASRA®) Conference, 13th August 2015, Queenstown, New Zealand.
8. **Rafea Naffa,** Meekyung Ahn, Richard Haverkamp and Gillian Norris. "Understanding the Molecular Basis of the Strength Differences in Skins Used in Leather Manufacture Part One: Quantitation of Amino acids", oral talk presented at the 65th Annual Leather and Shoe Research Association (LASRA®) Conference, 13th August 2014, Wellington, New Zealand.

1 CHAPTER ONE: Introduction

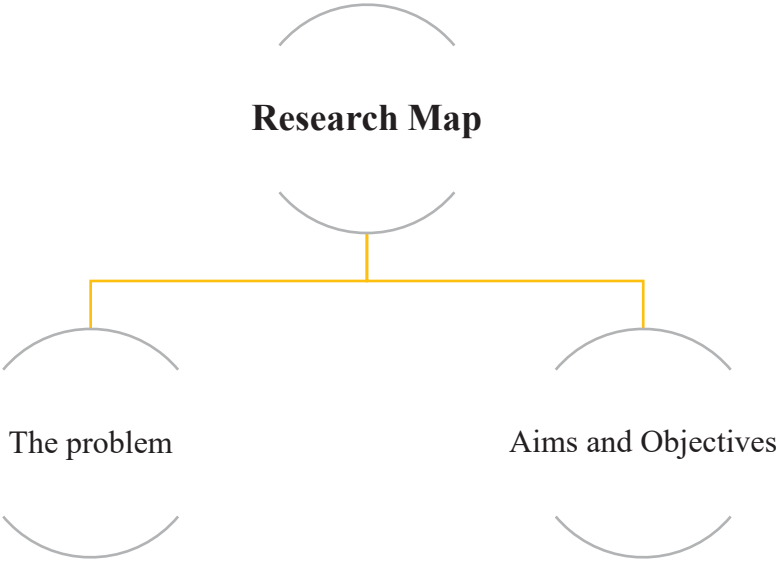

1.1 The Problem

Every year billions of animals are slaughtered for meat, producing millions of tons of hides and skins. These are converted to leather which is considered the most significant economic byproduct of the meat industry. New Zealand hides and skins particularly sheep skins contribute significantly to the world's leather industry by producing raw skins for the tanning industry [1]. The majority of skins produced in New Zealand are from sheep, cow, deer and goat. In 2011, 75% of lamb and sheep skins (dry weight) were exported overseas mainly for the garment industry [1].

Leather is used for many manufactured products because of its physical and aesthetic properties [2]. One of these properties is strength which is critical for many leather products especially footwear. Leather is manufactured by stabilizing the fibrous collagen networks of animal skins using chemical reagents, a process that is colloquially known as tanning [2]. The origin of the skins and the processing methods used in tanning, play a crucial role in determining the properties of the final leather product [2, 3].

Different animal skins, with different physical characteristics are used to make leather. Strong leather is used for footwear and upholstery while weaker softer leather is used for clothing. Skins from cow, goat and deer produce strong leather, while sheep skin produces weak leather (Table 1) [4]. Several factors that potentially affect skin strength have been studied including crosslinks between collagen, the weave of the collagen fibrils, their density and axial arrangement (D-periodicity) [4-8]. To the best of our knowledge, no relationship has been reported between the number and type of crosslinks in these different skins and other factors that affect strength.

It has been observed that during leather processing, the original strength of skins as measured by the tear test, is changed [2, 3, 9, 10]. Many studies have observed that a number of structural changes occur during leather manufacture, although these have not been related to the changes at the molecular level [3, 9, 10].

Table 1: Normalized tear strength for thickness of sheep, goat, deer and cow skin and leather [4].

Animal skin	Raw skin	Leather
	Tear strength normalized for thickness (N/mm)	
Sheep	30	20-40
Goat	60	70
Deer	83	108
Cow	160	63

Collagen is the main structural component of skin and its strength largely depends on the hierarchical architecture of the collagen structure [6]. The collagen molecule is made up from three α helical polypeptide chains which have a characteristic Gly-X-Y repeating sequence where X and Y are frequently proline and 4-hydroxyproline [11]. It also contains hydroxylated lysines which may or may not be modified by monosaccharides. Collagens are then assembled into suprastructures of striated fibrils which have a periodicity of 67 nm and diameters of 20-500 nm through the formation of different crosslinks [6, 11, 12]. These are then organized into fibre, with μm diameters, mediated by proteoglycans [12, 13].

The effects of collagen fibre orientation and periodicity on leather strength have been extensively studied [14-17]. It has been shown that strong leather is associated with a smaller orientation index (OI) which is associated with an alignment of fibres to the surface of leather (Figure 1 & 2) [4]. However, the correlation between D-periodicity and strength has not been reported [4, 18]. Most importantly, the differences in strength

have not been correlated to the crosslinking profile of animal skins and their variations in the number of types of crosslinks that occur during leather processing [4, 6, 19, 20].

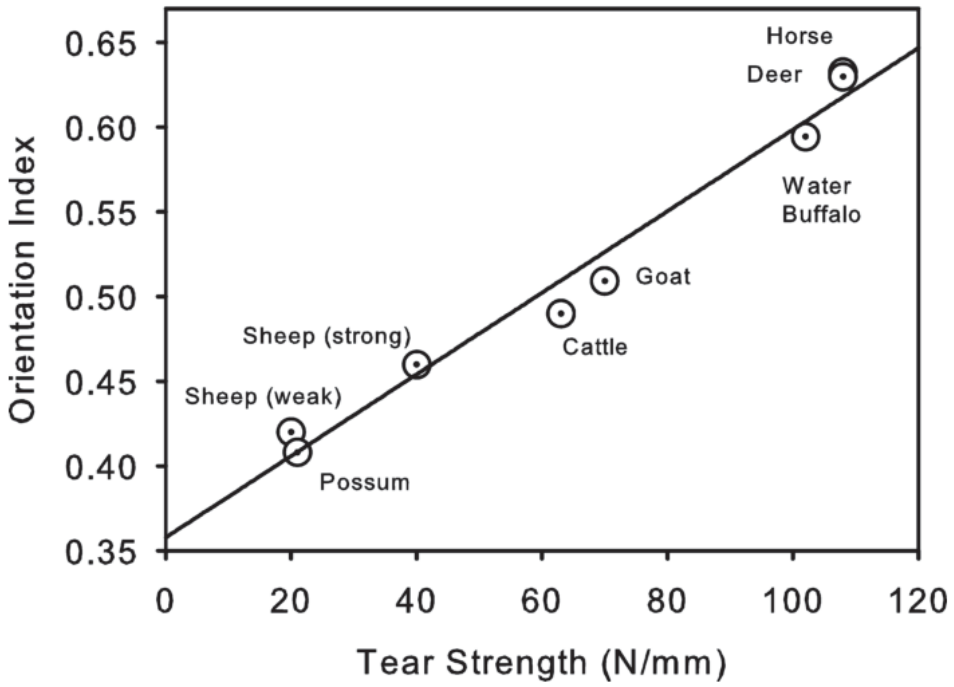

Figure 1: Collagen fibril orientation and tear strength for leather from different animals [4].

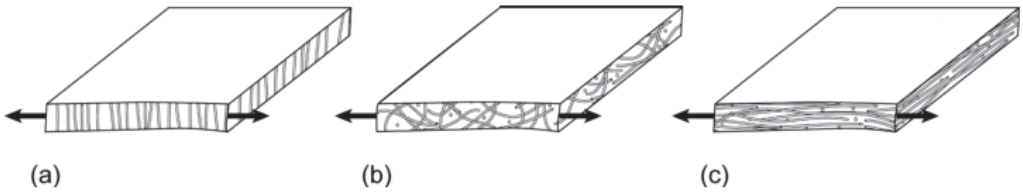

Figure 2: Relationship between collagen orientation index (OI) and strength of leather. OI measured edge-on with orientation that results in leather that is (a) very weak (vertical fibre defect), (b) medium strength (low OI), or (c) strong (high OI). Arrow indicates direction of applied stress in tear measurements [21].

It has long been known that leather becomes stronger when chemically crosslinked, suggesting that crosslinks play an important role in skin strength [2, 10, 22-25]. Although some of the physical features that differentiate strong from weak skins are understood, the molecular bases of these physical differences have not yet been explored [3, 4, 14, 20]. Surprisingly, there are no comparative data available on the molecular composition and structure at the micro-level of animal skins used in the leather industry.

This study involved the analysis and quantitation of molecular building blocks of animal skins including amino acids, collagen crosslinks, elastin crosslinks, glycosaminoglycans, carbohydrates and lipids. Secondly, small angle X-ray scattering (SAXS) was used to investigate the characteristic properties of collagen in skins, such as diameters, periodicity and the azimuthal angle of the fibrils. Finally, microscopic methods including laser confocal scanning microscopy (LCSM), transmission electron microscopy (TEM) and polarizing light microscopy (PLM) were carried out to visualize the micro and nano architecture of the skin. Tear strength, differential scanning calorimetry (DSC) and tensile strength of the skins were measured to obtain reference values to compare skins of sheep, goat, deer and cow.

For this study, four animal skins were chosen based on their different properties. Goat skin is thin but strong, sheep skin is weak and of medium thickness, deer skin is very strong and thin and cow hide is strong and thick [26]. These skins are also most commonly used in the New Zeeland tanning industry. It is possible the physical properties of the leather are influenced by chemical and mechanical processing.

It is predicted that the differences observed in the molecular analyses of the different skins will be reflected in their different physical characteristics, allowing us to understand the bases of these differences. We may also discover methods, in which skin processes could be improved to produce leather with specific properties.

This study asks the following questions:

(1) Are the strength differences in the sheep, goat, deer and cow skins reflected in differences in amino acid composition, the number of glycosaminoglycans, the type and number of covalent crosslinks, the concentration of carbohydrates, total lipids and the lipid profiles of the skins?

(2) How is the microarchitecture of collagen correlated to the molecular analyses of skins? This included diameters, D-periodicity, organisation and orientation of collagen fibrils.

(3) Is this correlation valid for all skins?

1.2 Aims and objectives

This work aims to improve our understanding of the molecular differences of animal skins and their effects on their physical properties. This study is focused on finding molecular-microstructure relationships between sheep, goat, deer and cow skins which will provide valuable and accessible information for the industry to refine skin processing protocols to produce sheep leather with improved physical properties especially strength. Moreover, this knowledge may be extended to help medical research by monitoring and evaluating any changes in skin structure to find biomarkers characteristics of diseased and healthy skins. It has recently been reported that the crosslink profile of skin changes in certain diseases [27].

The first objective of this study is to optimise the collection, preparation and storage of the skin samples to minimize any molecular or structural alterations in skins prior to the analysis. This should help to produce highly reliable, repeatable, robust and accurate measurements that reflect integrity of the skins. In Chapter 3 sample collection, preparation and storage conditions are presented and discussed as well as the experimental design and statistical implications. This chapter also presents and discusses the results of the physical measurements carried out on skins including thickness measurements, shrinkage temperature, tear strength and tensile strength.

Chapter 4 presents the optimization of amino acid analysis before the method was used to determine the amino acid concentrations in sheep, goat, deer and cow skins. The collagen content in each skin was then measured based on the concentration of hydroxyproline. In chapter 5, other molecular components of skins were measured including glycosaminoglycans, total carbohydrates and lipid total amounts and profile.

Chapter 6 contains the most challenging and crucial experimental part during this study which is the isolation and purification of crosslink standards which are essential for the development of the crosslinks quantitation. The approaches used for obtaining the crosslink standards were fully discussed. Several lengthy and complex separation steps were applied to purify the crosslink standards as they are not commercially available. This was started with Kgs of skin and finished by obtaining milligrams of highly purified crosslinks. The structure, purity and quantity of each purified crosslink were characterized, confirmed and determined using mass spectrometry and NMR. This was then followed in Chapter 7 by the development of a novel, fast and sensitive quantitation method for collagen and elastin crosslinks. This method was used to analyse the crosslinks in sheep, goat, deer and cow skins.

In Chapter 8, the organisation of collagen structure in sheep, goat, deer and cow skins was examined by small angle X-ray scattering (SAXS). All SAXS measurements were carried out at the Australian Synchrotron in Melbourne. In-house software was developed to process the SAXS data before being converted into an 11 × 11 map for each sample showing the diffraction patterns of the collagen. These maps used to compare the overall orientation of collagen fibrils of sheep, goat, deer and cow skins.

Chapter 9 has the micro and nano architecture of collagen structure in skin visualized using different microscopic imaging techniques. The general anatomical structures of each skin were first examined with both light and polarizing light microscopy (PLM) to determine the thickness and distribution of each skin layer. Laser confocal scanning microscope (LCSM) was then carried out by recording (80-250) of 2D images for each skin sample as the sample was scanned with the laser in the z plane by 0.25-0.4 μm

steps. These 2D images were combined to construct a 3D image of the microarchitecture of collagen fibres within skin. Visualizing the skin at the nano-level was then performed using transmission electron microscope (TEM) to estimate the collagen fibril diameters of each skin sample. These microscopic data helped us to visualize, annotate and compare the micro and nano architecture of collagen structure in sheep, goat, deer and cow skins and relate these differences to the molecular composition.

2 CHAPTER TWO: Literature Review

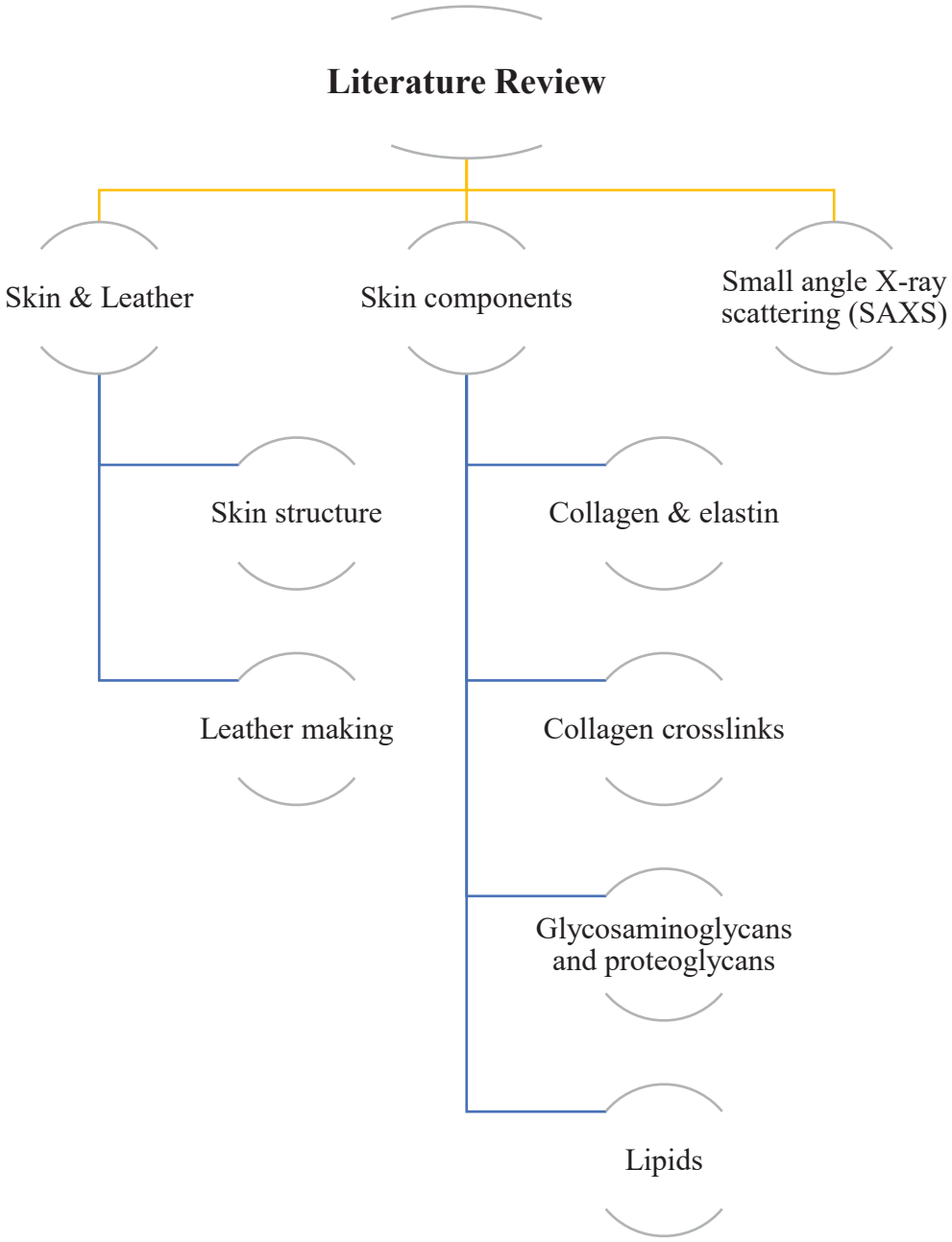

2.1 Skin to Leather

Skin is the largest organ in mammals and has many physiological functions, such as regulation of body temperature, creating a barrier between the organism and the environment and elimination of waste products [28, 29]. Skins and hides are by-products of the meat industry and the major raw material for the tanning industry where they are converted into leather to make garments, footwear and upholstery. Although skins of cow, sheep, goat and deer are the most common raw materials used in leather manufacture, skins of horses, pigs and reptiles are also used [26, 30]. For the tanner, a hide refers to large animal skins, such as cow, horse and buffalo, while skin is the term used to describe small animal skins such as sheep, goat and deer [31].

2.1.1 Skin

Skin has a complex structure composed mainly of collagen and elastin fibres that associate with proteoglycans [28]. Collagen is the major structural protein and the main component of skin [2]. Eight different types of collagen have been identified in skin, each of which has a specific function [6, 13, 32]. Collagen I is the major collagen, making up 70% of dry skin weight, followed by collagen III which makes up 10% [6]. Interestingly, the relative concentration of collagen III declines with maturation [33]. The collagen types are discussed in more detail in section 2.2.

Structurally, skin is composed of three well defined layers each of which has a specific organisation and distribution of macromolecular components which define their biological roles [34]. These are the epidermis, dermis and flesh layer (hypodermis) (Figure 3). The epidermis is the outside layer and composed mostly of keratinocytes

and barrier lipids while the flesh layer is mainly composed of fat cells underneath the dermis. The dermis layer is the middle layer and accounts for 90 % of the weight of skin. It is subdivided into the grain and the corium layers (Figure 3) [28, 34, 35]. The grain layer has a fine and loose collagen fibrous structure with a larger proportion of collagen III and is responsible for the distinctive appearance of leather [35, 36]. The corium layer contains a thicker and compact collagen fibre network running parallel to the skin surface that imparts the strength to skin [35]. Fibroblasts found in both grain and corium layers are the sites of biosynthesis of collagen, elastin and proteoglycans, together with immune-competent mast cells and macrophages [34, 37]. Generally, skin is composed of about 70% water, 25% protein, 2% lipids and trace minerals and nucleic acids. The major protein structures in skin are formed from fibrous collagen and elastin which are "glued" together by proteoglycans. Collagen fibres make up 70% of the skin, giving it strength and toughness while elastin maintains its normal elasticity and flexibility and the proteoglycans provide viscosity and hydration [34].

2.1.2 Leather

Skin is converted into leather through various physical and chemical processes. These processes retain or enhance several skin properties, such as tensile strength, flexibility, resilience, and resistance to decomposition and bacterial decay [2]. Leather is both a utilitarian and a luxury product that has many advantages over synthetic materials, such as aesthetic appeal, feel, texture, and breathability while retaining its strength [2]. The nature of the skin and its structural and molecular features determine the quality of the leather produced [30]. The conversion of skin into leather involves five major stages of preservation, pre-tanning, tanning, post-tanning and finishing (Figure 4).

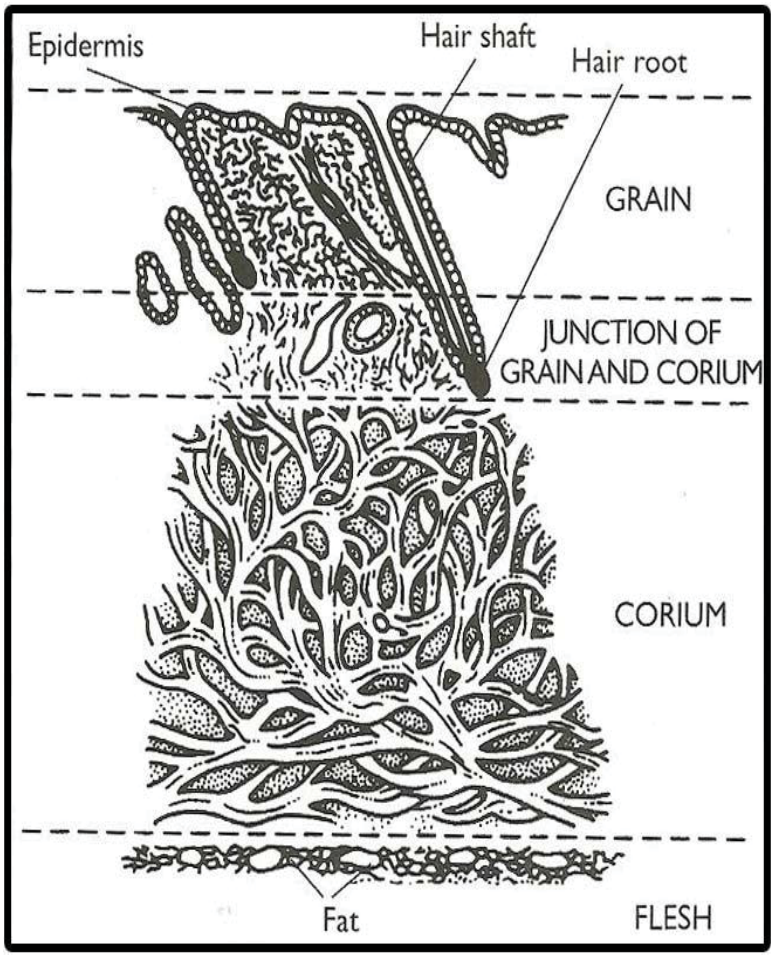

Figure 3: Diagram of skin showing its anatomical features [31].

2.1.2.1 Preservation

Fresh skin is removed from carcass by hand flaying or mechanical pulling, then is immediately washed with cold water to remove dirt and to slow the bacterial activity [2]. If it cannot be processed immediately, it must be preserved and any remaining meat tissues removed (fleshing). It is then trimmed which involves cutting off the unwanted edges. At this stage it contains approximately 70% water so the potential for bacterial activity is high [2]. To prevent this, the skin is dehydrated by applying dry crystalline salt at a rate of approximately 15% by weight to minimize putrefaction during storage

and transport. For short term storage, bioacids are used to reduce the degradative effect of the proteolytic enzymes on skin. After a period of drying, the skins are stacked in piles and stored.

2.1.2.2 Pre-Tanning

Water must saturate the skin structure to ensure uniform movement of reagents through skin layers during tanning. Salted skin is, therefore, soaked in water containing detergents and enzymes for several hours to a few days, which removes unwanted materials such as blood, complex sugars and hyaluronic acid [2].

The rehydrated skin is then painted on the flesh side with a solution containing sodium sulfide and lime (painting) which quickly penetrates the skin to the hair roots dissolving them [2, 31]. The hair is then removed from the raw skin by scraping using mechanical tools (depilation), after which the depilated skins are washed by rotation with water in drums [30]. This degrades the epidermis and removes most of the soluble proteins and proteoglycans from the collagen matrix, opening it up for further processing [2]. The skins are then washed further in water to lower the pH to between 8 and 9 before enzymes (mainly proteases) are added to the mix. This is called bating and its role is to remove the remaining unwanted protein from the skin. Finally the skin is preserved (pickling) in acidic solution (pH 1-2) at which stage it is stored [31].

2.1.2.3 Tanning

The tanning stage of leather production imparts stability, flexibility and aesthetic properties to the final product [33]. For chrome tanning, basic chromium sulfate is used which increases the pH to 4.0 to produce what is known as wet blue. It has been

reported that chromium (III) stabilizes the collagen through interaction with the amino and carboxylate sidechains of amino acids [2, 38].

A vegetable tanning step in which a mixture of natural plant polyphenols are applied to leather usually follows the chrome tanning. Studies have demonstrated that hydrogen bonding and hydrophobic interactions are involved in the stabilisation of collagen by the plant polyphenols [39].

2.1.2.4 Post-Tanning

Post-tanning consists of several steps which vary depending upon the final product [2]. Generally, excess moisture is removed by pressing the wet blue between rollers (sammying) after which the leather is horizontally sliced into the required thickness (splitting) and refined by shaving and trimming. The quality of the leather is then further improved by retanning with basic chromium sulfate or vegetable oils. Soft leather is eventually obtained by mixing the leather with natural and synthetic oils in a process known as fat liquoring. It is finally dyed using different types of dyes (dyeing) based on the leather applications.

2.1.2.5 Finishing

The leather production is concluded with several steps depending on the final leather product. These involve enhancing the fullness of leather (filling), restoration and repair of the appearance (buffing) and adjustments of the moisture to 14-25% (conditioning and toggling). For some leathers a surface coating such as a dye is applied to provide protection, decoration and durability [40].

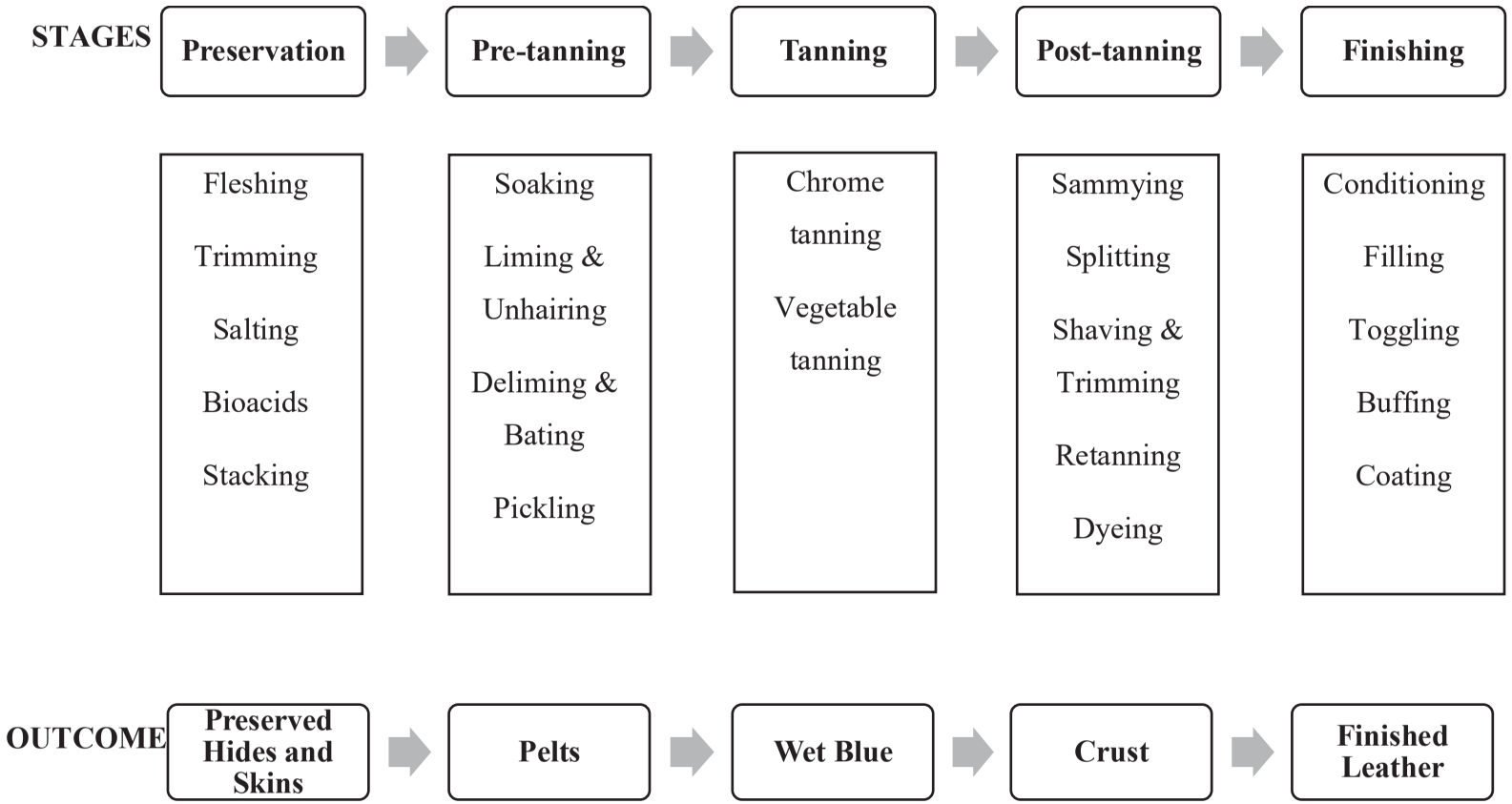

Figure 4: General flow diagram showing the steps in leather production.

2.2 Collagen

Collagen is the main structural protein found in the extracellular matrix of animal tissues. It makes up about 30% of total body protein and more than 50% is found in fibrous tissues, such as tendons, ligaments, skin, bone and teeth [6, 11, 13, 41]. Twenty-eight different types of collagen have been identified and categorised as fibrillar and non-fibrillar. The fibrillar collagens form long uninterrupted triple helix chains while the non-fibrillar collagens have a much shorter triple helix chain interrupted by non-collagenous domains. The non-fibrillar collagens have many different structures and as a result they are further divided into several subgroups (Table 2) [6, 11, 13, 42]. All collagens are, however, trimers with common characteristics. The most abundant types are I, II and III [11]. Collagens are either made up of three identical α helical polypeptide chains (homotrimeric) such as collagen types II, III, VII and X or more than one type, (heterotrimeric) including collagen types I, VI and V [6]. Although collagen type I usually forms heterotrimers, it has been reported as homotrimers in embryonic tissues and some diseases such as cancer, fibrosis and genetic disorders [531, 532]. Collagen VIII is the only known collagen which has both homo- and heterotrimers [43].

2.2.1 Collagen biosynthesis

The biosynthesis of collagen consists of complex intracellular and extracellular steps, which involve several post-translational modifications, chain association, stabilisation, folding and covalent crosslinking (Figure 5) [11, 44]. The synthesis starts with the formation of a particular α-polypeptide chain being translated on the ribosome and transported into endoplasmic reticulum (ER).

Table 2: Collagen classification [6, 42].

Family	Sub-family	Members	Location	Functions
Fibrillar Collagens		Types I, II, III, V, XI, XXIV and XXVII	Tendon, ligament, blood vessels, bone, cartilage, skin	I, II and II: resist tension V, XI: control fibril diameter
Non-Fibrillar Collagens	Fibril Associated Collagens with Interrupted Triple helices (FACITs)	Types IX, XII, XIV, XVI, XIX, XX, XXI and XXII	Co-assemble with fibril-forming collagens in cartilage	Interact with other matrix components
	Beaded filament forming collagen	Type VI	Ubiquitous in connective tissue	Bridges and anchors cells to other components of ECM
	Basement membrane and associated collagens	Types IV, VII, XV and XVIII	Basement membrane	Secures basement membrane to adjacent connective tissue matrix
	Short chain collagens and related proteins	Types VIII and X	VIII: cornea and vascular tissue X: hyaline cartilage	Unknown
	Transmembrane collagens and collagen-like protein	Types XIII, XVII, XXIII and XXV/CLAC-P.	XIII: blood vessel wall, glomeruli of kidney	Unknown
	Collectins and ficolin	Mannan binding protein; surfactant proteins A and D; conglutinin; CL-43; CL-46; CL-L1; CL-P1; L-, M- and H-fi CL-43	Non-extracellular matrix with homologies to collagen VIII and X	Diverse function in cell adhesion and signaling and immune system.
	Other collagens and collagen-like proteins	Emu1; collagen XXVI/Emu2; collagen XXVIII; acetylcholinesterase tail subunit		Diverse function in cell adhesion and signaling

Three modifications occur on the α-polypeptide chains leading to the formation of procollagen chains [45, 47, 48]. First, the signal peptide (propeptide) on the N-terminal is removed by specific proteases followed by the action of prolyl and lysyl hydroxylases which modifies specific proline and lysine residues producing hydroxyproline and hydroxylysine, respectively. Finally, glycosyltransferase and galactosyltransferases add glucose or galactose moiety to the hydroxy group of hydroxylysine [11, 46]. These modifications are essential for the formation of intra- and intermolecular cross-links which provide the correct maturation and assembly of the procollagen extracellularly into a triple helix of tropocollagen [45].

Conversion of the procollagen chains into procollagen molecules is initiated by the association of three C-terminals at a nucleation point stabilised by intrachain and interchain disulfide bonds [45, 48]. At this time the triple helix formation occurs in the C-terminus to N-terminus direction and propagates in a "zipper-like fashion" [49]. After synthesis in the endoplasmic reticulum, the procollagen molecule is moves through the Golgi apparatus from where it is secreted into the extracellular space. The C- and N- terminal ends are then trimmed by a group of metalloproteinases to produce "tropocollagen" which in case of collagen type I will have a length and diameter of 300 nm and 1.5 nm, respectively [11]. This significantly decreases its solubility resulting in a spontaneous assembly into quarter-staggered fibril which is then stabilized by the formation of several covalent crosslinks. It has been previously reported that the free propeptides are involved in feedback regulation of collagen synthesis [45].

The formation of the crosslinks is then initiated by lysyl oxidase which oxidatively deaminates specific lysine and hydroxylysine sidechains to produce aldehyde groups.

These spontaneously condense with other aldehydes or lysine and hydroxylysine sidechains to form intramolecular and intermolecular crosslinks [6, 11]. As a result, tropocollagen molecules spontaneously self-assemble into parallel and axially ordered fibrillar structures. These are organized in a staggered arrangement in which there is a part that consists of five tropocollagens, resulting in a gap region [(67 nm× 5) – 300 nm = 35 nm] and a part containing four tropocollagens resulting in an overlap region [300 nm – (67 nm × 4) = 32 nm], creating a periodicity of 67 nm, which can be seen under electron microscopy (Figure 6, left) [50]. The resulting fibrils have diameters of approximately 20-500 nm and are organized into fibres, with diameters in micrometers, mediated by proteoglycans (Figure 6, right) [51]. Remarkably, the mechanical properties of tissues are further refined by the varied alignment of the fibres that make it up. The random organisation of fibres in different tissues is responsible for their physical properties. In tendons, the parallel alignment of fibres is responsible for longitudinal strength while the tensile strength of bone results from the organisation fibres in concentric layers. In cornea, the precise organisation of the collagen fibrils provides the strength and transparency while the laminated layers in cartilage give its high flexibility [6].

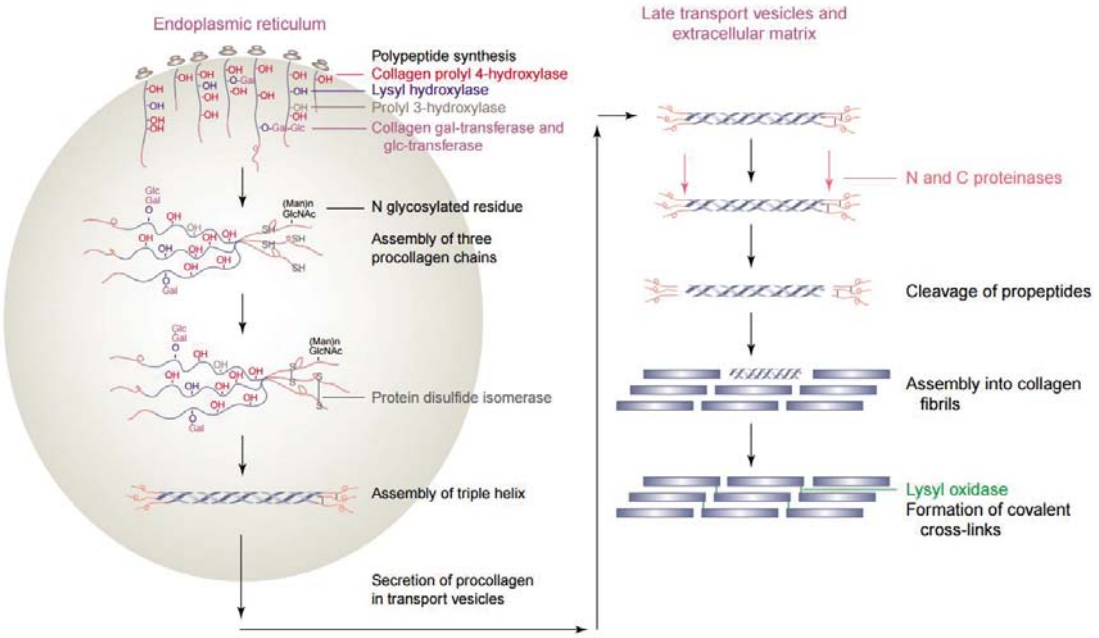

Figure 5: Schematic representation of the intracellular and extracellular steps involved in the synthesis of type I collagen into fibrils. Procollagen molecules are synthesized in the ER and Golgi apparatus before being transported to the plasma membrane. They then undergo several complex enzymatic modifications prior to being secreted in the extracellular space [52].

2.2.2 Collagen structure

The fibrous collagens are characterised by a helical domain which is composed of three left-handed polyproline-II chains coiled into a right-handed triple helix. The helical domain has a continuous Gly-X-Y repeating sequence where X and Y are frequently proline and 4-hydroxyproline, respectively [6, 32, 53]. This is flanked by short non-helical domains at both the N- and C-termini called telopeptides (Figure 7). Tropocollagen contains all the standard amino acids except for the largest amino acid tryptophan because it hinders the formation of the triple helix [2, 54]. Each chain in collagen type I has 1014 amino acids in the helical part, about (16 α1 and 9 α2 residues) 24 in N-terminal domain and 25 in the C-terminal telopeptide domain depending on the collagen type [55].

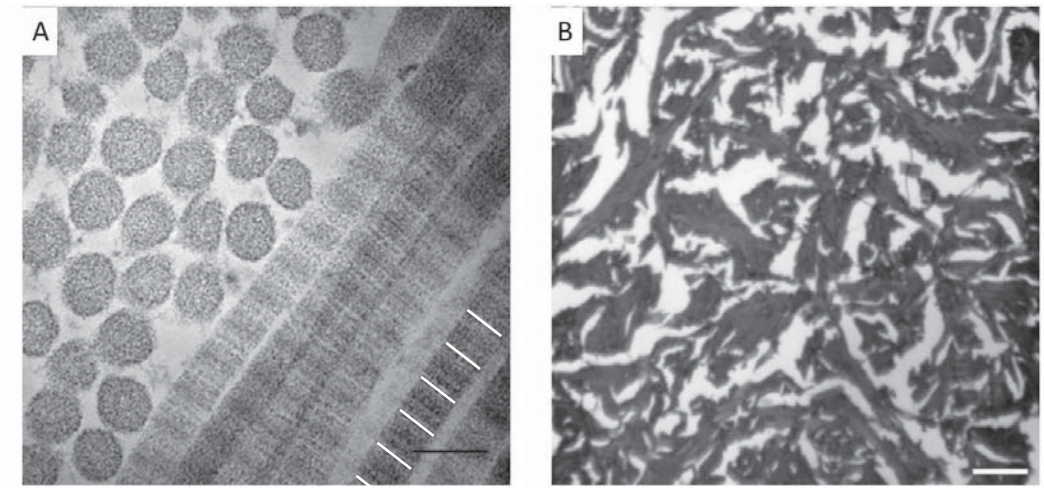

Figure 6: (A) Transmission electron microscopy (TEM) of transverse and longitudinal views of collagen fibrils in skin, scale bar 100 nm. The white lines show the D-periodicity (B) Light microscopy of collagen fibres, scale bar 400 μm.

Hydroxyproline and hydroxylysine are two non-standard amino acids found in tropocollagen. The most abundant amino acids in fibrous collagen are glycine, hydroxyproline and proline, which together make up about 55% of the total amino acids. Although present in low amounts (< 3%) lysine and hydroxylysine are essential for stabilizing the structure of the collagen fibrils through the formation of covalent crosslinks [6]. Every third residue in the tropocollagen helical domain is glycine, the smallest amino acid, which plays an important structural role by allowing close association of the three polypeptide chains that form the triple helix. Proline, hydroxyproline and hydroxylysine stabilize the tropocollagen molecular and fibrillar structure [46]. Charged amino acids such as arginine, glutamic acids and aspartic acid are involved in collagen fibril self-assembly while hydrophobic amino acids facilitate the hydrophobic interaction within the triple helix, contributing to fibril stability and orientation [56, 57].

Water is important for stabilizing the collagen structure and has been classified into three types based on its interaction with collagen. Type I stabilizes the triple helix structure by making hydrogen bonds between adjacent collagen molecules; type II is located on the fibril surface creating an extended network of hydrogen bonds which holds the microfibrils apart; type III is bulk water, which is weakly associated with collagen fibres and can be mechanically removed [33, 46].

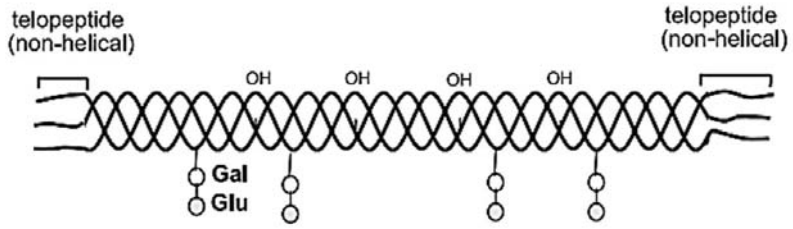

Figure 7: Structure of collagen molecule (collagen type I) showing the helical and non-helical parts with the glycosylation. Circles represent galactose (Gal) and glucose (Glu) residues attached to the lysine and hydroxylysine sidechains. Taken from [48] with permission of the publisher.

2.2.3 Collagens in skin

Nine types of collagen have been identified in the skin with type I being the most abundant and responsible for its mechanical strength (Table 3) [6, 33, 47, 58]. Type III, the next most abundant collagen in skin, forms fine fibrils (reticulin) that are mixed with type I collagen. Interestingly, type III makes up to 40% of foetal skin, being reduced to 10% when skin matures [32]. It is, along with types XIV and XII, the only homotrimeric collagen found in skin [2, 47]. Collagen IV is found in the basement membrane where it forms an open mesh structure. It is longer than the other fibrillar collagens (I and III), contains several discontinuities in the (Gly-X-Y) repeat and forms tetramers, that are stabilized by disulfide bonding [2, 6]. Collagen V is a minor collagen

that is found associated with collagen I and is thought to contribute to the formation of the fibril diameter. Collagen VI has a short triple helical domain with two tropocollagen molecules forming an antiparallel dimer that is stabilised by disulfide bonds; two dimers then aggregate to form a tetramer. Collagen IV maintains the skin tissue integrity and plays a role in fibril assembly and cell adhesion. Although collagen VII is the longest fibrillar collagen amongst vertebrates, it is not fibril forming [47]. It is found in the basement membrane at the dermal-epidermal junction in the form of anchoring filaments linking collagen IV [6]. Collagen types XII and XIV associate with the surface of collagen I to form fibril associated collagens with interrupted triple helices, the so-called FACIT collagens [59]. Collagen XII is localized in dense tissues containing collagen type I and collagen XIV is found in the basket-like structure around hair follicles [59]. Grassel *et al.* showed the collagen XVI was present at the dermo-epidermal interface where it interacts with anchoring collagens such as collagen VII [60].

Table 3: Collagen types in Skin [6, 32, 33, 47, 59].

Collagen Type	Molecular Structure	Remarks
I	$\alpha1(I)_2$, α2(I)	Fibril-forming collagens. Large fibril diameter. Principal components of skin > 90%.
III	$\alpha1(III)_3$	Fibril-forming collagens. Smaller fibril diameter. High in the grain layer of skin. Total amount in skin about 10%.
IV	$\alpha1(IV)_2\alpha2(IV)$; also α3(IV)α4(IV)α5(IV) α5(IV)2α6(IV)	Non fibrillar meshwork structure. Basement membrane. Form thin sheets (40-50 nm). N- and C- terminals called 7S and NC1, respectively. Tetramization of 7S domain and dimerization of NC1 domain form its structure.
V	α1(V)2α2(V)a α1(V)3	Regulatory fibril-forming collagens. Large N-terminus. Found in association with collagen I noncollagenous N-terminal domains.
VI	α1(VI)α2(VI)α3(VI) α (VI)α2(VI)α4(VI) α1(VI)α2(VI)α5(VI) α1(VI)α2(VI)α6(VI)	Beaded filaments. Periodicity 110 nm. Short helical domain and large non-helical domains. Associated into tetramers. Regulate the fibril assembly with decorin.
VII	α1(VII)3	Anchoring fibrils. Lateral aggregation of antiparallel dimers. Longest helical domain (420 nm). Found in the dermal-epidermal junction integrity.
XII	α1(XII)3	FACIT, non fibrillar. Structurally similar. Two collagenous domains separated by two short non-collagenous domains at C-terminal and very large N-terminal. Associated with the surface of collagen fibres and interacts with other ECM components.
XIV	α1(XIV)3	
XVI	α1(XVI)	

2.3 Collagen crosslinks

During collagen synthesis, several types of crosslinks are formed between tropocollagen molecules then developed within the fibrils defining the mechanical properties of the tissue [6, 12]., The crosslinking profile of skin, bone, tendon and cartilage are different, suggesting that the different types of collagen crosslinks are tissue specific rather than species specific [6, 61, 62]. Also the crosslink types reflect the relative stress on the tissue and its age as the mechanical properties of tissue are known to change with environment and age [6].

Essentially, collagen crosslinks are classified into two types based on their mechanism of formation, enzymatic and non-enzymatic [63]. The enzymatic crosslinks are strongly dependent on the location of the hydroxylysine and lysine in the helical and telopeptide domains [63]. Interestingly, there are significant differences in the hydroxylation and glycosylation of these residues, although their numbers and the locations in the α1-chains of collagen type I are conserved among mammalian species [6, 44, 61]. Unmodified lysine residues in collagen are involved in the formation of covalent enzymatic crosslinks in all mammalian species [44].

The adventitious reaction of specific lysine and arginine residues with glucose occurs during ageing and results in the formation of non-enzymatic crosslinks [6]. These are known as the advanced glycation end-products (AGE) and are linked to the decreasing mechanical strength of collagen fibres with age [64, 65].

2.3.1 Crosslink formation

During the early stages of extensive post-translational modification to the procollagen molecule, specific lysine residues are oxidized to hydroxylysine by lysyl hydroxylase [12, 66, 67]. It has been previously shown that the hydroxylysine content in different collagen types can vary from 15% to 90%, unlike hydroxyproline which does not significantly change among different species (11% to 14%) [44, 68]. Strikingly, the hydroxylation of lysine in collagen type I shows profound differences between tissues and even between the helical and telopeptide domains [44]. Investigations showed that lysyl hydroxylase uses different mechanisms; lysyl hydroxylase type 1 uses helical lysines as substrate while lysyl hydroxylase type 2 oxidises lysines in the telopeptide domain to produce hydroxylysine [44, 69].

Some of these hydroxylysine residues are glycosylated by the addition of galactose and some of them are further glycosylated with glucose to form galactosylhydroxylysine and glucosylgalactosylhydroxylysine, respectively [44]. It has been found that formation of the triple helix structure of collagen inhibits glycosylation, which is important for controlling collagen fibrillogenesis, crosslink formation and collagen-cell interaction [44, 70].

When collagen is secreted from Golgi apparatus into the extracellular space, it is subjected to further modifications. Specific lysine and hydroxylysine residues in the telopeptide domain are oxidised into allysine and hydroxyallysine aldehydes, respectively by the action of lysyl oxidase [71] which associates with the flexible telopeptide domain of the pre-assembled quarter staggered collagen fibril [72].

These enzymes require two factors to function, copper ions and the quinone derivative, lysine tyrosylquinone, which is produced by an enzyme catalysed reaction between tyrosine^{345} and lysine^{314} of the collagen polypeptide [72]. Five lysine and hydroxylysine residues are found in the telopeptide domain; two in the C-terminal (two α1-16^{C}), three in the N-terminal (two α1-9^{N}) and one α2-5^{N}) (Figure 8). These then undergo aldol condensation with other lysyl oxidase derived aldehydes or with lysine and hydroxylysine residues to form intra- and intermolecular covalent Schiff base crosslinks [71, 73-76]. The precise fibril alignment enables allysine and hydroxyallysine in the telopeptide domains to react with a juxtaposed helical amino group of hydroxylysine to form an immature enzymatic crosslink between allysine^{16C} (α1) and hydroxyallysine^{87} (α1 and α2) and between hydroxyallysine^{9N} (α1) or 5^{N}-hydroxyallysine^{5N} (α2) in the telopeptide domains and or hydroxylysine^{930} (α1) or hydroxylysine^{933} (α2) in the helical domains (Figure 9) [66, 67]. These are named the immature crosslinks and formed either in lysine or hydroxylysine rich domains producing aldimines and ketoamines, respectively [76, 77]. This double bond can be also reduced These divalent immature crosslinks are both acid and heat labile, and because of the Schiff base double bond, reducible. They can therefore be labelled by reducing agents such as tritiated sodium borohydride which was the first method used in the discovery of the collagen crosslinks [78-81].

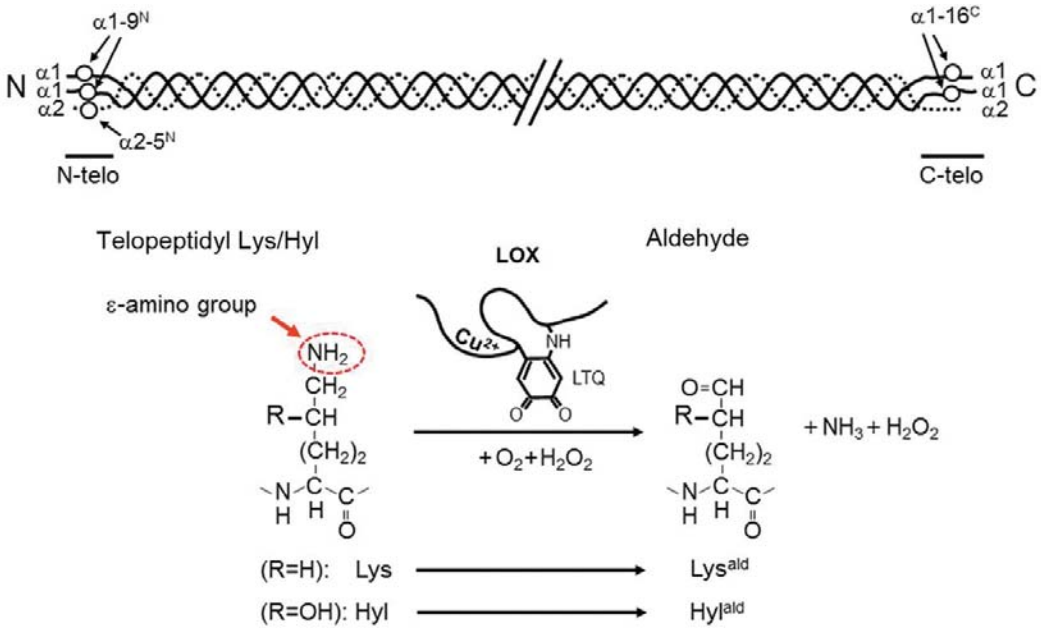

Figure 8: Oxidation of lysine and hydroxylysine residues in the telopeptide domain of collagen I by the action of lysyl oxidase. Lys and Hlys residues in the telopeptide domain are shown as circles (o). These five residues are oxidized by the copper (Cu^{2+})-dependent amine oxidase, LOX, to form their respective aldehydes, i.e. Lys^{ald} and Hyl^{ald}. Solid line, α1 chain; dashed line, α2 chain. Taken from Yamauchi and Sricholpech (2012) with permission of the publisher [44].

The synthesis and development of covalent crosslinks are crucial for the assembly and stabilization of collagen fibrils and critical for their biomechanical functions [77, 82]. The free aldehyde of the aldol or the immature crosslinks can further react with the amino group of a hydroxylysine or histidine residue in the helical domain to form trivalent and tetravalent mature cross-links (Figure 9). These link three and four collagen molecules in a head to tail fashion stabilizing fibril formation [6, 76]. The fibrils can then form fibril bundles, will eventually develop into fibres with varied alignments [33, 61].

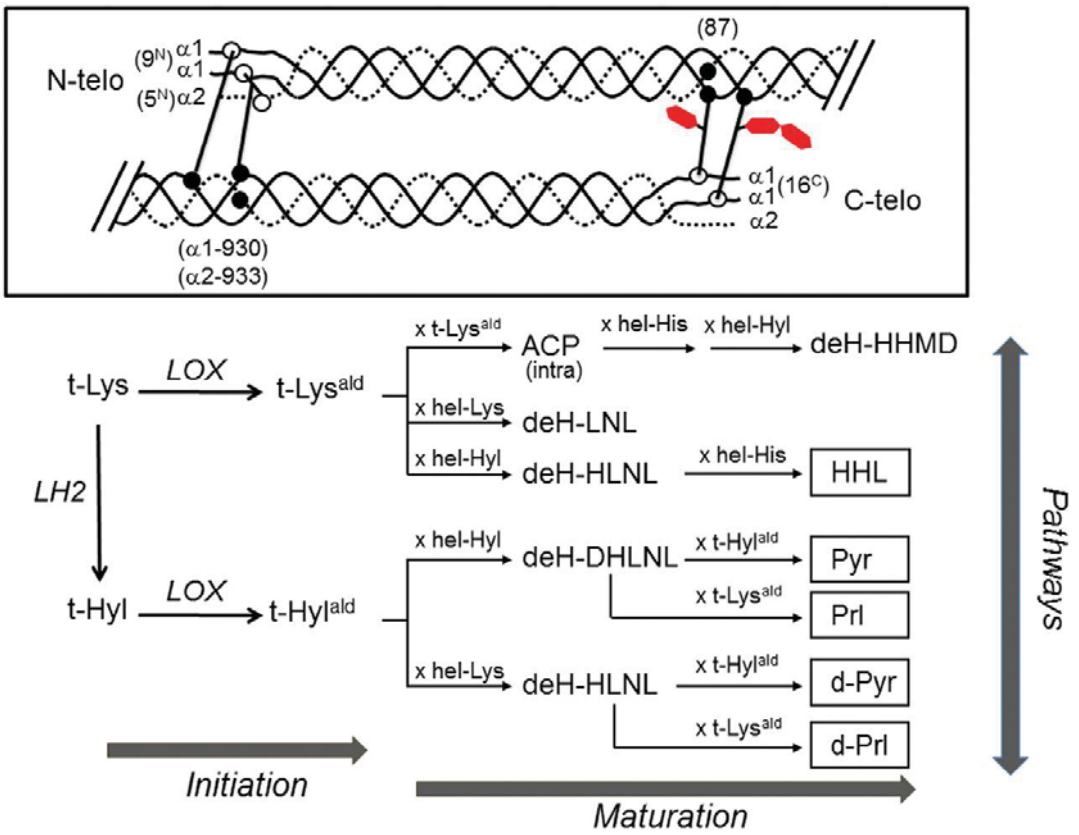

Figure 9: LOX-mediated collagen cross-linking: The top panel (boxed) shows the cross-linking sites of type I collagen. Black lines within and between the molecules indicate examples of the intra- and inter-molecular cross-linkages. Numbers in parentheses indicate the residue numbers of the telopeptidyl aldehydes (open circles) and the helical lysine or hydroxylysine residues (closed circles) involved in cross-linking. Red hexagon, galactose or glucose residues attached to the hydroxylysine involved in the tropocollagen crosslinking. Solid line, α1 chain; dashed line, α2 chain. The bottom panel summarises the initiation, maturation and various pathways of cross-linking. The boxed cross-link compounds are non-reducible cross-links. t, telopeptidyl; hel, helical; ald, aldehyde; d-, deoxyde-; H, dehydro. Taken from Yamauchi and Sricholpech (2012) with permission of the publisher [44].

2.3.2 Aldimines

When the rate of hydroxylation of lysine in the telopeptide domain is low, the reaction between allysine and hydroxylysine becomes predominant to form aldimines which are common in collagen of skin and rat tail tendon [83-86]. Two possible pathways have been shown to be responsible for the formation of aldimine crosslinks both involving allysine which reacts with either hydroxylysine or lysine to form dehydro-hydroxylysinonorleucine crosslinks (deH-HLNL) and dehydro-lysinonorleucine crosslinks (deH-LNL), respectively (Figure 10). The (X-Gly-His-Arg) amino acid sequence controls the type of the aldimine formed where X can be either hydroxylysine (as collagen in skin) or lysine (as in elastin) resulting in the formation of either deH-HLNL or deH-LNL, respectively [6, 87, 88]. Although deH-HLNL is classified as an aldimine, it also exists in a ketoamine form because of the reaction of allysine with lysine. This then spontaneously undergoes an Amadori rearrangement producing lysine-keto-norleucine (LKNL). Upon reduction with $NaBH_4$, the two forms cannot be separated [85]. DeH-HLNL is found in collagen while deH-LNL is found in elastin, both being essential for the formation of mature crosslinks [87, 88]. The two aldimine crosslinks deH-HLNL and deH-LNL can be further reduced by sodium borohydride to form the more stable HLNL and lysinonorleucine (LNL), respectively [80, 89, 90].

2.3.3 Ketoamines

In bone collagen, the hydroxylysine residue in the telopeptide is mainly hydroxylated [6]. It reacts with hydroxylysine in the helical domain sequence hydroxylysine-Gly-His-Arg to produce ketoamine crosslinks which are converted to hydroxylysine-keto-norleucine (HLKNL) through an amadori rearrangement (Figure 10) [90, 91]. The

ketoamines are more resistant to acid and heat than aldimines and are found mainly in bone and dentin but are not so common in skin [83, 84, 92]. Ketoamines generally predominate in connective tissues that bear large mechanical loads such as bone, cartilage and tendon [83].

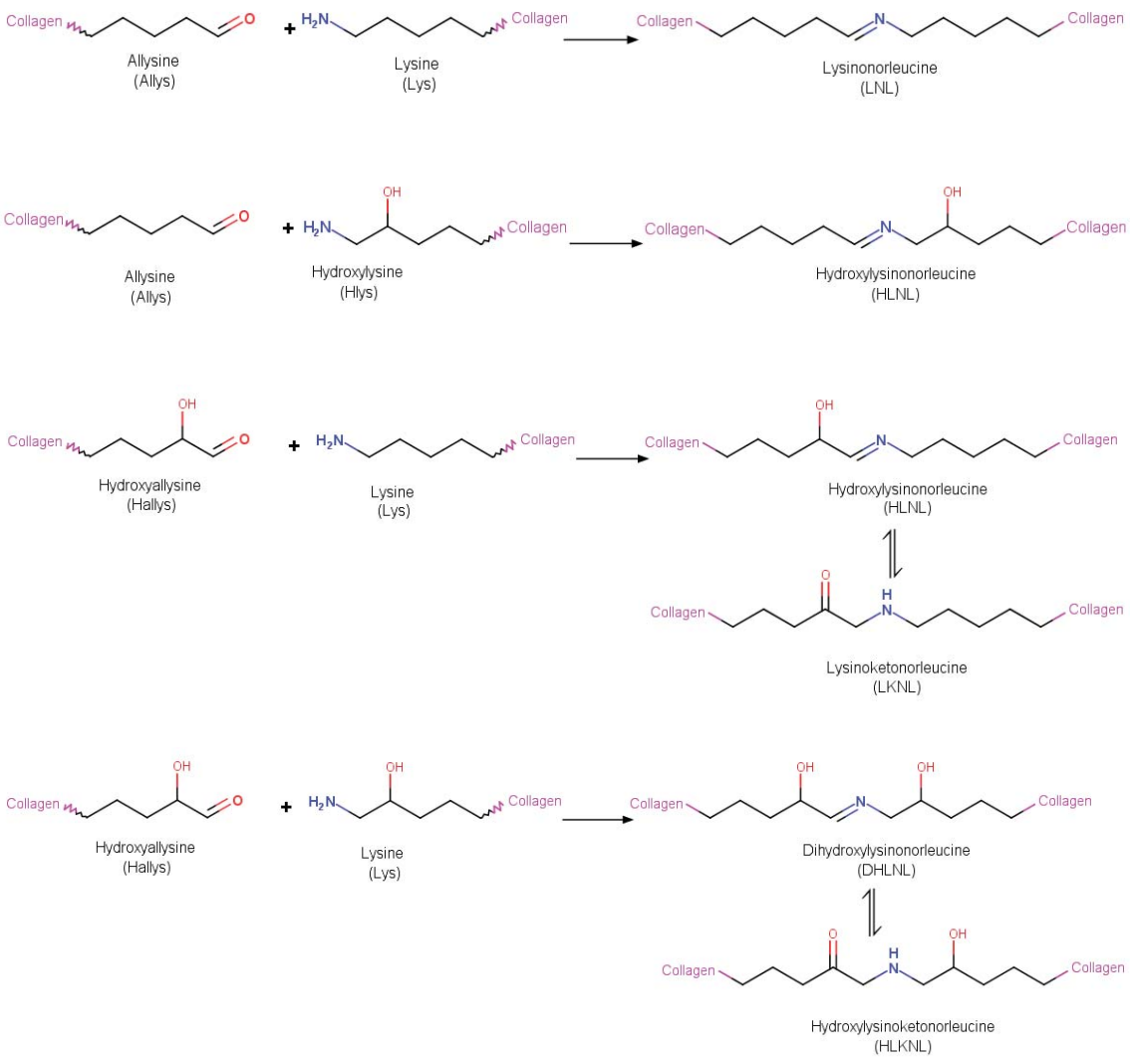

Figure 10: Formation of aldimine and ketoamine crosslinks.

2.3.4 Histidine-containing crosslinks

There are two crosslinks that contain histidine as a part of their structure: histidinohydroxylysinonorleucine (HHL) and histidinohydroxymerodesmosine (HHMD). They are formed however, by different mechanisms (Figure 11) [93-95]. HHL is a trivalent crosslink found mainly in skin and in some tendons at much lower concentrations [6, 93, 94, 96]. Its production starts at birth and is followed by an initial rapid increase in concentration followed by a more gradual increase with aging [97]. HHL is formed between two amino acids in the helical domain and one from the telopeptide [6]. Allysine from the C-telopeptide first reacts with hydroxyallysine^{87} from the helical domain producing a divalent HLNL crosslink which then reacts with histidine^{92} on the helical domain of the α2 chain to form HHL (Figure 11) [6, 94, 98]. Yamauchi *et al.* reported that the imidazole C-2 of histidine^{92} is linked to C-6 of norleucine (5-deaminated lysine from the helical domain) which is in turn linked to the C-6 amino group of histidine^{87} (see chapter 6 for the NMR results) [94]. Stiffness of skin has been linked to a decrease in the concentration of HLNL crosslinks and a concomitant increase in HHL crosslinks [12, 94, 96, 98]. It has been reported that UV radiation has no effect on the HHL structure [99]. The second histidine-containing crosslink is HHMD which consists of four amino acid residues making it a tetravalent crosslink. The formation of HHMD involving histidine, hydroxylysine and an aldol condensation product (Figure 11), and remains controversial [75, 94, 100]. Another mechanism is thought to involve the reaction of HHL with DHLNL [66, 93, 94, 101]. The presence of HHMD *in vivo* is debatable, despite it having been isolated and identified in different tissues by several researchers [90, 93, 102-104].

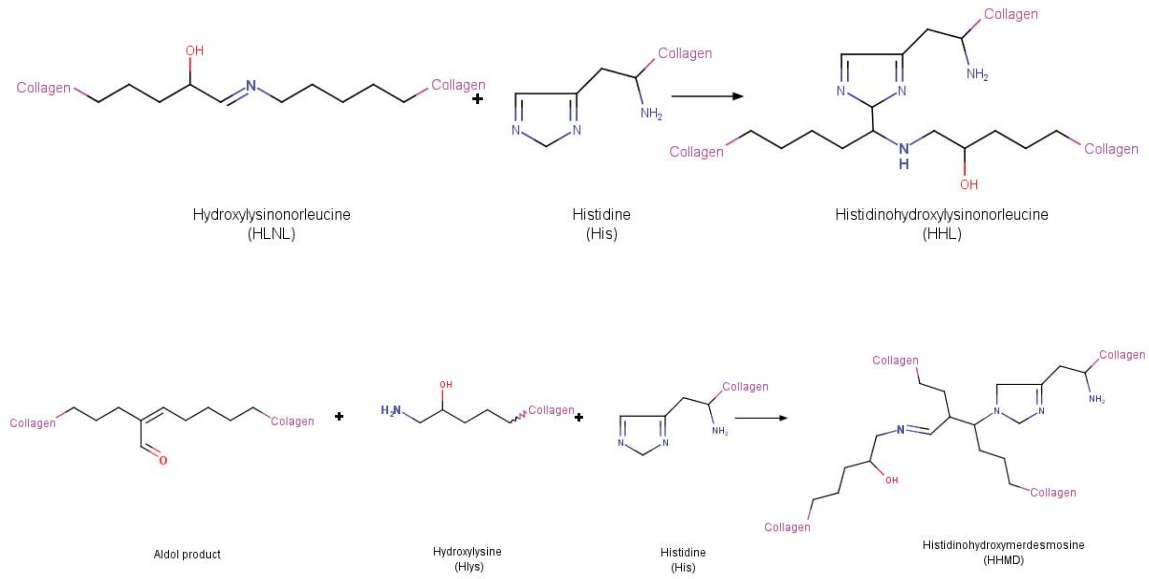

Figure 11: Formation of histidine-containing crosslinks.

2.3.5 Pyrrolic crosslinks

Pyrrolic crosslinks are the trifunctional maturation products of ketoamines and were detected by the formation of a pink colour when peptides isolated from connective tissues were reacted with Ehrlich's reagent (*p*-dimethylaminobenzaldehyde) [105-109]. Two compounds, lysyl pyrrole and hydroxylysyl pyrrole, are thought to be involved although they have not been separately isolated and verified [110]. The biosynthesis of pyrrolic crosslinks involves ketoamine, allysine or hydroxyallysine residues and aldimine (Figure 12) [106, 111].

2.3.6 Pyridinium crosslinks

Pyridinolines are stable crosslinks that were first isolated and characterised due to their fluorescence [112]. They are very common in bone, cartilage and tendon but rare in skin [61, 83, 113]. They are destroyed by exposure to UV radiation but are not reducible because they lack a Schiff base double bond [109, 114]. Their formation is associated

with a highly hydroxylated collagen telopeptide domain such as found in cartilage and bone collagen [6].

Pyridinoline (Pyr) and deoxypyridinoline (Dpyr) are two pyridinium crosslinks that were isolated and identified by Fujimoto *et al.* (1977) and Ogawa *et al.* (1982), respectively [112, 115]. Two mechanisms have been proposed for their formation [6]. Eyre and Oguchi reported that two keto-amines react together by releasing hydroxylysine (Figure 12) [116]. A second mechanism, based on the condensation of a keto-amine and hydroxyallysine was proposed by Robins and Duncan [117]. Although the two mechanisms are similar, they differ in the way the collagen molecules are linked. According to Eyre's mechanism, pyridinium crosslinks connect three collagen molecules while Robin's mechanism supports a linkage between two collagen molecules. The latter was supported by Light and Bailey who reported that Pyr crosslinked two type I collagen molecules [118].

2.3.7 Glycation

A complex series of non-enzymatic spontaneous condensation and rearrangement modifications occurs in collagen as a result of aging [61]. The different products formed are called advanced glycation end products (AGEs). These result from a Maillard reaction between reducing sugars and the amino functional groups on proteins [119-121]. This reaction generates several reactive intermediates that then undergo several oxidation reactions or non-oxidative rearrangements resulting in the formation of many sugar bridges between protein molecules [121-123]. Glycation is believed to be one of the major changes affecting the biomechanical properties of collagen during aging [121, 122].

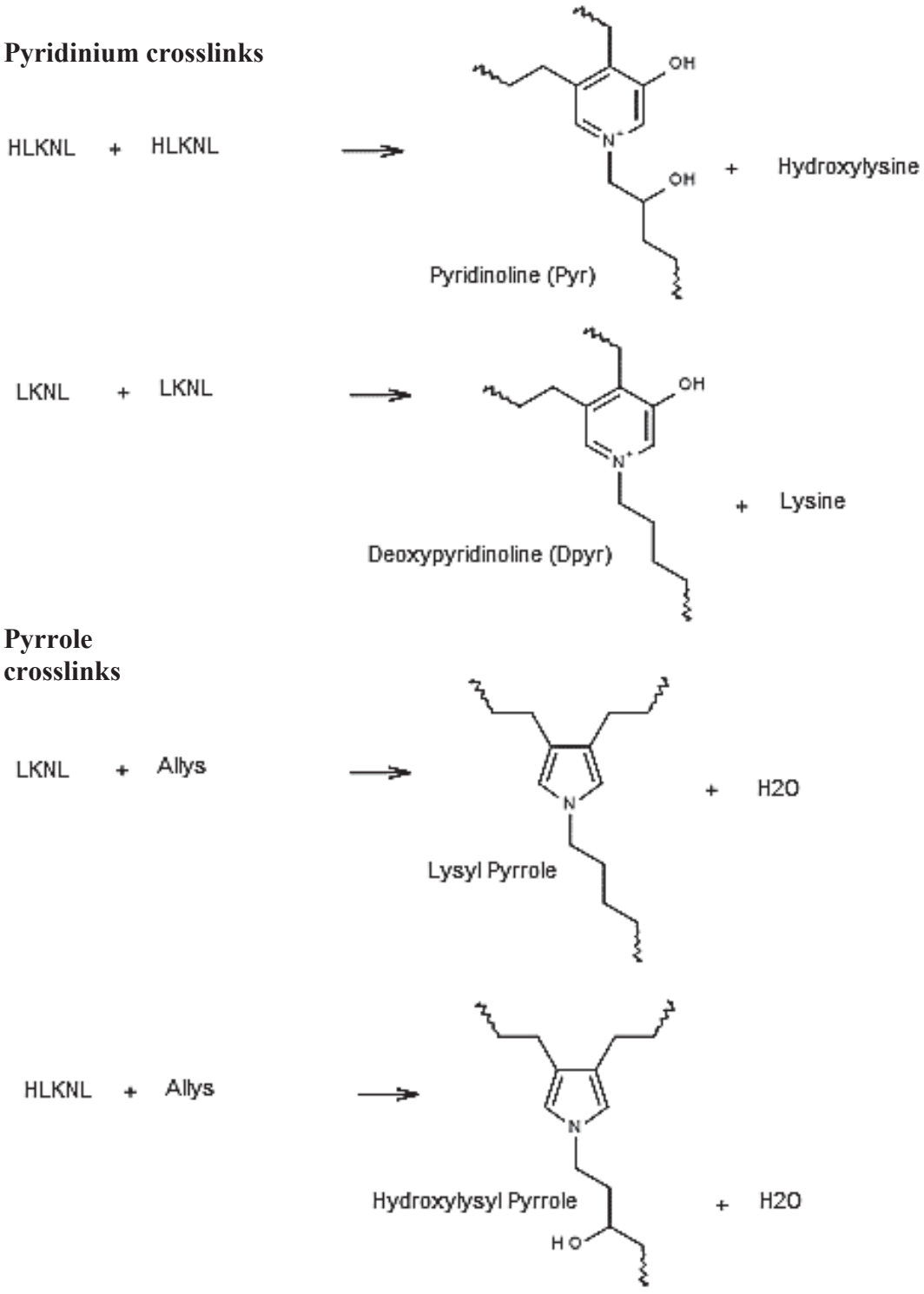

Figure 12: The formation of non-reducible crosslinks.

In spite of this, the concentration of AGE products is still much lower than those containing crosslinks formed by the activity of lysyl oxidase [6, 121].

Glucose, lysine and arginine are the major residues involved in the formation of AGE products and two well identified products, pentosidine and glucosepane have been isolated and measured (Figure 13) [124, 125]. Initially glucose reacts with a collagen lysine residue to form a glucosyl-lysine Schiff base. It then undergoes an Amadori rearrangement to produce fructose-lysine [126]. Subsequent reaction of fructose-lysine with arginine can result in two products: Pentosidine is formed by an oxidation reaction between ribose and arginine, while glucosepane is formed from the non-oxidative reaction between the same substrates (Figure 13) [122]. Studies have shown that glycation increases stiffness in tissues as well as their resistance to proteases [122]. Not surprisingly, the rate of glycation is accelerated in the presence of high glucose concentrations and radiation [122].

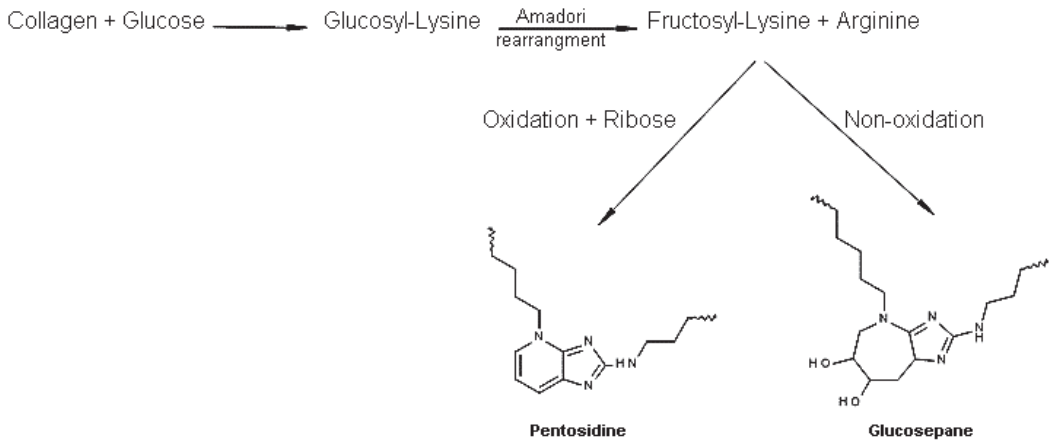

Figure 13: Possible pathways and the chemical structures of the two major AGEs.

2.3.8 Other crosslinks

Recently, Eyre *et al.* identified a new crosslink in cartilage formed by the spontaneous oxidation of a ketoamine with arginine to produce arginoline (Figure 14) [127].

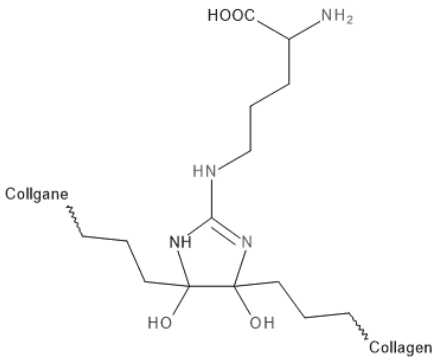

Figure 14: Chemical structure of arginoline

In keratin, fibrin and fibrillin, ε(γ-glutamyl)-lysine crosslinks are synthesized by transglutaminase (Figure 15) [128-130]. Collagen can also be stabilised by transglutaminase through the formation of ε(γ-glutamyl)-lysine links between lysine and glutamine residues [131, 132]. Because of the high glutamic concentration in collagen, such crosslinks could be important.

Another unusual collagen crosslink is found in marine mussels. It is formed by the reaction of oxidized 3,4-dihydroxyphenylalanine (DOPA *o*-quinone) and lysine residues as a result of the activity of catechol oxidase (Figure 15). The crosslink so formed then reacts with histidine residues or metal ions to form a more complex crosslink but the exact mechanism is still unknown [133-137]. An isotrityrosine crosslink has been isolated from cuticle collagen characterised, and shown to have an ether linkage (Figure 15) [138, 139].

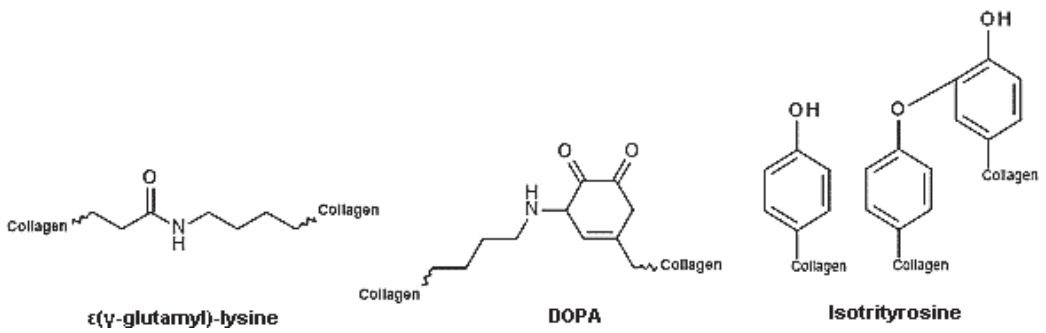

Figure 15: Chemical structures of other crosslinks.

2.3.9 Crosslinking profile of collagen

Collagen crosslinks have been extensively studied in many tissues, including bone, tendons, cartilage and skin. The different types of crosslinks have been isolated, and fully identified in each tissue (Figure 16) [6, 32, 140]. Moreover, the crosslinking profiles of different tissues at different stages of development have been analysed [6, 12, 141]. The critical factor that contributes to the formation of crosslinks is the amount and the location of hydroxylysine in the helical and telopeptide domains. This depends on the activity of the lysyl hydroxylase during the maturation of collagen [44, 48, 61, 82, 142, 143].

The number and location of lysine residues in the α1-chain are highly conserved among different species while the α2-chain shows slight differences [44]. Interestingly, all lysine residues in the telopeptide domains of both the α1 and α2 collagens are involved in the formation of crosslinks despite the extent of lysine hydroxylation being dramatically different between species [44]. For collagen I, the prevalence of hydroxylysine residues varies from tissue to tissue depending on its physiological condition [68]. The selective oxidation of specific hydroxylysine and lysine residues into aldehydes by lysyl oxidase is dependent whether or not they are glycosylated [12,

44, 66, 68, 144]. These observations strongly suggest that hydroxylation, oxidation and glycosylation of the lysine residues regulate the location, type and total number of crosslinks formed. It is likely that other factors such as the arrangement of different types of collagen in a particular tissue may also play an important role in crosslink formation [145-150].

2.3.9.1 Crosslinks in skin

Hydroxylation of lysine in the telopeptide domain of skin collagen is low, in contrast to the helical domain where it is high [6]. As a consequence, allysines are predominant in the telopeptide domain whereas hydroxyallysines are more common in the helical domain [44, 78, 83, 151]. Thus the formation of aldimine crosslinks is favoured in the helical domain of the collagen [44, 152]. As a result, collagen in immature skin is very soluble at acid pH or at higher temperatures because under these conditions aldimine crosslinks are easily broken [53, 90, 153, 154]. Compared with HLNL, LNL is usually present only in very low concentrations in skin, because the lysines in the helical collagen domain (X-Gly-His-Arg) are usually hydroxylated. The reaction of allysine with hydroxylysine is, therefore, more likely to occur with lysine to produce HLNL [6, 44, 78]. In foetal skin and during the initial stages of wound healing, the concentration of ketoamine crosslinks (DHLNL) is high, although it decreases rapidly as skin matures and aldimines become predominant [155].

Additionally, two mature crosslinks are detected in skin resulting from the reaction between three and four residues to make HHL and HHMD [66, 83]. Strikingly, the HHL crosslink is detected only in skin. The way it is formed is dictated by the unique geometry of collagen molecules in skin where the degree of bend is approximately 16^{o}

from the longitudinal axis of the fibril compared with bone collagen where it is only about 7^{o} [156]. This difference is generally supported by X-ray diffraction studies which show the D-periodicity of collagen in skin is approximately 65 nm compared to 67 nm in bone [156-158]. This puts α1-hydroxylysine^{87} and α2-histidine^{92} in the helical domain and α1-lysine^{13} in the C-telopeptide in close proximity, allowing them to react together to produce the HHL trivalent crosslink [156]. HHMD is formed using the same mechanism except that the aldol product participates in crosslink formation rather than the α1-Lysine^{13} residue [156, 159]. The structures of the HHL and HHMD were first confirmed by mass spectrometry then resolved by H^{1} and C^{13}-NMR by Yamauchi *et al.* and Hunt *et al.*, respectively [94, 104].

Although several crosslinks have been identified in skin, further work is required to explore the possible existence of others. For example, Housley and Tanzer isolated hydroxyaldol-histidine from cow skin, although this was refuted by Yamauchi *et al.* because of a possible product contamination [86, 94].

2.3.9.2 Crosslinks in bone

In bone collagen, the telopeptide lysines are more heavily hydroxylated, than the lysines in the helical domain, resulting in high concentrations of the more stable ketoamine crosslink, DHLNL [61, 83, 84]. As a result, bone collagen is hard to isolate by acid hydrolysis because the crosslinks are less soluble [160]. It has been shown that DHLNL reacts with other aldehydes to produce pyridinoline crosslinks during maturation [95, 161, 162]. Pyr is the major mature crosslink in bone and cartilage, while Dpyr is found mainly in bone. The occurrence of both Pyr and Dpyr in skin is rare [83, 95, 163].

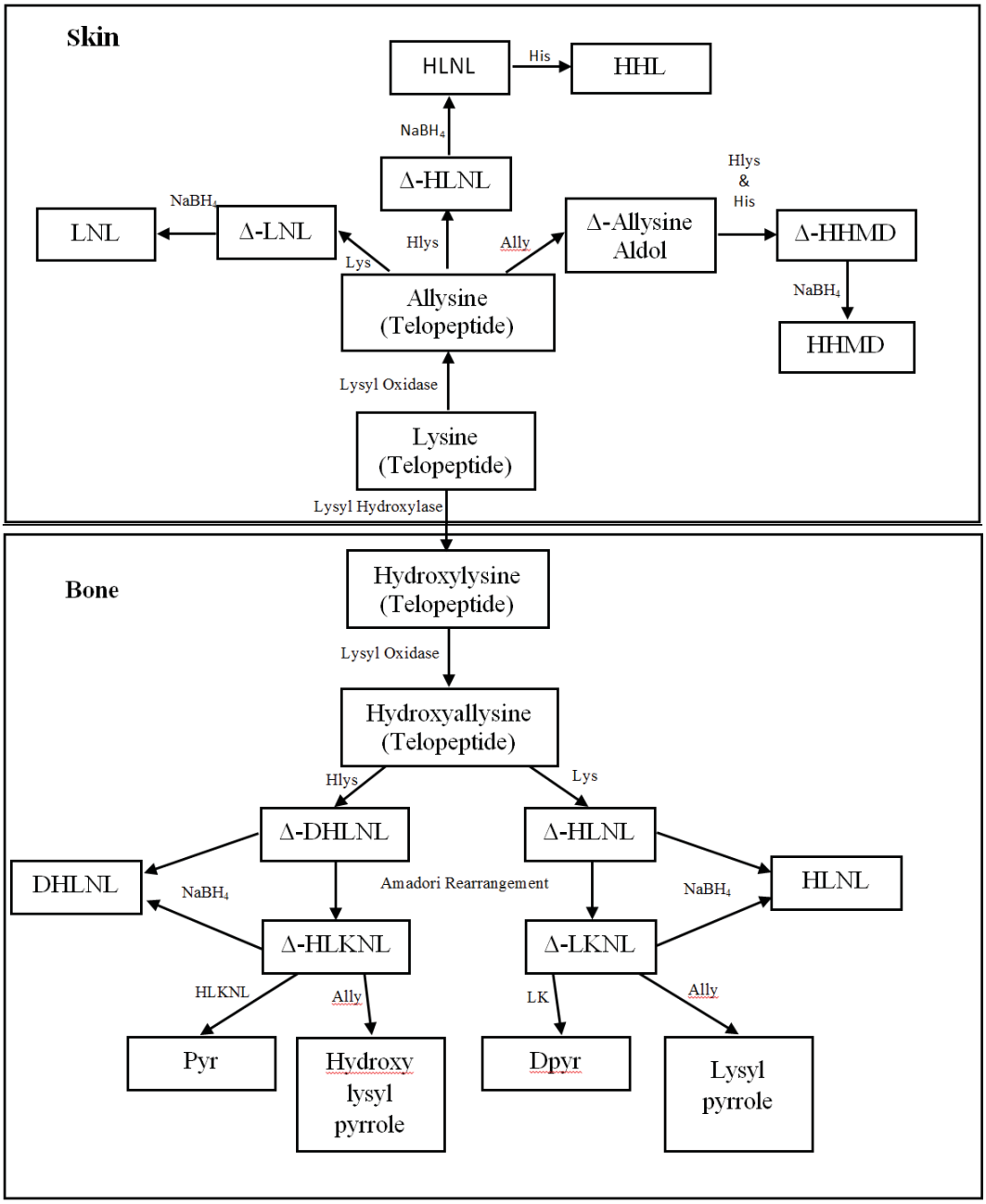

Figure 16: Possible pathways for the formation of crosslinks in skin and bone.

2.3.10 Quantitation of crosslinks

The sensitivity and reproducibility of crosslink analysis is critical to any method. The quantitation of crosslinks is carried out in three major stages [140, 164]. (i) Stabilisation of the acid and heat labile crosslinks by reduction before they are isolated from the tissue by acid or base hydrolysis at high temperature [140]. Treatment with 6 M of hydrochloric acid at 105ºC for 24-72 hours is the most common hydrolysis method [165]. (ii) Separation of the crosslinks from the free amino acids by fibrous cellulose chromatography to improve the detection sensitivity [140]. (iii) Detection and quantitation of the crosslinks [140].

2.3.10.1 Method development of crosslink quantitation.

The occurrence of the collagen crosslinks was first noted by several investigators who considered them to be "ester-like" linkages [166-168]. The first discovery of a crosslink was in 1963 when Partridge *et al.* showed, by titration, that the amino acid chains in elastin contained a fluorescent compound with 2 terminal α-carboxyl and 2 terminal α-amino groups [169]. This initiated a huge momentum to explore collagen and elastin crosslinks in tissues, using mainly tritiated borohydride labelling [80, 81, 170-174]. In 1968, Bailey and Peach resolved the first structure of a collagen crosslink by mass spectroscopy. HLNL was isolated from rat tail tendons and confirmed by synthesis [78]. Several quantitation methods were then developed resulting in the complete identification and quantitation of several collagen crosslinks.

2.3.10.2 Sample preparation

The efficiency of isolation of intact crosslinks from a crude sample determines the sensitivity and reproducibility of the analysis. Reduction of the sample with

borohydride is essential to stabilise reducible crosslinks as these are destroyed or modified by acid hydrolysis (Figure 17) [80, 174]. Pyridinoline crosslinks and advanced glycation products (AGEs) are, however, resistant to acid and heat and can be analyzed without prior reduction [116, 164]. Tritiated borohydride is sometimes used to facilitate the identification of the crosslinks during the pre-fractionation step [71, 175].

Crosslink quantitation is a big challenge because their numbers are very low compared to the amino acids [164]. Pre-fractionation of crosslinks from amino acids has been shown to improve all aspects of quantitation [164, 176]. Starcher (1976) and Skinner (1982) used liquid chromatography with a mobile phase of *n*-butanol:water:acetic acid (4:1:1) and a cellulose stationary phase to remove the amino acids from desmosine and isodesmosine owing to their low solubility in butanol [176, 177]. This method became an essential step for all subsequent methods used to quantitate collagen and elastin crosslinks [95, 164, 178-183]. Other methods, such as solid phase extraction (SPE), cation exchange and size exclusion chromatography, are less common [181, 184-186].

2.3.10.3 Separation of crosslinks

For reliable quantitatation, crosslinks must be fully separated to enhance the analytical sensitivity. Several methods have been developed to achieve this including cation exchange (CEX), size exclusion (SEC) and reverse phase high performace liquid chromatography (RP-HPLC) [187].

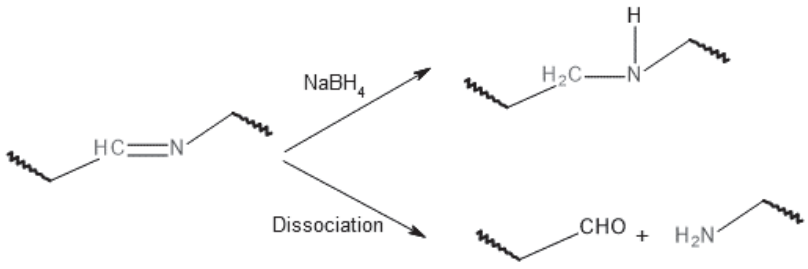

Figure 17: Reduction and acid cleavage reactions of aldimine crosslinks.

The first separation method involved a combination of two types of chromaotgraphy, CEX and SEC [188]. The sample was first reduced with tritiated sodium borohydride then hydrolysed in 6 M HCl. The resultant hyrolysate was then subjected to SEC (Sephadex G-10 or BioGel-P2). The reduced labelled crosslinks were eluted before the free amino acids due to their larger size and detected by radoiassay. Individual crosslinks were then separated by preparative CEX using a pyridine-formate buffer system followed by analytical CEX using citrate buffer [188]. Although successful, the method required large samples and long run times. It would therefore be an advantage to develop a more sensitive method with a reduced sample size and a shorter run time.

The method reported by Smolenski *et al.* used HPLC separation with scintillation detection and manual post-derivitization offered no improvement in sensitivity [89]. The most cited method for analysing crosslinks was reported by Sims and Bailey in 1992; collagen and elastin crosslinks were separated by CEX using a citrate buffer system and post-column derivatization with ninhydrin was used for detection [164]. Currently, this is the "golden method" for crosslink analysis. Although other methods have been develped using RP-HPLC none have been able to simultaneously analyse all crosslinks and elastin [109, 178, 181, 189-193].

2.3.10.4 Detection of crosslinks

To date, crosslink analysis has been performed mostly by HPLC using both fluorescence and UV detection [95, 164, 176, 178, 190]. Most of the crosslinks are determined using post-column derivitization with ninhydrin except for the pyridinolines and AGEs which have a conjugated system of aromatic rings and therefore fluoresce naturally [140, 164, 194]. In spite of the usefulness of the post-column ninhydrin method, it has many limitations including long run times (> 60 minutes), low sensitivity (nmol range) and the need for a dedicated insturment. New methods are, therefore, being developed every year to improve the detection sensitivity and to shorten the run time as well as to simplify sample preparation steps.

Pre-column derivitization methods have been succesfully utilized in amino acid analysis however it has not proved suitable for measuring crosslinks due to the fomration of multiple derivatives which complicates quantitation [140]. Mass spectrometry on the other hand, does not require any derivitization and all crosslinks can be detected simultaneously with excellent sensitivity and selectivity regardless of their spectroscopic properties [178, 189]. Kindt *et al.* (2000) were the first to use mass spectrometry to detect pyridinium crosslinks [189]. In 2010, Gineyts *et al.* described the use of electrospray ionization mass spectrometry to detect four crosslinks (HLNL, DHLNL, Pyr and Dpry). While the sensitivity of this method was good, other major crosslinks (HHL and HHMD) were not analysed [178].

Fourier transform infrared (FTIR) has been successfully used to measure the relative amounts of nonreducible to reducible crosslinks in collagen without the need for preparation and pre-fractionation steps [164, 195]. It was found that the area ratio of

the two amide I bands of the collagen spectral peaks (1660:1690) cm^{-1} is related to the secondary structure of collagen and corresponds to the ratio of pyridinoline to DHLNL crosslinks [196-198]. While this technique provides the relative proportions of some crosslinks, it also requires much data manipulation and background elemination, which limits its usefulness.

2.4 Elastin

2.4.1 Elastin structure

Elastin is the major component of the elastic fibres found in the extracellular matrix of vertebrates [13]. Unlike collagen, elastin can stretch to twice its length without fracturing and imparts elasticity to the tissues and organs allowing them to recoil to their original shape after being stretched. This property is important for skin, lungs, ligaments, tendons, and blood vessels [199]. The relative amount of elastin varies in different tissues, being less than 4% of dry skin weight and more than 50% in arteries [200, 201]. Elastic fibres consist of two major structural components, soluble immature elastin (amorphous) known as tropoelastin, which is the major fraction and mature crosslinked microfibrils which are located more peripherally [13].

The amino acid composition of elastin is similar to that of collagen with a high proportion of hydrophobic amino acids particularly valine and alanine. Interestingly, it contains no hydroxylysine, histidine or methionine [13, 202]. The low lysine, arginine and aromatic amino acid content makes elastin resistant to proteolysis by trypsin and chymotrypsin. It can, however, be degraded by elastases which recognize alanine, valine, glycine, and leucine amino acids [13, 203]. Alanine-rich α-helical and hydrophobic domains are characteristic of elastin [204, 205]. In the helical domain,

lysines are separated by two to three alanine residues which is crucial for the formation of crosslinks [206]. The hydrophobic domain contributes significantly to the elasticity especially to fibre recoil in the stable state (Figure 18) [207]. It has been reported that elastin microfibrils can generate signals when tissues are damaged thereby activating tissue repair [208].

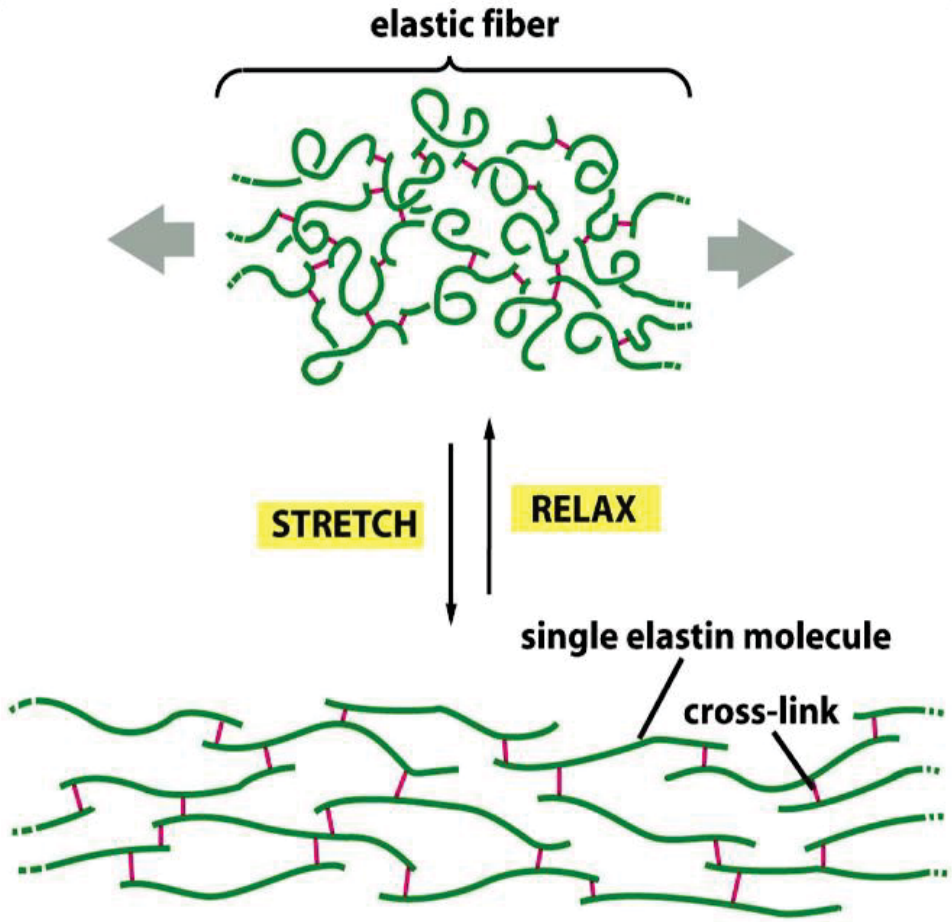

Figure 18: A schematic diagram showing an elastin network and its elastic properties. Elastin chains are in green and crosslinks are in red. Taken from Alberts, Bray, Hopkin, Johnson, Lewis, Raff, Roberts and Walter [209] with permission of the publisher.

2.4.2 Elastin biosynthesis and crosslinking

Synthesis and deposition of elastin into the extracellular matrix is a complex process [13]. First, a 60–70 kDa monomer called tropoelastin is synthesized, after which proteoglycans bind to its C-terminus. This initiates elastin self-microassembly, in which tropoelastin molecules aggregate into correct register with the help of n Fibulin-4 before being cross-linked [210-212]. Lysyl oxidase then oxidatively deaminates certain lysine residues to form aldehyde groups (allysine) [213]. Spontaneous condensation of allysine with lysine creates dehydro-lysinonorleucine (deH-LNL) followed by condensation of two allysine residues to give allysine aldol (ACP) (Figure 19) [213]. deH-LNL reacts with ACP to produce desmosine making stable elastin microfibrils. The removal of the tropoelastin lysine sidechains as they become involved in crosslinks results in a decrease in its isoelectric point from 11 to 6 causing the elastin microfibrils to become insoluble [13, 214].

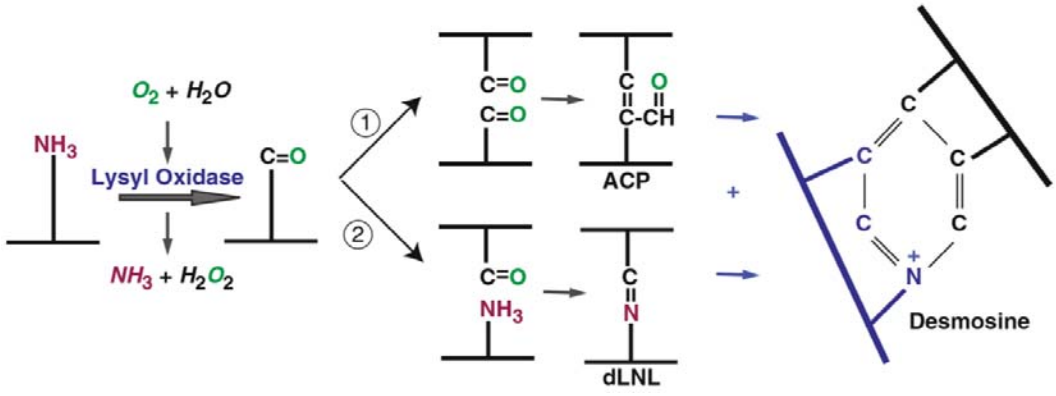

Figure 19: Desmosine crosslink formation in the tropoelastin molecule. Taken from [13] with permission of the publisher. ACP = allysine aldol and dLNL = dehydro-lysinonorleucine.

The formation of other crosslinks has been reported including dehydromerodesmosine, cyclopentenosine, desmopyridine and isodesmopyridine [215]. Desmosine and isodesmosine are, however, the major elastin crosslinks and have been isolated from and fully identified in elastin [215-218]. It has been proposed that these tetrafunctional crosslinks can be synthesised by the reaction of dehydromerodesmosine with dehydro-lysinonorleucine, or the reaction of two allysine groups with dehydro-lysinonorleucine (Figure 20) [199, 200, 215, 218]. The interaction between tropoelastin hydrophobic domains results in the formation of aggregates which are further stabilized by crosslinks [219], contributing to the unique mechanical recoiling function of elastin fibres. Interestingly, the extensive crosslinking of elastin results in an extremely slow protein turnover that is estimated in years [220-222].

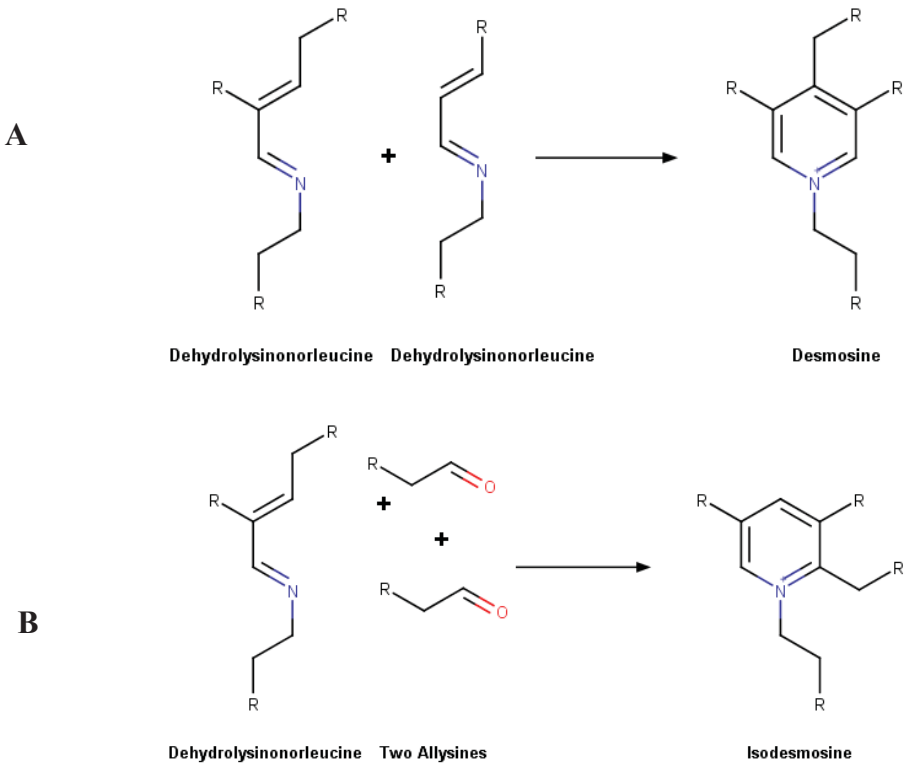

Figure 20: Proposed mechanism for the formation of (A) desmosine (B) isodesmosine.

2.4.3 Elastin quantitation

Traditionally, quantitation of elastin is carried out gravimetrically. Elastin is first isolated by boiling in acid (α-elastin) or base (κ-elastin) before being weighed [223-225]. Weighing limits the accuracy of detection therefore other methods have been developed [177]. It was discovered that desmosine and isodesmosine are only found in elastin therefore their quantitation is used to quantitate the concentration of elastin in biological samples [177, 183, 201].

Several methods have been developed to measure the concentration of desmosine and isodesmosine including electrophoresis, radioimmunoassay, enzyme immunoassay, thin layer chromatography (TLC), high performance liquid chromatography (HPLC) and mass spectrometry [176, 183, 226-229]. TLC and electrophoresis techniques did not prove to be useful for accurate quantitation. On the other hand, immunoassay methods require extensive sample preparation, specific antibodies and have limited sensitivity [228, 230]. HPLC and mass spectrometry can simultaneously determine desmosine and isodesmosine concentrations with high accuracy [177, 183, 191, 230]. Both methods require acid hydrolysis of the sample to release the crosslinks followed by separation from the bulk amino acids by RP-HPLC and detection by UV or by mass spectrometry [183, 227, 231]. The elastin content is then calculated from a calibration curve formed by different concentrations of either an elastin standard, containing a known amount of desmosine, or from pure desmosine and isodesmosine [177, 201, 228].

2.5 Glycosaminoglycans and proteoglycans

Glycosaminoglycans are long linear, sulfated and negatively charged polysaccharides with a molecular weight of 10-100 kDa [232]. They can be covalently attached to a core protein through O- or N- linkages to form proteoglycans [233, 234]. Proteoglycans have multiple cellular roles, depending on the number and type of glycosaminoglycans and the structure and size of core protein [232, 235, 236]. Their functions include distribution of water and salt, cell-cell interactions, cell-matrix interactions and importantly in skin, collagen fibril organisation during fibrillogenesis [237-240].

2.5.1 Glycosaminoglycans

Heparin was the first glycosaminoglycan discovered in 1917 as an anti-coagulant and was initially characterized as chondroitin sulfate [241, 242]. Structurally, most glycosaminoglycans are made up of either a glucuronic or iduronic acid, linked to either a glucosamine or a galactosamine to form a repeating disaccharide motif in which the saccharide moieties can be sulfated on either C4 or C6 (Figure 21) [234]. There are different types of glycosaminoglycans (Table 4): Dermatan sulfate, chondroitin sulfate, heparin and hyaluronic acid are found in skin [232].

2.5.1.1 Chondroitin sulfate

Chondroitin sulfate consists of a monosulfated repeating disaccharide composed of D-glucuronic acid and N-acetyl-galactosamine. The N-acetyl-galactosamine is monosulfated on either C4 or C6 to give chondroitin-4-sulfate or chondroitin-6-sulfate, respectively, both of which have similar properties [35, 243]. Ten parentage of chondroitin sulfate is non-sulfated and the di-sulfated disaccharide rarely occurs [243].

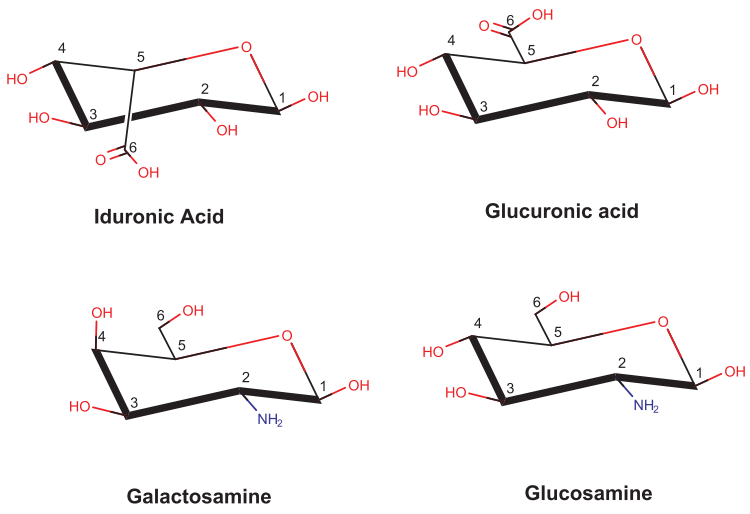

Figure 21: Structure of the saccharide moieties of glycosaminoglycans.

Chondroitin sulfate attached to proteoglycans is present in virtually all connective tissues of the body. Interestingly, different sulfation patterns determine specific biological activities of chondroitin glycosaminoglycan chains [244-246]. Chondroitin sulfate and its core protein play an important role in the collagen fibrillogenesis, and the saccharide of chondroitin sulfate has been shown to facilitate collagen crosslinking [247-249]. Interestingly, it has been shown the chondroitin sulfate content of skin is increased by exposure to UV light [250].

2.5.1.2 Dermatan sulfate

Dermatan sulfate, also known as chondroitin sulfate B, consists of repeating units of L-iduronic acid and N-acetyl-galactosamine (Table 4) [235, 239]. Dermatan sulfate and chondroitin sulfate are considered structural isomers in which epimerization of the carboxyl group around C5 of glucuronic acid creates the iduronic acid of dermatan sulfate. The presence of iduronic acid plays an important role in determining the specificity of glycosaminoglycan-protein interactions [251]. Dermatan sulfate is the

major glycosaminoglycan found in skin and when associated with decorin, is directly involved in collagen fibril formation [239, 240].

2.5.1.3 Heparin/ heparan sulfate

Heparin and heparan sulfate are linear polysaccharides consisting of glucuronic acid and glucosamine repeating disaccharide units [252]. Structurally, they are the most complex members of the glycosaminoglycans, with about 24 different disaccharide units, due to different substitutions on the disaccharide units including N- and O-sulfation and N-acetyl groups [252]. Although heparin and heparan sulfate are structurally related, heparin is the most sulfated glycosaminoglycan having the highest negative charge density of any known biological molecule [253]. Heparin is found only in mast cells while heparan sulfate is located in most of mammalian cells, particularly on the cell surfaces and in the extracellular matrix [252]. The biological functions of heparin and heparan sulfate are a result of their high affinity to proteins [252].

Some studies have reported heparin sulfate exists in skin [254, 255]. While its *in vitro* functions in skin are not yet been fully understood, an *in vivo* study suggested heparin sulfate inhibits collagen fibrillogenesis by inhibiting lysyl oxidase activity [254].

2.5.1.4 Keratan sulfate

Keratan sulfate consists of repeating disaccharides of D-galactose and N-acetylglucosamine with sulfation occuring primarily on C6 of the D-galactose [235]. Unlike other glycosaminoglycans, keratan sulfate can be O-linked to threonine or N-linked to aspargine residues in the protein core [235]. In skin, keratan sulfate side

chains, are covalenty linked to lumican, which is associated with fibrillar collagen [256].

2.5.1.5 Hyaluronic acid

Hyaluronic acid is synthesized as a non-sulfated polymer that is non-covalently linked to any protein [257]. It contains thousands of repeating disaccharides of D-glucuronic acid and N-acetylglucosamine [258]. As a result, it has a very high molecular weight and because of its linear polyanion character, it holds a high concentration of water [258]. It is found in synovial fluid, articular cartilage, skin, vitreous humor and ECM of loose connective tissue [259].

Hyaluronic acid is the major component of extramolecular matrix of skin where it maintains the normal hydration of skin and distributes salts and nutrients [259, 260]. Interestingly, skin hyaluronic acid accounts for 50% of total body hyaluronic acid [249, 261]. It has been shown that hyaluronic acid enhances the enzymatic resistance and the mechanical properties of collagen [262, 263]. Strikingly, the concentration of hyaluronic acid in skin does not change with age but its length and its saccharide units change [260, 264]. It is found in both the dermis and epidermis although the concentration of hyaluronic acid in dermis is significantly higher than in the epidermis. In dermis, it is found associated with both collagen fibrils and elastin fibres, and is involved in their structure and organisation [260, 265].

Table 4: Repeating disaccharide units of various glycosaminoglycans [244].

Glycosaminoglycans Molecular weight	Disaccharide units	Localization	Features
Dermatan Sulfate **15-40 kDa**	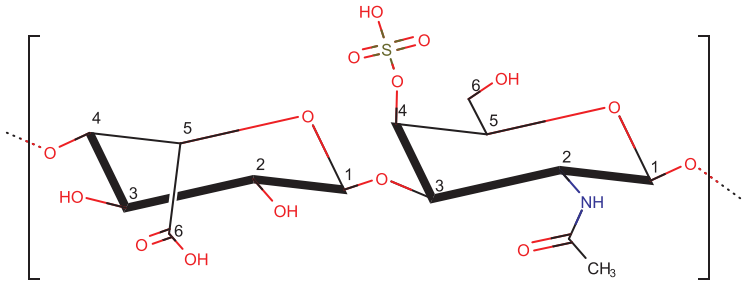	Skin, blood vessels, heart valves, tendons, lung.	L-iduronic sugar moiety. Major GAG in skin. Key role in formation of collagen fibril.
Chondroitin Sulfate **5-50 kDa**	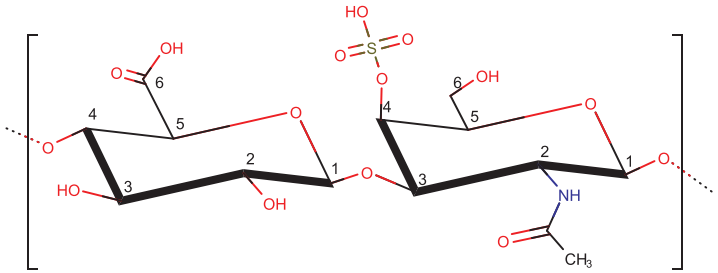	Cartilage, bone, heart valves.	Most abundant GAG in the body. Form proteoglycans called hyalectans, major component of the ECM.
Keratan Sulfate **4-19 kDa**	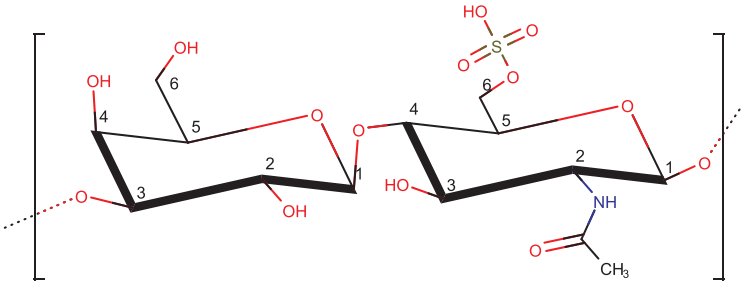	Cornea, bone, cartilage aggregated with chondroitin sulfates.	Most heterogeneous GAG. Two types KS I and KS II. KS I is found in the cornea. KS II is found in cartilage aggregated with CS.

Heparan Sulfate 10-70 kDa	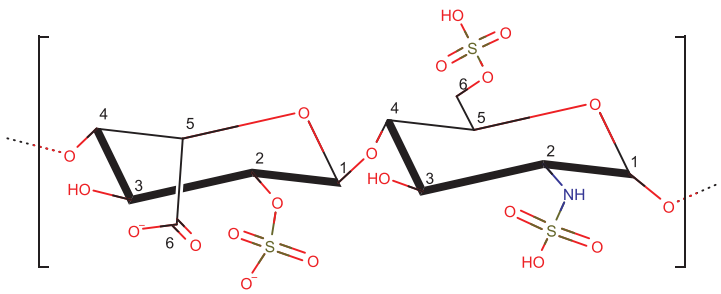	Component of intracellular granules of mast cells.	Most sulfated GAG. Highest negative charge among all biological molecules.
Heparin 10-12 kDa	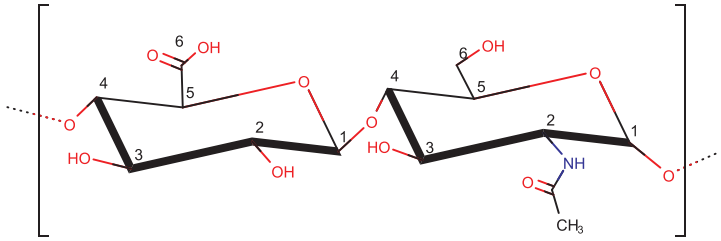	Basement membranes, components of cell surfaces.	Highest acetylated glucosamine associated with (HSPG).
Hyaluronic Acid (Non Sulfated) 4-8000 kDa	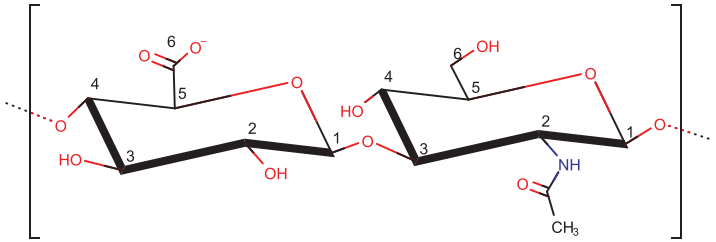	Synovial fluid, articular cartilage, skin, vitreous humor, ECM of loose connectivetissue.	Non-sulfated. Non-covalently attached to protein.

2.5.2 Proteoglycans

Glycosylation is one of the most common protein post-translational modifications [236]. It occurs when a mono or oligosaccharide is covalently added to a polypeptide chain by specific enzymes called glycosyl or oligosaccharyl transferases [266]. Linkages can either be through the side chain of an asparagine residue (N-glycosylation) or through the side chains of serine, threonine, hydroxyproline or hydroxylysine residues (O-glycosylation) [266]. Recently it has been found that sugars can be linked through the thiol sulfur cysteine [267]. The sugar moiety is called a glycan and has many functions that range from physicochemical through to recognition [233].

Proteoglycans (PGs) are a special type of glycoprotein in which the glycan moiety is any GAG chain except for hyaluronic acid (Figure 22) [233, 268]. They play many important roles in the regulation of cellular processes that depend on both the protein and the type, number, length and sulfate content of the glycosaminoglycan moiety [257, 269]. In skin, proteoglycans are known to play a major role in regulating collagen fibril assembly [233, 270-272]. Proteoglycans are classified into small leucine-rich proteoglycans (SLRP), large chondroitin sulfate proteoglycans (Hyalectans) and cell surface proteoglycans [233].

2.5.2.1 Small leucine rich proteoglycan

Small leucine-rich proteoglycans (SLRPs) are a family of PGs that share common multiple repeats of a leucine rich structural motif flanked by cysteines [274]. SLRPs

are classified into three subgroups according to their sequence homology at both the protein gene level and at the cysteine-rich regions [233].

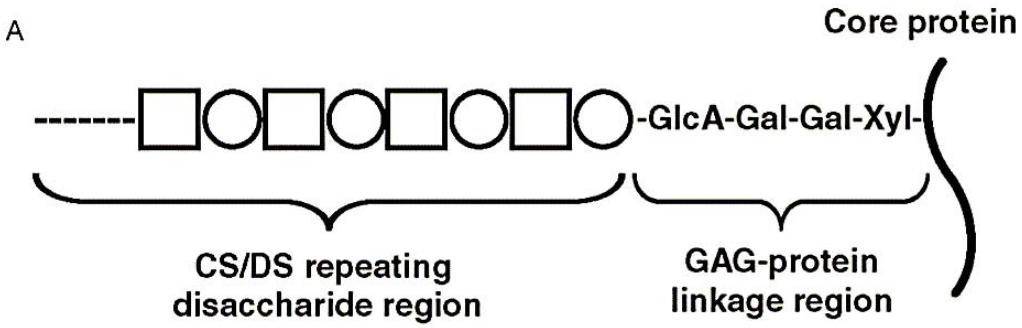

Figure 22: Chondroitin sulfate (CS) and dermatan sulfate (DS) chains are covalently attached to the core protein through the common GAG-protein linkage region tetrasaccharide, GlcA-Gal-Gal-Xyl (where GlcA, Gal, and Xyl stand for D-glucuronic acid, D-galactose, and D-xylose, respectively). The circles and squares indicate GalNAc and GlcA (or IdoA), respectively. Taken from [273] with permission of the publisher.

Class I includes decorin, biglycan and aspirin, class II includes fibromodulin, osteoadherin and lumican, and class III includes opticin, osteoglycin/mimecan and epuphycan/PHLb [275]. Extracellular matrix 2 (ECM2), chondroadherin and nyctalopin are leucine rich repeat proteoglycans with significant homology to the small leucine-rich proteoglycans (SLRPs) [276]. All SLRPs are involved in the protein-protein interactions and regulate various biological processes as well as organizing the extracellular matrix [233, 257]. Several studies have shown that SLRPs bind to type I and II collagens resulting in an interruption of fibril formation resulting in thinner fibres [238, 239, 271, 274, 277]. Decorin, the main proteoglycan in skin, biglycan, fibromodulin, lumican and versican are members of this family (Table 5) [274, 278].

2.5.2.1.1 Decorin

Decorin is the most abundant SLRP in skin, accounting for approximately 80% of the total PG content [209, 279]. It is also the major proteoglycan found in skin and it is localized in the dermal extracellular matrix where it is associated with collagen fibrils [272]. It consists of a small leucine-rich protein domain of 36 KDa and one chondroitin sulfate or dermatan sulfate glycosaminoglycan chain [272, 280, 281]. In skin, decorin binds near the C-terminal of collagen and strikingly close to one of the intermolecular covalent crosslinks [282]. Several studies have described the role of decorin in regulating collagen fibrillogenesis, ordering the spatial arrangement of collagen molecules and, thus, influencing crosslinking patterns [240, 271, 274, 277, 282-285]. It has been shown that decorin facilitates fibrillar slippage in skin, improving its tensile properties [240, 286]. A recent study reported that the average size of the decorin glycosaminoglycan chain reduces with age. It is, therefore, possible that the increase in skin fragility with aging is related to the changes in the decorin glycosaminoglycan [272].

2.5.2.1.2 Biglycan

Biglycan is a leucine-rich proteoglycan which has a core protein of 38 kDa and two attachment sites for glycosaminoglycans, in skin, these side chains can be either dermatan sulfate or chondroitin sulfate [281, 287]. Although biglycan and decorin both bind to collagen, it has been reported that biglycan is localized to both the epidermis and dermis, unlike decorin which is found only in the dermis [272]. Other studies have reported that biglycan is concentrated in the epidermis where it associates with the pericellular matrix and not the fibrillar elements of skin [287, 288]. Although biglycan

binds to collagen VI *in vitro*, it's *in vivo* function is not fully understood [257, 289, 290].

2.5.2.1.3 Lumican

Lumican is the major keratan sulfate proteoglycan found in the cornea, skin, and muscle connective tissues [256]. Some studies have shown that lumican plays an important role in the development of highly organised collagenous matrices and its deficiency has a profound effect on the skin fragility [256, 291]. The specific sites of its interactions with collagen have, however, not been identified [256]. Lumican is structurally very similar to decorin and biglycan in that it has a cysteine free protein core with a molecular weight of 38 kDa. One difference to decorin is the presence of an N-linked keratan sulfate on different asparagine residues [292].

2.5.2.2 Large Proteoglycans and Glycoproteins (Versican and tenascin)

Large proteoglycans such as versican, aggrecan and tenascin consist of a high molecular weight core protein (200-400 kDa) with up to 1000 chondroitin or dermatan sulfate glycosaminoglycan chains [293-295]. The large core proteins have relatively high affinity to hyaluronic acid creating several potential binding sites for other molecules [296]. Versican plays an essential role in extracellular matrix assembly where it interacts with important ECM molecules such as hyaluronic acid, fibulin-1, fibulin-2 and proteins associated with elastin [297, 298]. Some studies have suggested that versican is present primarily in the elastic fibres of skin where its concentration increases concomitantly with that of elastin and decreases with aging [256, 299, 300]. Tenascin is another member of the large glycoprotein that found in skin including

Tenascin-C and Tenascin-X [278]. It is the most complex glycoprotein in skin having 30 domains each of which have an independent function [295]. Tenascin is prominent in embryonic skin where it is associated with the development of the new skin [301, 302]. A few reports have suggested that it is not present in the adult skin while others have found it concentrated under the dermal-epidermal junction where it associates with collagen XVI [60, 301, 303].

Table 5: Functions and characteristics of skin proteoglycans [304, 305]

Proteoglycan	**Class**	**Core protein size kDa**	**glycosaminoglycan chains (number of chains)**	**Function and characteristics**
Decorin	SLRP	36	CS/DS (1), or CS/DS (1) + KS (1)	Binds to fibrillar collagen and regulates fibrillogenesis; predominant SLRP in tendon.
Biglycan	SLRP	38	CS/DS (1-2)	Binds to fibrillar collagen and regulates fibrillogenesis.
Lumican	SLRP	38	KS (2-3)	Binds to fibrillar collagen and regulates fibrillogenesis, inhibits size of collagen fibrils.
Versican		200-400	CS/DS (10-30)	Linked to hyaluronic acid, increases viscoelasticity, maintains cell shape.

2.6 Lipids

Lipids or fats are water insoluble substances that include triglycerides, wax esters, fatty acids and smaller amounts of cholesterol, cholesterol esters, ceramides and squalene (Table 6). They are essential components of skin and are concentrated in the upper layer of the epidermis, stratum corneum, and subcutaneous layer (Figure 23) [28]. Although lipids are unevenly distributed in mammalian skin, they can make up to 30% of the skin dry weight [2].

Lipids are synthesized in the sebaceous gland which secretes a fatty mixture called sebum [306, 307], whose composition varies among mammalian species [28, 308]. Lipids, are however, crucial for skin integrity, with functions that include waterproofing, antibacterial, membrane formation and energy storage [309, 310].

Phospholipids, sphingolipids and cholesterol are all involved in membrane formation while triglycerides are the major components of fat cells located in the subcutaneous layer [308]. The most hydrophobic lipids are waxes that are very stable and resistant to oxidation, hydrolysis, and heat and act to protect and lubricate the skin [28]. Squalene is unique in human sebum and has not been detected in other mammalian species [28]. It is a marker of sebaceous gland activity in human skin and has been shown to play a key role in blocking UV light [311].

The stratum corneum provides a permeability barrier. Lipids are packaged in secretory organelles called epidermal lamellar bodies (LB) that contain mainly cholesterol, glucosylceramides and phospholipids in addition to a variety of proteins including enzymes [308]. When keratinocytes are differentiated into corneocytes, lipids are

released from lamellar bodies into the extracellular space. After several enzymatic processes, the resulting mixture is converted into a hydrophobic matrix which occupies the extracellular spaces of the stratum corneum. This matrix prevents the movement of water across the skin [28].

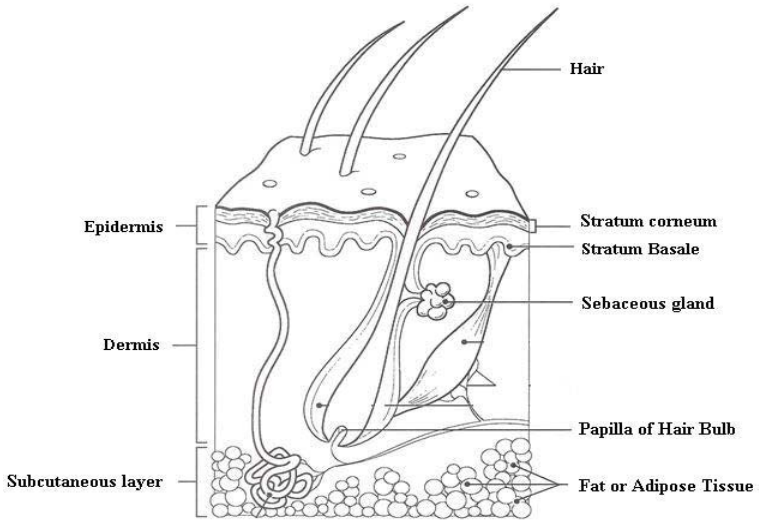

Figure 23: Schematic diagram of Skin.

Sebaceous glands in animals produce triglycerides and wax esters [312]. Several studies have shown that lipids vary widely amongst animals [306, 312-314]. Sterols and sterol esters have been found in the skin of most animals although some animals do not produce wax monoesters and triglycerides [314, 315]. It has been noted that surface lipids in sheep skin are subjected to a high rate of autoxidation and activity from microbial enzymes making them substantially different to those of other animals [316]. Remarkably, sheep skin has the highest total lipid content, up to 30% of dry skin weight. This is due to the fat layer between the epidermis and dermis layers that is not present in other animal skins [2]. Cow skin contains mainly waxes, triglycerides, cholesterol and cholesterol esters [313].

Although several studies have shown that collagen has high affinity for lipids, there are few reported studies on its interaction with lipids [317-319]. It is thus most unlikely that lipids affect collagen stability. It is possible, however, that their presence affects the accessibility of chemicals and enzymes to the skin, which may influence the interaction of collagen with other proteins [317, 318, 320].

Table 6: General Structure of Lipids.

Classification	General struture
Free Fatty Acids	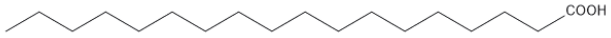
Triglycerides R1, R2 = H, Monoglycerides R1 = H Diglycerides	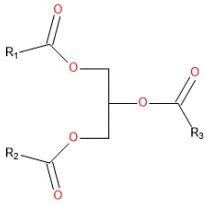
Wax Ester	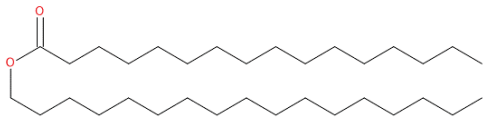
Cholesterol ester R1 = H, Sterol (Cholesterol)	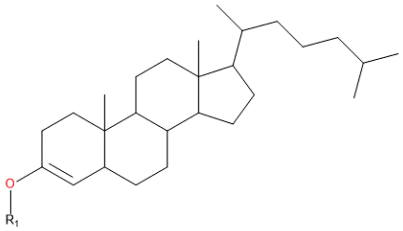
R1= H, Ceramides R1= Phosphate group, Phospholipids R1= Carbohydrates, Glycolipids	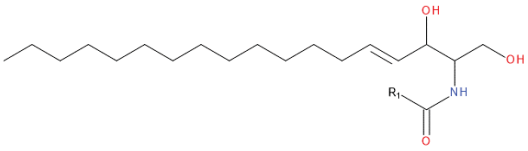
Squalene	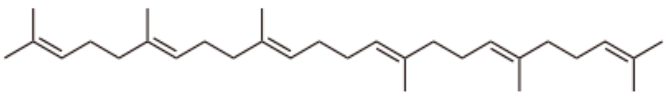

2.7 Small angle X-ray scattering (SAXS)

When an X-ray beam passes through a sample, it will interact with individual particles where it can be either scattered or absorbed [321]. Absorption occurs when X-ray photons are absorbed by molecules in the sample which causes the electrons to become excited to higher energy level. The release of this energy is associated with the production of other forms of energy such as heat [321, 322]. Scattering of the X-rays can occur with loss of energy (inelastic) or without loss of energy (elastic) scattering. Inelastic scattering (Compton scattering) is characterized by energy loss from the photons, resulting in a scattered beam of higher wavelength that is incoherent with the incident radiation. As a result, it does not carry any structural information about the particles and is part of the background radiation [323]. In elastic scattering (Rayleigh and Thomson scattering), photons hit the electrons without energy transfer causing electrons to oscillate at the same frequency as the incident beam. This results in a coherent scattering that has structural information [322, 323].

The X-ray beam is scattered at different angles (Figure 24), each of which contains information about the shape and the size of the particles. This angle depends on the electron density around the particle thus size, sample-to-detector distance and the wavelength of the X-ray beam [322]. At small angles, only elastic scattering is observed since the inelastic scattering is weak [323]. The larger the particles are, the smaller the angle is [323]. Depending on the angle, X-ray scattering can be classified into two types, small angle X-ray scattering (SAXS) and wide angle X-ray scattering (WAXS) (Figure 24) [321].

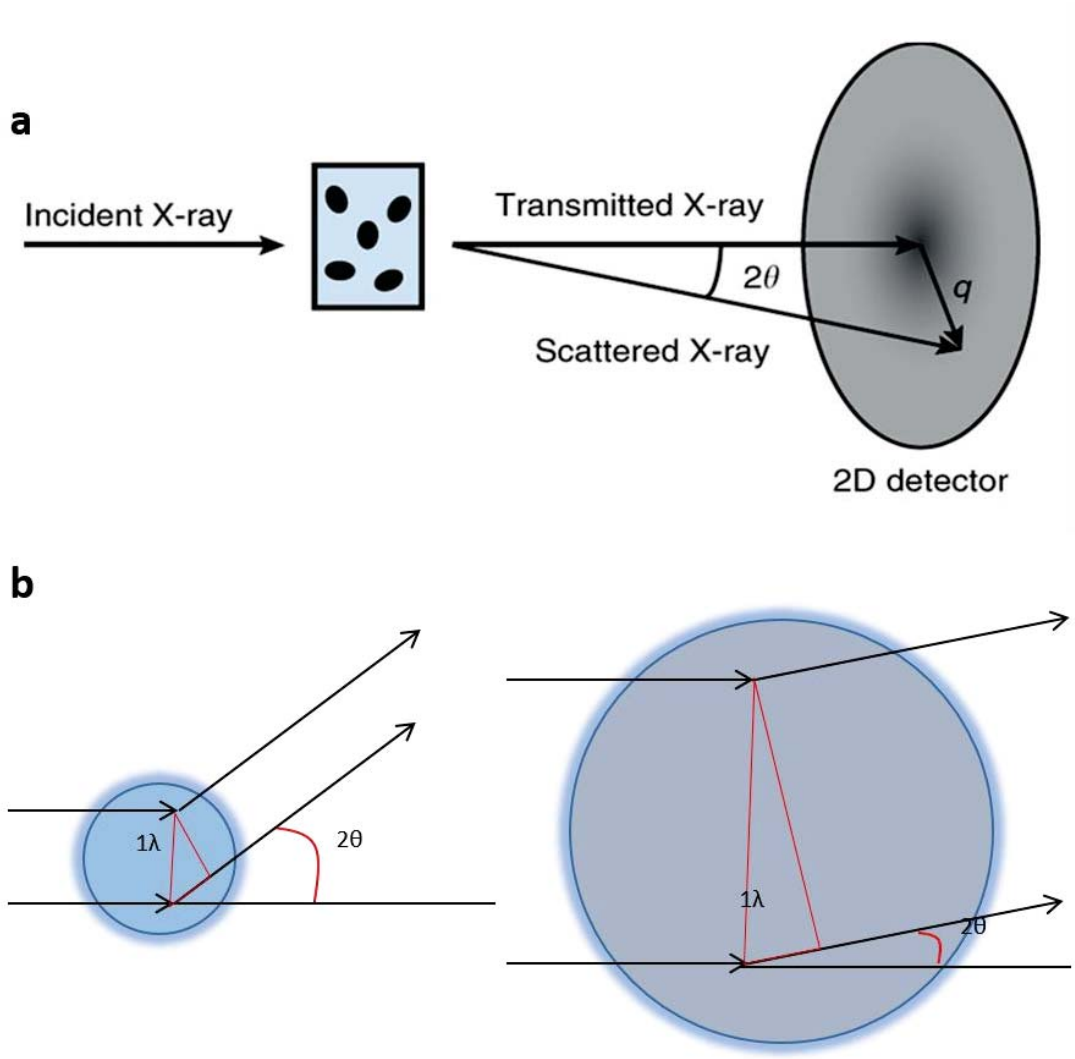

Figure 24: (a) An X-ray beam incident on the sample generates scattered X-rays, which are imaged by a detector. The scattering vector q, describes the change in direction of the elastically scattered X-rays. (b) Representation of the scattering differences for small and large particles. Left represents WAXS while right represents SAXS.

2.7.1 SAXS of skin

SAXS is a non-destructive technique that does not require any sample preparation such as the staining or dehydration that are necessary for electron microscopy [324, 325]. SAXS provides excellent insights into the structural organisation of collagen fibrils and fibres in tendon, skin, bone and teeth [20, 326-333]. When collagen interacts with X-rays, it produces, equatorial and meridional diffraction patterns that depend on the structural organisation of the collagen in the tissue (Figure 25).

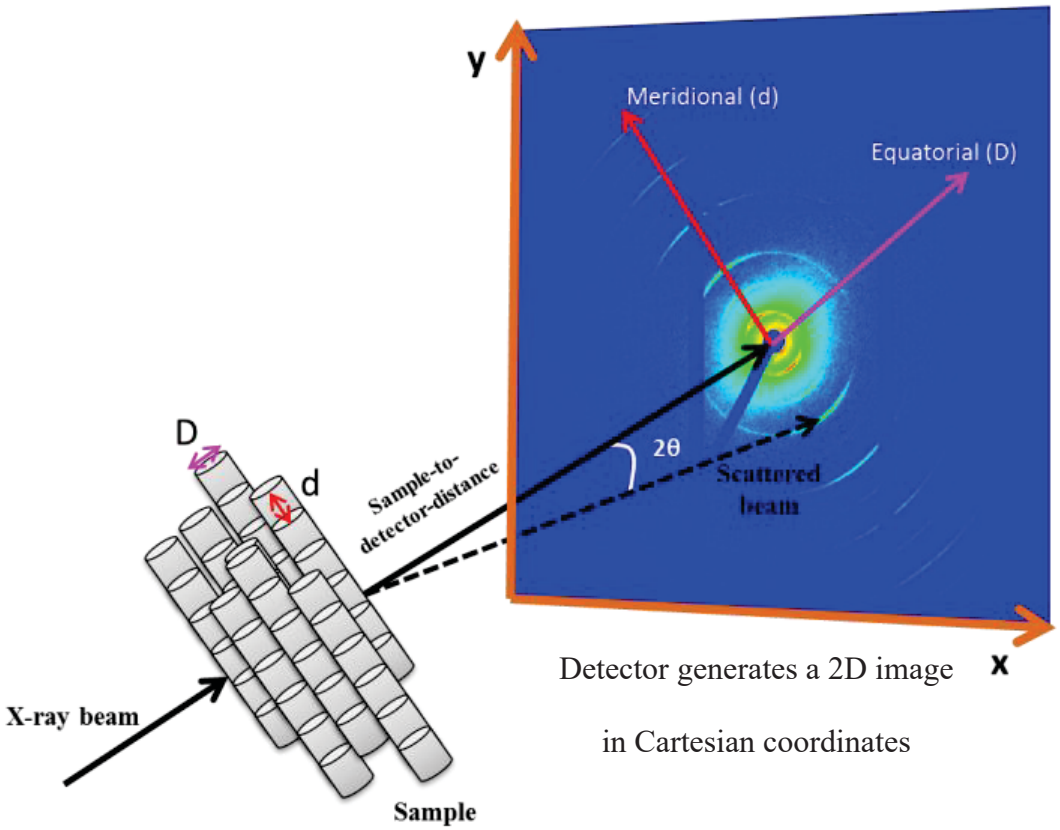

Figure 25: Schematic representation of the sample SAXS diffraction pattern showing the meridional (d) and equatorial (D) scattering from collagen.

Skin is made of networks of collagen fibres which give the skin its extensibility and strength [334]. These fibres contain large number of fibril bundles that result from the formation of covalent crosslinks within collagen molecules. These fibrils are arranged axially in staggered arrangements creating a periodicity called d-spacing (Figure 26). This regular arrangement results in a characteristic diffraction pattern of meridional rings where the distance between the arcs is directly correlated to the d-spacing of the fibrils.

Hulmes *et al.* also reported that the axial D-periodicity of collagen could be used to analyse different types of collagen, interaction of collagen with other components such as proteoglycans and the orientation of the fibrils [324]. On the other hand, several studies have shown that equatorial scattering is useful to determine the fibril diameter of collagen [335, 336].

2.7.2 Interpretation of SAXS data

The smallest structural details that produce measurable effect by SAXS are in a range of few nanometers therefore D-periodicity and fibril diameters can be determined accurately [324, 336]. Experimentally, SAXS creates a 2D image which has an equatorial streak and meridional diffraction rings (Figure 27A). The meridional rings are produced from the scattering of D-periodicity (Bragg peaks) while the equatorial streak is produced due to the scattering from the fibril diameters (Figure 27A).

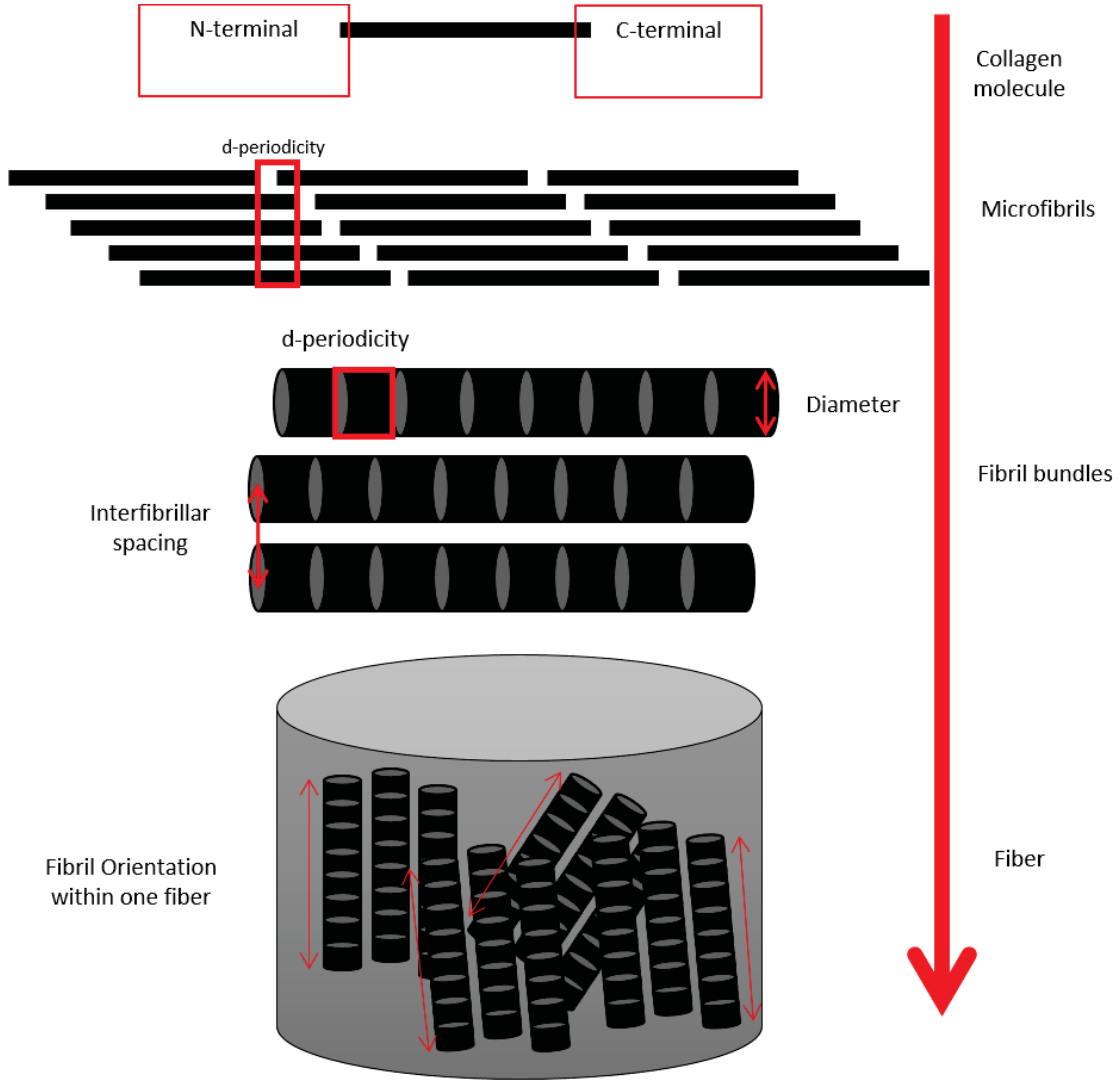

Figure 26: Schematic representation of the collagen hierarchy.

The first step in the analysis of SAXS data is to convert the one dimensional (1D) image with the Cartesian coordinates (x,y) (Figure 27A) into a 1D image with polar coordinates (r,θ) (Figure 27B). Data are then extracted from this image and used to generate three plots. Two are constructed by plotting the intensity against the magnitude of the scattering vector, q ($q = \frac{4\pi}{\lambda} \sin\theta$, where θ is half of the radial angle), in both the meridional and equatorial directions. Bragg peaks are shown in the meridional plot and used to determine the D-periodicity by taking the average of all diffraction peaks (Figure 27C). The equatorial plot is correlated to the fibril diameter and organisation (Figure 27D). The third plot shows the orientation of the collagen fibrils (Figure 27E) and is obtained by Integration of the intensity over an azimuthal range of 30 degrees in both on- and off-axis directions (where the on-axis corresponds to the highest intensity of the collagen diffraction).

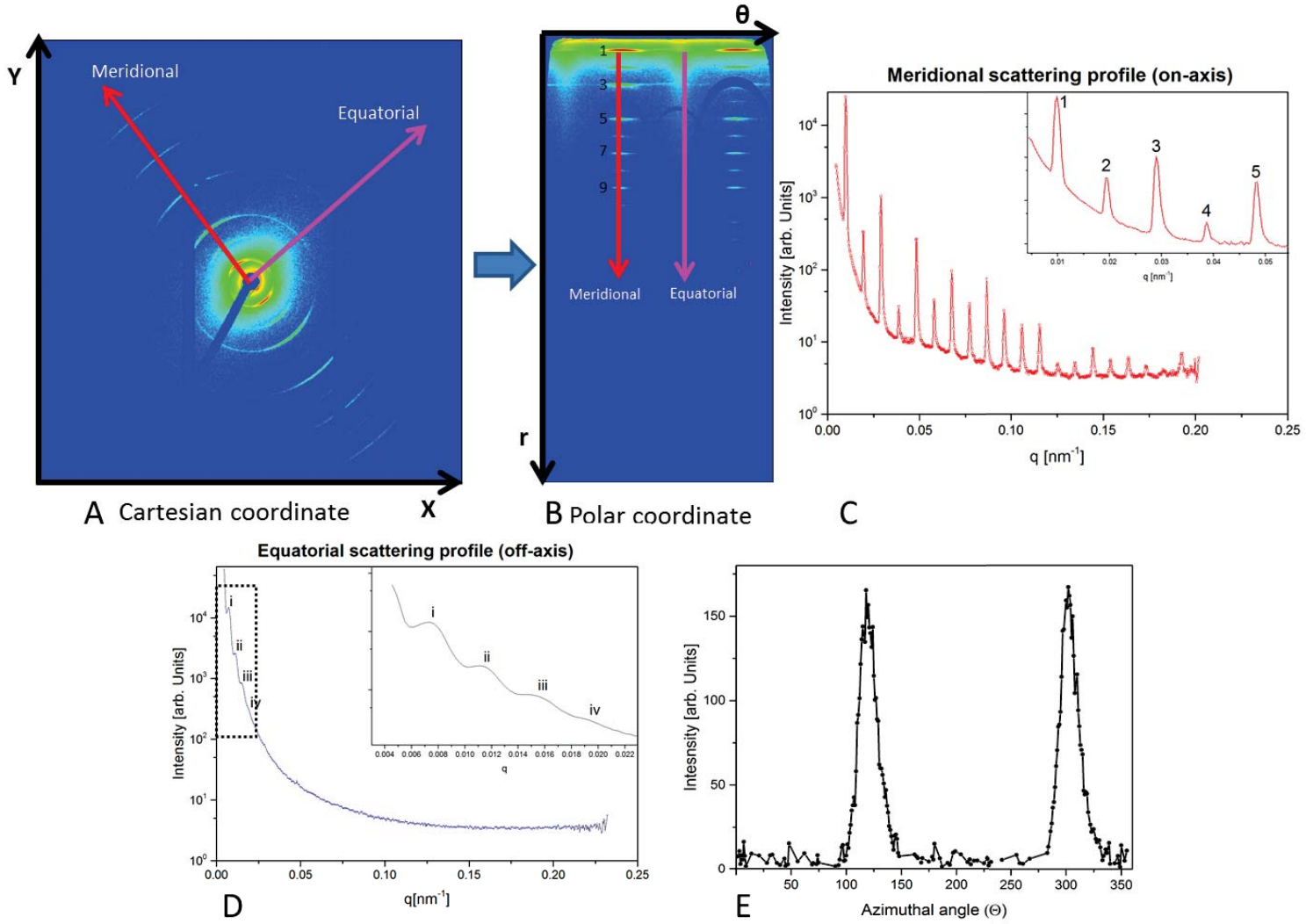

Figure 27: SAXS data and interpretation

2.7.3 SAXS calculations

Bragg's law (shown below) describes the relationship between incident and scattered X- radiation from a regular array of objects [337].

$$\mathbf{n\lambda = 2d\ sin\theta}$$

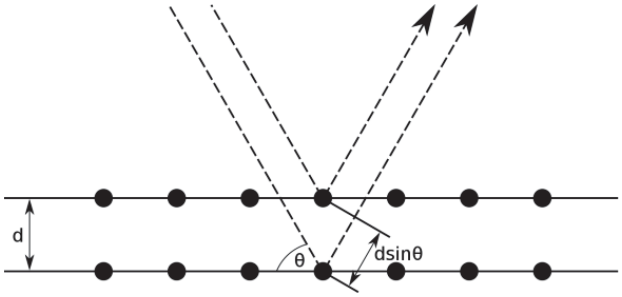

n = positive integer (releated to the diffraction ring number).

λ = the wavelength of the incident x − ray beam.

d = the periodicity of the order within the scattering structure.

θ = the angle between the incident and scattered x − ray beam.

For mathematical convenience, the scattering factor is calculated using the intensity (I) as a function of the amplitude of the scattering vector (q).

$$\boldsymbol{q = 4\pi sin\theta/\lambda}$$

Alternatively, this equation can be expressed using S.

$$\boldsymbol{S = \frac{q}{2\pi} = 2\ sin\theta/\lambda}$$

Both S and q can be related to the D-periodicity of collagen using Braggs' law.

$$\boldsymbol{d = \frac{\lambda}{2\ sin\theta} = \frac{2\pi}{q} = 1/S}$$

2.7.4 Orientation of collagen fibrils

Generally, X-ray scattering produces information about the spacing between ordered scattering objects and their orientation [20, 338]. For collagen fibrils, the scattering axis is defined as the meridian which relates to the gap and overlap spacing of collagen molecules (D-periodicity). The perpendicular scattering axis is, related to the diameter and packing of the collagen fibrils [336]. The angular spread is obtained from the distribution of diffraction peaks which appear as arcs with an angular spread that is related to the orientation of collagen fibrils (Figure 28).

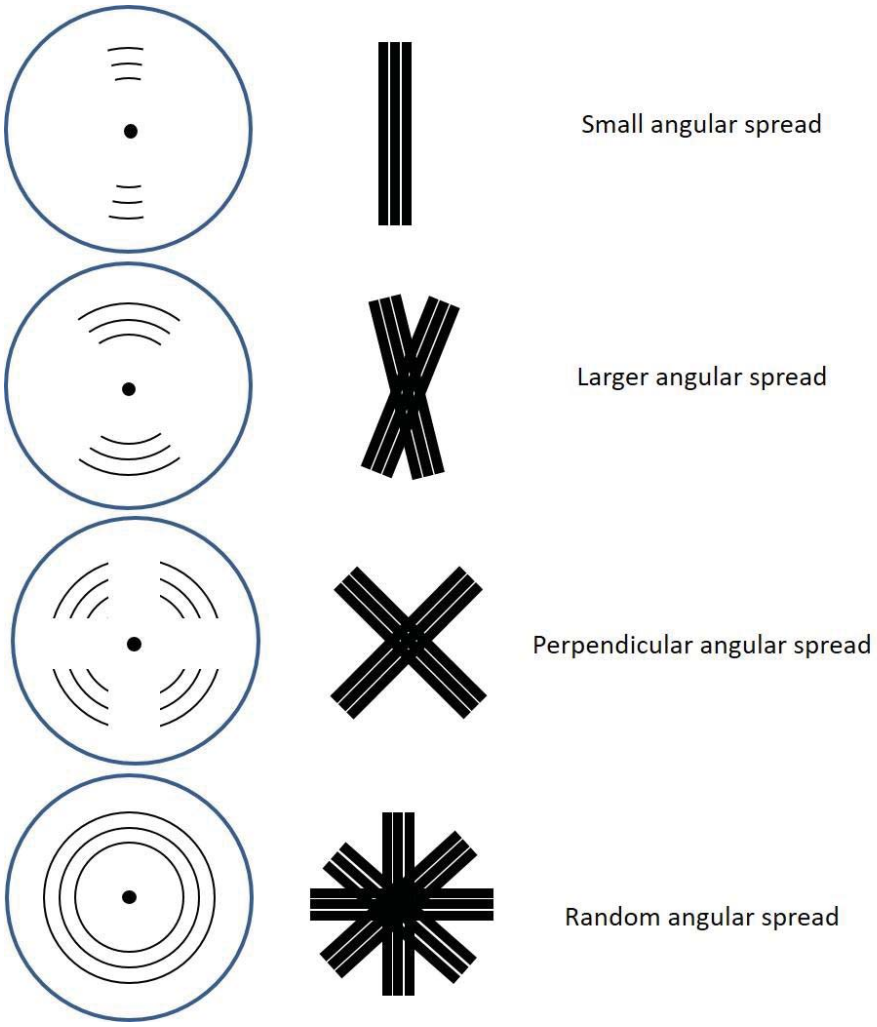

Figure 28: Angular spreading of the collagen fibrils and it relation with the diffraction peaks on the meridional axis.

3 CHAPTER THREE: Sample Collection, Preparation and Analysis

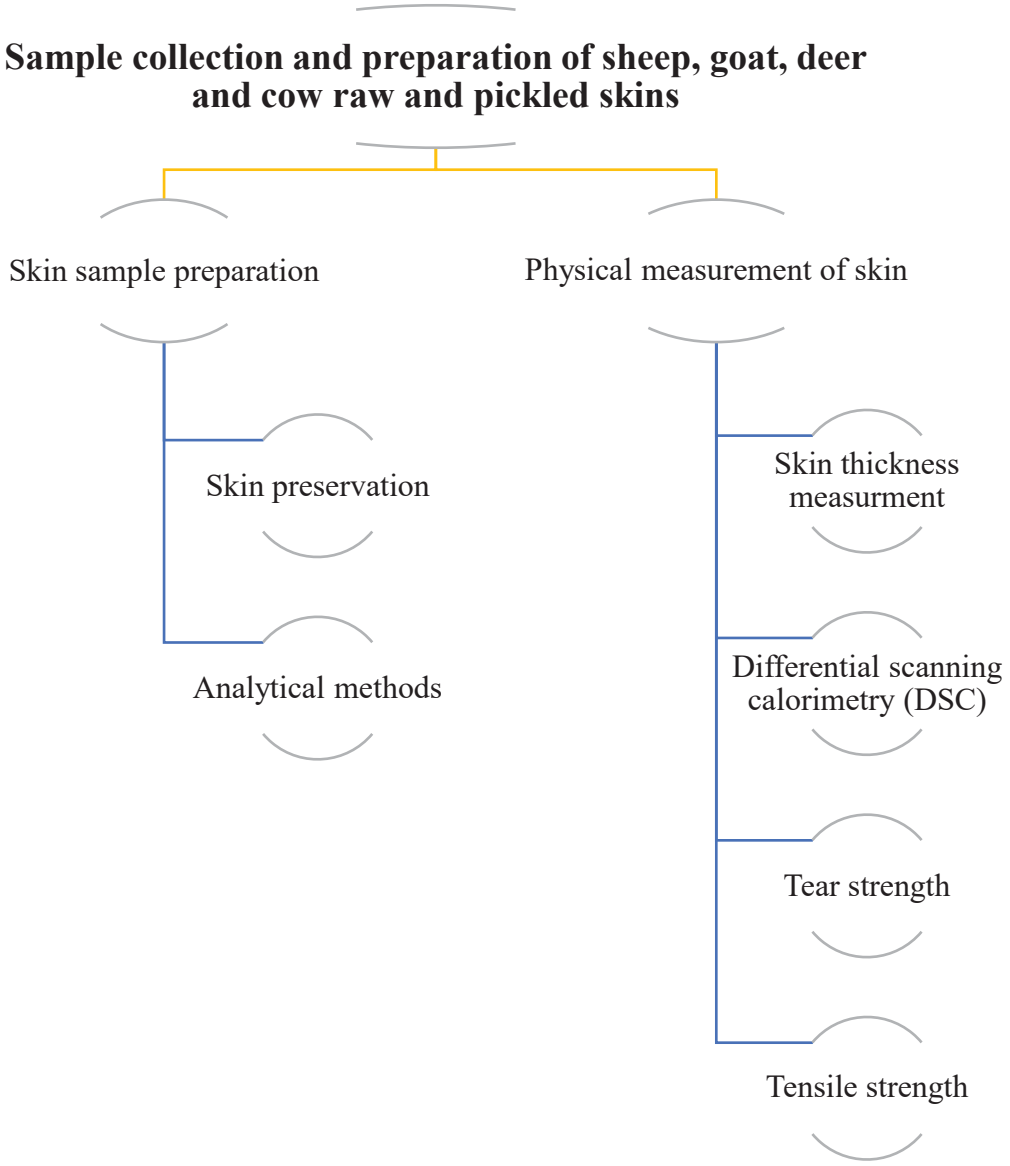

3.1 Introduction

To ensure high quality results, skin samples of sheep, goat, deer and cow have to be carefully collected, handled and stored. A common problem with analysing the molecular properties of raw skin is its rapid deterioration due to bacterial contamination [2]. This is rapid at room temperature but also continues at 4 °C, albeit more slowly. To the best of our knowledge, most of the previous published data on studying the strength of skins of sheep, goat, deer and cow utilising the SAXS techniques have used mainly salted skins as the severe dehydration caused by salt minimizes the bacterial damage [339, 340]. However, water is an integral part of collagen structure, so that skin dehydration must result in significant structure variations prior to SAXS measurements [33, 341].

As SAXS analysis required the transport from New Zealand to Melbourne in Australia, it was imperative that they were maintained in "fresh" state for a minimum of 3-4 days. A common method of preservation involves the application of crystalline salt, which dehydrates the skin, and results in the removal of proteins and glycosaminoglycans when the skin is rehydrated. A series of tests was, therefore, carried out to determine the most appropriate treatment of the raw shaved sheep and goat skins to maintain their integrity at 4 °C. Then, in order to assess the possible effects of these treatments on skin integrity, solutions used for treatment were analysed for leeched collagen, glycosaminoglycans, uronic acid, and carbohydrates as other work in our laboratory had shown these to be easily removed by soaking in various solutions.

Several physical measurements were also carried out on the collected skin including thickness measurements, tear strength, tensile strength and differential scanning calorimetry (DSC).

3.2 Experimental procedure

3.2.1 Chemicals and reagents

Sodium azide, benzamidine, ethylenediaminetetraacetic acid disodium salt (EDTA), phenylmethylsulfonyl fluoride (PMSF) and N-ethylmaleimide (NEM) were purchased from SIGMA. Bate enzyme was Tanzyme® purchased from (Tryptec, Biochemicals, New Zealand). The following commercial grade chemicals were used: sodium sulfide (LASRA®), hydrated lime (Websters, Hydrated Lime Co. Ltd., New Zealand), starch thickener (Solvitode, Avebe, Netherlands), ammonium sulfate (Clark Products, New Zealand).

3.2.2 Collection of sheep, goat, deer and cow skins

All animal skins analysed were those commonly used to produce leather and New Zealand farm-raised. Sheep skins were 11-12 months old Romney crosses taken from local farms in the Manawatu, processed at Ovation Ltd, Feilding. The skins were removed from the carcass and washed with cold water through a rotary screen to drop skin temperature to under 8 ºC. Skins were selected directly from the screen and transported to LASRA® where they were sampled and preserved within two hours of collection. The red deer skins (Cervus elaphus) were 21 months old from locally sourced hinds, processed by Venison Packers Feilding Ltd. These were collected fresh from the slaughter board and transported to LASRA® for fleshing, sampling and

temporary preservation. Feral goat skins were 12-18 months old and were sourced from the Waikato region, processed at Te Kuiti Meat Processors Limited and shipped overnight to Tasman Tanning, Whanganui where they were held in chilled storage. The next day, skins were transported to LASRA® for fleshing, sampling and temporary preservation. Cow hides were 5 years old and were locally sourced, slaughtered at AFFCO Land Meats, Whanganui and then transported within the hour to Tasman Tanning where they were green fleshed and sent to LASRA® for sampling and temporary preservation. Five sheep skins, five goat skins, four deer skins and four cow hides were provided by LASRA® for each SAXS visit. All skin samples were cut from the official sampling position (OSP) of the skins (Figure 29). Three technical replicates were taken from each cut which were made of parallel and perpendicular to the animal backbone.

3.2.3 Skin sample preparation

To find the optimal conditions for prevention of bacterial contamination, known weights of fresh skins (3 x 6 cm pieces or ~5 g) were treated with 25 mL of the following antimicrobial agents for 5 and 15 minutes, 2, 6 and 24 hours.

(a) 0.5 % sodium azide, 1 mM benzamidine, 5 mM EDTA, 1 mM PMSF, 1 mM NEM,

(b) cOmplete™ at the recommended concentration (Roche Applied Science, 68298 Mannheim, Germany) with 0.5 % sodium azide,

(c) 0.5 % sodium azide and

(d) deionized water (control).

Skins were then blotted with tissue to remove excess liquid and stored in plastic bags at 4 ^{o}C for one week. During this time, they were tested for bacterial growth every day for one week using Hygiene Check Slides (Fort Richard Laboratories Auckland, New Zealand).

3.2.4 Analysis methods

Skin samples were tested for leach of collagen, glycosaminoglycans, uronic acid, and carbohydrates. Uronic acid and carbohydrates were tested using the previously published procedures [342-344]. The carbazole assay was used for uronic acid analysis and the phenol-sulfuric acid assay was used for carbohydrate analysis [343, 344]. For collagen analysis, sircol red (Sircol™ Collagen Assay, Biocolor Ltd., Northern Ireland) was used, while 1,9-dimethylmethylene blue assay (Blyscan™ Glycosaminoglycan Assay, Biocolor Ltd., Northern Ireland) was used for glycosaminoglycan assay following the manufacturing protocols.

3.2.5 Leather processing steps

Leather was produced from skin using conventional methods. The flesh (inner) side of sheep, goat and deer skins was painted with a mixture of sodium sulfide (140 g/L), lime (50 g/L) and starch thickener (25 g/L), pH of 13.5. This dissolved the hair roots within two hours allowing the hair or wool to be pulled off the skin by hand. Cow hide was placed in a drum, containing sodium sulfide and lime (pH ~ 13.5), for 2 hours until all the hair was removed. The dehaired skins were then placed in a drum and washed with several changes of water to remove the sodium sulfide, then pH was adjusted to 8.0 with 2% (W/V) ammonium sulfate. Skins were further processed by adding a mixture

of bate enzymes to remove unwanted materials, before they were stored in 2% sulfuric acid and 10% sodium chloride solution (pH 1-2) at which stage they became pickled pelts. The pickled pelts were pre-tanned with oxazalodine then tanned with chromium sulfate to produce “wet blue”. Finally, the resultant “wet blue” was treated with vegetable oil prior to drying and dyeing.

3.2.6 Differential scanning calorimetry (DSC)

For DSC measurements, skin samples (5-7 mg) were encapsulated in hermetically sealed aluminum pans (10 μL). They were then placed in the cell of a DSC Q2000 differential scanning calorimeter (TA Instruments, Newcastle, Delaware, USA). The temperature was calibrated using indium as a standard and a heating rate of 5 ^{o}C/min. All measurements were carried out over a temperature range of 20 to 120 ^{o}C. The average values of the shrinkage temperature of three skin samples were reported.

3.2.7 Skin thickness measurements

The thickness of the skin samples was first measured using an instrument developed by Wodzicka (1958), which has an accuracy of 0.01 mm [345]. The thickness of grain and corium layers was measured under the light microscope. Three fully hydrated samples of each skin were mounted on a glass slide, then checked for the thickness of the grain and the corium layers under the light microscope.

3.2.8 Tear strength

Tear strength was carried out using a Texture Analyzer (stable Micro Systems, model TA.XT Plus, Surrey, UK) according to the international standard ISO 3377-2:2002 [346]. Skin samples from sheep, goat, deer and cow skins were cut into

rectangular shaped pieces (50 mm × 30 mm) with a direction parallel and perpendicular to the animal backbone (see Appendix-chapter-3). Before carrying out the tear test, samples were stored at a constant temperature of 23ºC and a relative humidity of 48%. A slit was cut in the center of the rectangular sample and the thickness of the leather at either end of this slit was measured to provide an average thickness for the test sample. The slit was placed over the two hooks of the instrument and the skin stretched at a constant rate with the long axis of the slit at right angles to the direction of pull until rupture and the force (N) required to tear the skin recorded. The tear strength was calculated as tear force divided by the thickness of the tested sample (N/mm). The final tear strength was the average of the calculated tear strength of five replicates.

3.2.9 Tensile strength

Samples were cut into a "dogbone" shape of 100 mm × 20 mm dimensions (Figure 34A). Tensile strength tests were carried out at room temperature on the Texture Analyser (stable Micro Systems, model TA.XT Plus, Surrey, UK) controlled by exponent software. Uniaxial tensile tests were conducted using a load cell of 7500 N. Five samples of each skin were analysed with the sample ends being securely clamped into specifically designed grips. Samples were then stretched at strain rates of 0.2 mm/sec and 1.0 mm/sec. The sample effective height (h) was 50.0 mm and length (l) 10.0 mm. Force (N) was plotted against distance (mm) for each skin until rupture. Stress (N/mm^2) was calculated from force (N) divided by the sample cross-sectional area (mm^2), calculated from thickness (mm) × width (mm). Strain (mm/mm) was obtained from distance (mm) divided by sample length (mm). The tensile strength curve was generated by plotting the strain against stress.

3.3 Results and discussion

3.3.1 Collection of skin samples

Skin is divided into three areas including neck, belly and OSP (Figure 29) [2]. Because of skin is anisotropic, its structure and properties vary significantly within these areas [2, 26, 347]. For the best comparison of the properties of different animals, the OSP area was used. Also, since the structure of animal skins is influenced by breed, age, diet and environmental conditions, several biological replicates of each animal were collected to account for these natural variations [2].

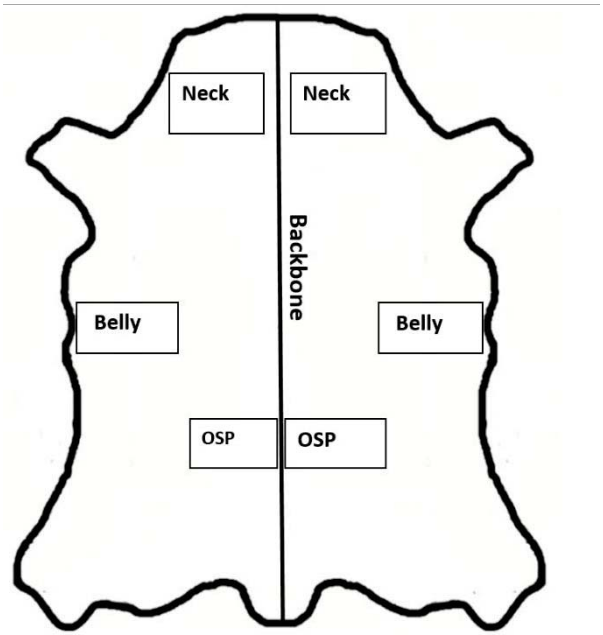

Figure 29: Skin diagram shows the standard collection areas particularly the official sampling position (OSP).

As the physical properties of skin, such as tear strength and tensile strength, are affected by the anisotropic properties of the skin, samples were collected in both parallel and perpendicular directions to the animal backbone [2]. Generally, samples perpendicular to the backbone have been shown to have a higher strength that those in the parallel direction [2, 348]. All samples were handled with care to minimize any deformation of the skin prior to the mechanical testing.

3.3.2 Skin sample preparation

As soon as the animal is slaughtered, the skin putrefaction begins. It is known that fresh skins are very susceptible to bacterial damage due to the production of proteolytic enzymes which break down the skin proteins including collagen [2, 349-351]. Collagen degradation causes structural changes in skin which may result in significant structural variations and changes in its mechanical properties. A common method of preservation involves the application of crystalline salt. However, this dehydrates the skin and removes proteins and the glycosaminoglycans resulting in modifications of skin structure [2]. Therefore, another way had to be found to prevent bacterial growth on the skins. It was shown that untreated skin had a significant bacterial growth while skin treated with different protease inhibitors, the inhibitor mixture of sodium azide, benzamidine, EDTA, PMSF and NEM, showed no sign of bacterial growth (Figure 30). This protease inhibitor mixture was used to treat all subsequent skin samples to minimise any bacterial damage that might occur to the skin during storage. Similar results were obtained with cOmplete™ and sodium azide, however neither were used. Next, the effect of these protease inhibitor treatments on the structure of the skins was investigated. After soaking, the solutions were analysed for the leeched collagen, glycosaminoglycans, uronic acid and carbohydrates. Preliminary results showed that sheep skin lost the largest amount of collagen and glycosaminoglycans, therefore sheep skin was used to optimise the procedure.

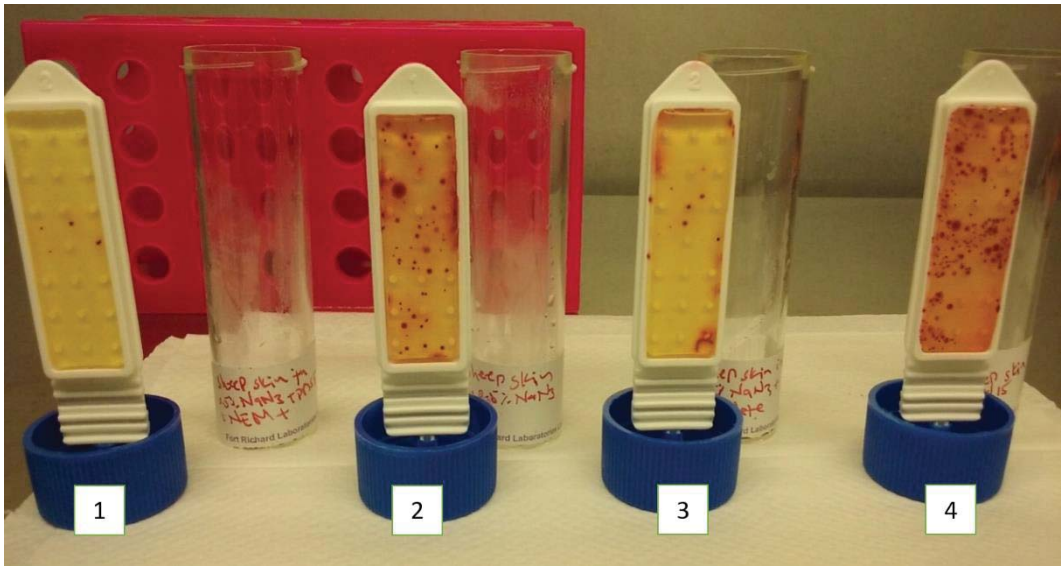

Figure 30: Check slides after exposed to the fresh sheep skin, stored at 4 ºC for one week, then incubated for 24 hours at 37 ºC. (1) Fresh sheep skin incubated in 1 % NaN_3, 1 mM PMSF, 1 mM NEM, 1 mM benzamidine and 5 mM EDTA, (2) with 0.5% NaN_3, (3) with 0.5% NaN_3 and cOmplete™ (a protease inhibitor cocktail), (4) in water. It is clear that the first and the third slides have the minimum bacterial growth suggesting that PMSF, NEM, EDTA and cOmplete™ have significantly minimized the bacterial growth in the fresh sheep skin.

The release of glycosaminoglycans and collagen from sheep skin was measured after soaking in buffer containing the protease inhibitor mixture for 1 and 24 hours at room temperature. It was found that after soaking for 24 hours, 0.24 % of glycosaminoglycans and 10% of collagen were removed from skins. However, the testing different soaking times showed that 1 hour exposure to the protease inhibitor cocktail achieved the optimum anti-microbial effect with a minimal loss of glycosaminoglycans and collagen (Figure 31).

3.3.3 Skin thickness

The total skin thickness was measured in mm using an instrument developed by Wodzicka (1958), which has an accuracy of ± 0.01 mm. The thickness of each of grain and corium layers was then measured using a light microscope [345]. The total

thickness of the skin and the thickness of grain and corium layers was used to calculate the percentage of corium in sheep, goat, deer and cow skins (Table 7). There are significant differences in the thicknesses of sheep, goat, deer and cow skins, with deer skin being the thinnest and cow skin being the thickest.

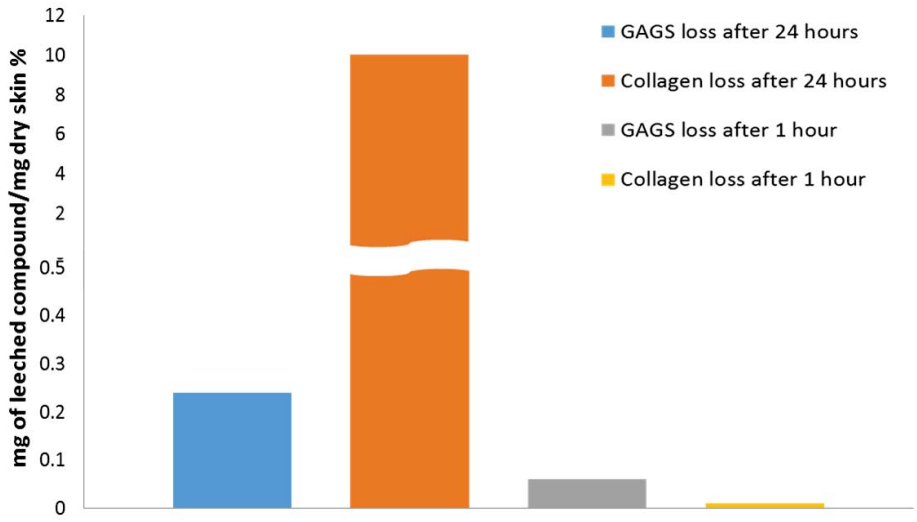

Figure 31: Loss of glycosaminoglycans and collagen from sheep skin after soaking in buffer containing a protease inhibitor mixture for 1 hour and 24 hours.

The corium layer is the main part of the skin and is responsible for its integrity and strength [352]. The grain layer, however, is responsible for the appearance of the skin [2]. It has been observed that in all animal skins so far examined, the corium contains thicker, more organised collagen fibres in contrast to the grain which is made up of smaller and randomly organized fibres [334, 348]. Deer skin has the highest percentage of corium followed by cow, then goat and sheep skins. On the other hand, sheep skin has the thickest grain layer making up of about 55% of the total skin thickness.

Table 7: Total skin thickness and the thickness of the corium and grain layers of sheep, goat, deer and cow skins. The percentage of corium layer is based on the total skin thickness.

Sample	Total (mm)	Grain (mm)	Corium (mm)	Corium %
Sheep	2.35 (±13.03 %)	1.29	1.06	45.1
Goat	1.80 (±13.72 %)	0.59	1.21	67.2
Deer	1.62 (±11.58 %)	0.19	1.43	88.3
Cow	5.60 (±8.37 %)	1.06	4.54	81.1

3.3.4 Differential scanning calorimetry (DSC)

DSC is used to measure the shrinkage temperature of skin, which is related to the denaturation temperature (Ts) of collagen [353]. The denaturation of collagen is accompanied by the absorption of heat producing an endothermic peak. The shrinkage temperature is determined either as the onset of the peak or the peak maximum [354] (Figure 32) and appears to be directly related to the hydroxyproline content of the collagen fibres [168, 355, 356]. Several studies have also suggested that it is affected by intermolecular forces [144, 353, 355, 357, 358].

The shrinkage temperatures of sheep, goat, deer and cow skins are shown in Table 8. Not surprisingly, sheep and goat skins have lower shrinkage temperatures compared to deer and cow skins. These findings are at odds with the accepted correlation between skin shrinkage temperature and its hydroxyproline content (see Chapter4). In this study, other factors must therefore be contributing to the thermal stabilization of collagen in skin, such as collagen crosslinks and collagen fibril and fibre organisation [355, 357]. Table 8 also shows the shrinkage temperature for pickled skins. It is clear that the

pickled cow skin has a much higher shrinkage temperature than all the other skins tested, although there are no significant differences in the amino acid composition of these skins.

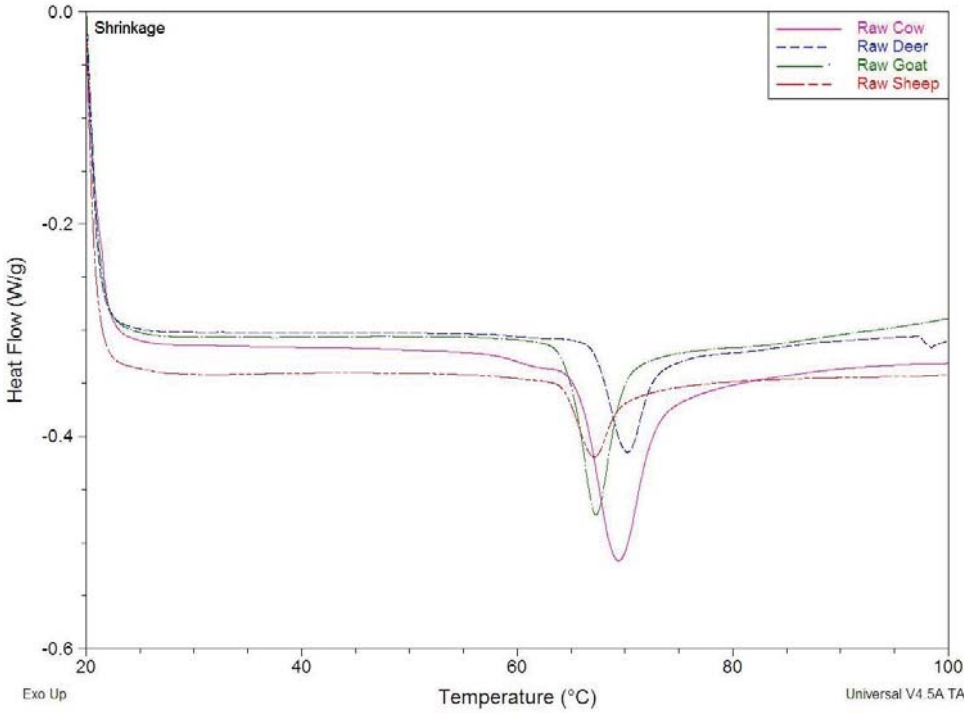

Figure 32: Differential scanning calorimetry (DSC) thermograms of sheep, goat, deer and cow skins.

Strikingly, the biggest decease in the shrinkage temperature between the raw and the pickled state was seen for the deer skin (66.81 ºC for raw skin, 51.31 ºC for pickled skin). Sheep and goat skins had also reductions in their shrinkage temperature of 12.32 ºC and 11.86 ºC, respectively.

Table 8: Shrinkage temperature (Ts) of sheep, goat, deer and cow raw and pickled skins. Data represent the mean values of three technical replicates.

Skin	Ts of raw skin (°C)	CV* %	Ts of pickled skin (°C)	CV* %
Sheep	64.15	0.24	51.83	1.86
Goat	64.90	0.76	53.04	1.86
Deer	66.81	0.38	51.31	1.70
Cow	66.53	0.14	57.80	2.86

* CV = Coefficient of variation.

The shrinkage temperatures of sheep skins measured at specific steps during leather processing are shown in Table 9. There is a significant decrease in shrinkage temperature after liming/dewooling because at high pH, the skin swells, resulting in opening up of the fibres and a reduction in the water-retention of collagen. After deliming, the shrinkage temperature steadily increases as the matrix becomes more rigid due to the removal of water and the introduction of crosslinks during tanning [35, 360].

Table 9: Shrinkage temperatures of sheep skin during selected leather processing steps. Data represent the mean values of three technical replicates.

Skin	Ts of skin (°C)	CV %
Raw Sheep	64.15	1.24
Liming/dewooling	57.84	3.19
Deliming/Bating	62.98	1.98
Pickling	51.83	1.86
Oxazolodine	74.09	1.51
Chrome Tanning	110.31	1.62
Oil Veg	119.60	1.33
Fat Liquor	120.08	1.40

3.3.5 Tear Strength of sheep, goat, deer and cow skins

The tear strength sheep, goat, deer and cow skins was measured parallel to the backbone then normalized to the total thickness of skins. Figure 33 shows clearly that cow skin had the highest normalized tear strength followed by deer, goat and sheep skins (228.9, 130.1, 59.4 and 38.7 N/mm, respectively).

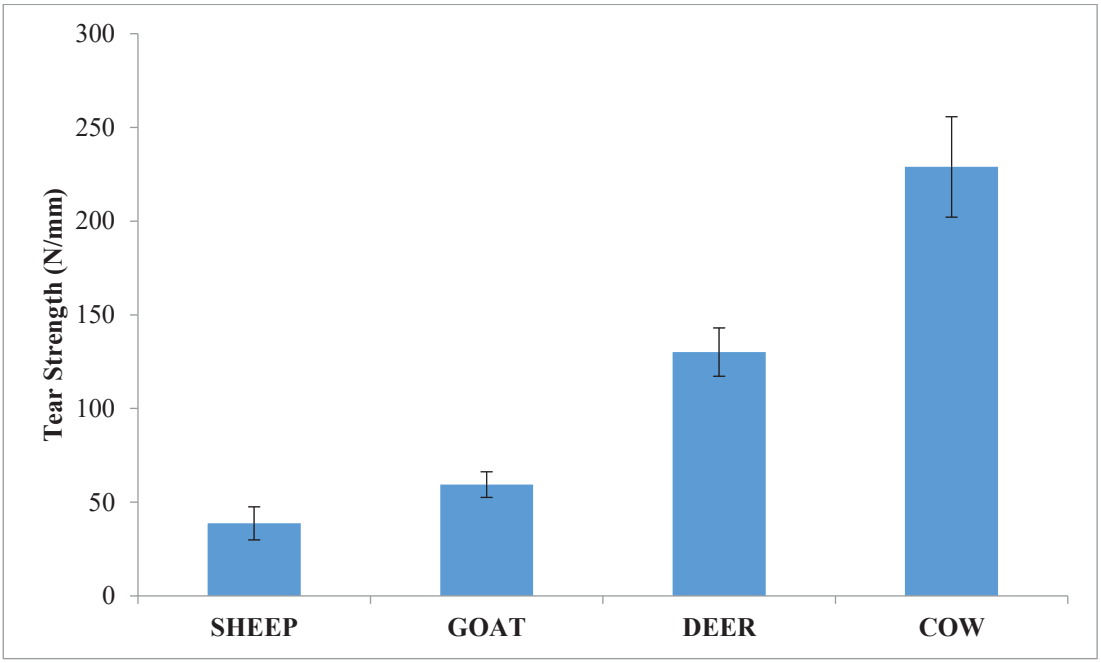

Figure 33: Tear strengths of sheep, goat, deer and cow skins. Average of five individual measurements. Error bars represent the standard deviations.

3.3.6 Tensile strength of sheep, goat, deer and cow skins

The mechanical behaviour of biological tissues is effectively described by the stress-strain curve and has been previously reported for different tissues, such as tendon [361, 362], cartilage [363, 364] and skin [365-367]. To the best of our knowledge, a comparison of the stress-strain curves of the sheep, goat, deer and cow skins has not been previously reported and discussed in terms of their macro and microscopic properties and stress-strain curves. Ultimately, the understanding of the mechanical

behaviours of weak and strong skins will identify the differences in their underlying properties. This may lead to a significant optimisation in skin processing steps, which could result in an improvement in the strength of the final leather product. Generally, a stress-strain curve of skin is produced from the uniaxial tensile strength experiment where a "dogbone" shaped piece of skin is stretched in one direction and the force applied is measured until the skin sample ruptures (Figure 34).

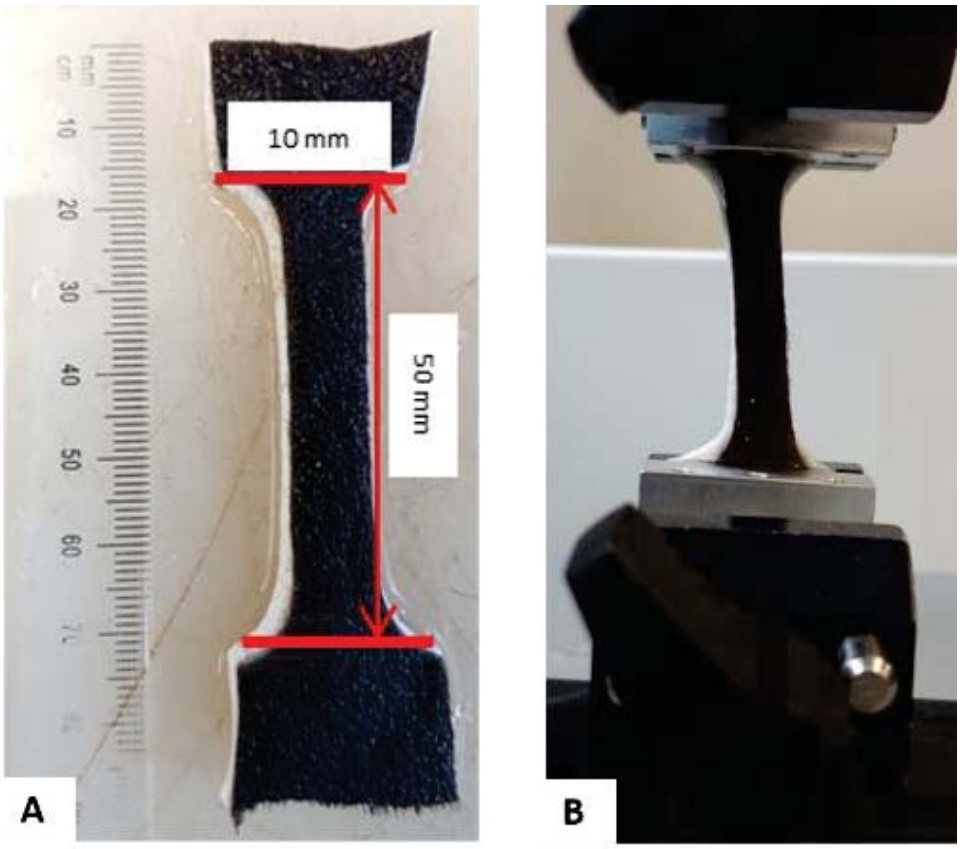

Figure 34: (A) "dog-bone" shaped skin sample. (B) Skin sample clamped in the tensile strength instrument.

The force applied (N) is then divided by the skin cross-sectional area in mm^2 (thickness in mm × width in mm) to calculate stress (N/mm^2) and the distance (mm) is divided by the sample length to get strain (mm/mm). A stress-strain curve is then generated by plotting the stress against strain [365, 368]. A typical stress-strain curve of skin shows three regions (Figure 35), which include toe, heel and linear regions [365, 368, 369]. The toe or elastic region is seen at low strain where the macroscopic crimps in the fibres are removed by rotation to the direction of the applied force, which is a reversible process [370]. At high strain, the fibrils become aligned in the direction of the force and the fibres slide relative to one another to accommodate the strain until rupture [6, 365] resulting in a significant increase in the gap region [370]. In the heel region, non-linearity prevails with a transition in phase from floppy to rigid that is accompanied by a significant increase in skin stiffness [371-373]. Although the toe and linear regions are well understood, the nonlinear region is still poorly explored [371, 373]. Misof *et al.* (1997) have, suggested that several factors are contributing to the heel region including reorientation, straightening and stretching of the fibres [374].

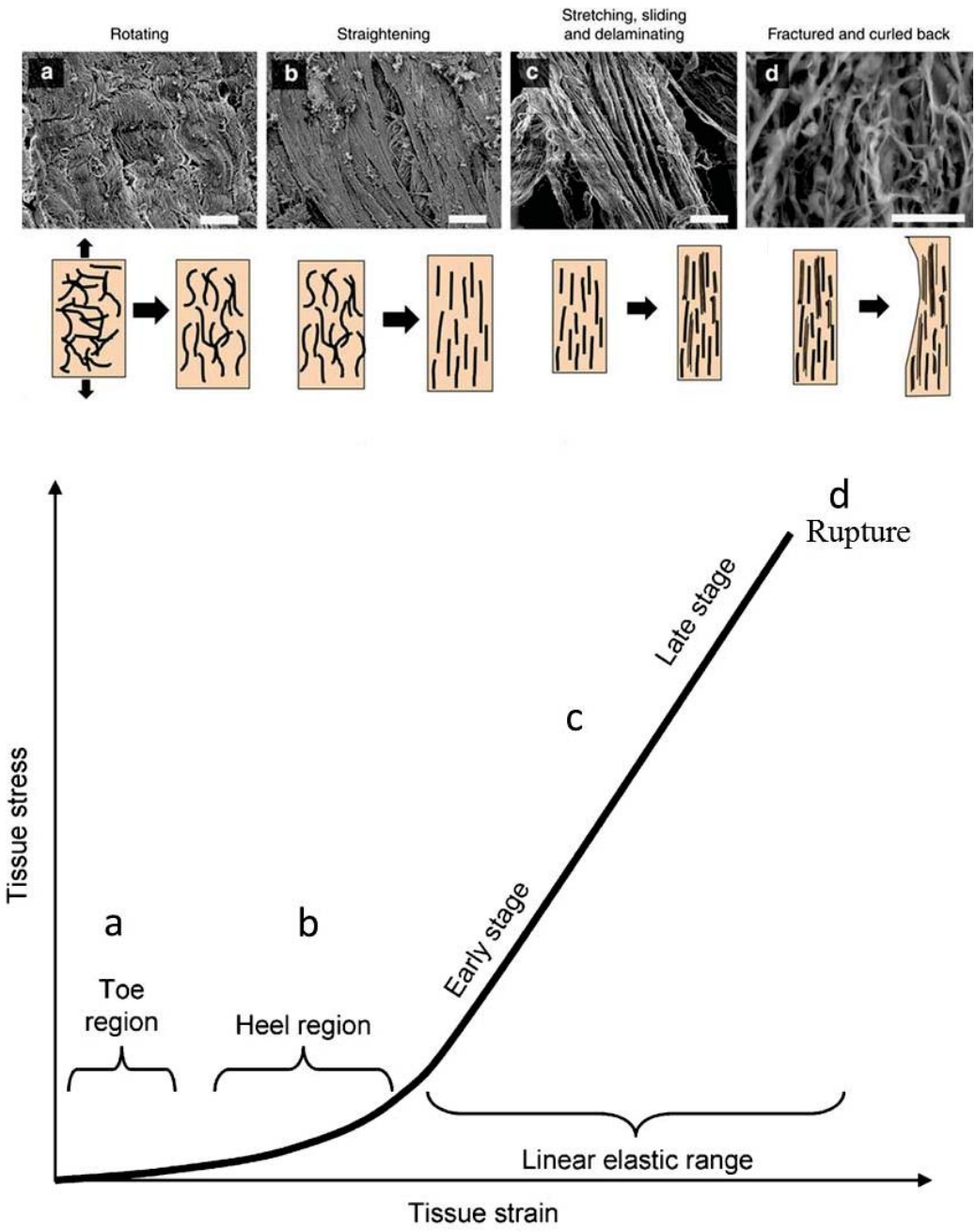

Figure 35: Typical stress-strain curve of skin showing the three major regions and the corresponding changes at the fibrillar level with applied tensile stress. First, (A) at very low stress, the curve shows a linear region with a very small slope due to the removal of the collagen fibre crimps by rotation. This is followed by (B) the heel region, where the kinks in the collagen molecules are straightened out. Finally, (C) at larger strains the straight collagen molecules are stretched and glide resulting in the stress–strain relationship becoming linear [6, 365]. Eventually, (d) the skin ruptures and curls back.

To compare the mechanical properties of the sheep, goat, deer and cow skins, the tensile strength was measured by stretching the skin samples over a constant distance (mm) and the applied force (N) was recorded. All the samples measured were cut parallel to the animals' backbone.

All skins showed typical stress-strain curves with the toe, heel and linear regions (Figure 36) in an excellent agreement with previously published results [365-367, 375, 376]. The curves at low strain (toe), medium strain (heel) and high strain (linear) were compared and their slopes analysed.

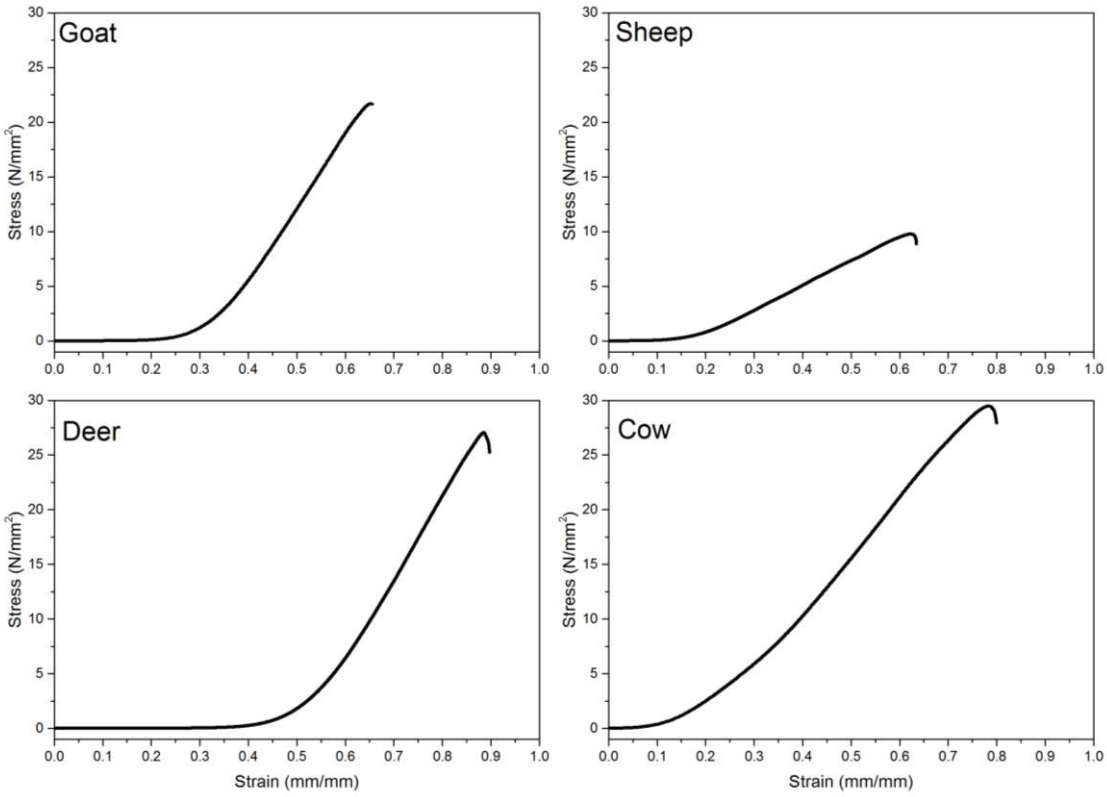

Figure 36: Stress-strain curves of sheep, goat, deer and cow skins.

Table 10 shows the force, stress and strain at rupture for sheep, goat, deer and cow skins. Forces at rupture were 1343.2 N for cow skin, 452.8 N for deer skin, 240.8 N for goat skin and 124.1 N for sheep skin. It is known that thickness contributes to the tensile strength, therefore force at rupture was divided by the cross-sectional area (sample thickness × width) to determine stress (N/mm^2) of each skin [4, 377]. This modified the results, so that cow skin withstood 29.2 N/mm^2 maximum stress and was close to the maximum stress of 28.3 N/mm^2 for deer skin. Goat skin could withstand 17.2 N/mm^2 stress while sheep skin was the weakest, withstanding a maximum stress of only 7.3 N/mm^2. When the strain at rupture was measured, deer was found to have the highest at 0.83 mm/mm strain while sheep again had the lowest maximum strain of 0.62 mm/mm. Goat and cow skins showed similar values of strain at rupture of 0.71 mm/mm and 0.72 mm/mm, respectively.

Inspection of the stress-strain curves shows that deer skin had the longest toe region with the shallowest slope of 0.051 and 0.4 strain mm/mm (Figure 36). This strongly suggests that deer has the largest and highest number of fibre crimps and the smallest fibril diameter which is in an excellent agreement with Diamant *et al.* (1971) who reported that the toe region gets shorter and steeper by ageing due to increasing the fibril diameter and decreasing fibre crimps [370]. Looking at the SAXS date (see chapter 8), fibril diameter of deer was the smallest among all animal skins which supported by the longer toe region. On the other hand, the stress-strain curve of cow skin, shows that it has the shortest and steepest toe region, suggesting that it contains fewer crimps in the collagen fibres and fibrils. The microscopic appearance of the

collagen fibres of cow and deer skins (see chapter 9) was consistent with the above findings

Table 10: Tensile strength results for sheep, goat, deer and cow skins (parallel to the backbone).

Skin	Thickness (mm)	Force at rupture (N) (CV %)	Stress at rupture (N/mm^2)	Strain at rupture (mm) (CV %)
Sheep	1.7	124.1 (18%)	7.3	0.62 (11%)
Goat	1.4	240.8 (12%)	17.2	0.71 (14%)
Deer	1.6	452.8 (14%)	28.3	0.83 (3.3%)
Cow	4.6	1343.2 (12%)	29.2	0.72 (16%)

Table 11 shows the slopes at high strains of sheep, goat, deer and cow skins. Deer had a 78.1 N/mm^2 slope and goat had 68.4 N/mm^2 slope, and both were higher than those of sheep and cow skins with 22.7 N/mm^2 and 55.8 N/mm^2 slopes, respectively. It has been reported that a steeper slope is associated with a stiffer skin, suggesting that deer and goat skins are stiffer than sheep and cow skins at high strain [370]. These variations can be explained in term of shear strain which is measured by the Poissons' ratio. Shear strain is the deformation of the sample dimensions under applied force and Poissons' ratio is the measurable ratio of transverse to axial strain during uniaxial tensile strength [378]. During the uniaxial tensile strength test, it was observed that deer and goat skins tend to show a lower transverse strain (thinner) than sheep and cow skins. Because goat and deer skins are stiffer, they have a higher shear strain but a smaller Poissons' ratio which is seen as a greater slope at high strain [372, 379, 380].

To visualise the linear and nonlinear ranges in the stress-strain curves accurately, first derivative curves of the stress-strain curves of sheep, goat, deer and cow skins were calculated (Figure 37). Generally, a linear curve has a constant slope so its first

derivative has zero slope while the slope of the non-linear curve changes in a way that gives the first derivative a constant slope [381].

Table 11: Slopes at low and high strains of the tensile strength curves for sheep, goat, deer and cow skins.

Sample	Slope at low strain	Strain at the maximum change in slope	Slope up to max change in slope	Slope at high strain
Sheep	0.52	0.18	2.5	22.7
Goat	0.40	0.32	3.5	68.4
Deer	0.17	0.52	2.5	78.1
Cow	1.20	0.12	4.7	55.8

It is clear in Figure 37 that all skins have two linear regions (toe and linear) and one non-linear region (heel). However significant differences were observed in their ranges. Cow skin had the shortest toe region while deer skin had the longest. Sheep skin had the longest linear region at the high strain while cow skin had the shortest. Interestingly, cow skin had the longest non-linear range which was extended for about 0.45 strain while sheep, goat and deer skins had a shorter non-linear range of around 0.2 strain only.

Fratzl *et al.* (1997) have correlated the transition from the toe to the linear region (heel region) of these profiles to the removal of kinks in the collagen molecule. Others have suggested several additional factors affect these measurements, including the fibre network geometry, the fibril diameter, collagen density, crosslink density and crosslink strength [371-373, 376, 380]. The long non-linear range in cow skin is evidence that its fibres are large and long suggesting there is a high concentration of crosslinks present. On the other hand, the long linear range seen in the sheep skin is most likely

due to smaller fibre diameters, and consequently, a lower concentration of crosslinks which will allow the fibrils to slide over one another leading to early rupture [382, 383].

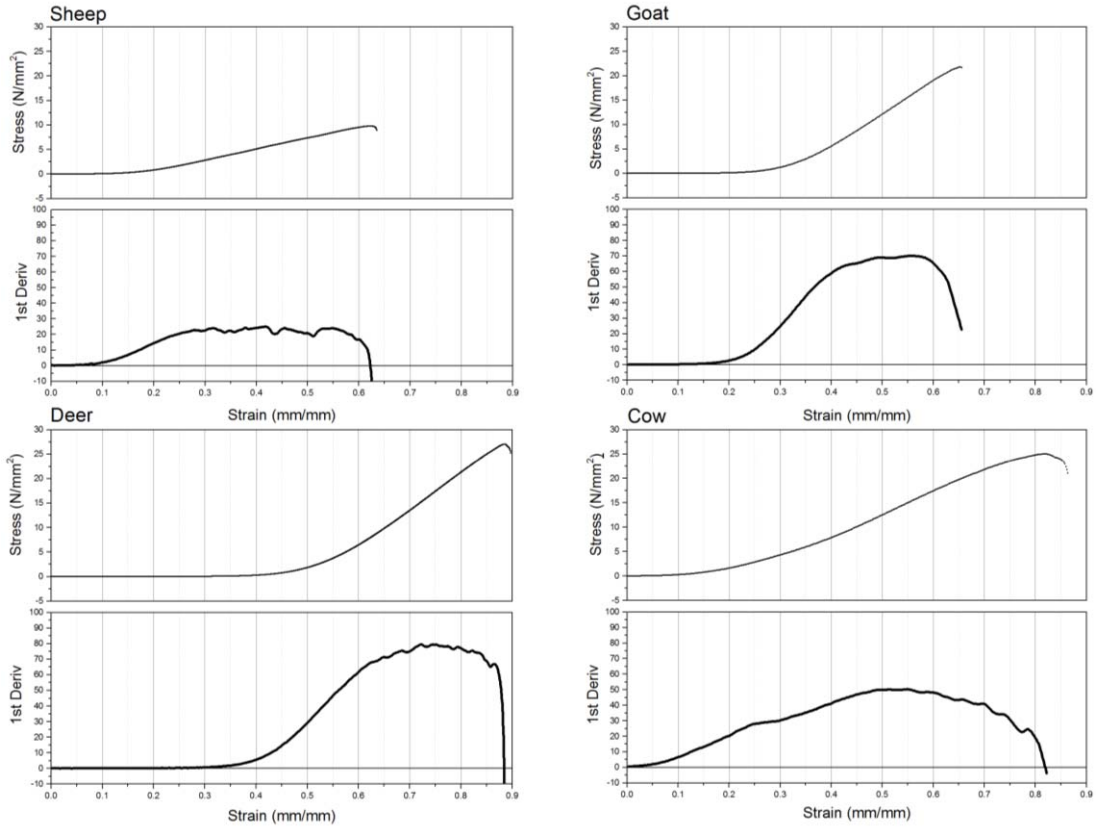

Figure 37: The stress-strain curves of sheep, goat, deer and cow skins along with their first derivative curves.

4 CHAPTER FOUR: Method Development and Quantitation of Amino Acids

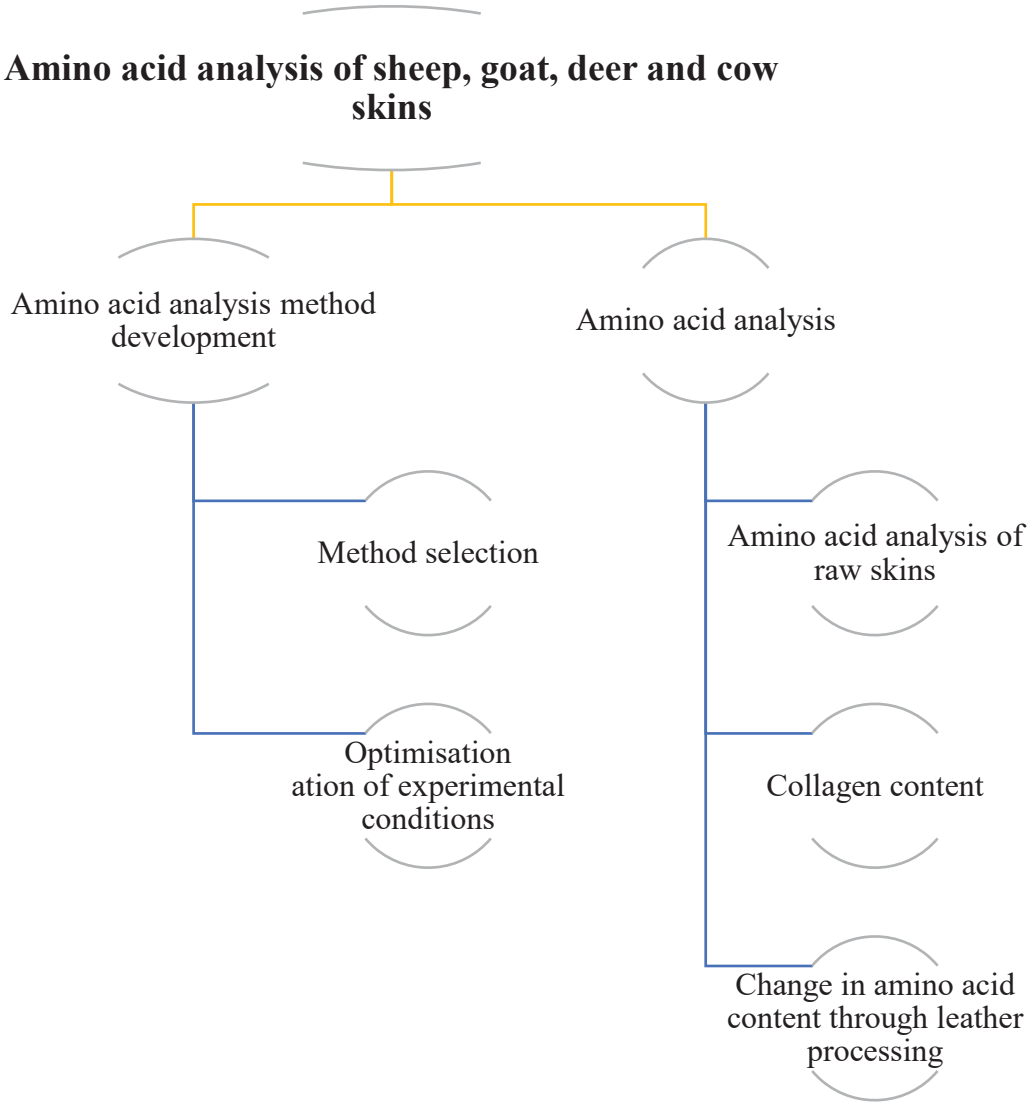

4.1 Introduction

Increasing demand for information about the quality of leather produced from different animal skins has led to the need to understand the molecular differences between the skins. The first step towards understanding the differences at a macro-level of the skin is to determine the molecular content of skin then investigate how the different molecules interact with each other. The major building block of the structural proteins in skin is collagen, which contains all the regular amino acids, except for tryptophan, plus the two unusual amino acids which are unique to collagen, hydroxyproline and hydroxylysine [32]. Hydroxyproline is responsible for the hydrothermal stability of collagen through its ability to form hydrogen bonds with water molecules [46]. Hydroxylysine is directly involved in the formation of covalent crosslinks between collagen fibrils which are responsible for the stability of microfibrils and fibrils [6]. The number and positions of these crosslinks are therefore related to the differences in the biochemical properties of skin collagen and elastin, and the concentrations of lysine and hydroxylysine are directly related to these [12, 79]. Furthermore, the amino acid composition of the skin at different stages of processing can give a snapshot of the effect of the different chemical treatments on the proteins.

6-aminoquinolyl-N-hydroxysuccinimidyl carbamate (AQC) was chosen due to its rapid reaction with both primary and secondary amino acids to produce a stable fluorescent derivative [384]. The rapid (within seconds) derivatization reaction was carried out in a borate buffer (pH = 9.0) (Figure 38). It was allowed, however, to proceed for 10 minutes at 55 ^{o}C to guarantee complete conversion and production of stable derivatives [384]. Complete conversion was evaluated by the presence of a 6-

aminoquinoline (AMQ) peak in the chromatogram, as it is eluted before any of the amino acids.

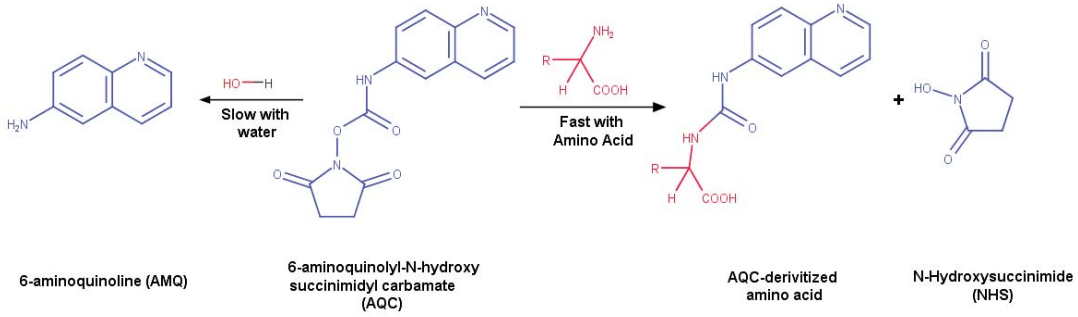

Figure 38: Derivatization reaction of amino acids by AQC.

4.2 Experimental procedure

4.2.1 Chemicals and reagents

Amino acid standards were purchased from SIGMA (Steinhaim, Germany). Norleucine, boric Acid and triethylamine (TEA) were from SIGMA (St. Louis, MO, USA). 6-aminoquinolyl-N-hydroxysuccinimidyl carbamate (AQC) was purchased from SYNCHEM (Altenburg, Germany). Acetonitrile was from Panreac (Barcelona, Spain). Sodium acetate trihydrate was purchased from Riedel-Dehaan AG (Seelze, Germany) and ammonium acetate was from Ajax Finechem chemicals (Auburn, Australia). Ethylenediamine tetraacetic acid (EDTA) was from J.T.Baker (Center Valley, PA, USA). Deionized water was obtained from a Milli-Q Ultra- pure ThermoFischer water system (Dubudue, IA, USA).

4.2.2 Preparation of amino acid standards

Stock solutions of amino acid standards and as the internal standard norleucine were prepared in 100 pmol/µL by serial dilution (except for cystine at 50 pmol/µL and

proline and hydroxyproline at 500 pmol/µL). Ten microliters of the standard solution were taken and derivatized (see section 4.2.4 below). Norleucine was chosen as internal standard because it does not naturally occur in skin and its concentration response is linear. It was added to the amino acid and skin solutions to correct any variations during sample preparation and derivatisation.

4.2.3 Amino acid extraction from skins

Skins of sheep, goat, deer and cow were prepared as described in chapter 3 (section 3.2.2). Skin samples (100 mg) were placed in clean, acid washed 6 x 50 mm screw cap (PTFE) borosilicate glass tubes and 5.0 mL of 6 M HCl, containing 3% phenol, was added to the samples. Phenol is used to minimize the destruction of amino acids by oxidation during hydrolysis [165, 385]. The skin pieces were then hydrolysed at 110 ^{o}C for 24 hrs. After hydrolysis, any undissolved material was removed by filtering through plastic syringes plugged with glass-wool. The resultant hydrolysates were lyophilized, dissolved in 1.0 mL of water then diluted 100 fold with water and finally derivatized (see below).

4.2.4 Derivatization of amino acids by AQC

Ten µL of either a standard amino acid solution or a skin hydrolysate extract and 10 µL of 100 pmol/µL of norleucine were mixed with 60 µL of 0.2 M borate buffer (pH 9.0), and 20 µL of 15 nmol/µL of AQC, dissolved in acetonitrile, was added. The mixture was incubated for one minute at room temperature then for 10 min at 55 °C. The resultant AQC-derivatized mixture was diluted by adding 900 µL of water, then centrifuged for 30 minute at 14,100 × g prior to injection on HPLC.

4.2.5 Separation of AQC-amino acids using high performance liquid chromatography (HPLC)

Amino acid analysis was carried out using a Dionex HPLC system equipped with a P580 pump and an ASI-100 auto-sample injector. One to five µL samples were injected on to a Phenomenex® Gemini C18 (150 mm x 4.6 mm, 5 µm) HPLC column or a Zorbax eclipse XD8-C18 Agilent (50 mm × 4.3mm, 3.6 µm) HPLC column both of which were protected with a guard column. The analysis was performed at 25 ºC and 37 ºC using two different gradients. For the first gradient system, solvent a contained sodium acetate (140 mm), sodium azide (7.5 mm), EDTA (0.26 mm) and TEA (15 mm), in water, adjusted to pH of 5.05 with concentrated phosphoric acid. Solvent B was 60% (v/v) of acetonitrile in water [386]. For the second gradient system, solvent A contained ammonium acetate (5 mm) in water adjusted to pH 5.02 with glacial acetic acid and solvent B was 60% (v/v) of acetonitrile in water. Each system was optimised to get the optimum amino acid separation. Eluted peaks were monitored using a fluorescence detector (Dionex RF 2000) with excitation and emission wavelengths set at 245 nm and 395 nm, respectively. At the end of each run, the column was washed with 10 column volumes of solvent B followed by re-equilibration in 20 column volumes of solvent A.

4.2.6 AQC-Amino acid separation and detection by mass spectrometry

AQC-amino acids were separated on a Phenomenex Gemini C18 (150 mm x 4.6mm, 5 µm), HPLC column protected with a guard column. The analysis was performed at 25 ºC using the optimised gradient. Monoisotopic masses of the AQC-amino acids in the eluted peaks were measured using mass spectrometry.

The mass spectrometer used was an Agilent 6520 Accurate-Mass quadrupole time-of-flight (Q-TOF) liquid chromatography mass spectrometry (LC/MS) system (Agilent 6520 Q-TOF, Agilent Technologies, Hanover, Germany) with an electrospray ionization (ESI) source. The HPLC was an Agilent 1200 series with a temperature controlled autosampler. Detection was carried out in positive mode using a mass range of 100-1200 m/z, a fragmentor voltage of 145 V and a skimmer voltage of 55 V. The nitrogen gas temperature was set at 330 ^{o}C with a flow rate of 6 L/min. Agilent Mass Hunter Workstation Qualitative Analysis software version B.06.01 SP1 (Agilent Technologies, Santa Clara, CA, USA) was used for qualitative analysis.

4.2.7 Method validation

For method validation, the determination of limits of detection (LOD), limit of quantitation (LOQ), linear dynamic range (LDR) and reproducibility of retention time were obtained. Calibration curves were produced using serial dilutions of the standard solution, and injection volumes of a 1.0 to 5.0 µL. All samples were spiked with norleucine as an internal standard. The concentration ranges were from 0.1 pmol/µL to 10.0 pmol/µL. An average of three replicates of each standard was used to construct the calibration curve.

4.2.8 Amino acid quantitation in skins

For animal skins, 4 or 5 biological replicates of sheep, goat, deer and cow skins were prepared as above, and three technical replicates of each biological replicate were used for quantitation. The amino acid concentrations in the different skin samples were then

determined and standard deviations calculated for the technical and biological replicates before retention times were calculated.

4.3 Results and discussion

4.3.1 Separation of AQC-amino acids by HPLC

Work done previously in our laboratory reported the separation of AQC-derivatized amino acids using a Gemini column and a mobile phase composed of a binary gradients of sodium acetate and acetonitrile [386]. In summary, solvent A contained sodium acetate (140 mM), sodium azide (7.5 mM), EDTA (0.26 mM) and TEA (17 mM) as an ion pairing agent. Solvent B contained 60% acetonitrile in water [386]. Unfortunately, under these conditions, glycine, histidine, threonine, arginine, cystine, lysine and the two diastereomers of hydroxylysine were not well resolved. To achieve complete separation of these amino acids, several experimental conditions were optimised including buffer pH, column temperature, buffer concentration, flow rates and different columns.

No improvement in resolution was achieved by changing either buffer pH or concentration. It was found, however, that the quality and the high concentration of the sodium acetate buffer used significantly affected the separation. Interestingly, the resolution could be enhanced by using different flow rates and decreasing the column temperature to 34 ^{o}C (Table 12). Under these conditions, all amino acids were fully resolved (Figure 39A), apart from glycine and threonine which co-eluted with histidine and arginine, respectively. Most importantly, hydroxyproline and hydroxylysine, the amino acids unique to collagen, were completely resolved.

Table 12: Optimised gradient for amino acid separation using Gemini Phenomenex and Zorbax Eclipse HPLC columns. Column temperature was set at 34 ºC.

Time (min)	Gemini Column Flow rate (mL/min)	Zorbax Column Flow rate (mL/min)	Buffer B %(v/v)
0.0	1.00	1.50	0
0.5	1.00	1.50	1
15	1.00	1.50	4
23	1.00	1.50	7
28	1.00	1.50	8
46	0.60	1.50	11
52	0.60	1.50	21
71	0.60	1.50	31
76	0.60	1.00	35
79	0.60	0.60	40
80	0.60	0.60	100
110	1.00	1.00	100

Resolution between threonine and arginine was achieved by changing the column to the Zorbax Eclipse. This change, however, did not improve the resolution between glycine and histidine (Figure 39B).

Although several other parameters were investigated, glycine and histidine could not be resolved. Furthermore, the high concentration of sodium acetate (140 mM) required frequent changes of the guard column due to the blockage resulting from salt precipitation.

The use of ammonium acetate rather than sodium acetate was evaluated for three reasons. (1) to improve the resolution of glycine and histidine. (2) Ammonium acetate is a volatile buffer, and therefore compatible with mass spectrometry which can be used to detect and confirm the structures of both the mono- and di-derivatized AQC-amino acids [384]. (3) To develop a method suitable for the separation of collagen crosslinks as well as amino acids.

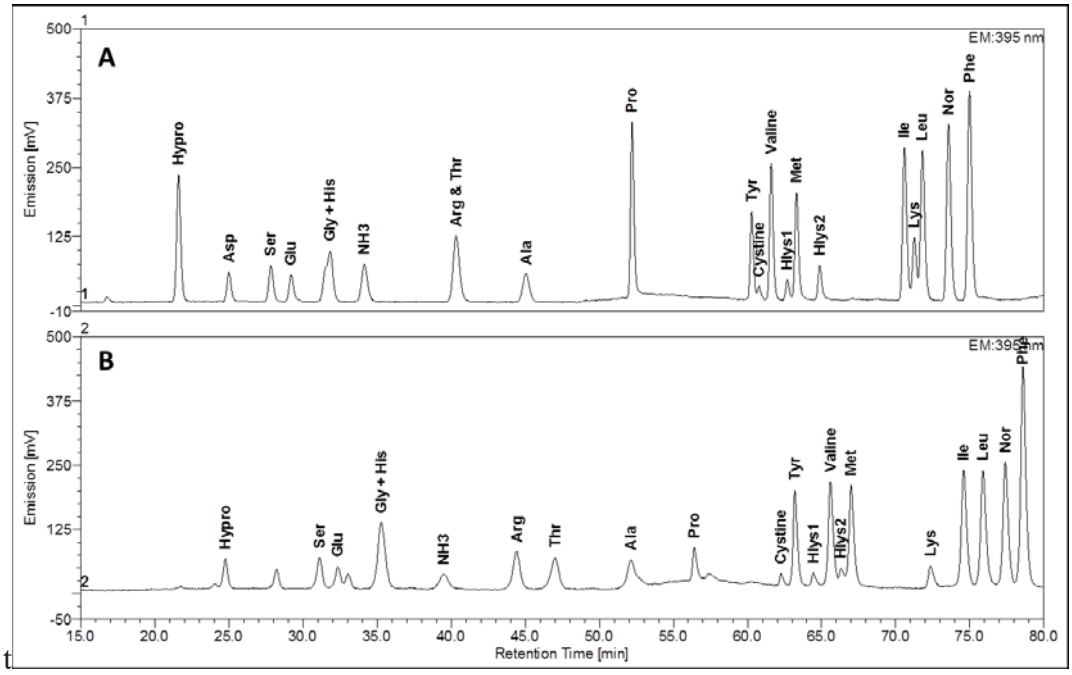

Figure 39: Separation of AQC-amino acids using (A) A Gemini column (B) A Zorbax column. Buffer A contained sodium acetate (140 mM), sodium azide (7.5 mM), EDTA (0.26 mM) and TEA (15 mM) at pH 5.05 adjusted with H_3PO_4 and buffer B was 60% (v/v) of acetonitrile in water. Table 11 shows the detailed separation conditions.

First, it was important to optimise the concentration of ammonium acetate in the buffer. Several concentrations ranging from 5 to 50 mM were prepared, and the buffer pH adjusted to 5.02 using glacial acetic acid. Sodium azide, EDTA and TEA were excluded from the buffer as they suppress the ionisation and significantly affect the performance of the mass spectrometer on the long term use [387, 388].

It was found that when 5 mM ammonium acetate (pH 5.02) was used, glycine and threonine were successfully separated from histidine and arginine, respectively (Figure 40). Interestingly, the resolution of all other amino acids was unchanged except for hydroxylysine2 which was merged with the methionine peak.

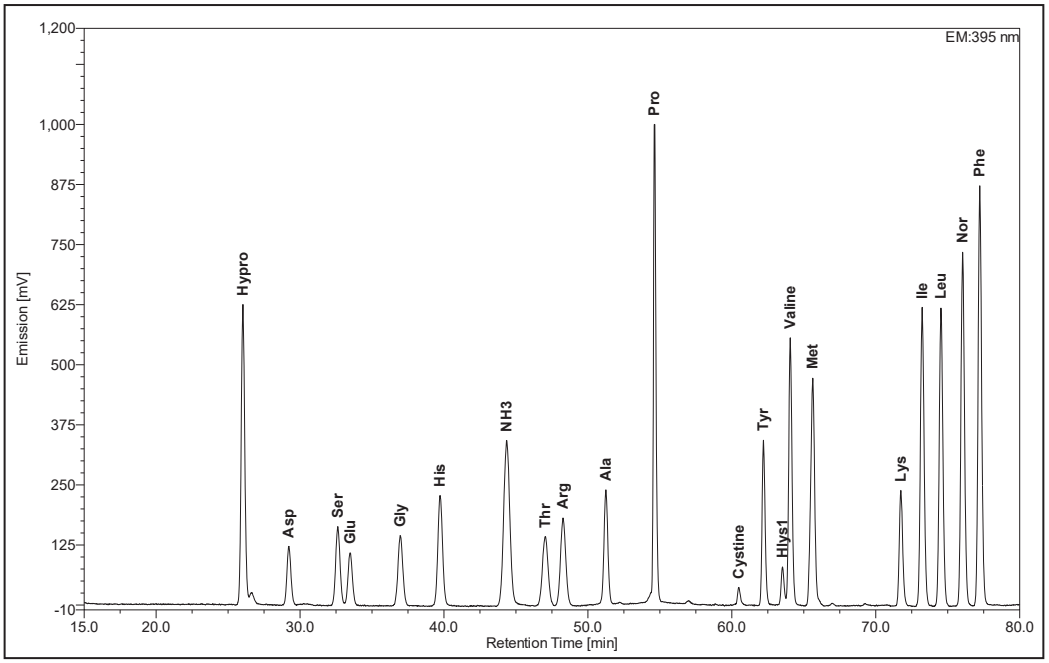

Figure 40: Separation of AQC-amino acid using a Gemini HPLC column. Solvent A contained 5 mM ammonium acetate (pH 5.02) and solvent B was 60% of acetonitrile in water. Flow rate was 1.0 mL/min using the same above gradients (Table 12).

4.3.2 AQC-Amino acid separation and detection by on mass spectrometry

Mass spectrometry is a technique which allows the determination of the compounds in a complex matrix with high sensitivity. It can be used to characterise compounds based on their monoisotopic masses [389]. Few established methods have successfully used mass spectrometry to separate and detect AQC-derivatized amino acids [390, 391]. Using the ammonium acetate buffer system, all amino acids, including hydroxyproline and diastereomers of hydroxylysine, could be detected by mass spectrometry as they eluted from the Gemini Phenomenex® column (Figure 41).

Mass spectrometry detection allowed the accurate identification of the AQC-derivatized amino acid products corresponding to each peak and showed the resolution was similar to that obtained using HPLC-fluorescence detection (see section 4.3.2).

The monoisotopic masses were extracted for both the mono and di- AQC-derivatized amino acids (Table 13).

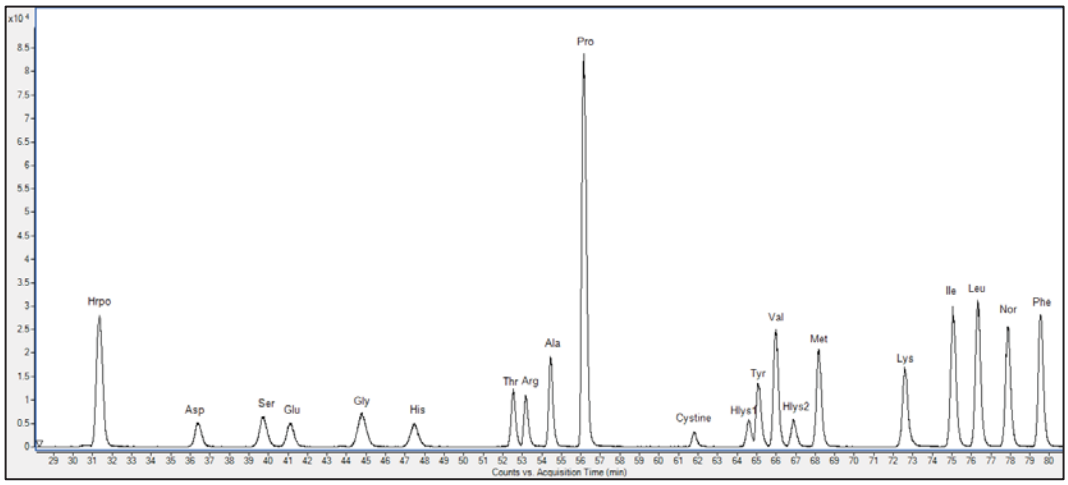

Figure 41: Extracted ion chromatogram of the AQC- amino acids separated on Gemini HPLC column. Solvent A contained 5 mM ammonium acetate (pH 5.02) and solvent B was 60% of acetonitrile in water. Flow rate was 1.0 mL/min using the same above gradients (Table 12).

Since the AQC reagent reacts with amino groups to give urea derivatives, it was expected that all amino acids would produce mono-derivatized products except for lysine, hydroxylysine, cystine and tyrosine (Figure 42) [384, 392]. It was also observed that AMQ, the hydrolysis product of AQC, eluted prior to the amino acids with a retention time of 30.70 minutes. Its presence confirms the complete quantitative conversion of the amino acids under the reaction conditions in an excellent agreement with previous results [384]. All amino acids formed mono-derivatized AQC products except for lysine which produced both the mono and di-derivatized products. The mono-derivatized product of lysine was detected at around 43.70 minutes, although produced a significantly smaller peak than that of the di-derivatized product.

Table 13: Accurate extracted masses of $[M+H]^+$ and $[M+2H]^{2+}$ charged ions of AQC-derivatized amino acids.

Amino acid	Retention time (sec)	Monoisotopic mass (m/z)	$[M+1H]^+$ of AQC-derivative (m/z)	$[M+2H]^{+2}$ of AQC-derivative (m/z)
AMQ	30.70	145.0801	-	-
Glycine	44.77	76.0320	246.0420	-
Alanine	54.45	90.0477	260.0577	-
Serine	39.73	106.0426	276.0526	-
Proline	56.14	116.0633	286.0733	-
Valine	65.99	118.0790	288.0890	-
Threonine	52.54	120.0582	290.0682	-
Hydroxyproline	31.36	132.0582	302.0682	-
Isoleucine	75.06	132.0946	302.1046	-
Leucine	76.32	132.0946	302.1046	-
Norleucine	77.88	132.0946	302.1046	-
Aspartate	36.37	134.0475	304.0450	-
Lysine	72.60 (di)	146.1055	316.1155	486.1255
Glutamate	41.12	148.0532	318.0632	-
Methionine	68.18	150.0510	320.0610	-
Histidine	47.48	156.0695	326.0795	-
Hydroxylysine1	64.60 (di)	163.1004	333.1104	503.1204
Hydroxylysine2	66.88 (di)	163.1004	333.1104	503.1204
Phenylalanine	79.54	166.0790	336.0890	-
Arginine	53.17	175.1117	345.1217	-
Tyrosine	65.06	182.0739	352.0839	522.0939
Cystine	61.81	241.0239	411.0339	581.0339

It has also been reported that hydroxylysine and cystine react with the AQC reagent to produce mono and di-derivatized products [384], however only the di-derivatized products were detected in our chromatogram with retention times 61.81 for cysteine and 64.60 and 66.88 minutes for hydroxylysines 1 and 2. The retention times of all amino acids were a good match with those obtained using the Dionex HPLC system with fluorescence detection.

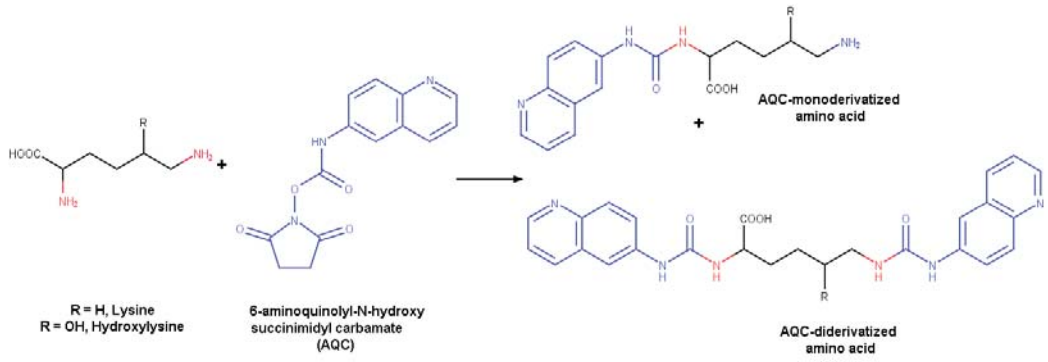

Figure 42: Reaction of lysine and hydroxylysine with AQC reagent producing the mono and di-derivatized products.

4.3.3 Separation of collagen crosslinks

Collagen crosslinks are made up of two, three or four lysine and hydroxylysine amino acids, so they react with AQC in the same way as lysine and hydroxylysine except for the possibility of producing tri and tetra-derivatized products. The use of AQC with mass spectrometry detection was investigated in order to quantitate collagen crosslinks using the same method that was developed above for amino acid analysis.

With no further optimisation, dihydroxylysinonorleucine (DHLNL) was derivatized with AQC using the same protocol as used for amino acid analysis. The formation of three products was predicted based on the structure of DHLNL which has three free amino groups (Figure 43). The extracted ion chromatogram showed that mono-, di- and tri-derivative products of DHLNL were formed, and were well resolved from the amino acids on the Gemini column (Figure 44). The intensity of the mono-derivatized product was, however, very low (<0.001% of the intensity of others).

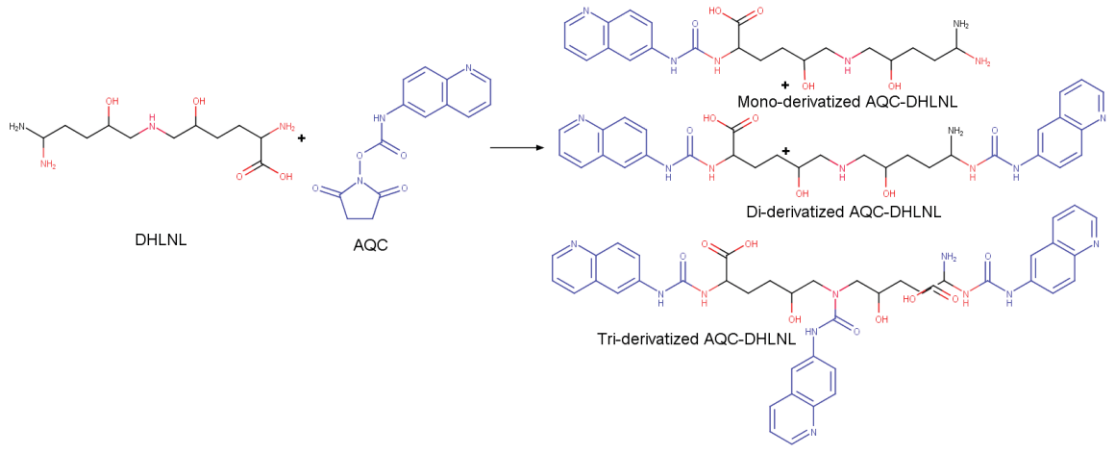

Figure 43: Three possible AQC derivatives of the DHLNL collagen crosslinks.

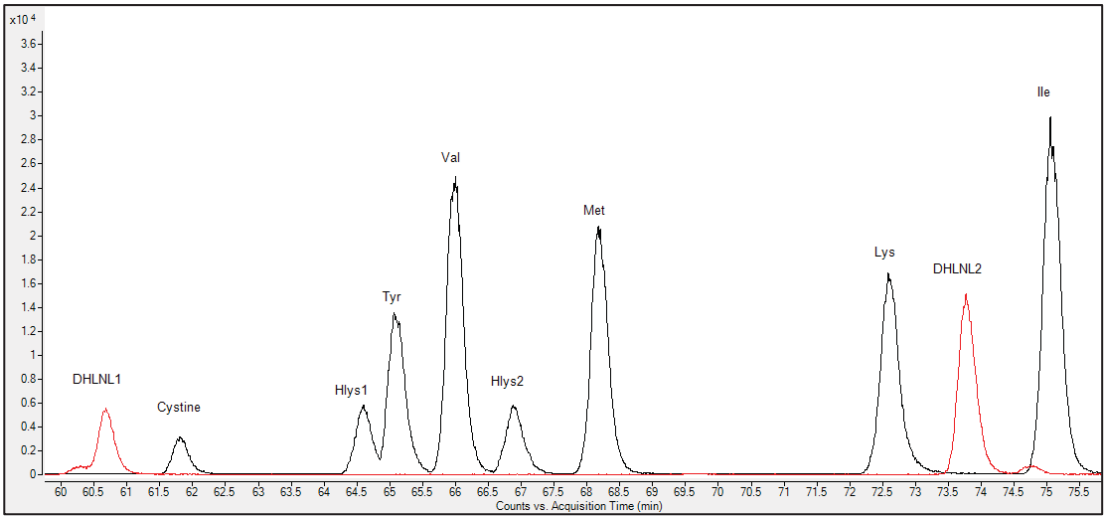

Figure 44: Extracted ion chromatogram of AQC-amino acids and AQC-DHLNL. DHLNL1 and DHLNL2 are the di-derivatized and the tri-derivatized AQC-DHLNL products, respectively. Solvent A contained 5 mM ammonium acetate (pH 5.02) and solvent B was 60% of acetonitrile in water. Flow rate was 1.0 mL/min using the gradient shown in Table 12.

Although it initially appeared that analysis of collagen crosslinks could be carried out by AQC derivatization, it was only possible for DHLNL and HLNL, both of which formed only two products. The multiple AQC derivatives of the HHL and HHMD were not detected which suggests that either they did not react with AQC or that their signals

were suppressed. No further work was carried out to solve this problem because a derivative-free method of crosslink analysis was subsequently developed (see chapter 7) [393].

4.3.4 Quantitation of amino acids

4.3.4.1 Total protein, collagen and non-collagenous content in skins

All amino acids were quantified in dry skins for sheep, goat, deer and cow after being separated using the methods described in section 4.2.5 (For details see the accompanying CD; folder labelled "Chapter 4-amino acid Analysis-calculations"). The total protein, collagen and non-collagenous content in dry skins was then calculated as follows.

- Total protein was calculated from the entire amino acid amount in mg.
- The amount of collagen was based on the hydroxyproline content of each skin.
- Finally, subtraction of the amount of collagen (mg) from the total protein (mg) gives the content of the non-collagenous protein (mg) in the dry skin (Figure 45).

It has been shown that the hydroxyproline content of collagen from various mammals is about 13.5% (w/w). It is not found in any other protein except elastin [32, 394]. The percentage of collagen in a dry skin can be calculated using the following equation [395, 396]

Collagen % = weight of hydroxyproline/ dry weight of skin × (100/13.5) × 100)

It is clear from the results obtained that sheep skin had the lowest total protein content and cow skin the highest (76.5% and 92.6%, respectively). Not surprisingly, the collagen content in sheep skin was 36.0 %, which is the lowest of all four animals tested. Cow skin with 70.9% collagen contained the most, and deer and goat skins with 61.9 % and 58.8 %, respectively were intermediate. Sheep skin had 40.5% of non-collagenous content followed by deer (26.8%), goat (27.7%) and cow (21.7%).

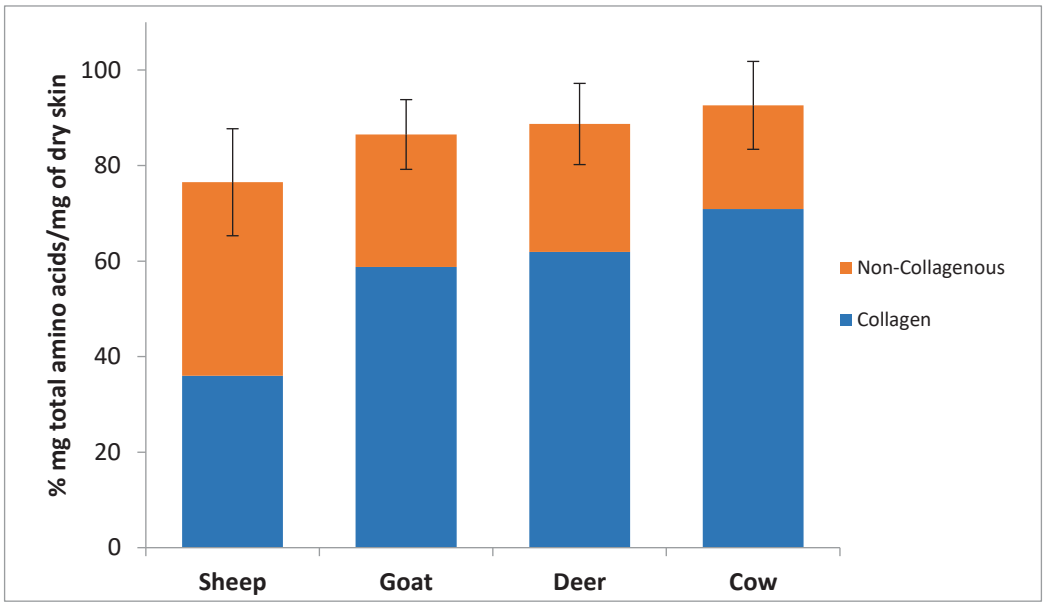

Figure 45: Total protein content in dry skin based on the total amino acid content (mg) in dry skin (mg). The collagen was calculated based on hydroxyproline content. Error bars represent standard deviation.

4.3.4.2 Amino acid content in skins

The concentration of each amino acid in sheep, goat, deer and cow skins was calculated using the mole percentage of amino acids present (Table 14). The reproducibility between measurements was based on four biological replicates for cow and deer skins and five biological replicates for sheep and goat skins. The coefficient of variation (CV %) for the technical replicates of most amino acids was less than 5 %. For the biological

replicates, the CV % for most amino acids was less than 10 % except for hydroxylysine, which had a variance up to 45 %. Generally, large variations in hydroxylysine content were expected because hydroxylation of lysine residues in collagen varies significantly between different animals with different genetic makeups and even varies within collagen type I among different tissues [44, 397]. Furthermore, the largest variance calculated in hydroxylysine2 (~ 45 %) for sheep skin was affected by the low concentration of hydroxylysine2 found in sheep skin (~ 0.03 %).

Generally, it is apparent that glycine, proline, hydroxyproline, alanine, arginine and glutamic acid are predominant in all skins. On the other hand, tyrosine, histidine, methionine and hydroxylysine are the least abundant amino acids [398]. Interestingly, while cystine was quantified in the sheep skin, it could only be detected in traces in goat, deer and cow raw skins. This is because sheep has a higher concentration of non-collagenous protein (Figure 45), such as proteoglycans and elastin, both of which contain multiple disulfide bonds in their structure (Table 15) [399, 400].

Hydroxylysine was well separated from other amino acids, and, in fact, was separated into its two diastereomers [401]. Generally, the hydroxylysine percentage was in good correlation with the value for hydroxyproline as they are both unique amino acids found in collagen [6]. The more hydroxyproline the skin had, the higher the hydroxylysine concentration. Sheep skin with the lowest hydroxylysine concentration had the lowest hydroxyproline content and cow skin with the highest hydroxylysine had the highest hydroxyproline content. The ratio between the concentrations of hydroxyproline and hydroxylysine was calculated for sheep, goat, deer and cow skins. The ratio was 20.5 in cow skin, 28.8 in deer skin, 31.8 in goat skin and 35.8 in sheep skin. The low ratio

indicates the higher hydroxylysine relative to hydroxyproline concentrations. These significant variations in the ratios strongly suggest that hydroxylation of lysine residues in the collagen making up the animal skins varies between the animal skins. Subsequently, these variations would be reflected in the concentration of the crosslinks found in skins (see chapter 7).

Table 14: Average of mole percentage of amino acids in dry sheep, goat, deer and cow skins determined using AQC labelling and RP-HPLC. Data represent the mean values of 5 biological replicates of sheep and goat and 4 biological replicates of deer and cow skins. The average of three technical replicates were measured for each biological replicate.

	Sheep	CV%	Goat	CV%	Deer	CV%	Cow	CV%
Hyp	5.74	4.50	7.95	4.78	8.07	2.19	8.82	1.57
Asp	5.58	1.90	4.96	2.11	4.76	2.19	4.68	1.72
Ser	4.27	6.97	3.42	3.47	3.32	8.18	3.39	11.33
Glu	10.70	2.56	8.96	1.66	8.61	1.78	8.33	1.66
Gly	24.27	3.28	30.31	1.37	30.57	1.45	31.00	1.79
His	0.83	2.92	0.63	7.23	0.60	3.95	0.57	14.87
Arg	7.07	2.95	6.57	1.80	6.40	2.07	6.22	0.42
Thr	1.80	6.00	1.14	7.95	1.15	3.00	0.95	2.99
Ala	9.51	1.92	10.26	2.40	10.48	2.05	10.80	0.80
Pro	9.85	3.60	11.44	3.43	12.04	2.75	12.38	0.34
Cystine	0.88	15.74	traces	-	traces	-	traces	-
Tyr	1.50	7.17	0.99	3.70	0.84	9.90	0.66	8.81
Hyl1	0.13	10.30	0.16	12.01	0.14	7.04	0.15	17.22
Valine	4.05	5.47	2.86	2.17	2.73	3.38	2.40	1.68
Hyl2	0.03	46.98	0.09	19.14	0.14	24.62	0.28	11.20
Met	0.95	3.94	0.76	2.85	0.66	5.50	0.63	11.96
Lys	3.67	1.72	3.02	2.95	2.97	3.36	2.82	1.09
IIe	2.29	4.76	1.68	3.04	1.57	3.60	1.43	1.11
Leu	4.89	4.97	3.43	2.70	3.25	3.64	2.87	0.90
Phe	2.01	2.64	1.65	1.08	1.55	2.21	1.45	2.20

It is clear from table 14 that sheep skin has a different amino acid composition compared to goat, deer and cow skins. Aspartic acid, serine, glutamic acid, tyrosine, valine, isoleucine, leucine and phenylalanine all seem to be higher in sheep skin relative

to the other three skins. The high hydrophobic amino acid content in sheep skin might be correlated to a higher elastin and glycosaminoglycan content in sheep skin. Both elastin and decorin are known to have a higher content of hydrophobic and acidic amino acids compared to collagen I (Table 15) [13, 199]. In sheep skin, hydroxyproline, glycine, arginine, proline, hydroxylysine are present in lower relative concentrations compared to other skins, in agreement with the lower concentration of collagen found in sheep skin.

4.3.4.3 Hydroxylysine diastereomers in skins

It is known that hydroxylation and glycosylation of lysine are crucial for the formation of collagen crosslinks, thus stabilizing fibril structure [44]. Hydroxylysine diastereomers were named originally as hydroxylysine and allohydroxylysine (Figure 46) [401, 404]. Although Piez (1954) and Hamilton (1654) reported the presence of the hydroxylysine diastereomers in collagen, Hamilton refuted their existence based on the assumption that allohydroxylysine was produced due to the epimerization of hydroxylysine during acid hydrolysis [401, 405]. Strikingly, Kimura (1971), showed that hydroxylysine diastereomers existed even after basic hydrolysis [406-408] and Brownell and Veis (1975) and Oikarinen *et al.* (1975) detected hydroxylysine diastereomers in both alkaline and acidic hydrolysates [407, 408].

Table 15: Amino acid composition of collagen I, collagen III, elastin and decorin. Values expressed as a percentage of the total amino acids (mole %).

	Collagen I[a]	Collagen III[b]	Elastin[c]	Decorin[d]
Amino acid	%	%	%	%
Hyp	10.80	11.73	0.80	0.00
Asp	4.37	4.86	0.39	13.67
Ser	3.54	4.39	0.88	6.83
Glu	7.22	6.86	1.27	8.63
Gly	33.11	34.80	32.91	6.47
His	0.45	0.76	0.00	2.88
Arg	5.04	4.67	0.68	3.24
Thr	1.66	1.33	1.17	4.68
Ala	11.14	8.58	21.62	4.68
Pro	11.24	11.72	11.98	6.12
Cys	0.00	0.19	0.29	2.16
Tyr	0.35	0.38	0.97	2.88
Valine	2.20	1.43	12.95	6.83
Met	0.57	0.86	0.00	1.08
Lys[e]	3.42	3.62	0.97	8.27
IIe	1.15	1.43	2.53	5.40
Leu	2.49	1.53	5.45	13.31
Phe	1.25	0.86	5.94	2.88

[a] Based on the Bovine amino acid sequence [398, 402].
[b] Based on the Bovine amino acid sequence [398, 402].
[c] Based on the Bovine amino acid sequence [225, 403].
[d] Based on the Bovine amino acid sequence [275].
[e] This represents the sum of lysine and hydroxylysine because the hydroxylation of lysine varies significantly among species.

Hamilton (1955) noted that "inversion took place by epimerization predominantly at the α-carbon atom. It was not proved conclusively that epimerization at the δ-carbon atom did not occur" [405]. This quote states clearly more work is required to show whether epimerization of hydroxylysine was more likely to occur at the α- or δ-carbon.

According to Hudson's rule, the allohydroxylysine lactone is much less stable than hydroxylysine lactone (Figure 46) [404, 409]. Witkop (1956) showed that when both diastereomers were treated with HCl in ethanol, only the hydroxylysine-, not the allohydroxylysine- lactone was formed [409] suggesting that upon acid hydrolysis, the formation of hydroxylysine is favoured over allohydroxylysine.

Strikingly, significant differences in the concentrations of hydroxylysine diastereomers were reported for collagen extracted from different sources. While Piez used collagen extracted from human dentin, Hamilton used gelatin extracted from cow skin [401, 405]

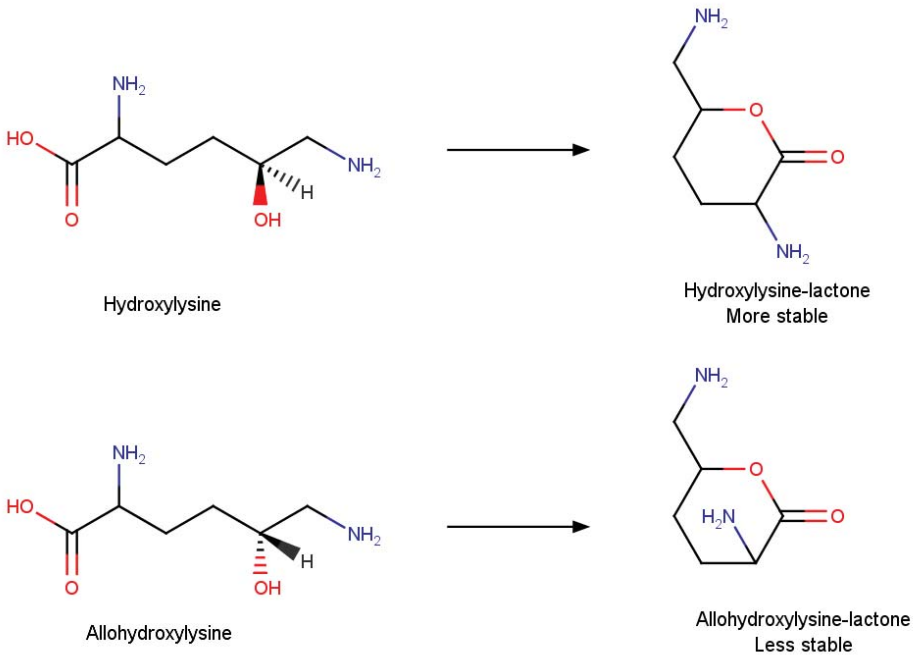

Figure 46: Structures of hydroxylysine diastereomers and their conversion into lactones.

Nakornchai *et al.* showed that the hydroxylysine content in human teeth varies across the dentin layers. This strongly suggests that the hydroxylysine content significantly varies within tissues [410]. It has been reported that the extent of lysine hydroxylation can vary between 15 to 90% depending on the collagen types. Also, it significantly differs within collagen type I from tissue to another tissue [44, 68]. This explains the significant differences observed between the concentrations of the hydroxylysine diastereomers reported by Hamilton and Piez [401, 405].

In this study, the percentage distributions in the concentrations of hydroxylysine diastereomers compared to the total hydroxylysine content in sheep, goat, deer and cow skins are different (Table 16). However, the concentrations of diastereomers in cow skin are in an excellent agreement with those reported by Hamilton in that 35% hydroxylysine and 65% of allohydroxylysine were measured after 25 hours hydrolysis [405]. This result strongly suggests that sheep, goat and deer skins have different rates of hydroxylation of lysine compared to that seen in cow skin.

Interestingly, while the concentration of hydroxylysine1 in the different animal skins hardly changed, the concentration of hydroxylysine2 changed significantly (Table 16). Hydroxylysine1 had a percentage distribution between 34.9-81.3 while that for hydroxylysine2 was 18.7-65.1.

It is clear that sheep skin has the highest percentage of hydroxylysine1while cow skin has the lowest. Deer skin on the other hand appears to have equal amounts of hydroxylysine1 and hydroxylysine2. These differences are intriguing and could be linked to the different hydroxylation and glycosylation patterns of lysine residues in skin, which may in turn have an important role in the formation and the location of collagen crosslinks.

Table 16: The concentrations and the percentage distribution of hydroxylysine diastereomers compared to the total hydroxylysine content in sheep, goat, deer and cow skins given in Table 14.

	Sheep (mol %)	Goat (mol %)	Deer (mol %)	Cow (mol %)
Hlys1	0.13	0.16	0.14	0.15
Hlys2	0.03	0.09	0.14	0.28
Total Hlys	0.16	0.25	0.28	0.43
%Hlys1	81.3	64.0	50.0	34.9
%Hlys2	18.7	36.0	50.0	65.1

4.3.4.4 Collagen I/III ratio in skins

Sommer and Larsen reported an analytical method that could determine the amount of the collagen III using amino acid analysis based on the calculated ratio of isoleucine (IIe):valine (Val) (Table 17) [402]. This was used to calculate the collagen III content in the sheep, goat, deer and cow skins. Using their quadratic equation, the collagen III content in sheep, goat, deer and cow skins was calculated to be 12.46 % for sheep skin, 16.59 % for goat skin, 13.61 % for deer skin and 18.69 % for cow skin. Although sheep skin had the thickest grain layer, this equation showed it to have the lowest collagen III content. This result could be due to the high content of non-collagenous proteins that contain high concentrations of both IIe and Val as shown in Table 14. Consequently, this method is not applicable for calculating the amount of collagen III in sheep skin and therefore results for sheep skin have not been included in Figure 47.

Using this method to compare the collagen III content in goat, deer and cow skins, it was found that cow skin had the highest collagen III content and deer skin had the lowest. This is perfectly correlated to the thickness of the grain layer which is rich in collagen III.

Table 17: Theoretical correlation of the IIe/Val ratio to percentage of collagen III [402].

% Collagen III	IIe/Val
0	0.522
5	0.538
10	0.554
15	0.571
20	0.589
25	0.607
30	0.626

Cow skin had the thickest grain and deer skin had the thinnest grain layer (Figure 47) [149, 150, 402].

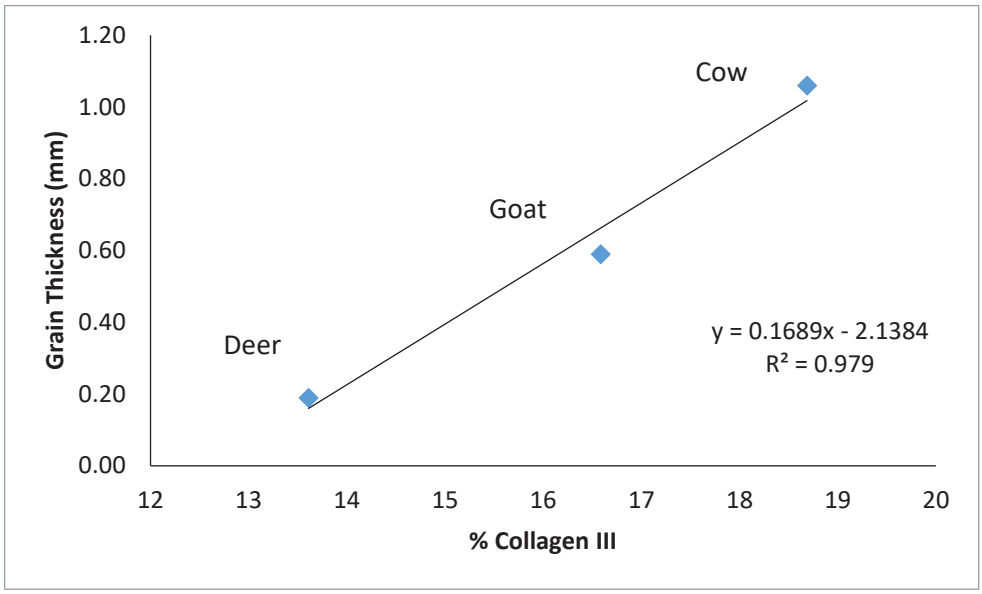

Figure 47: Plot of % collagen III estimated from the IIe/Val ratio against the grain thickness (mm) of goat, deer and cow skins.

4.3.4.5 Amino acid content in pickled skins

Results for the pickled skins of sheep, goat, deer and cow are summarised in Figure 48. Surprisingly, there were no significant differences in the relative concentrations of amino acids between sheep, goat, deer and cow skins. However, the relative concentrations of hydroxyproline and proline increased significantly in pickled sheep skin whereas in pickled goat, deer and cow skins it remained fairly constant. The processes used to remove wool from sheep skin are the same as those that have been used for centuries to dehair goat, deer and cow skins [2]. It is obvious that the process is removing a greater proportion of protein from the sheep skin, particularly the non-collagenous protein rich in hydrophobic amino acids, and as a result the pickled sheep skin is mainly composed of collagen [2, 411, 412].

Figure 49 shows the collagen content in raw and pickled skins based on the hydroxyproline content. The collagen content in sheep skin is low compared to that in deer, goat and cow skins. However, the fact that the collagen content in the pickled skins is higher than raw skins does not represent an increase in the absolute collagen content of the skin, rather an increase in the concentration relative to the other proteins present. It is due to the loss of the non-collagenous protein during liming and further removal of these proteins during the deliming and bating steps. It has been shown that alkaline treatment of skin opens up the collagen fibre structure but does not significantly degrade the collagen [2, 411]. These results show that sheep skin appears to be more vulnerable to this process than goat, deer and cow skins and suggests that sheep skin structure is different, swelling more in alkaline conditions resulting in greater loss of the non-collagenous protein compared to that from goat, deer and cow skins. This effect can be further explained by calculating the weight ratios between the sum of major amino acids in collagen, hydroxyproline, proline and glycine, and the sum of each of the following groups of amino acids; hydrophobic, acidic and basic amino acids. Figures 50 and 51 show these weight ratios for sheep, goat, deer and cow raw and pickled skins, respectively. It is clear that all weight ratios of raw sheep skin are higher than those for its pickled skin.

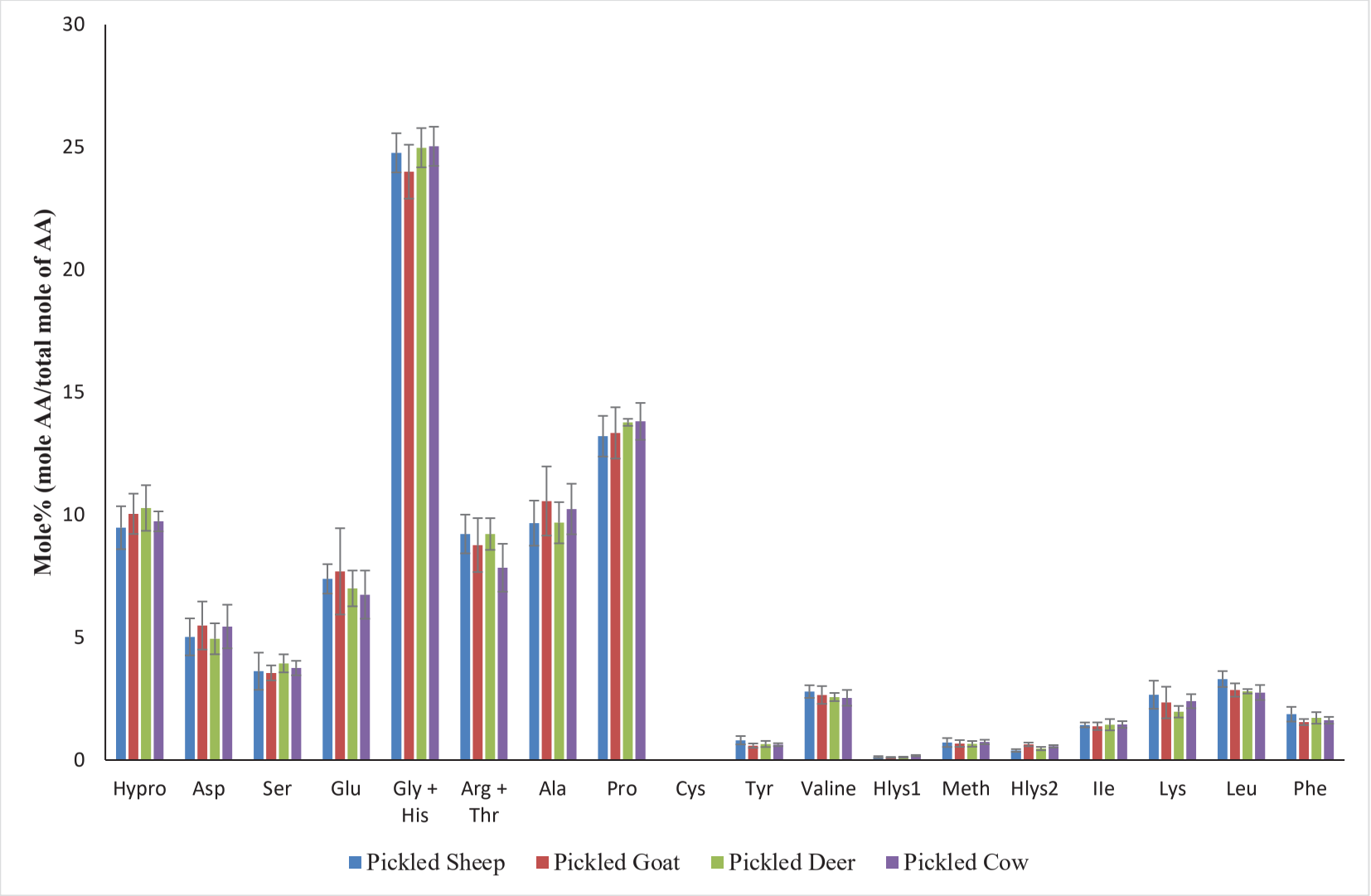

Figure 48: Mole percentages of amino acids in sheep, goat, deer and cow pickled skins.

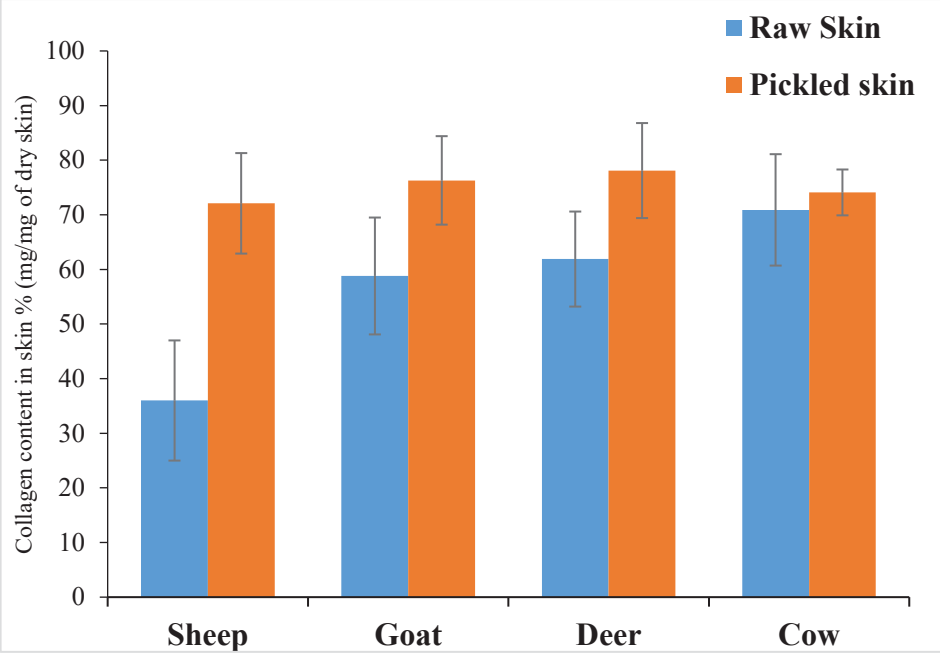

Figure 49: Collagen content in sheep, goat, deer and cow raw and pickled skins.

The weight ratios for goat and cow raw and pickled skins remained fairly constant although there was a small increase in the case of the deer pickled skin. Collagen is composed mainly of hydroxyproline, proline and glycine, allowing these to be correlated with the amount of collagen in the same skin sample. The remaining amino acids are a reflection of the non-collagenous proteins present in the skin. Assuming that the collagen content of skin remains fairly constant during processing and the remaining proteins are removed during leather production [2], any change in their concentrations will be inversely proportional to the calculated weight ratio. An increase in the weight ratio of the pickled skins, therefore shows a greater loss of the non-collagenous proteins. From Figure 51, it is clear that sheep pickled skin had the highest increase in the weight ratio, suggesting a significant loss of its non-collagenous proteins and glycosaminoglycans (for details see chapter 5). An independent study showed that the tear strength of sheep and deer pickled skins significantly decreased during

processing compared with goat and cow pickled skins, indicating that sheep and deer skins are more adversely affected by the processing than goat and cow skins (M. Ahn, personal communication).

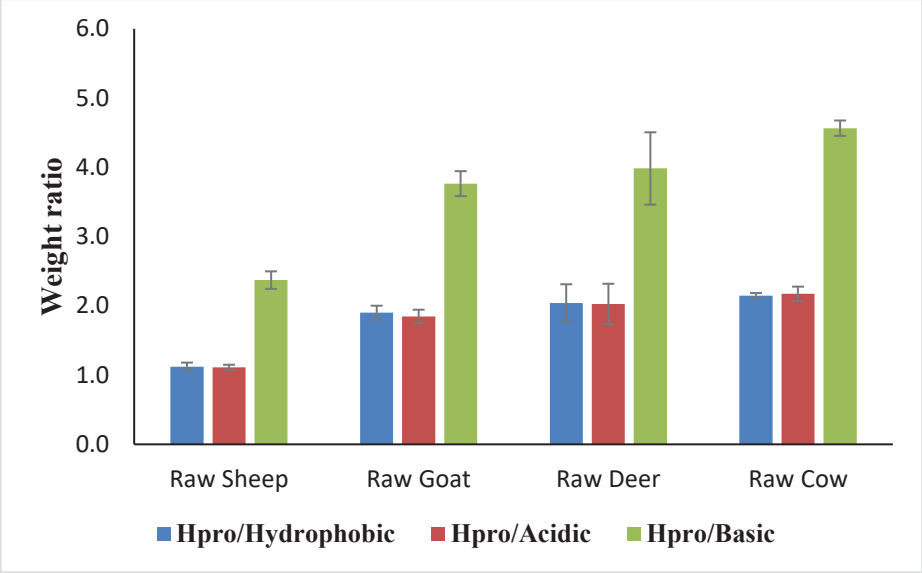

Figure 50: A comparison of the weight ratio of different amino acids in sheep, goat, deer and cow skins. Hydroxyproline is the sum of the hydroxyproline + proline; hydrophobic is the sum of leucine+ isoleucine + phenylalanine + alanine + valine; acidic is the sum of (glutamic acid+ aspartic acid); basic is the sum of (lysine + arginine).

4.3.4.6 Amino acid content through sheep leather processing steps

The relative amino acid content of sheep skin at different steps during the leather processing is shown in Figure 52. Generally, there were no significant changes in amino acid concentrations between different processing stages and the mole percentage of each amino acid remained relatively constant, except for hydroxyproline and proline, which increased after the liming/dewooling step.

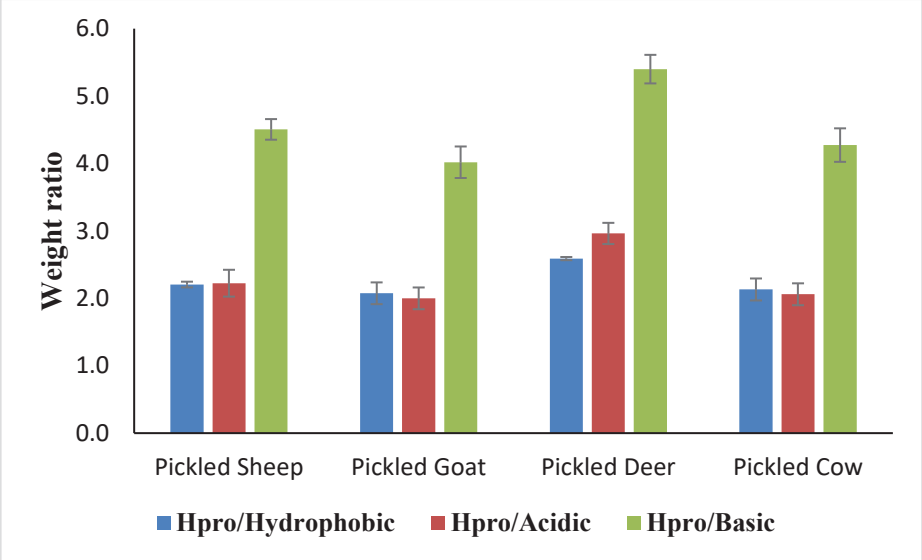

Figure 51: A comparison of the weight ratio of different amino acids in pickled sheep, goat, deer and cow skins. Hydroxyproline is the sum of the hydroxyproline + proline + glycine; hydrophobic is the sum of leucine+ isoleucine + phenylalanine + alanine + valine; acidic is the sum of glutamic acid + aspartic acid; and basic is the sum of lysine + arginine.

4.3.4.7 Amino acid content in pickled skins

Other work in our laboratory has shown many proteins are depleted from sheep skin during processing including collagen VI and proteoglycans (E. M. Ahn, personal communication). As these proteins are rich in all amino acids, except for proline and hydroxyproline, their removal in the liming and deliming steps results in the same weight of pickled skin, containing a greater proportion of collagen than the raw skin. This is reflected in the significant increase in hydroxyproline and proline concentrations compared to the other amino acids. As this difference was greatest in sheep skin, it is clear that sheep skin is being most significantly affected by the dewooling procedure, with the treatment adversely affecting its physical properties. The complete removal of cystine from sheep skin also suggests that the skin is being subjected to a harsher treatment than may be necessary.

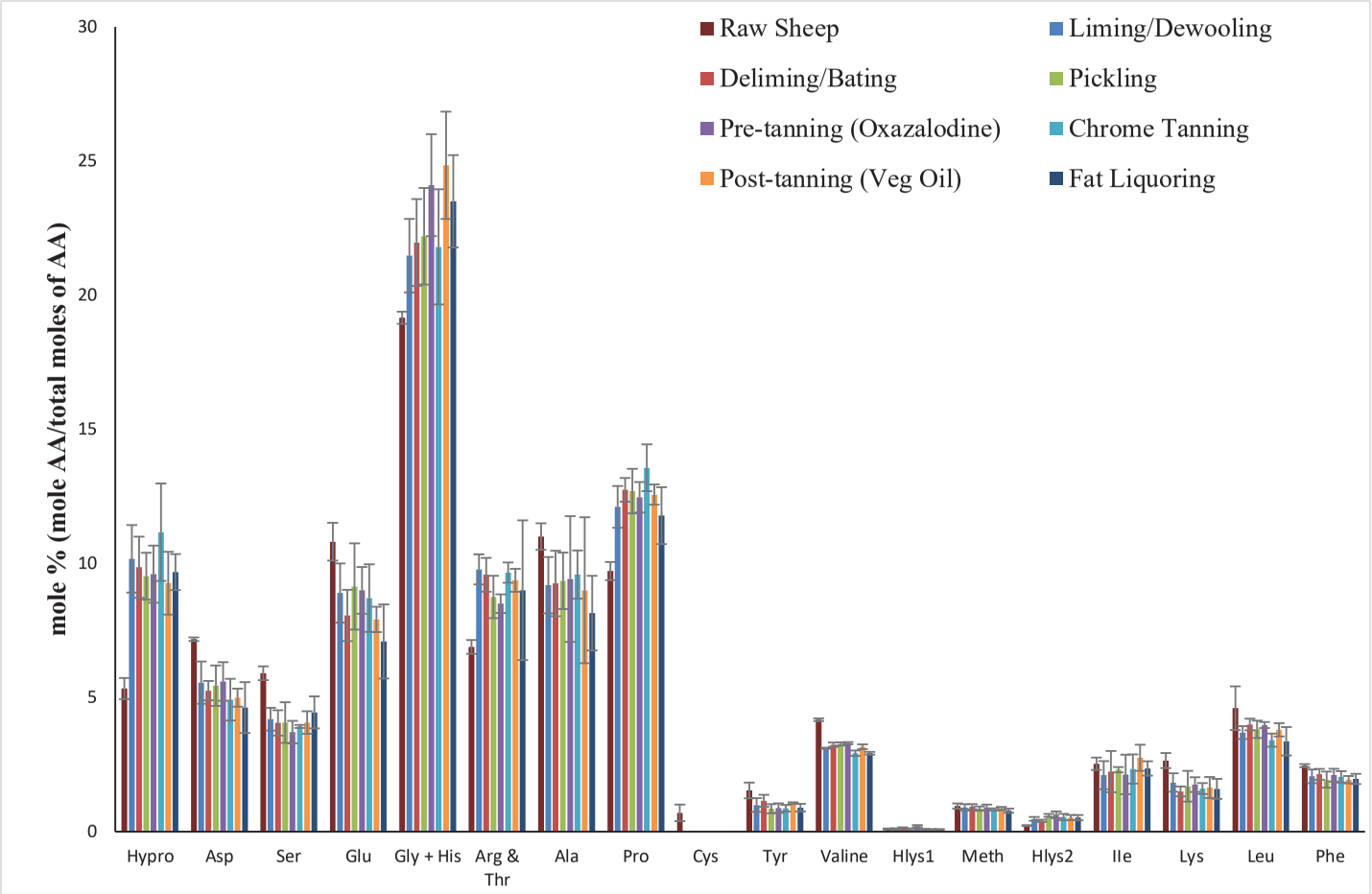

Figure 52: Mole percentages of amino acids of 100 mg of sheep skin at different steps during leather processing.

5 CHAPTER FIVE: Analysis of Glycosaminoglycans, Carbohydrates and Lipids

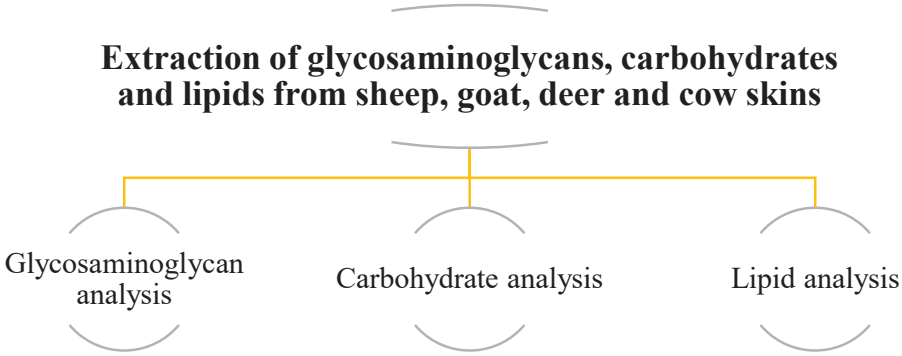

5.1 Introduction

Glycosaminoglycans are anionic polysaccharide linear chains, consisting of repeating disaccharide units [232]. Except for hyaluronic acid, glycosaminoglycans are sulfated and are covalently O-linked linked to a core protein through a serine or threonine sidechain to form proteoglycans [232]. Glycosaminoglycans are common constituents of the extracellular matrix, including skin, where they play a number of roles that include cellular processes and structural functions [232].

Many methods have been developed for quantitation of glycosaminoglycans [413] including spectrophotometric methods that are commonly used to measure the total concentration of sulfated glycosaminoglycans in biological samples [414]. The glycosaminoglycan assay, based on the use of 1,9-dimethymethylene blue (DMMB), was used in this study because it binds specifically to sulfated glycosaminoglycans to form a precipitate. The precipitate is then dissolved, releasing DMMB, to produce a colored solution that absorbs at a wavelength of 565 nm. The intensity of the adsorption is directly proportional to concentration of glycosaminoglycans [414].

5.2 Experimental procedure

5.2.1 Chemicals and reagents

The Blyscan glycosaminoglycan assay kit was purchased from Biocolor Ltd., Northern Ireland. Papain was from MP Biomedical, France, and norleucine was from Sigma & Aldrich, USA. Sodium acetate trihydrate was from Riedel-De haën AG, Germany and EDTA was from J.T.Baker, USA. Cysteine hydrochloride 98% was from Sigma. Chloroform was from SDS, France, methanol was from Labserv, USA, molybdic Acid was from M&B, UK, 4-methyl-2,6-di-tertbutylphenol and

molybdenum powder were from BDH, UK. TLC silica plates were purchased from Macherey-Nagel, Germany and bromothymol blue was from LabChem, USA.

5.2.2 Optimization of the glycosaminoglycan extraction from skins

Skins of sheep, goat, deer and cow were prepared as described in chapter 3 (sections 3.2.2). Glycosaminoglycans were extracted from skin samples using the following optimised procedure. Skin samples (50 mg) were weighed into clean labelled 1.5 mL Eppendorf tubes then 1.0 mL of 200 mM phosphate buffer (pH 6.4) containing 100 mM sodium acetate, 50 mM EDTA and 5 mM cysteine chloride were added. Papain was dissolved in the same phosphate buffer, then added in a ratio of 20:1 (w/w) skin:papain. The mixtures were then incubated at 65 ^{o}C for 24 hours, after which time, insoluble materials were pelleted by centrifugation at 14,100 × g at room temperature for one hour. The supernatants were transferred to new 1.5 mL eppendorf tubes and the remaining pellets were digested twice more with fresh papain as above. The concentration of glycosaminoglycans in each supernatant was determined using the Blyscan glycosaminoglycan assay. Extraction of glycosaminoglycans from skin samples was tested using two different papain concentrations, 1:20 and 1:100 (w/w) sample:papain, different incubation times between 12 to 72 hours and the number of extractions.

5.2.3 Glycosaminoglycans quantification

The Blyscan glycosaminoglycan assay protocol was used with slight modification [415]. In brief, glycosaminoglycan standards were prepared from chondroitin sulfate using concentrations of 0.5, 1.0, 1.5, 2.0 and 2.5 µg in 1.0 mL of Milli-Q water. One mL of a 0.1 M solution of DMMB dye was added to each of the chondroitin sulfate solutions and to 10-50 µL of papain-extracted skin supernatants.

Three replicates were used for each animal skin. The tubes were mixed by rotation for one hour, then the insoluble material was removed by centrifugation at 14,100 × g for 60 min at room temperature. The supernatants were discarded and tubes were kept inverted for a few minutes on tissue to remove any residual liquid. Once dry, the pellets were dissolved in 1.0 mL of dissociation dye solution, containing a mixture of guanidine chloride, *n*-propanol and sodium dodecyl sulfate (provided by the manufacturer) then vortexed. The resultant solutions were mixed thoroughly by rotation for 30 minute at room temperature then centrifuged at 14,100 × g for 60 minutes. Two hundred µL of each solution was then transferred to a 96 well microplate in triplicate and absorption measured at 656 nm.

5.2.4 Extraction and quantification of carbohydrates from animal skins

Measurement of carbohydrate was carried out using the phenol-sulfuric acid method [416]. Three replicates of each animal skin were used. Twenty-five mg of each skin was weighed then mixed with 2.0 mL of 1.0 M sulfuric acid. The mixtures were incubated at 100 ºC for 8 hours and then allowed to cool to room temperature. Undissolved material was pelleted by centrifugation for one hour at 14,100 × g at room temperature. The supernatants were then transferred to a 1.5 mL Eppendorf tubes and the pellets were discarded. Ten µL of each skin extract was placed in a 96-well microplate and 150 µL of concentrated sulfuric acid was added, followed by 30 µL of 5% phenol. The microplate was heated for 10 minutes at 90 ºC in a water bath then allowed to cool to room temperature and the absorbance measured at 490 nm. A calibration curve was produced using different concentrations of (0, 5, 10, 20, 40, 60, 80 and 100 nmol) glucose.

5.2.5 Extraction of lipids from skin

Lipids, including phospholipids, triglycerides, diglycerides, monoglycerides, sterols, sterol esters, free fatty acids and others, were extracted from skin samples using the Folch method with a mixture of chloroform:methanol (2:1) v/v [417-419]. One gram of skin was transferred into a cellulose thimble (Whatman, UK). The thimble was plugged with fat-free cellulose wool, and placed in the extraction chamber. Fifty mL of chloroform:methanol (2:1, v/v) was added to a clean and dry pre-weighed boiling flask, and the Soxhlet apparatus set up as shown in Figure 53. The boiling flask was placed in a water bath and heated at 100 ºC for two hours to extract all skin lipids. After cooling the extract to room temperature, the organic phase was removed by rotatory evaporator at 30 ºC. The remaining liquid material was lyophilized for two hours after which the lipid residues were weighed before being completely dissolved in chloroform to a concentration of 20-60 µg/µL. Oxidation of lipids was minimised by the immediate addition of 4-methyl-2,6-di-tertbutylphenol (0.005%)[420]. The lipid extracts were then washed with potassium chloride solution to remove any non-lipid substances, before being analysed by silica and cellulose TLC.

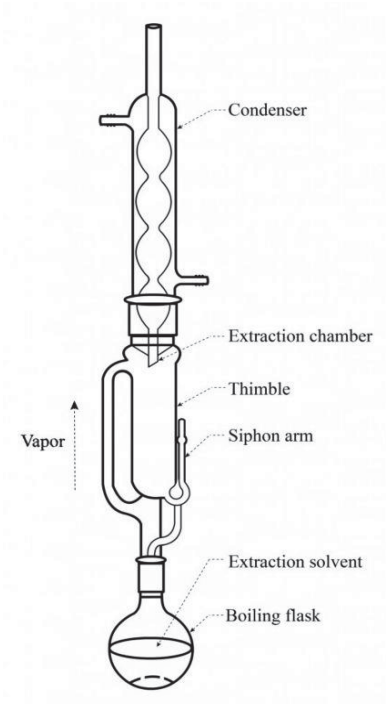

Figure 53: Soxhlet Apparatus

5.2.6 Preparation of lipid stains

The locations of the lipids of the TLC were examined using three different stains. The first stain was prepared by mixing 100 mL of concentrated H_2SO_4 with 900 mL

milli-Q water to produce a 10 % aqueous H_2SO_4. The second stain was made up of 0.01 % bromothymol blue (BTB) by dissolving 0.1 g of BTB in 10 % ethanol/water (v/v) then the addition of 5 drops of concentrated ammonia solution. The third stain of molybdenum blue, was made up of the following two solutions. First, solution I was prepared by dissolving 8 g of MoO_3 in 200 mL of hot concentrated H_2SO_4 to produce a light blue solution after standing overnight. Solution II was prepared by dissolving 0.4 g molybdenum powder in 100 mL of solution I. The resultant mixture was then boiled for 15 minutes, cooled to room temperature and filtered to remove any solid material. Finally, equal volumes of solution I and II were mixed and diluted twice with water to obtain a dark green solution of stain number three.

5.2.7 Thin Layer Chromatography (TLC) of Lipid extracts

The developing tank was prepared at least 30 minutes prior to the immersion of the TLC plate by lining the tank with filter paper, adding chloroform to a depth of 10 mm then covering it to saturate the atmosphere with chloroform vapour. The lipid samples were applied to oven-dried silica plates using micropipettes to give different concentrations of 60, 120 and 180 µg/µL. After the spots had dried, the TLC plate was placed into the tank, developed until the solvent front reached the top of the plate, then removed and air-dried in the fume hood for 2 hours.

The stains were applied to the plates using a sprayer (DESAGA SG1, Sarstedt-Gruppe, Wiesloch, Germany) then allowed to air dry in the fume hood. Plates sprayed with 10 % H_2SO_4 were heated in an oven at 110 ºC for 2 hours. General lipids including phospholipids, triglycerides, diglycerides, monoglycerides, sterols, sterol esters, free fatty acids and others, were detected using 10 % H_2SO_4 and bromothymol blue. Phospholipids were also stained using molybdenum blue.

5.3 Results and discussion

5.3.1 Optimisation of glycosaminoglycan extraction from skin

Quantitation of glycosaminoglycans by 1,9-dimethylmethylene blue assay requires the complete extraction of glycosaminoglycans from skin [414, 415].

The influence of the papain digestion time was investigated first and showed that a longer digestion time resulted in a higher concentration of extracted glycosaminoglycans. There was, however, no significant increase after 24 hours digestion, suggesting that this time is sufficient to extract all available glycosaminoglycans from the skin sample.

The same skin sample was sequentially digested three times, each digestion lasting 24 hours in order to test the efficiency of extraction. When the concentration of glycosaminoglycans in each digest was measured, it was found that the first and second skin digestions extracted more than 99% of the glycosaminoglycans from the skin sample (Figure 54). Based on this result, two sequential digestions used in subsequent analyses.

Sheep, goat and cow skins showed a significant drop in the concentration of the glycosaminoglycans from the second papain digestion, whereas deer skin showed only a small decrease suggesting that the glycosaminoglycans in deer skin are more resistant to the papain digestion than those in sheep, goat and cow skins. This could be because deer skin contains glycosaminoglycans that are more difficult to extract because of size, or glycosylation compared to those in sheep, goat and cow skins. Alternatively, it may be that the matrix itself is less amenable to papain digestion.

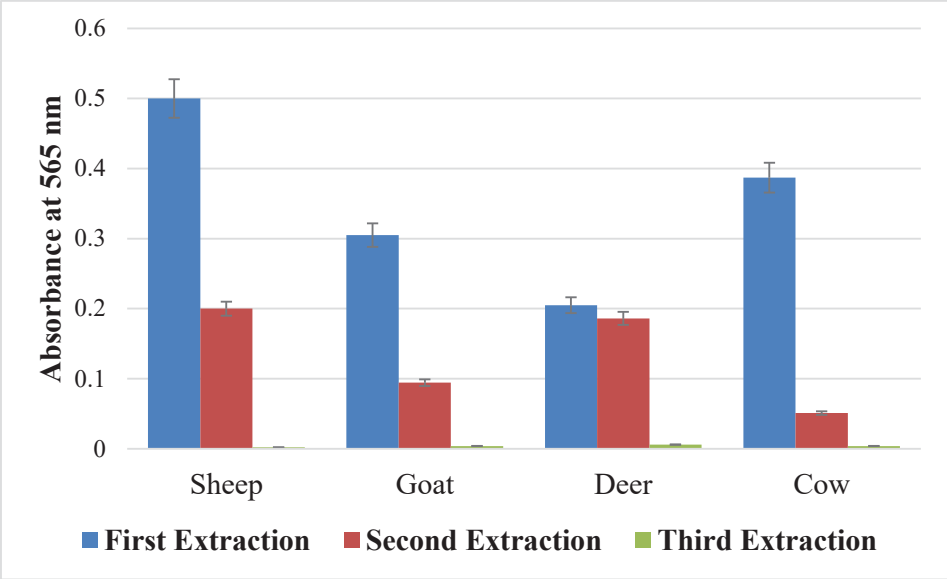

Figure 54: Absorbance of first, second and third glycosaminoglycan extractions. Error bars represent standard deviation.

The effect of different papain concentrations was tested using 1:20 and 1:100 (w/w) of skin:papain. It was found that a ratio of 1:20 of sample:papain enzyme concentration extracted more glycosaminoglycans in sheep and deer (Figure 55). However, there was no significant change in the glycosaminoglycans extracted from goat and cow skins. This again suggests again that there is something different about the glycosaminoglycans or the matrix of goat and deer skins.

5.3.2 Quantitation of glycosaminoglycans in skin

A calibration curve was generated using a range of chondroitin sulfate concentrations between 0.5-2.5 µg/L (Figure 56).

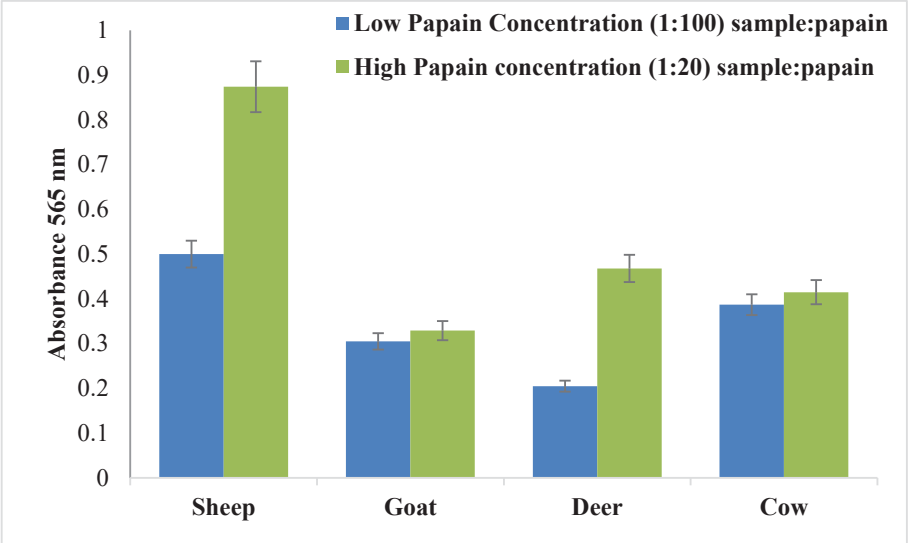

Figure 55: Absorbance of first glycosaminoglycan extraction fraction after 24 hours digestion time using two different concentration ratios of the sample to papain. Error bars represent standard deviation.

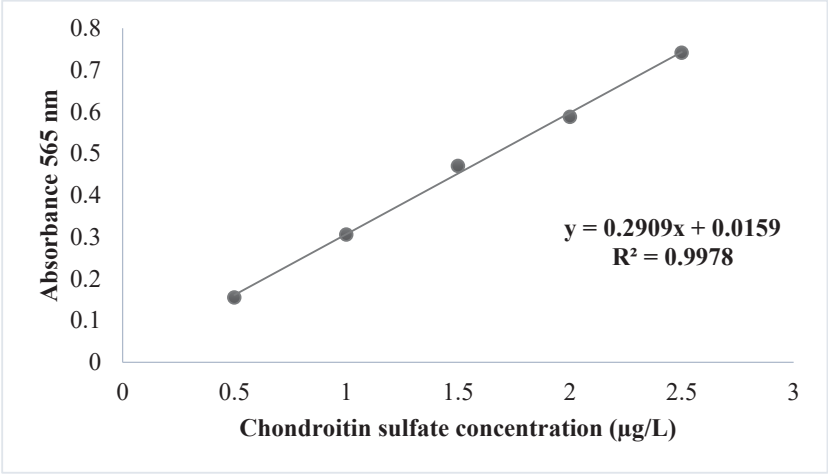

Figure 56: Calibration curve of chondroitin sulfate standards.

The glycosaminoglycans were extracted from two biological samples of raw and pickled sheep, goat, deer and cow skins. There was a significant difference in the glycosaminoglycan content of the four animal skins as shown in Figure 57. Sheep skin had the highest glycosaminoglycan content and goat skin had the lowest, while deer and cow skins had similar glycosaminoglycan content. The glycosaminoglycan concentration significantly decreased in all pickled skins in

common with the trend observed for amino acid concentrations (see Chapter 4) with sheep skin showing the largest decrease. (Figure 57).

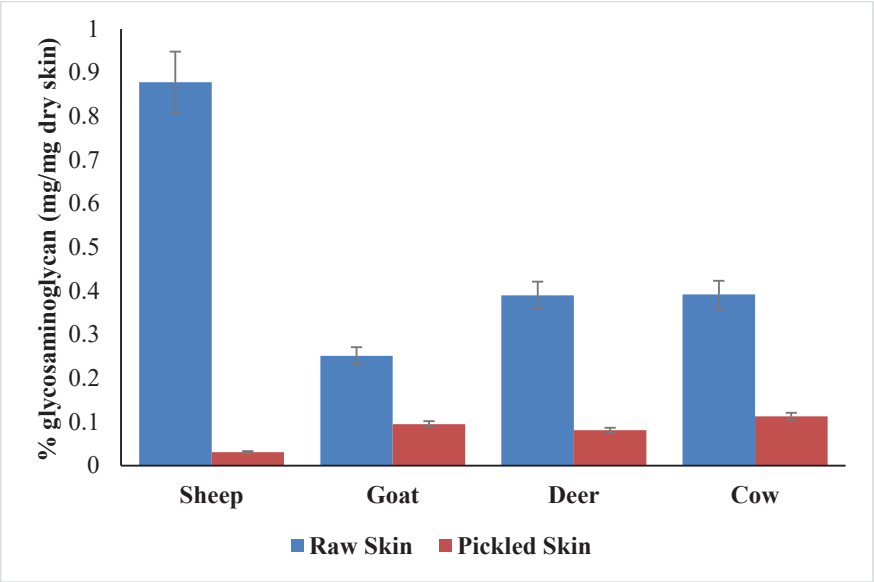

Figure 57: Sulfated glycosaminoglycans percentage in sheep, goat, deer and cow raw and pickled skins. Error bars represent standard deviation.

This has implications for the processing of sheep skin to make leather. Sheep skin appears to have different properties to the other skins in all analyses carried out. A significant concentration of both amino acids (protein) and glycosaminoglycans (proteoglycans, hyaluronic acid) were removed from sheep skin during the liming and deliming steps, which agrees with reports by Covington (2009) and Fathima (2010) (Figure 58). This is because the alkaline conditions open up the inter-fibrillar collagen structure facilitating removal of proteoglycans, and the effect is clearly the greatest in sheep, perhaps because of the differences in the skin structure highlighted in this study. Further losses occurred after bating, where proteases are used to break down the non-structural proteins in the matrix [2, 421]. As alkali-treated collagen is more vulnerable to proteases, their ready access to the non-collagenous matrix results in significant degradation and loss of

glycosaminoglycans. It is also possible that the bating enzymes contain low concentrations of glycosidases that may degrade O-linked glycans linked to collagen, further loosening the skin matrix and allowing degradation of the protein.

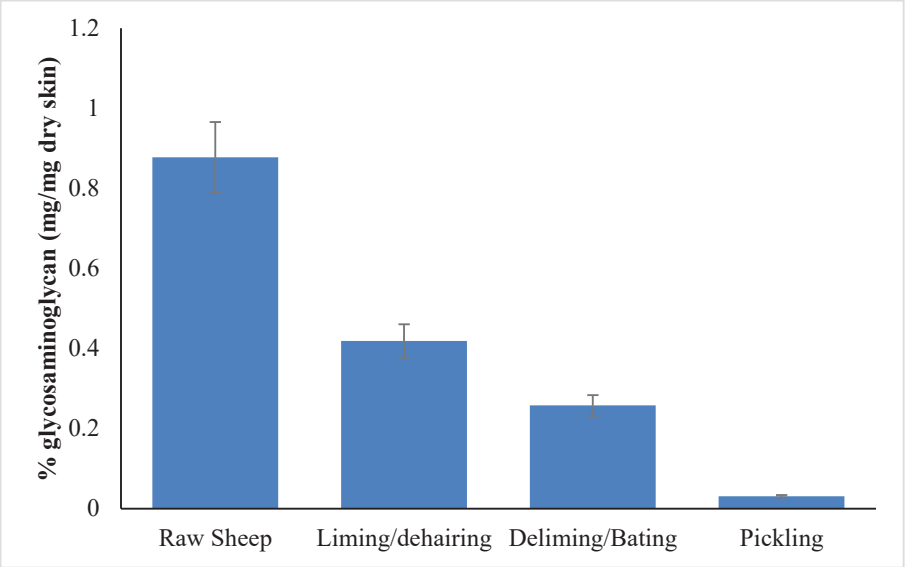

Figure 58: Glycosaminoglycan content of sheep skin during the leather processing steps. Error bars represent standard deviation.

5.3.3 Quantitation of carbohydrates in animal skins

Carbohydrate content was measured using the phenol-sulfuric acid method in a microplate format [416]. This is an easy and reliable method that can be used to measure the total carbohydrates in oligosaccharides, proteoglycans, glycosaminoglycans, glycoprotein and glycolipids [416, 422-424].

Carbohydrates were released from skin samples by hydrolysis with 1.0 M sulfuric acid at 100 ºC for 8 hours. These conditions have been shown to extract most of the carbohydrates from the sample [425]. A calibration curve was obtained using different concentrations of glucose from 20, 40, 60, 80 and 100 pmol/well (Figure 59).

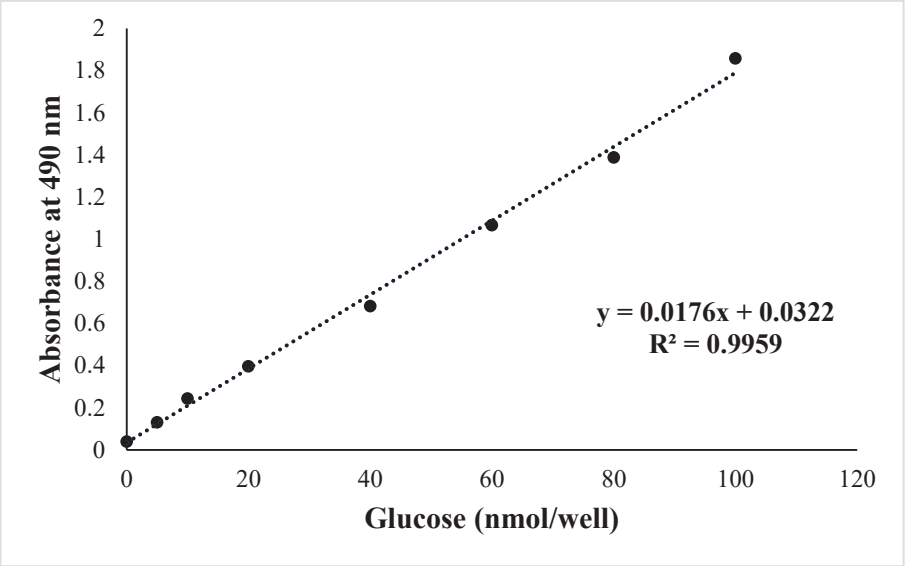

Figure 59: Calibration curve of glucose.

The total carbohydrate content of sheep, goat, deer and cow skins was in good agreement with the results obtained from the glycosaminoglycan analysis. Sheep skin had by far the highest concentration of carbohydrates while that of deer and cow skins was similar (Figure 60). While goat skin had a lower glycosaminoglycan content than that of either cow or deer skin its total carbohydrate content was approximately the same as those skins. This implies that goat skin may contain fewer sulfated oligosaccharide chains than the other skins, but must have more *O*-linked or even *N*-linked glycans associated with either proteins or lipids in the skin. Further work needs to be done to find the source of these differences. Figure 61 shows that carbohydrate content is lost from sheep skin in even steps during processing. This is at odds with the results of the glycosaminoglycan assay, which showed a big drop in glycosaminoglycan content after liming and after bating. This suggests that some carbohydrates are not associated with the glycosaminoglycans. It is also possible that hyaluronic acid resists the processing conditions more than

has been predicated. Another more likely explanation is that some carbohydrates are linked through N- or O- glycosylation

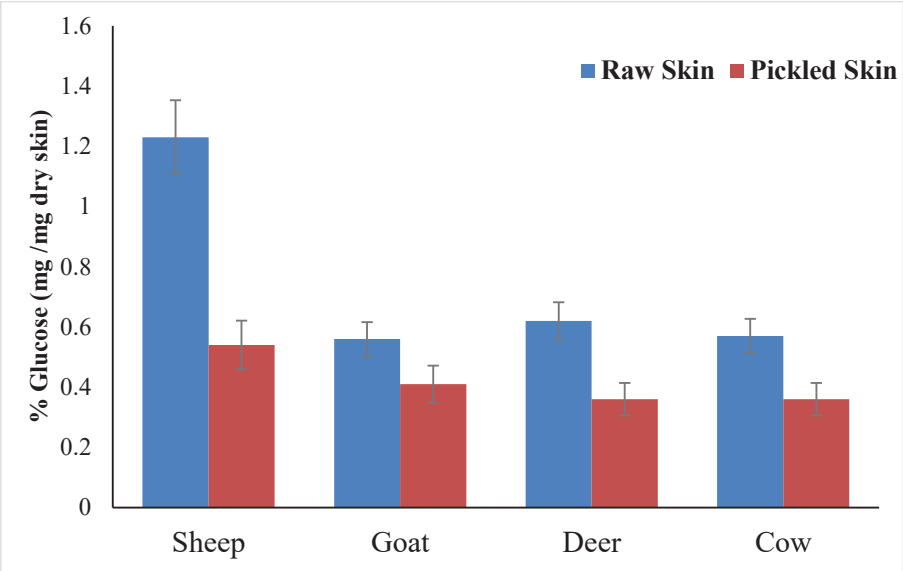

Figure 60: Carbohydrate content in sheep, goat, deer and cow in raw and pickled skins. Error bars represent standard deviation.

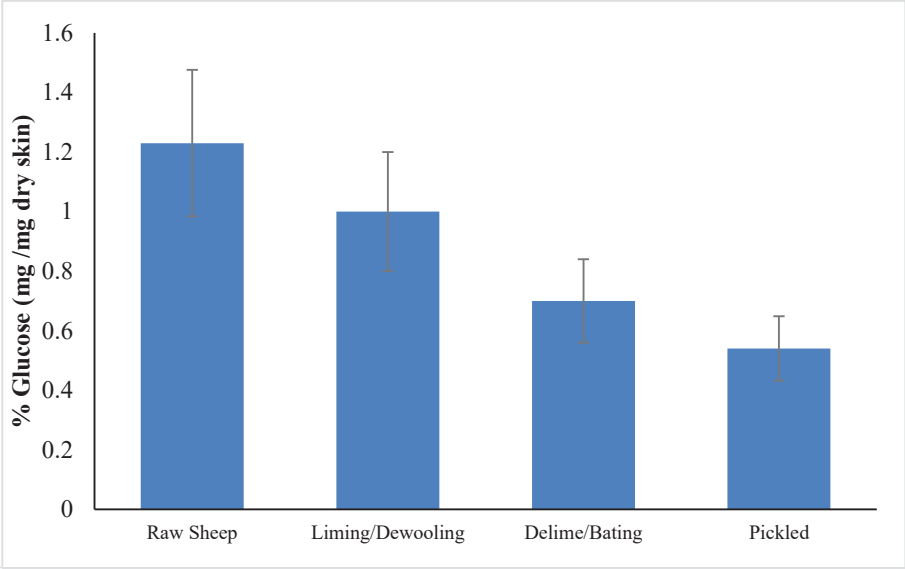

Figure 61: Carbohydrate content in sheep skin during various processing steps. Error bars represent standard deviation.

5.3.4 Analysis of lipids in animal skins

It is clear that the skins of different animals contain different amounts of total lipid (Figure 62). Sheep raw skin appeared to have more lipid, which is not surprising as it is known to have a fat layer between the grain and corium layers [2]. Goat, deer and cow skins appeared to have similar concentration of lipid.

Although both 10 % H_2SO_4 and bromothymol blue stained all lipids, charring the plates with 10 % H_2SO_4 gave more intense spots. Figure 63 shows typical results of the lipid spots on a silica TLC plate that become visible when charred in the presence of 10 % H_2SO_4. It shows the distribution of the various lipid classes in the raw skins of sheep, goat, deer and cow. The different lipids can be identified on the basis of comparison with other studies [312, 315, 418, 419, 426, 427].

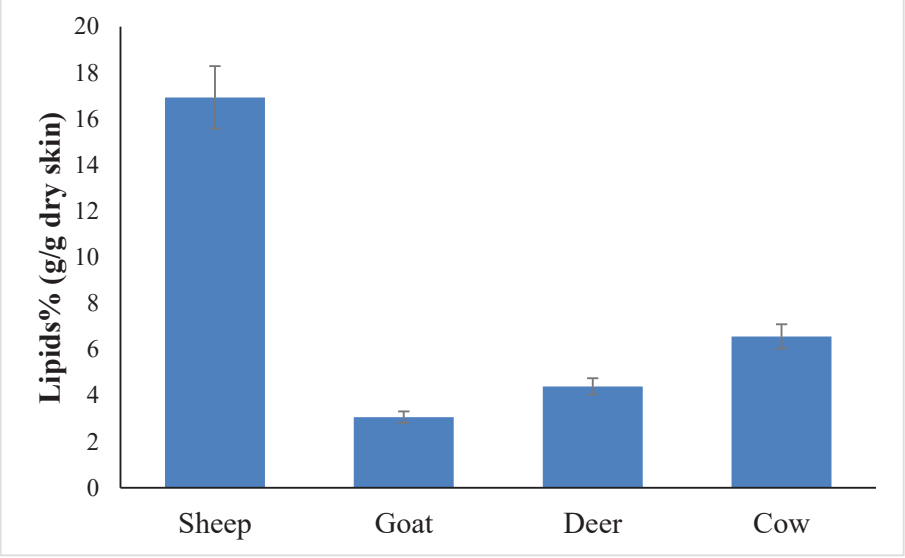

Figure 62: Lipid content in sheep, goat, deer and cow skins. Error bars represent standard deviation.

When the TLC plates were sprayed with molybdic blue stain to detect phospholipids, it was seen that phospholipids had not moved in the gradient [418, 427]. After spraying 10 % H_2SO_4 then charring, both sterols and sterol esters

appeared at the beginning of heating as pink to red spots which was used to locate them on the TLC plate [418, 419].

Interestingly, the lipid distribution in each animal skin was different. The animal skins showed appreciable amounts of phospholipids, although deer and goat skins seemed to have slightly higher concentrations than sheep and cow skins. In the free fatty acid and monoglycerides region, well resolved spots could be seen for all animal skins although sheep and cow skins had slightly more than goat and deer skins. It is also appeared that goat and deer skins have more sterol and sterol esters than sheep and cow skins. The triglyceride region shows the most significant differences between the different animal skins. Sheep and cow skins show significant amounts of triglycerides, while goat and deer skins either show faint or no spots in this region.

The plasmalogens appeared in sheep and cow skins, while O-alkyl diglycerides appeared only in sheep skin. In the sterol ester region, goat skin had the most intense spots and cow skin the lightest spots. Fatty acids, methyl esters and waxes appeared in the region between the plasmalogens and sterol esters. Goat and deer skins seemed to have more of sterol esters than sheep and cow skins [428, 429]. Some spots of shorter chain length of fatty acids appeared between spots 3 and 4 (Figure 63) [430]. These were not detected in goat, deer and cow skins whereas they were clearly present in sheep skin.

Although cellulose TLC (Figure 64) did not separate all lipids, it was used as a complimentary tool to confirm results previously obtained and discussed (Figure 63). Only four spots were detected on the cellulose TLC plate compared to 11 spots observed on the silica TLC plate, due to incomplete separation. During heating the

TLC plate in an oven, it was observed that spots 2 and 4 were initially turned into pink and were therefore identified as sterols and sterol esters. These were more intense in goat and deer skins than sheep and cow skins suggesting that sterols and sterol esters are present in higher concentrations in goat and deer skins than sheep and cow skins. Spot 1 representing the phospholipids appears to be more intense in goat and deer skins compared to sheep and cow skins. Spot 3 was observed in sheep and cow skins and not in goat and deer skins.

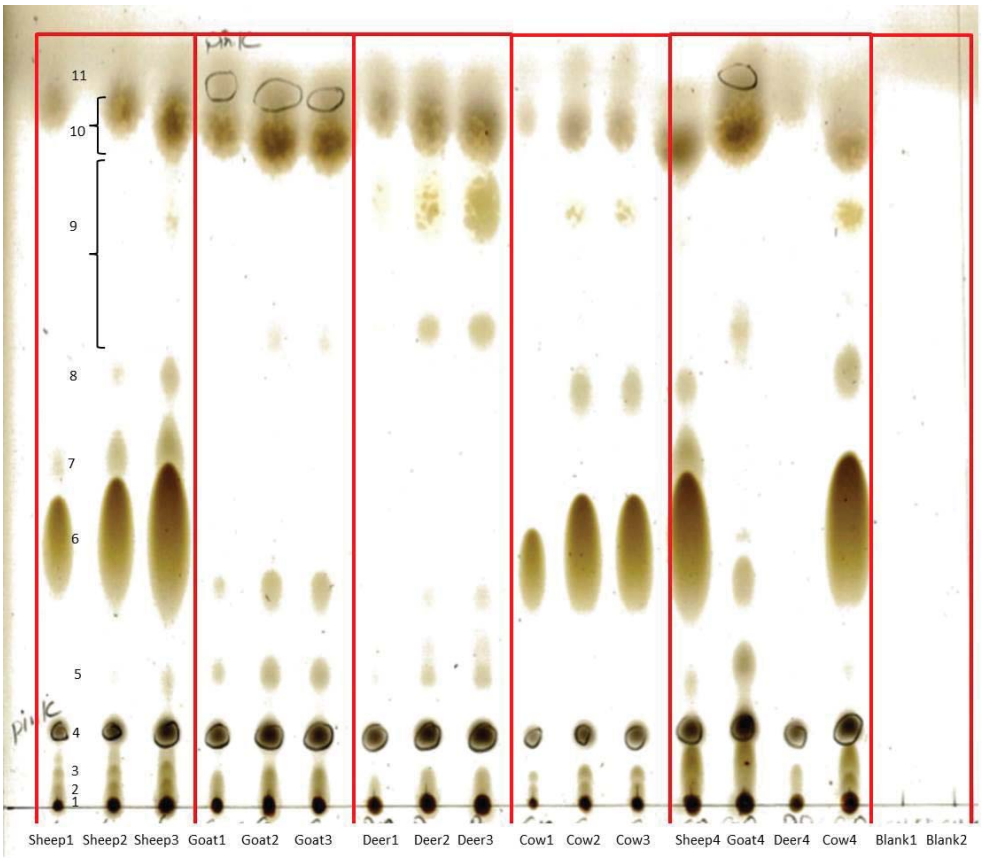

Figure 63: Silica TLC of total lipid extracts of the sheep, goat, deer and cow raw skins. Skin1, skin2 and skin3 indicate increased application volumes of total lipid. (1) Phospholipids (PLS), (2) Monoglycerides (MG), (3) Free fatty acids (FFA), (4) Sterols (S), (5) Diglycerides (DG), (6) Triglycerides (TG), (7) O-alkyl diglycerides (OAD), (8) Plasmalogens (P), (9) fatty acids esters (FFE), (10) Waxes and (11) Sterol esters (SE). [315, 418, 426]. The TLC plate was developed using chloroform then the plate was charred with 10 % H_2SO_4. Spots 4 and 11 were pink before turning black. Blank 1 and 2 are extraction solvent.

This strongly indicates that goat and deer skins contain a much lower concentration of triglycerides compared to sheep and cow skins. The results from cellulose TLC (Figure 64) perfectly match the results obtained from silica TLC (Figure 63).

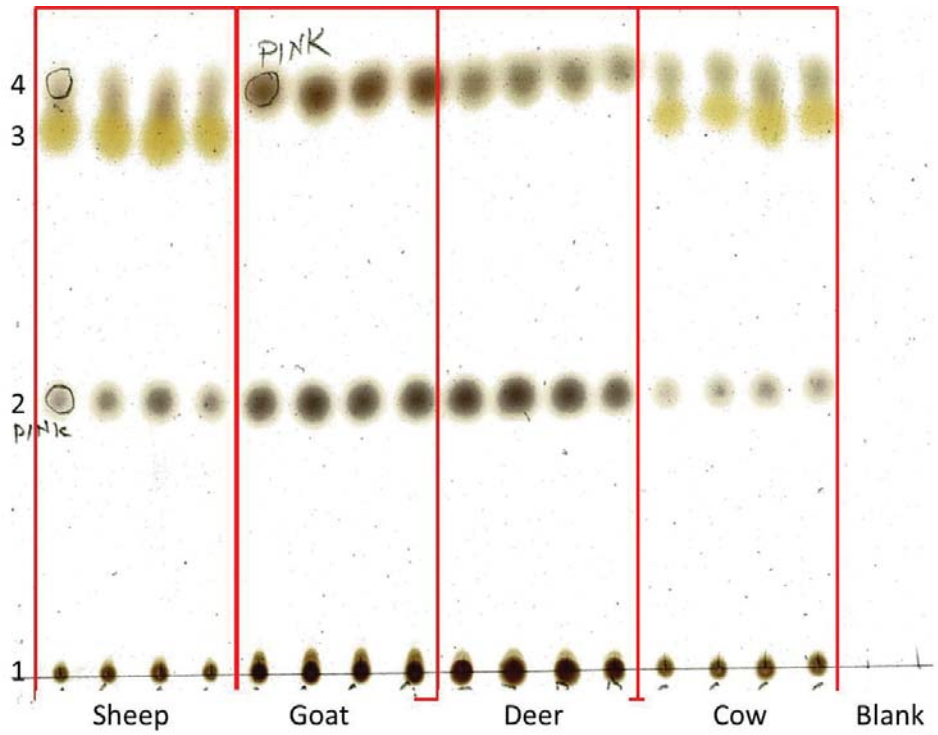

Figure 64: Cellulose TLC of total lipid extracts of the sheep, goat, deer and cow raw skins. (1) Phospholipids, (2) Sterols, (3) Triglycerides, (4) Sterol esters. Plate developed using chloroform then charred with 10 % H_2SO_4. Spots 2 and 4 were pink before turning black. Several lipid classes were not separated as well as by silica TLC. Blank 1 and 2 are extraction solvent.

6 CHAPTER SIX: Isolation, Purification and Characterisation of Crosslinks

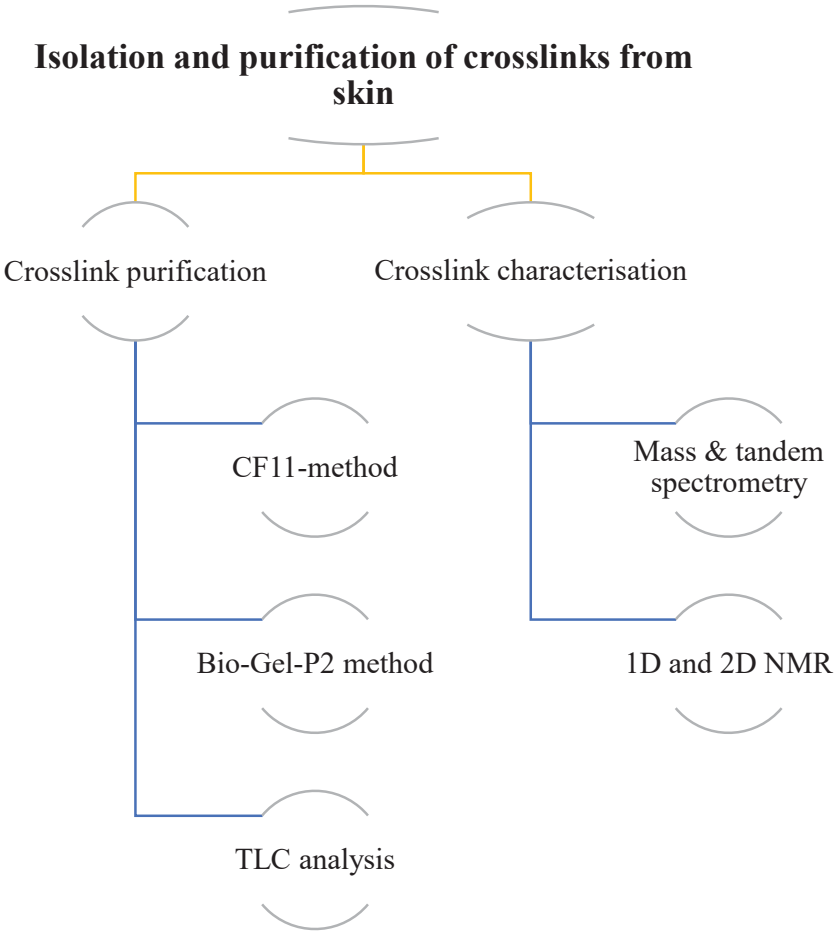

6.1 Introduction

The development of the quantitation method for collagen crosslinks requires crosslink standards. However, the major crosslink standards in skin (HLNL, HHL and HHMD) are not commercially available. These crosslinks, therefore, had to be isolated, purified and their chemical structures verified before work could begin to develop the quantitation method. To do this, crosslinks were isolated from skin using several sequential purification steps based on previously published methods. The concentration of crosslinks is very low in skin, so this required the processing of large quantities of skin (~ 100 g).

To isolate the crosslinks from skin samples, skin was reduced using sodium borohydride before the crosslinks were released from the reduced skin by acid hydrolysis. They were then enriched by CF11-column chromatography, which removed most of the amino acids and produced a solution containing mainly crosslinks. Next, they were fractionated by preparative size exclusion chromatography using Bio-Gel®-P2 (Fine, Bio-Rad) as the stationary phase packed in two sequentially linked columns (1.5 cm × 90 cm) and (0.7 cm × 140 cm). The eluting solvent was 0.5 M acetic acid [94, 176]. Small fractions (0.5 – 1 mL) were collected from both columns using TLC to monitor their crosslink content. The fractions were then analysed by mass spectrometry. The resultant crosslink rich samples were further purified using preparative TLC and characterised using mass spectrometry, tandem mass spectrometry and NMR. Mass spectrometry measures the accurate monoisotopic masses and the fragmentation patterns of the crosslinks can be used to verify their structures. In order to resolve their complete chemical structures, 1D and 2D NMR spectra were recorded and analysed.

6.2 Experimental procedures

6.2.1 Chemicals and reagents

Sodium phosphate, sodium chloride, sodium hydroxide, phenol, methanol, cellulose fibrous (CF11), ethyl acetate and formic acid were purchased from Sigma. Amino acid standards, sodium borohydride (>99%), Deuterium oxide (99.9 atom % D) were purchased from Sigma Aldrich (St. Louis, MO, USA). Deionized water was obtained from a Milli-Q Ultra-pure water system (Dubuque, IA, USA). Mass spectrometry grade water, acetonitrile, methanol and formic acid (>99%) were purchased from Fisher Chemical (Fair Lawn, NJ, USA). Hydrochloric acid and acetic acid were purchased from Panreac (Barcelona, Spain). *n*-butanol (97%) was purchased from Ajax Finechem, Univar (TarenPoint, NSW, Australia).

6.2.2 Preparation of skin samples

All skin samples were obtained as described in Chapter 3, Section 3.2.2.

6.2.3 Reduction of skin samples

Skins from sheep, goat, deer and cow were prepared as described in chapter 3 (sections 3.2.2). Skin samples of about 100 g were suspended in 1.0 L of 0.1 M phosphate buffer, containing 0.15 M sodium chloride and pH adjusted to 7.5. They were then homogenized using a Polytron homogenizer (Janke & Kunkel, IKS, Germany) to produce a skin-buffer mixture. This mixture was then reduced by sodium borohydride (3.5 g) dissolved in a minimum volume of 1 mM cold sodium hydroxide before being added to the skin-buffer mixture. This mixture was incubated at 25 ºC for 24 hours then reduction was stopped by adjusting the pH to 3.0 using glacial acetic acid. The resulting mixture was centrifuged at 23,000 × g for 30 minutes, the supernatant discarded and the pellet was washed three times

with water to remove any excess of acetic acid and salt. The reduced skin was then lyophilised and stored at - 20ºC for further analysis. This was repeated several times to obtain about 1.0 kg of dry reduced skin.

6.2.4 Hydrolysis of skin samples using 6 M hydrochloric acid

A dry reduced skin sample was mixed with a 2.0 L of 6 M hydrochloric acid containing 3 % phenol and refluxed at 105 ºC for 72 hours. The large volume of the dark brown hydrolysate produced was filtered, and dried using a rotatory evaporator. The resulting viscous brown liquid was then rehydrated in a minimum volume of water (~ 100 mL) to obtain the maximum concentrations of soluble amino acids and crosslinks.

6.2.5 Crosslink Enrichment of crosslinks by CF11 column chromatography

A 5 % of CF11 slurry was prepared by suspending 100 g of CF11 powder in 2.0 L of butanol-water-acetic acid (4:1:1, v/v/v). A 1.0 cm × 100 cm column plugged with glass-wool was filled with the 5% CF11 slurry and washed three times with 500 mL of butanol-water-acetic acid (4:1:1, v/v/v). The skin hydrolysate was applied and the initial eluent discarded. The column was then washed ten times with 250 mL of butanol-water-acetic acid (4:1:1, v/v/v) containing 10% methanol (v/v). Ten mL fractions were collected and their amino acid and crosslink content monitored by TLC. Once most of the amino acids had been removed, the crosslinks were eluted using 2.0 L of water. The resulting crosslink-rich solution was dried on a rotatory evaporator then rehydrated in about 10.0 mL of water. Before proceeding to the next stage, the presence of the crosslinks in the sample was confirmed by mass spectrometry.

6.2.6 Crosslink purification by size exclusion chromatography

One mL samples produced as described above, were loaded onto a calibrated Bio-Gel P2 column (1.5 cm × 90 cm) equilibrated with 0.5 M acetic acid. The column was washed with 0.5 M acetic acid at a flow rate of 20 mL/hour and 5.0 mL fractions were collected. The elution of the crosslinks from the column was monitored using TLC with either butanol:water:acetic acid (4:1:1, v/v/v) or ethyl acetate:water:acetic acid (1.5:1:1, v/v/v). The fractions containing only crosslinks were pooled together then lyophilised and rehydrated in 200 µL of water. A second sequential purification was carried out on a calibrated Bio-Gel P2 column (0.7 cm × 140 cm) using 0.5 M acetic acid at a flow rate of 2.5 mL/hour and collecting 0.2 mL fractions. Each fraction was analysed by mass spectrometry and fractions containing pure crosslinks of HLNL, HHL or HHMD were pooled together, lyophilised and rehydrated in 0.2 mL of deuterium oxide.

6.2.7 Characterization of crosslinks by NMR

NMR spectra were recorded using a 700 MHz NMR spectrometer Bruker Avance (Bruker Biospin, Rheinstetten, Germany) operating at a ^{1}H frequency of 700.13 MHz and equipped with a cryoprobe. ^{1}H spectra were recorded using the standard Bruker "zgpr" pulse sequence with a spectral width of 14.3 kHz digitised with 64k points. A presaturation field strength of 50 Hz was used to suppress the residual HOD signal in conjunction with a recycle delay of 2 s. ^{13}C and ^{13}C DEPT-135 spectra were recorded using a spectral width of 42 kHz and digitized with 64k points and a recycle delay of 2 s. Two dimensional double-quantum filtered COSY, multiplicity edited HSQC and HMBC spectra were recorded with the following COSY parameters: spectral width 8.4 kHz digitised with 2048 x 400 points and a

recycle delay of 2 s. The residual HOD signal was suppressed using a weak pre-saturation pulse with a field strength of 7 Hz. HSQC spectral widths of 11.3 kHz (^{1}H) and 29.2 kHz (^{13}C) were digitised with 1024 x 400 points. Bi-level adiabatic ^{13}C decoupling was used during the acquisition followed by a recycle delay of 1.5 s. HMBC spectral widths of 7.2 kHz (^{1}H) and 35.2 kHz (^{13}C) were digitised with 4096 x 256 points. A low-pass filter was used to suppress $^{1}J_{CH}$ couplings. The spectrum was acquired without ^{13}C decoupling and used a recycle delay of 1.5 s. All 2D spectra used pulsed-field gradients for coherence selection. Spectra were processed with Topspin 2.1.8 (Bruker Biospin, Rheinstetten, Germany) using standard parameters. Quantitation of the crosslinks in the samples purified as described above was preformed using ^{1}H NMR spectra as above but employing a 30^{o} pulse without solvent presaturation and with a recycle delay of 4 s. Signals from the solute were integrated against the signal of formic acid, which was added to the sample at a concentration of (1-100) mM.

6.2.8 Characterisation of crosslinks by liquid chromatography-mass spectrometry

Samples of 2 µL were injected directly into the mass spectrometer (Agilent 6520 Q-TOF, Agilent Technologies, Hanover, Germany) using a solvent of 50 % acetonitrile in water containing 0.1 % (v/v) formic acid and a flow rate of 200 µL/min. The capillary voltage of the electrospray ionisation source was 3.3 kV and positive mode scans from 100-1000 m/z were obtained using fragmentor and skimmer voltages of 145 and 55 V, respectively. The total ion chromatograms (TIC) produced were examined using Agilent MassHunter Workstation Qualitative Analysis software version B.06.01 SP1 (Agilent Technologies, Santa Clara, CA, USA).

6.3 Results and discussion

6.3.1 Stabilization of crosslinks by reduction

The reducible crosslinks (DHLNL, HLNL and LNL) were first stabilised by reduction with sodium borohydride [164]. The imine bond was reduced into a secondary amine which did not degrade upon hydrolysis with 6 M hydrochloric acid (Figure 65) [431]. The HHMD crosslink was also stabilised by reduction, although its unreduced structure, dehydro-histidino-hydroxymerodesmosine (deH-HHMD), is still controversial [6]. However, Tanzer *et al.* (1973), Hunt *et al.* (1973) and Bernstein *et al.* (1980) have reported that deH-HHMD is one of the major crosslinks in skin [103, 104, 159].

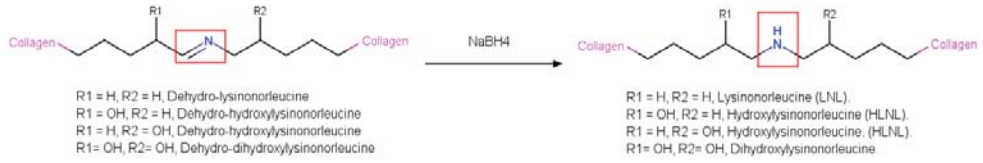

Figure 65: Stabilisation of the reducible crosslinks by reduction with sodium borohydride where the imine bond is reduced into secondary amine which is acid resistance.

6.3.2 Removal of amino acids by CF11 column chromatography

CF11 chromatography was first used by Ledvina and Bartos (1976) and Starcher (1977) to remove the amino acids from the elastin crosslinks (desmosine and isodesmosine) [177, 432] and has become a common procedure for the analysis of crosslinks because it improves detection sensitivity [164, 177, 178]. As a result of this study, a new method was developed that can quantitate crosslinks without the need for CF11 [393]. When a sample containing crosslinks was loaded on CF11 column, free amino acids were washed off the column using butanol-water-acetic

acid (4:1:1). This work found that the addition of 5% (v/v) methanol significantly improved the removal of basic and acidic amino acids. This is because crosslinks are far more hydrophilic than amino acids and therefore remain strongly adsorbed to CF11 [433]. As a result, amino acids were largely removed as seen by TLC analysis of the fractions (Figure 66). Most of the amino acids appeared to be eluted by the organic solvent while fractions of lysine, hydroxylysine, histidine, proline, hydroxyproline and crosslinks were eluted in the water washes (Figure 66). The TLC results were confirmed by amino acid analysis using AQC-derivatization followed by LC-MS (Figure 67). It is clear that butanol-water-acetic acid washes contained mainly acidic and neutral amino acids while the water washes contained proline, hydroxyproline and basic amino acids.

6.3.3 Purification of the crosslinks by size exclusion chromatography

CF11 chromatography did not completely remove all amino acids from the sample. However, because the crosslinks have higher molecular weights than basic amino acids they were successfully removed prior to crosslink purification by size exclusion chromatography using Bio Gel-P2 [434].

The Bio Gel-P2 columns were calibrated using cytochrome C to determine the void volume and cyanocobalamin to mark the position of lysine. Ascorbic acid and sodium chloride were also used to mark the position of other amino acids and salts, respectively [434]. In previous reports, desmosine eluted between the void volume and lysine suggesting that the crosslinks HLNL, HHL and HHMD should behave in a similar manner because of their similar sizes [435, 436].

The separation of the crosslinks from all traces of amino acid was successfully achieved using SEC. Eluted fractions were visually identified by TLC (Figure 68)

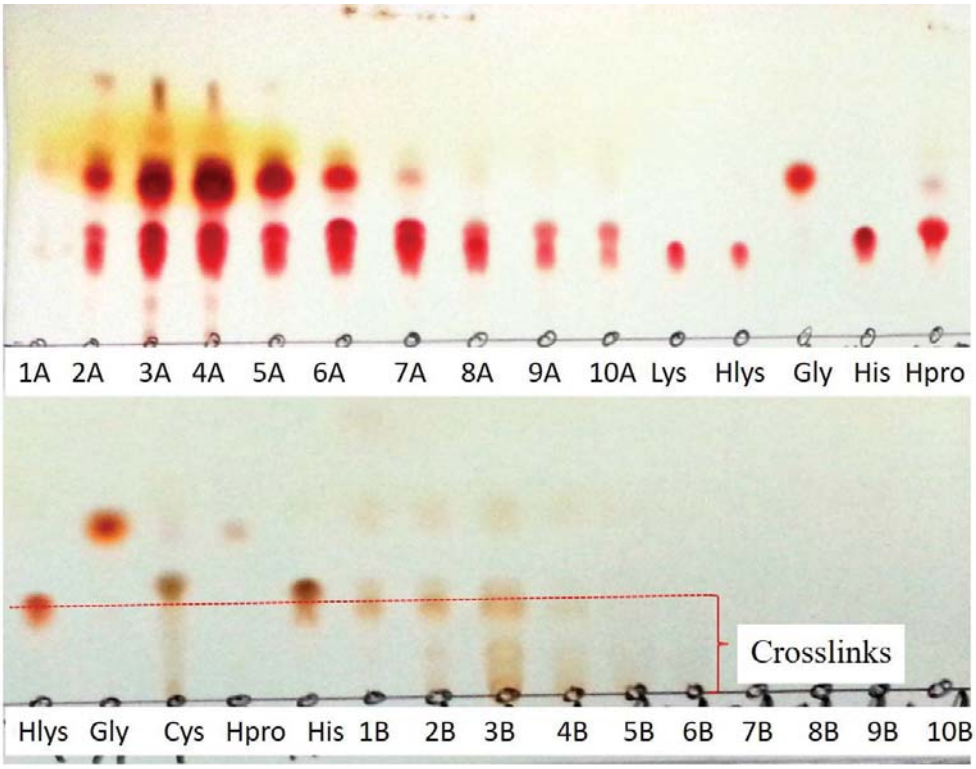

Figure 66: TLC carried out using ethyl acetate:water:acetic acid (1.5:1:1) on the fractions eluted with butanol-water-acetic acid (4:1:1) (1A to 10A) and water (1B to 10B). Cystine (Cys), Lysine (Lys), hydroxylysine (Hlys), glycine (gly), histidine (His) and hydroxyproline (Hpro) standards were used to mark the location of the different spots. To detect the spots, the TLC plate was sprayed with ninhydrin then heated at 100 ºC for 20 minutes.

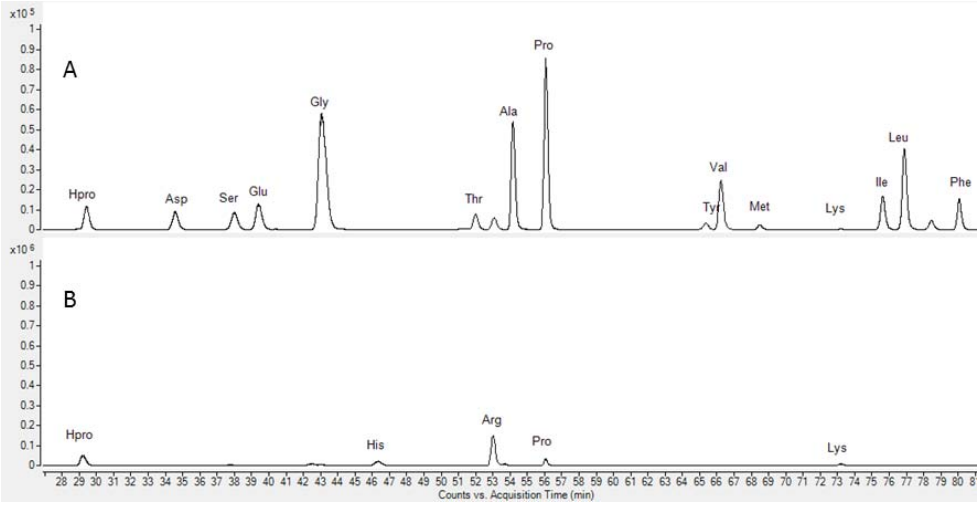

Figure 67: HPLC separation of amino acids using AQC-derivatisation of (A) amino acids in butanol-water-acetic acid (4:1:1) fractions and (B) amino acids in water fractions from the CF11 column. See chapter 4 for the separation conditions.

and mass spectrometry (Figure 69). It is clear that amino acids (fractions 66 and 71) were completely removed to produce pure crosslinks (fraction 28 to 40). Interestingly, HHMD was obtained pure while HHL and HLNL still required further purification (Figures 68 & 69). A longer and narrower Bio Gel-P2 column of 0.7 cm × 140 cm was therefore used to obtain pure HHL and HLNL with the same procedure.

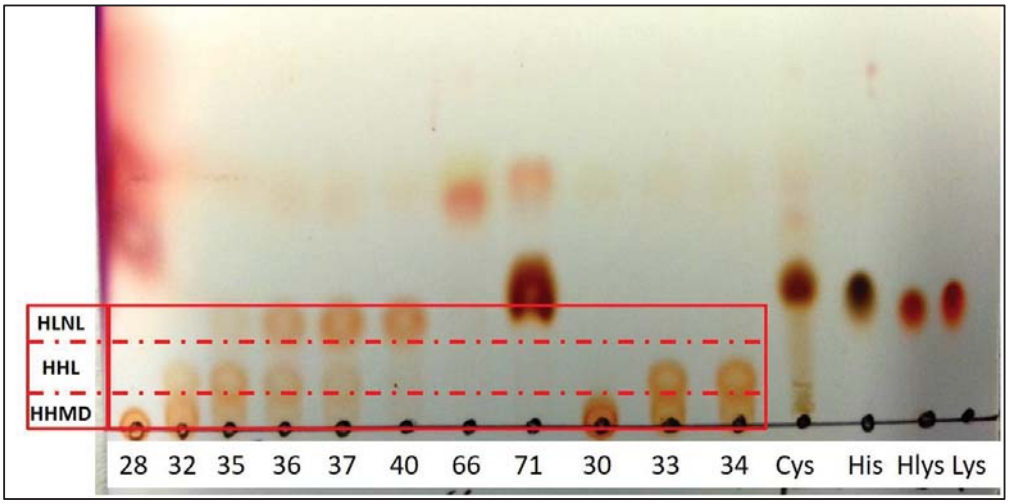

Figure 68: Fractions from size exclusion chromatography were analysed using TLC with ethyl acetate:water:acetic acid (1.5:1:1) as the mobile phase. HHMD is seen pure in spot 28 while HHL and HLNL are partially pure in spots 32 to 37. Lysine (Lys), hydroxylysine (Hlys), histidine (His) and hydroxyproline standards were used to mark the location of the different spots. To detect the spots, the TLC plate was sprayed with ninhydrin then heated at 100 ^{o}C for 20 minutes.

6.3.4 Characterisation of HHMD, HHL and HLNL crosslinks

6.3.4.1 Introduction

It was important to check the purity of the purified crosslink fractions after each separation step. It was also crucial to verify their structures, as although accurate mass gives elemental composition, there is the possibility of isobaric structures. To do that, tandem mass spectrometry and NMR were utilized. The accurate concentrations of the purified crosslink samples were also measured using ^{1}H NMR

with formic acid as an internal standard. Prior to NMR, the purity of crosslinks was checked using mass spectrometry. The monoisotopic masses of the

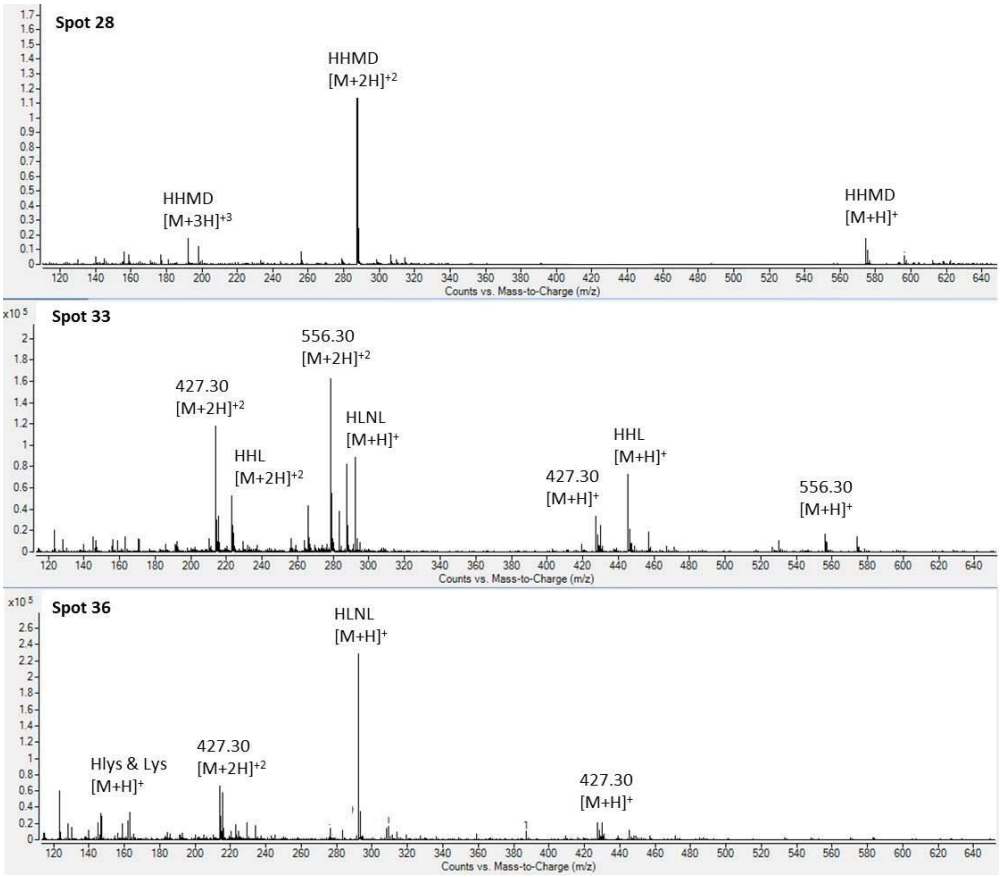

Figure 69: Total ion chromatogram of the mass spectra of three spots 28, 33 and 36 as analysed by TLC in Figure 68. Spot 28 appears to be pure HHMD while spots 33 and 36 have a mixture of HHMD, HH, HLNL and basic amino acids and suspected new crosslinks of 427.30 and 556.30 m/z. See section 6.2.8 for experimental conditions.

crosslinks and their relative intensities were recorded. Their fragmentation patterns were also analysed by tandem mass spectrometry. For NMR, all purified crosslink samples were dried under high vacuum then rehydrated in 200 μL of deuterium oxide and placed in a Shigemi NMR tube to improve the NMR data collection.

The complete chemical structures of HLNL, HHL and HHMD were resolved using 1D (^{1}H, ^{13}C and DEPT-135) and 2D NMR (COSY, HSQC and HMBC) spectra. The 1D NMR spectra of the major moieties of crosslinks, including lysine and hydroxylysine and histidine, were also recorded to help with the interpretation of the NMR spectra of the crosslinks. Finally, the concentration of each crosslink was accurately determined using formic acid as an internal standard in ^{1}H NMR. All recorded NMR spectra are recorded in the appendices (See Appendix under "Chapter 6-NMR Spectra" folder).

6.3.4.2 Histidine, lysine and hydroxylysine used for NMR

Norleucine and histidine were diastereomerically pure. Lysine contained a mixture of two diastereomers at C-2 and hydroxylysine was a mixture of four diastereomers at C-5 and C-2 (Figure 70). All NMR spectra recorded for histidine, lysine, hydroxylysine and norleucine are listed in the appendix. All NMR spectra of ^{1}H, ^{13}C and DEPT-135 for histidine, lysine and hydroxylysine were analysed and summarised (Table 18).

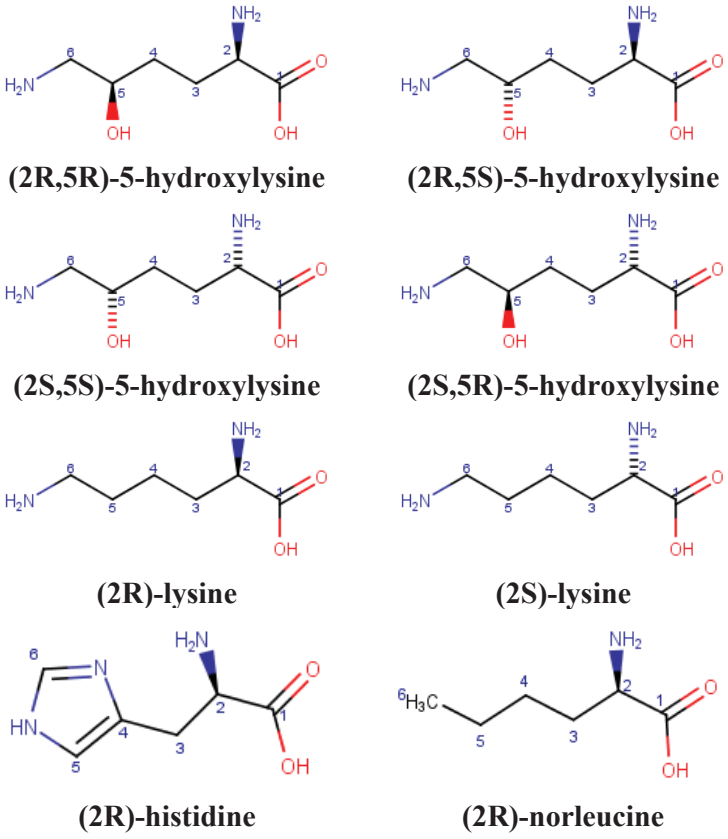

Figure 70: Chemical structures of lysine, hydroxylysine, histidine and norleucine including their diastereomers.

6.3.4.3 Mass spectra of lysine, hydroxylysine and histidine

The monoisotopic masses of lysine, hydroxylysine and histidine were measured by mass spectrometry and their fragmentation patterns were investigated by tandem mass spectrometry. The monoisotopic masses of lysine, hydroxylysine and histidine were 146.1055, 162.1004 and 155.0695 g/mol, respectively in agreement with theoretical values.

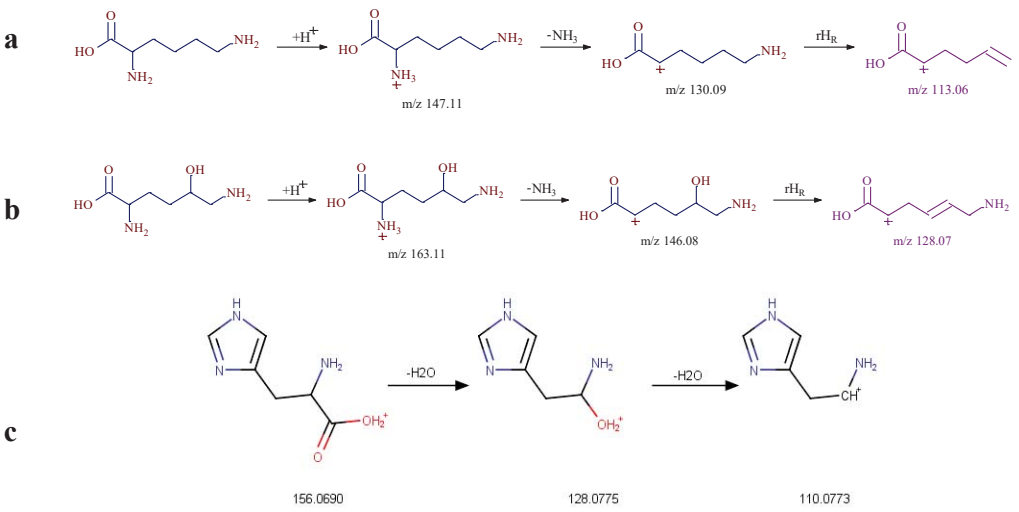

Figure 71: Fragmentation pathway of (a) lysine, (b) hydroxylysine and (c) histidine.

Only singly charged ions were observed and their optimum CID energy ranged from 10-15 KeV. Lysine produced product ions of 130.09 m/z, 113.06 m/z and several masses below 100 m/z (Figure 71a). Fragmentation of hydroxylysine gave 146.08 m/z, 128.07 m/z and several masses below 100 m/z (Figure 71b). Histidine fragmentation gave two characteristic product ions of 128.08 m/z and 110.07 m/z (Figure 71c).

6.3.4.4 NMR of Histidine

The ^{1}H and ^{13}C NMR spectra of histidine were recorded (see appendix). Histidine is made up of 6 carbon atoms so 6 singlet peaks were observed in the ^{13}C spectrum. Its imidazole ring gives three characteristic peaks at 127.38, 134.00 and 117.68 ppm which are in good agreement with previous reports [437]. The peak of the quaternary carbon at 127.38 ppm disappeared in the DEPT-135 spectrum and the peaks of tertiary carbons at 134.00 ppm and 117.68 ppm were positive in the DEPT-135 spectrum. The chemical shift of C-2 (the α-carbon) was observed at 53.52 ppm

and was positive in the DEPT-135 spectrum while the chemical shift for C-3 was observed at 25.73 ppm and was negative in the DEPT-135 spectrum. The most deshielded carboxy carbon was observed at 174.51 ppm due to its direct attachment to oxygen.

The full integration of the ^{1}H spectrum of histidine is 5 which is corresponded to the total number of protons in histidine. Its imidazole protons at C-6 and C-5 gave two characteristic broad singlet peaks at 8.58 ppm and 7.31 ppm, respectively [438]. The chemical shift of the proton attached to C-2 was observed at 3.95 ppm. This was a triplet due to coupling with two protons on C-3 [438]. Finally, the chemical shift of the two protons attached to C-3 was observed at 3.27 ppm which was a doublet of doublet of doublets (ddd) due to long range coupling with imidazole ring protons [438].

6.3.4.5 NMR of Lysine

The ^{1}H and ^{13}C NMR spectra of lysine were recorded (see the appendix for this chapter). Lysine is made up of 6 carbon atoms, and 6 peaks were observed in its ^{13}C spectrum. Although lysine contains two diastereomers, all peaks on ^{13}C spectrum were seen singlets, which suggests that the stereoisomerism around C-2 has no influence on the NMR to produce peaks at different intensities. In other words, lysine diastereomers are not distinguishable by NMR. The most deshielded carboxy quaternary carbon was observed at 174.30 ppm, and this disappeared in the DEPT-135spectrum. The chemical shift of C-2 (the α-carbon) was observed at 54.48 ppm which was positive in the DEPT-135 spectrum. The chemical shifts of the remaining secondary carbons (C-6, C-3, C-5 and C-4) were observed at 39.06 ppm, 29.84 ppm, 26.37 ppm and 21.40 ppm, respectively.

In the ^{1}H spectrum of lysine, the most deshielded protons, those attached to carboxy C-2, were observed at 3.67 ppm as a triplet. The chemical shifts of protons attached to C-6 were observed as a triplet at 2.94 ppm. The diastereotopic protons attached to C-3 were observed at 1.82 ppm as a multiplet due to their different couplings. The quintet observed at 1.64 ppm was assigned to the protons attached to C-5 and the multiplet at 1.40 ppm was assigned to protons at C-4.

6.3.4.6 NMR of hydroxylysine

The ^{1}H, ^{13}C, DEPT-135, COSY, HQC and HMBC spectra of hydroxylysine were recorded (see the appendix for this chapter). Hydroxylysine is made up of 6 carbon atoms, therefore 6 peaks were observed in its ^{13}C spectrum. The chemical shift of the proton attached to C-5 was observed at 3.80 ppm and its ^{13}C chemical shift was observed at 67.15 ppm. This carbon is the major glycosylation site of the collagen molecule and therefore influences crosslink formation [407, 408]. It is also a stereogenic center which results in the production of two stereoisomers of the hydroxylysine. These naturally occurring hydroxylysine diastereomers are controversial [401, 405, 409].

Strikingly, all the peaks in the ^{13}C spectrum of hydroxylysine were appeared to be doublets (Table 18) (see appendix "Chapter 6-NMR spectra/Hydroxylysine ^{13}C NMR) which is due to the presence of hydroxylysine diastereomers as a result of the chirality around C-5 (the δ-carbon) [439, 440]. This diastereomeric mixture of hydroxylysine results in different chemical shifts of ^{13}C peaks of each of hydroxylysine diastereomers.

Looking at the ^{1}H NMR, the two protons attached to C-6 were observed at 3.08 ppm as a doublet of doublets (dd) and at 2.85 ppm as doublet of doublet of doublets

(ddd). The (dd) and (ddd) result from one proton coupled to two and three neighbouring protons by different coupling constant, respectively [445]. The diastereotopic protons on C-6 seen at 2.85 ppm and 3.08 ppm are coupled with protons on C-5 and C-6 through the ^{3}J and ^{2}J couplings, respectively. The other diastereotopic proton on C-6 is also likely to have a long-range proton-proton couplings (^{4}J) with proton on C-4. This supports that idea that the C-5 has two configurations (R and S), resulting in a diastereomeric mixture.

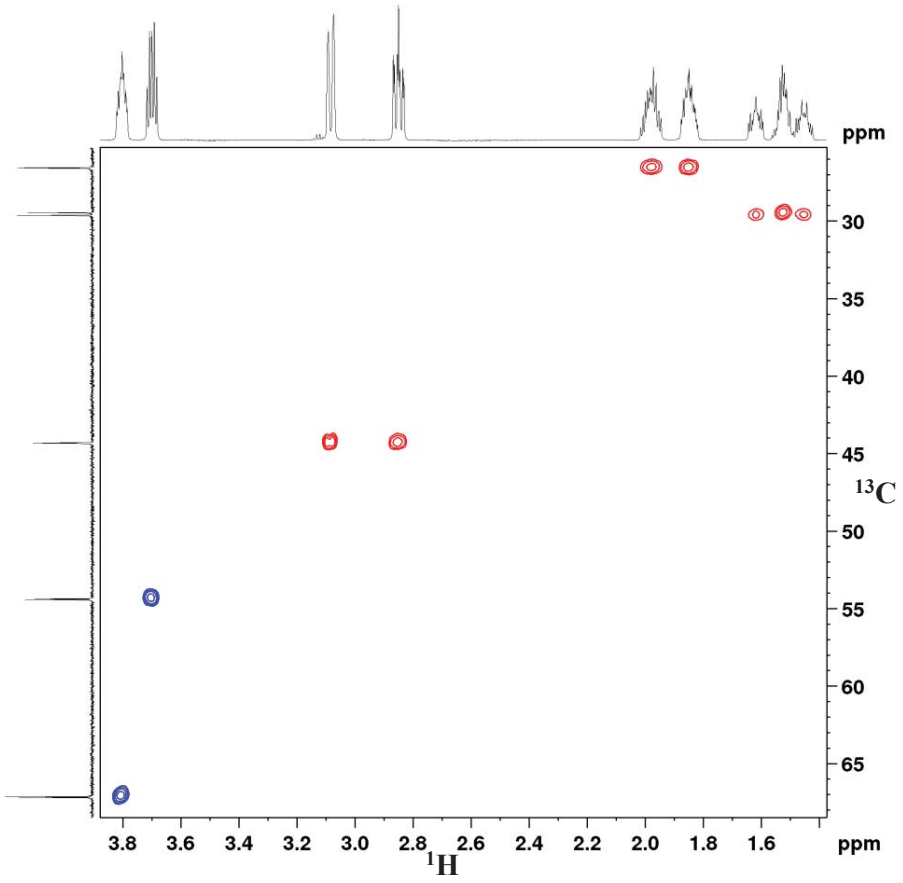

Figure 72: HSQC of hydroxylysine. Blue spots are positive peaks (CH_3 or CH) while red spots are negative peaks (CH_2) in DEPT-135 spectra.

The 2D HSQC confirmed the significant effect of the diastereomers on chemical shifts of the ^{13}C peaks (Figure 72). It is clear that C-6 is correlated to two different protons, at 3.08 ppm and 2.85 ppm. C-4 is also correlated to two different protons one at 1.45 ppm and 1.62 ppm and another at 1.52 ppm. C-3 is correlated to protons at 1.86 and 1.98 ppm. These findings support both the presence and the significant effect of diastereomers on NMR properties of hydroxylysine.

6.3.4.7 Characterisation of the HLNL crosslink

The structure of the HLNL was first suggested by Bailey and Peach in 1968 [78]. Tanzer *et al.* (1970) and Davis and Bailey (1972) synthesised HLNL and used periodate chemical degradation to confirm its structure (Figure 73) [441, 442]. Although two diastereomers of HLNL were isolated and identified from skin, their existence is controversial [154, 401, 405, 442]. It had previously been shown that hydroxylysine diastereomers form even after basic hydrolysis (see chapter 4 for details) [406, 407]. It was therefore, suggested that diastereomers of hydroxylysine will eventually produce HLNL diastereomers (see below for details).

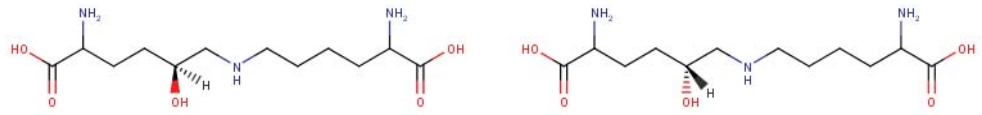

Figure 73: Chemical Structure of the two possible diastereomers of HLNL.

Nieuwendijk *et al.* (1999) and Cribiu *et al.* (2005) obtained HLNL by chemical synthesis and recorded its NMR. The NMR spectrum of HLNL isolated from skin has, however, not been previously reported [443, 444].

Table 18: The ^{1}H and ^{13}C chemical shifts of lysine, hydroxylysine and histidine.

Lysine		Hydroxylysine		Histidine	
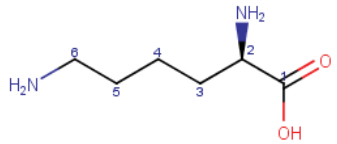		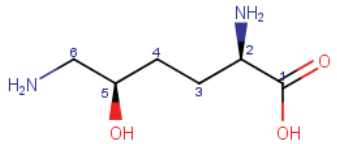		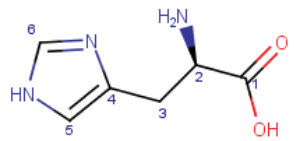	
^{1}H	**^{13}C**	**^{1}H**	**^{13}C**	**^{1}H**	**^{13}C**
1.40 (2H, m, H-3)	21.4 (C-4)	1.45, 1.52, 1.62 (2H, m, H-4)	26.52 & 26.55 (C-3)	3.27 (2H, ddd, H-3)	25.73 (C-3)
1.64 (2H, q, H-4)	26.37 (C-5)	1.86, 1.98 (2H, m, H-3)	29.45 & 29.54 (C-4)	3.95 (1H, t, H-2)	53.52 (C-2)
1.82 (2H, m, H-5)	29.84 (C-3)	2.85 (ddd), 3.08 (dd) (2H, m, H-6)	44.29 & 44.32 (C-6)	7.31 (1H, s, H-5)	117.68 (C-5)
2.94 (2H, t, H-6)	39.06 (C-6)	3.70 (1H, m, H-2)	54.35 & 54.41 (C-2)	8.58 (1H, s, H-6)	127.38 (C-4)
3.67 (1H, t, H-2)	54.48 (C-2)	3.80 (1H, m, H-5)	67.12 & 67.19 (C-5)		134.00 (C-6)
	174.55 (C-1)		174.29 & 174.33 (C-1)		172.51 (C-1)

6.3.4.7.1 Mass spectrum of HLNL

The monoisotopic mass of HLNL was measured as 291.2010 g/mol, which is in good agreement with previous reports [78, 442]. The mass spectrum of HLNL shows two characteristic singly and doubly charged ions at 146.6030 and 292.2010 m/z, respectively (Figure 74), and is evidence of the purity of the HLNL sample.

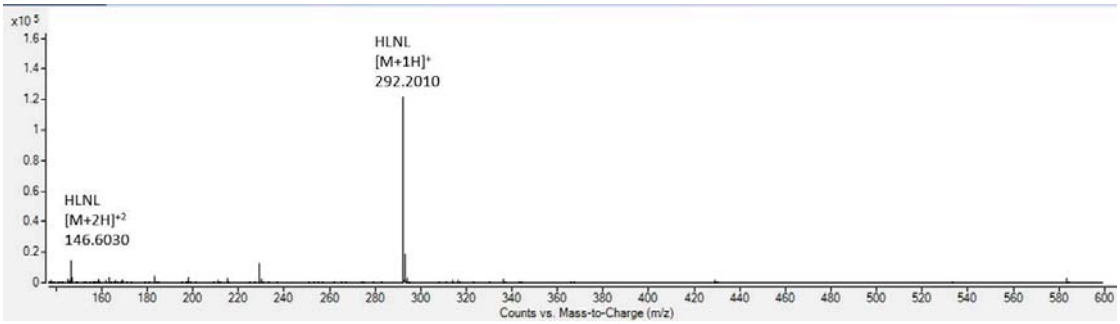

Figure 74: Mass spectrum of the HLNL showing the singly (292.2010 m/z) and doubly (146.6030 m/z) charged ions.

The energy required to fragment the singly charged HLNL (292.2010 m/z) was optimised at 17 KeV and 5 KeV for the doubly charged ion (146.6030 m/z). Figure 75 shows the typical product ions formed from the fragmentation of singly charged HLNL at 17 KeV.

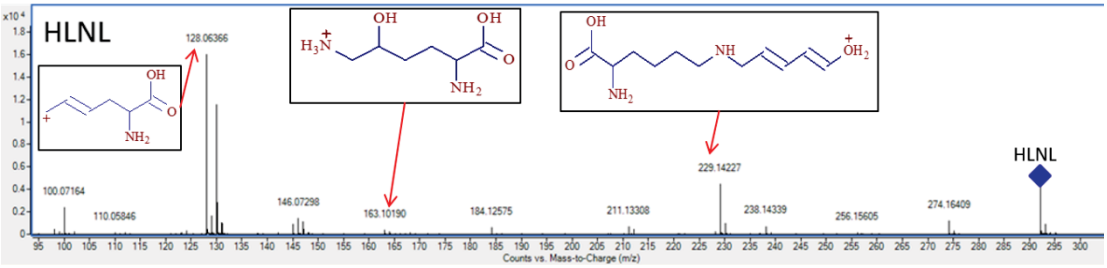

Figure 75: The major product ions formed from the fragmentation of HLNL at 17 KeV. Insets show the possible structures of selected ions. The blue diamond represents the parent ion. All possible major structures of HLNL fragments are given in the appendix for this chapter. (see "chapter 6 - MS-MS – fragments" folder).

The fragmentation pathway of HLNL is initiated by protonation either of the hydroxyl or amino groups to form water or an ammonium ion, respectively. This is followed by the cleavage and rearrangement of several bonds occurring in consecutive steps, each step producing an ion. Two of the possible pathways are given in Figure 76. These pathways produced ions that are similar to those produced by lysine and hydroxylysine, the two major moieties of HLNL. Such product ions are useful for the characterisation and quantitation of HLNL by tandem mass spectroscopy.

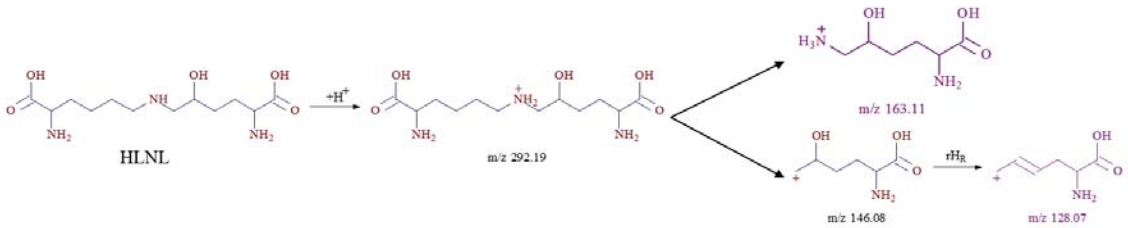

Figure 76: Two possible fragmentation pathways of HLNL which result in the production of 163.11, 146.08 and 128.07 m/z ions.

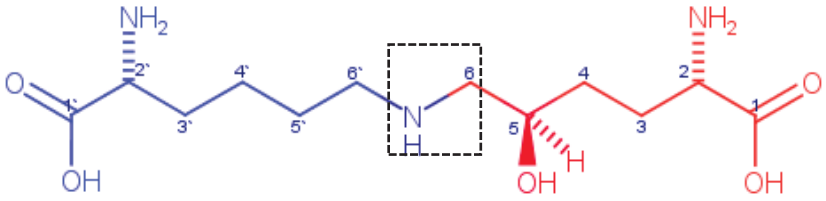

Figure 77: The chemical structure of HLNL. The blue part shows the lysine moiety and red part shows the hydroxylysine moiety. The dashed box shows the new bond formed between the lysine and hydroxylysine moieties to produce HLNL.

6.3.4.7.2 NMR of HLNL

HLNL is made up of lysine and hydroxylysine moieties (Figure 77). Therefore ^{1}H and ^{13}C spectra of lysine and hydroxylysine were used to interpret the NMR spectra of

HLNL. The ^{1}H, ^{13}C and DEPT-135 spectra for HLNL were recorded, which was then followed by the COSY, HSQC and HMBC spectra.

^{13}C NMR spectra were more useful in interpreting the structures of the crosslinks because they are recorded over a range of 200 ppm. This means overlapping signals are less likely to occur than for ^{1}H NMR, where signals are generated over a narrower range of 10 ppm and are therefore prone to overlap [93, 94, 104]. All chemical shifts of ^{1}H, ^{13}C and DEPT-135 spectra of HLNL are listed in Table 19.

HLNL is made up of 12 carbon atoms including 2 quaternary, 3 tertiary and 7 secondary carbon atoms as shown in Figure 73. In the ^{13}C spectrum 12 peaks were observed matching the number of carbon atoms in HLNL. In the DEPT-135 spectrum, the quaternary carbon atom produces no peaks while the primary and tertiary carbon atoms produce positive peaks. On the other hand, the secondary carbon atom produces a negative peak. In the DEPT-135 spectrum of HLNL (see appendix), only 10 peaks in total were observed. This is because the 2 quaternary carbon atoms produced no peaks and the 3 tertiary and 7 secondary carbon atoms produced 3 positive and 7 negative peaks, respectively [445]. The chemical shifts of all carbon atoms in the DEPT-135 spectrum were the same as those peaks seen in the ^{13}C spectrum.

The two quaternary carboxy atoms of C-1 and C-1′ are the most deshielded carbons as they are directly attached to oxygen. They were, therefore, located downfield at 176.27 and 176.11 ppm, respectively. Furthermore, the C-1 and C-1′ peaks were absent in the DEPT-135 spectrum confirming their quaternary configuration. These findings demonstrate the divalent properties of the HLNL crosslink with two carboxylic acid

ends linking two collagen molecules [6, 78, 442]. The chemical shifts of the C-2 and C-2′ atoms are 56.03 and 55.99 ppm, respectively. They produced two positive peaks in the DEPT-135 spectrum which is evidence that C-2 and C-2′ are tertiary carbons.

The C-5 atom was located further downfield with a chemical shift 67.91 ppm as it is attached to the hydroxy group producing a high electronegative region. This was in good agreement with the chemical shift of C-5 of hydroxylysine which is a moiety in HLNL (Table 18). ^{13}C NMR peaks are not prone to splitting because 99% of the neighbouring carbons are carbon-12 and do not have a nuclear spin. As a result, coupling between adjacent carbon atoms is not observed in ^{13}C NMR unlike coupling between adjacent protons which is clearly observed in ^{1}H NMR [445]. The C-5 peak was, however, observed as a doublet with a chemical shift difference of around (0.05 ppm - 0.2 ppm) (Table 18). This is in excellent agreement with the difference in the chemical shift of C-5 peak of hydroxylysine at 67.15 ppm. This suggests that the hydroxylysine moiety in HLNL structure has two conformations (R and S) and therefore HLNL is likely to exist as two diastereomers. Further support for this is provided by the C-6 peak at 53.82 ppm, which appeared as doublet matching with the the C-6 peak for hydroxylysine at 44.31 ppm. However, the significant increase in the chemical shift of the C-6 peak of HLNL (53.82 ppm) compared with that of C-6 peak of hydroxylysine (44.31 ppm) is due to the new bond formed between the amino group and C-6 resulting in the formation of HLNL (Figure 77). Furthermore, all ^{13}C peaks in the HLNL ^{13}C spectrum that correlated to the lysine moiety were observed as singlets, while the ^{13}C peaks correlated to the hydroxylysine moiety were observed as doublets

(Figure 78). These exactly matched the pattern of the peaks observed in the ^{13}C spectra of lysine and hydroxylysine (Figure 78).

Table 19: ^{13}C chemical shifts of HLNL. DEPT-135 signals are given in brackets for the experimental chemical shift: Quaternary carbon (none), tertiary and primary carbon (positive) and secondary carbon (negative).

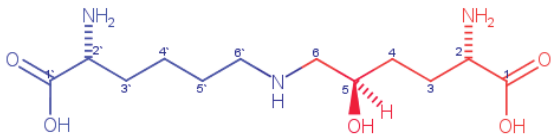

Atom number	**Predicted***	**Adrianus et al. (1999) and Cribiu *et al.* (2008) [443, 444]**	**Experimental**
4′	22.34	22.57	23.06 (Negative)
3	29.40	25.96	26.56 (Negative)
5′	29.50	26.96	28.16 (Negative)
4	30.42	30.30	31.32 (Negative)
3′	32.90	30.55	31.46 (Negative)
6′	49.38	48.20	48.71 (Negative)
6	52.98	52.70	53.82 (Negative)
2′	53.94	53.13	55.99 (Positive)
2	55.33	53.83	56.03 (Positive)
5	71.50	67.21	67.91 (Positive)
1′	174.47	172.99	176.11 (None)
1	175.95	173.19	176.27 (None)

* ^{13}C spectrum was predicted by Marvin Sketch software (version 16.12.26.0, 2016, ChemAxon Ltd., Budapest, Hungary).

The chemical shifts of the remaining secondary carbons were located slightly upfield between 23.06 and 31.46 ppm and all were negative peaks in the DEPT-135 spectrum (see appendix). The unidentified peak observed at 24.8 ppm and 183.01 ppm and the positive peak in the DEPT-135 spectrum was for the primary carbon of residual acetic acid.

The ^{1}H NMR of HLNL was recorded, and compared with the sum of ^{1}H spectra of lysine and hydroxylysine shown in Figures 79 and 80 respectively. Generally, the ^{1}H spectrum of HLNL perfectly matched the summed ^{1}H spectra of lysine and hydroxylysine. The chemical shift of the proton attached to C-5 was downfield at 3.85 ppm (Figure 79) and was the most deshielded proton in HLNL due to the hydroxy group. The peak was multiplet, which perfectly matched the ^{1}H spectrum of hydroxylysine (Figure 80) confirming the presence of a number of diastereomers [439, 440, 443]. The multiplet observed at 3.67 ppm was correlated to the protons on C-2 and C-2′ which are attached to the amino group. This is equal to the sum of the lysine and hydroxylysine peaks observed at 3.67 ppm and 3.70 ppm, respectively.

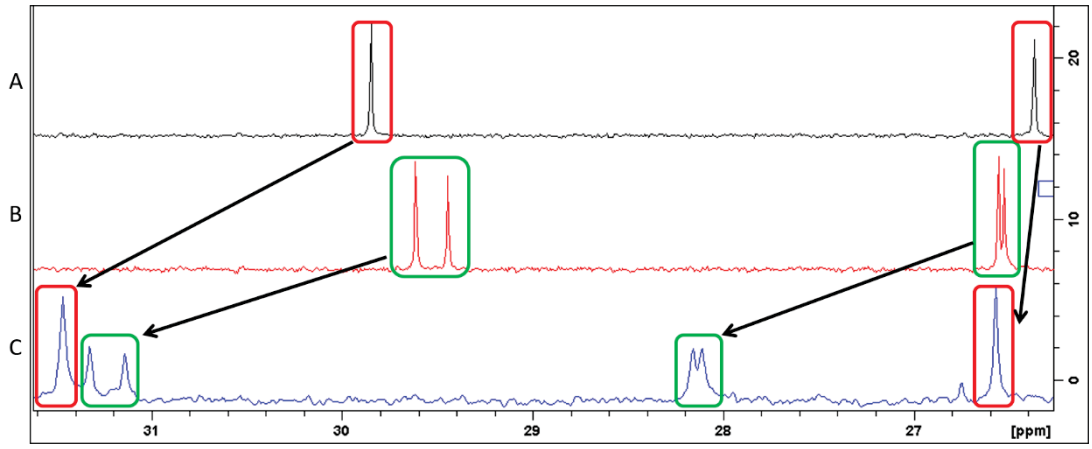

Figure 78: The ^{13}C spectra of (A) hydroxylysine (B) lysine and (C) HLNL. The singlets and doublets in HLNL matched up with those in hydroxylysine and lysine, respectively. Boxes show the correlation between the peaks of HLNL and those for lysine and hydroxylysine.

The two diastereomeric protons on C-5 of the hydroxylysine moiety appeared at different chemical shifts and proton coupling. The doublet of doublets (dd) at 3.11

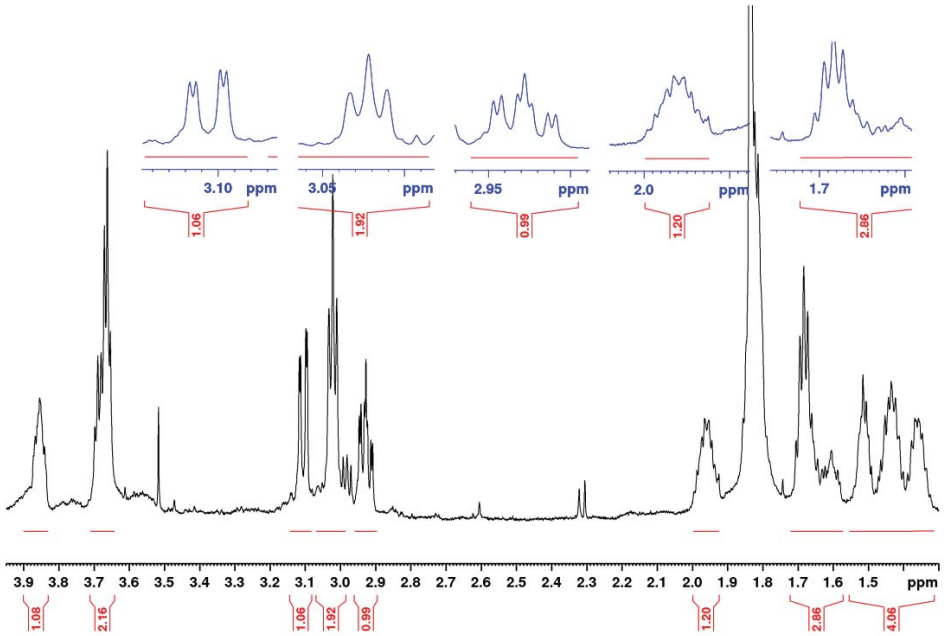

Figure 79: ^{1}H NMR spectrum of HLNL.

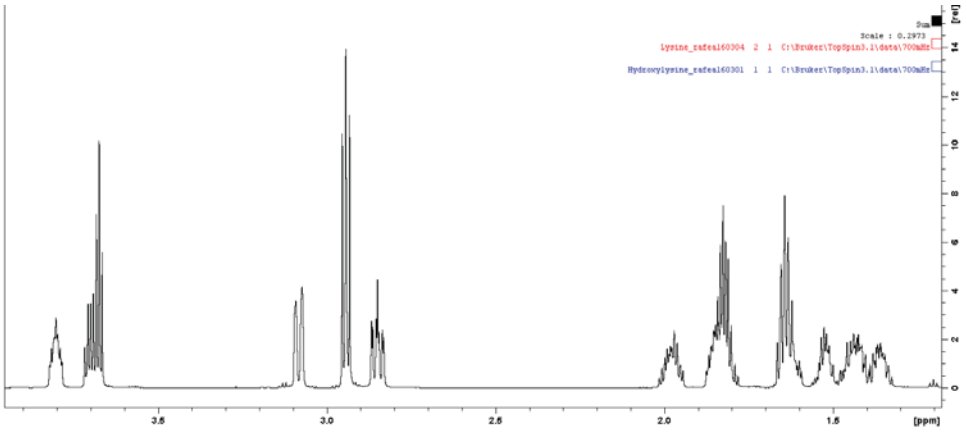

Figure 80: The sum of ^{1}H spectra of lysine and hydroxylysine

ppm was correlated to the first diastereomeric proton and the doublet of doublet of doublets (ddd) at 2.91 ppm was correlated to the second proton. On the other hand, the triplet at 3.01 ppm was assigned to the two protons on C-5′ of the lysine moiety. The remaining peaks were located between 1.4 and 2.0 ppm. COSY, HSQC and HMBC 2

D spectra of HLNL were fully assigned showing the correlations between protons and between protons and each carbon atom (see appendix).

6.3.4.8 Characterisation of the HHL crosslink

HHL is made up of HLNL and histidine (Figure 81). Despite it only being more than 80% pure as determined from the formic acid internal standard method, its 1D NMR spectra (including ^{1}H, ^{13}C and DEPT-135 and 2D NMR spectra of COSY, HSQC and HMBC) were recorded.

HHL was first described by Fairweather *et al.* in 1972 [86, 159] and its structure was first proposed by Bernstein and Mechanic in 1980 [86, 159]. Yamauchi *et al.* showed that C-6′ of the HLNL moiety is linked to C-5″ of the histidine moiety (Figure 81) [94].

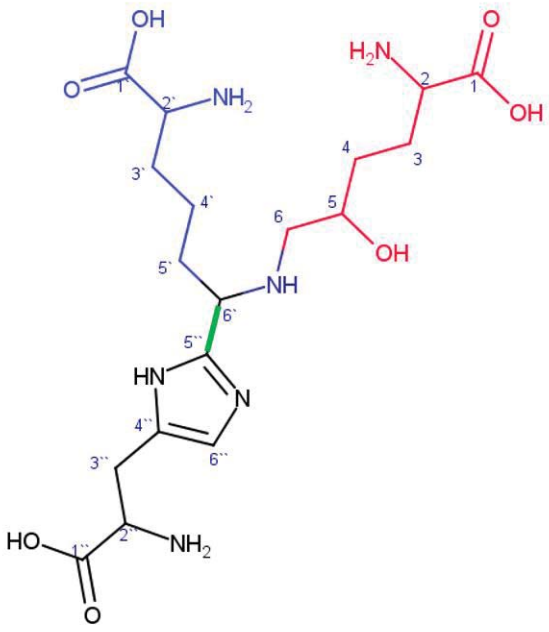

Figure 81: Chemical structure of HHL proposed by Yamauchi *et al.* (1987). Hydroxylysine moiety (red); lysine moiety (blue); histidine (black). The green bond shows where HLNL is linked to the histidine moiety. The combined structures of lysine and hydroxylysine gives HLNL.

6.3.4.8.1 Mass spectrum of HHL

The monoisotopic mass of the HHL crosslink was recorded as singly and doubly charged ions. Triply charged ions were not detected. The monoisotopic mass of 283.1370 m/z is always detected in the mass spectrometry of HHL.

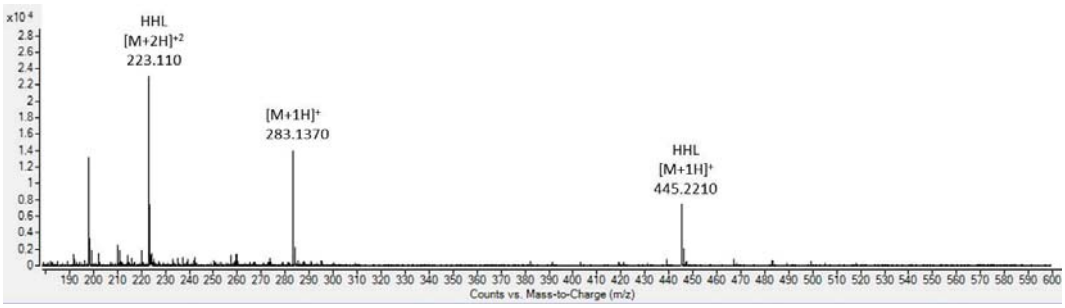

Figure 82: Mass spectrum of the HHL showing the singly (445.2210 m/z) and doubly (223.1100 m/z) charged ions. The 283.1370 m/z monoisotopic mass is a characteristic mass of HHL.

The energy used to fragment the singly charged ions was 22 KeV and for the doubly ions charged was 5 KeV. Several product ions were detected, however two ions 283.1555 m/z and 156.0853 m/z were most abundant (Figure 83).

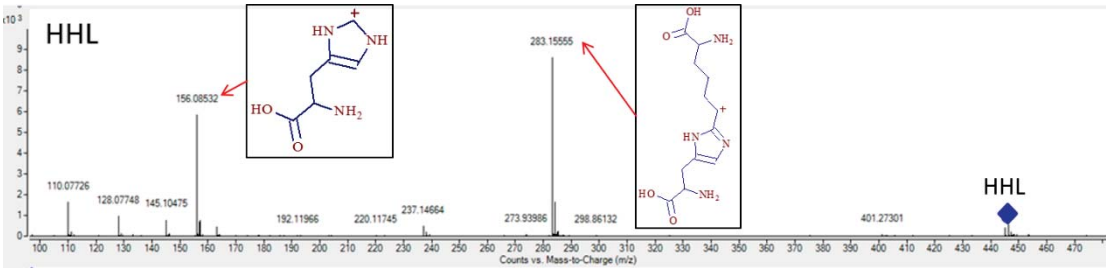

Figure 83: The major products ions formed from the fragmentation of HHL at 22 KeV. Insets show the possible structures of selected ions. The blue diamond represents the parent ion. All possible major structures of HHL fragments are given in the appendix for this chapter ("chapter 6 - MS-MS – fragments" folder).

The proposed pathway for the formation of the 283.14 m/z ion is through the loss of the hydroxylysine fragment (Figure 84).

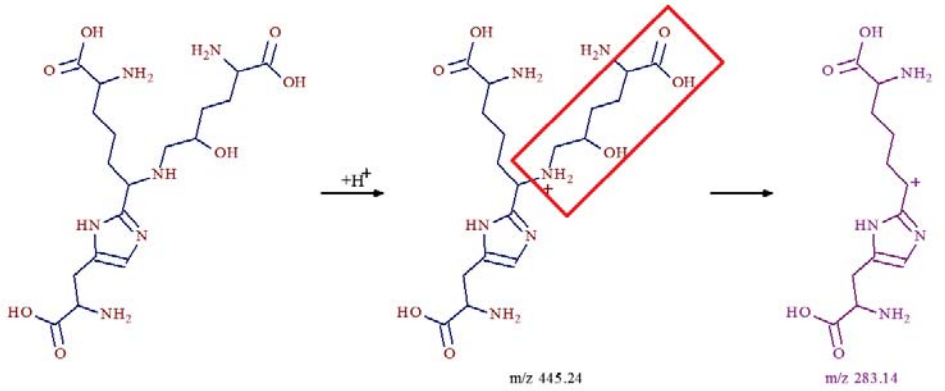

Figure 84: HHL fragmentation pathway showing the formation of the 283.14 m/z ion. The red box shows the fragment lost.

The 156.08 m/z ion is formed after the histidine is fragmented from HHL (Figure 85) and the 128.07 m/z and 110.07 m/z ions are identical to those produced from the fragmentation of histidine.

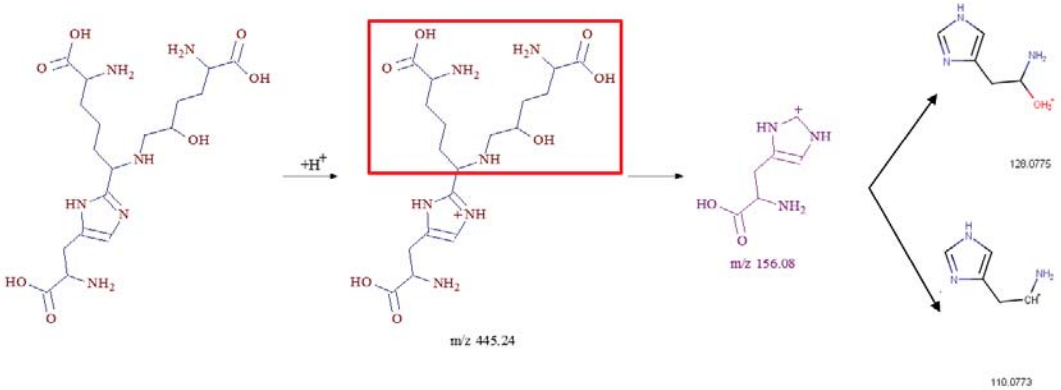

Figure 85: HHL fragmentation pathway showing the formation of the 156.08 m/z ion. The red box contains the fragment lost.

6.3.4.8.2 NMR of HHL

The interpretation of the NMR spectra of HHL was based on that of the HLNL and histidine moiety. In general, the ^{13}C spectrum of HHL was in good agreement with that previously reported by Yamauchi *et al.* (1986) [94] and that predicted by Marvin Sketch software (version 16.12.26.0, 2016, ChemAxon Ltd., Budapest, Hungary). A few differences in the chemical shifts of some signals were, however, observed. Furthermore, a few extra peaks were observed in the ^{13}C spectrum of HHL, which were associated with possible impurities in the HHL sample. Because their intensities were very low, they did not affect the interpretation. Table 20 summarises the chemical shifts of the ^{13}C spectrum taken from the literature, predicated by software, and this study.

The three signals observed at 174.34 ppm, 174.28 ppm and 173.28 ppm were assigned to the quaternary carboxy carbons (C-1, C-1′ and C-1″), respectively. These are the most deshielded carbon peaks due to their direct attachment to an oxygen atom. These quaternary carbons were also confirmed by the disappearance of their peaks in the DEPT-135spectra (see Appendix). The presence of these three carboxyl groups in the HHL ^{13}C spectrum strongly suggests that HHL is a trivalent crosslink linking three collagen molecules [94].

The chemical shifts of the imidazole ring carbons (C-5″, C-4″ and C-6″) were observed at 141.15, 134.06 and 118.33, respectively. In the DEPT-135 spectrum, the peak of C-

4″ was positive while the other two peaks for C-5″ and C-6″ disappeared. This is in good agreement with the imidazole ring peaks observed in the ^{13}C spectrum of histidine (see Appendix). However, the peak for C-5″ in histidine is tertiary while in HHL it is quaternary. This conversion from tertiary configuration in histidine to a quaternary configuration in HHL confirms that C-5″ is involved in making the bond between HLNL and the histidine moieties to produce HHL (Figure 81-green bond) [93, 94]. Yamauchi *et al.* (1986) assigned the ^{13}C peak of C-5″ peak based on a difference in the chemical shift compared with what is seen for substituted histidine [94]. In this study, however, the disappearance of the C-5″ peak in the DEPT-135 spectrum indicates that C-5″ does have a quaternary configuration [94].

The ^{13}C peak of the tertiary C-6′, was observed at 54.24 ppm and was positive in the DEPT-135 spectrum confirming its tertiary configuration. The chemical shift of C-6′ in HLNL was observed at 48.71 ppm and was negative in the DEPT-135 spectrum suggesting it has a secondary configuration (Table 20). The conversion from secondary to tertiary suggests that a bond is being formed between C-6′ of HLNL and C-5″ of histidine to produce HHL as shown in Figure 81.

The three peaks observed at 54.37, 54.47 and 55.08 ppm, which were positive in the DEPT-135 spectrum, were assigned as tertiary carbons attached to the amino groups

(C-2′, C-2 and C-2″), respectively. The remaining peaks were consistent with the chemical shifts observed for HLNL (Table 19) and histidine (Table 18) carbons all of which are located between 20 and 31 ppm. These carbons are all secondary (-CH_2-), and so have negative peaks in the DEPT-135 spectrum.

The singlet peak at 66.36 ppm was assigned to C-5 of the hydroxylysine moiety. Although smaller peaks were observed close to it, their relative intensities and chemical shifts does not match with those peaks seen for C-5 in hydroxylysine and HLNL. These smaller peaks were more likely to be due to impurities found in the HHL preparation and are not a result of diastereomers. It was therefore concluded that the hydroxylysine moiety in HHL could have only one configuration (R or S), unlike HLNL and hydroxylysine. More investigation is, however, required to support these results.

Figures 86 and 87 show the ^{1}H NMR spectra of HHL histidine. It is clear that the two imidazole protons of histidine are observed at 8.6 and 7.3 ppm, while for HHL the peak at 7.3 ppm shifts to 7.02 ppm and the other peak at 8.6 ppm disappears. The disappearance of the peak at 8.6 ppm indicates that the histidine moiety in HHL is linked to the HLNL moiety through C-5``. This results in the conversion of the C-5`` configuration from tertiary in histidine to quaternary in HHL through the loss of a

proton resulting in the disappearance of its ^{1}H NMR peak. The remaining proton peaks in HHL were not fully interpreted due to the presence of impurities resulting in

Table 20: ^{13}C chemical shifts of HHL. DEPT-135 signals are given in brackets for the experimental chemical shift: Quaternary carbon (none), tertiary and primary carbon (positive) and secondary carbon (negative).

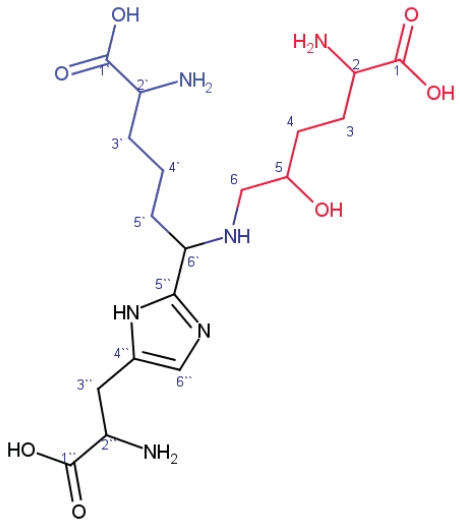

Atom number	**Predicted**	**Yamauchi (1987)[94]**	**Recorded**
4′	23.11	20.8	20.57 (Negative)
5′	31.69	26.7	26.37 (Negative)
3	29.29	27.9	27.68 (Negative)
3′	27.24	29.9	29.53 (Negative)
3″	30.99	29.9	29.63 (Negative)
4	23.51	30.9	30.64 (Negative)
6	51.04	50.8	50.49 (Negative)
6′	56.26	54.8	54.24 (Positive)
2′	55.33	54.8	54.37 (Positive)
2	56.33	54.8	54.47 (Positive)
2″	56.75	55.3	55.08 (Positive)
5	71.50	66.7	66.36 (Positive)
6″	125.03	118.7	118.33 (Positive)
4″	130.09	134.1	134.06 (None)
5″	146.63	141.7	141.15 (None)
1″	174.30	173.7	173.46 (None)
1′	175.33	174.5	174.28 (None)
1	175.95	174.5	174.34 (None)

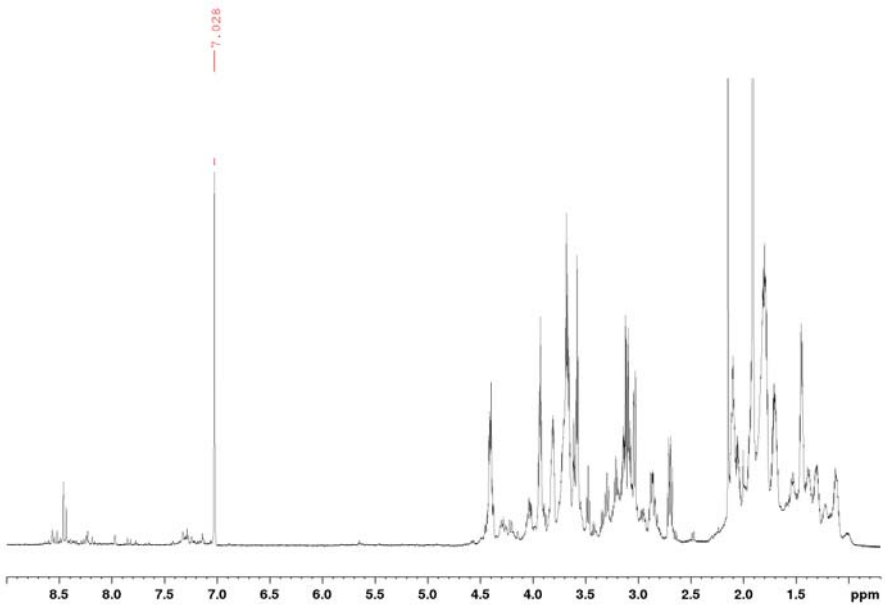

Figure 86: [1]H NMR spectrum of HHL showing the peak at 7.02 ppm.

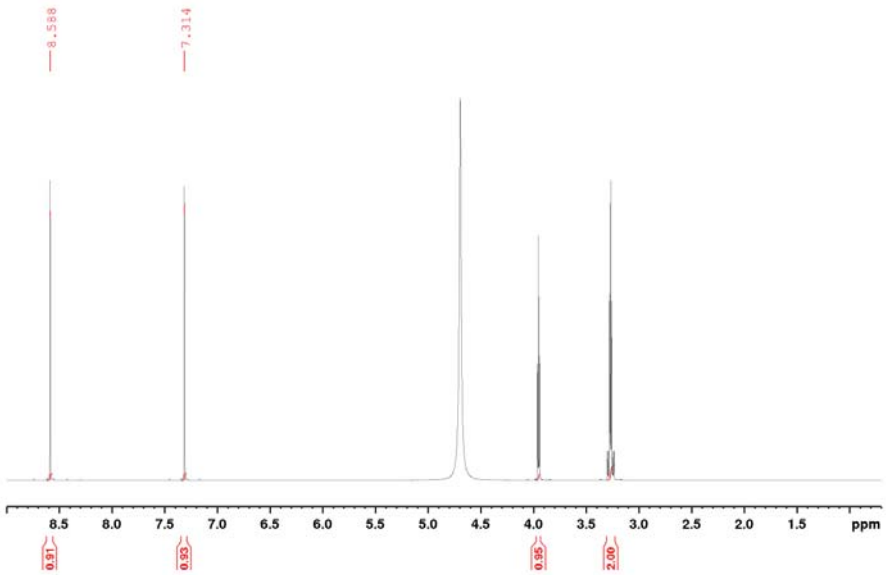

Figure 87: [1]H NMR spectrum of histidine showing the two peaks of the imidazole at 8.60 ppm and 7.30 ppm.

several overlapping signals. The 2D COSY, HQSC and HMBC spectra were also of poor quality due to the impurities and were not used.

6.3.4.9 Characterisation of the HHMD crosslink

HHMD is made up of four amino acid residues and was first characterised in 1973 by Tanzer *et al.* [93, 104]. Its existence is, however, controversial based on the work of Robins and Bailey (1976) who suggested that HHMD is an artefact of alkaline reduction and hydrolysis [446]. This was later refuted by Bernstein and Mechanic (1980) who succeeded in isolating HHMD from iodinated collagen fibrils using pepsin [159]. In 1973, Tanzer *et al.* proposed that the HHMD structure linked four collagen molecules similar to desmosine and isodesmosine elastin crosslinks [93, 103].

The HHMD structure was resolved by Hunt and Morris (1973) using a low resolution ^{1}H and ^{13}C NMR (100 MHz) [104]. No other attempts were made to confirm the HHMD structure using high resolution NMR [104]. To aid interpretation, HHMD was treated as containing HLNL, histidine and norleucine moieties (Figure 88).

6.3.4.9.1 Mass spectrum of HHMD

The HHMD mass spectrum showed the sample was pure, producing ions with three charge states. (single, double and triple charges (Figure 89)).

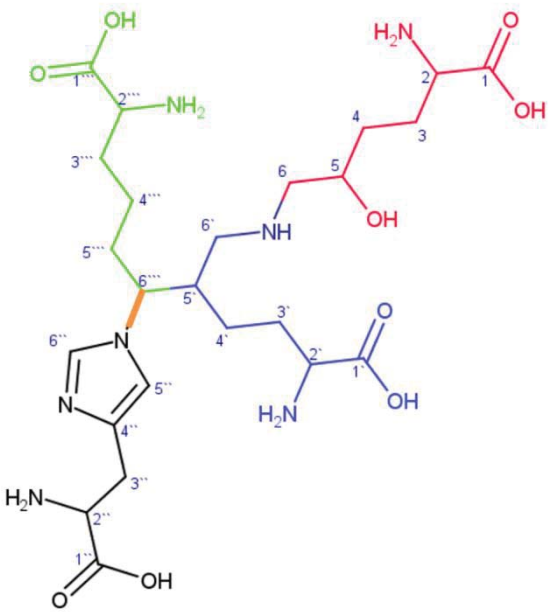

Figure 88: The chemical structure of HHMD showing the four major moieties. Red, hydroxylysine; blue, lysine; black, histidine and green, norleucine. The red and blue moieties give HLNL. The orange line shows the bond made between the histidine and norleucine moieties.

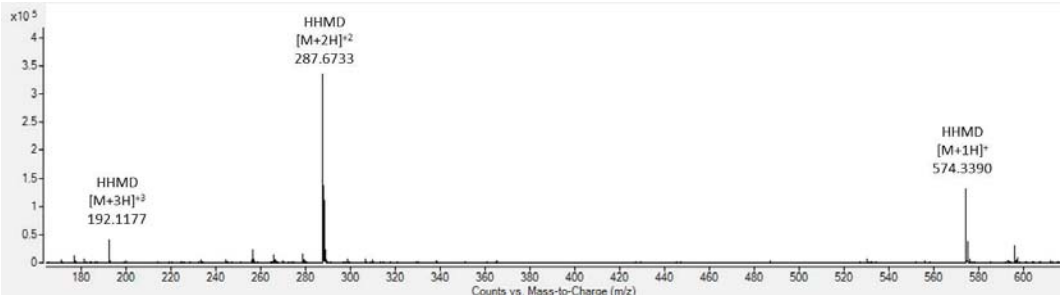

Figure 89: Mass spectrum of HHMD showing singly (574.3390), doubly (287.6733) and triply (192.1177) charged ions.

Singly charged ions of HHMD required 35 KeV for fragmentation while the doubly charged ions required 12 KeV. These are much higher values than those used for HHL and are probably due to the free imidazole nitrogen in HHL which can be easily protonated. The fragmentation pathway and product ions of singly charged of HHMD

were analysed (Figure 90), and the complete list of the product ions is given in the Appendix named “chapter 6 - MS-MS – fragments” folder.

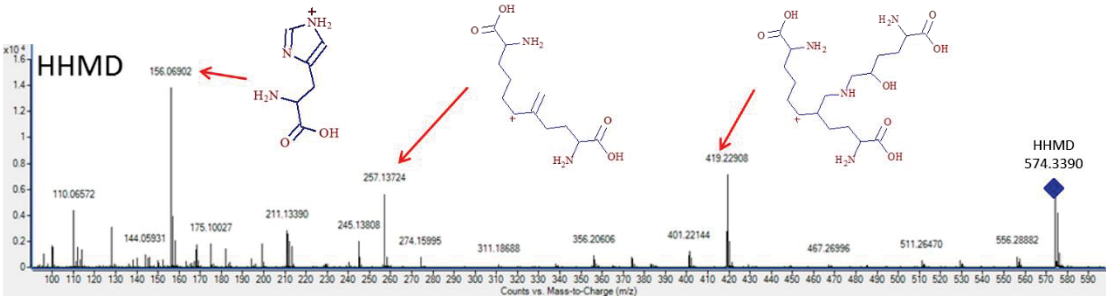

Figure 90: The major product ions formed from the fragmentation of HHMD at 35 KeV. Insets show the possible structures of selected ions. The blue diamond shows the parent ion. All possible major structures of HHMD fragments are given in Appendix “chapter 6 - MS-MS – fragments”).

Below is an example of the fragmentation pattern pathway of singly charged HHMD ion that produces product ions of 419.22 and 156.08 m/z (Figure 91).

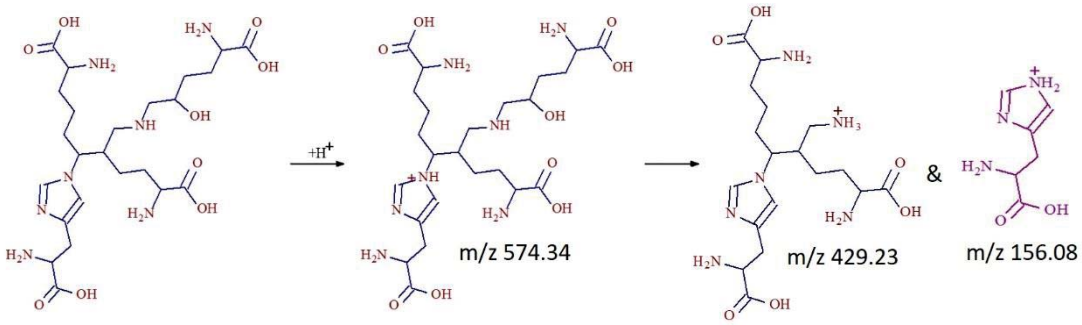

Figure 91: MSMS spectra of HHMD singly charged ions to produce product ions of 419.23 m/z and 156.08 m/z.

6.3.4.9.2 NMR of HHMD

The ^{13}C chemical shifts of the HHMD are summarised in table 21. Generally, they are in good agreement with the ^{13}C spectra reported by Tanzer *et al.* (1973), Hunt and Morris (1973) and the ^{13}C spectrum predicted by Marvin Sketch software (version 16.12.26.0, 2016, ChemAxon Ltd., Budapest, Hungary). Slight shifts in the chemical shifts of some signals were observed, which is due to the differences in the experimental conditions such as pH and concentration [93, 104].

The four quaternary carboxy carbons (C-1, C-1′, C-1″ and C-1‴) are observed at 173.08, 174.96, 174.91 and 173.56 ppm, respectively and all disappeared in the DEPT-135 spectrum, suggesting that HHMD contains four terminal carboxy groups linking four collagen molecules [103, 104].

The imidazole carbons (C-6″, C-4″ and C-5″) of the histidine moiety were observed at 136.70, 131.16 and 120.50 ppm, respectively. The quaternary C-4″ at 131.16 ppm disappeared while the tertiary C-5″ and C-6″ at 136.70 and 120.50 ppm, were positive peaks in DEPT-135. This perfectly matches with the three peaks seen in the ^{13}C spectrum of histidine (Table 18) which suggests that none of the imidazole ring carbon atoms in HHMD are involved in linking the HHMD moieties. This leaves the nitrogen to make a bond with C-6‴ of the norleucine moiety. Peaks due to the tertiary C-6‴ and C-5′ were observed at 62.56 and 41.29 ppm, respectively and both produced positive peaks in the DEPT-135 spectrum.

The carbons attached to the amino groups (C-2, C-2′, C-2″ and C-2‴) were observed between 55 and 54 ppm and all gave positive peaks in the DEPT-135 spectrum. The combination of ^{13}C and DEPT-135 spectra has clearly resolved the complete structure

of HHMD, which is in excellent agreement with the previously published data [93, 104].

The chemical shift of C-5 was observed at 67.53 ppm and was positive in the DEPT-135 spectrum. This peak was a doublet which matched the peaks seen in HLNL at 67.91 ppm and hydroxylysine at 67.15 ppm but did not match the peak seen in HHL (Figure 92). This supports the existence of HHMD diastereomers which has also been suggested by Tanzer *et al.* (1973) and Hunt and Morris (1973) [93, 104].

Although the ^{1}H NMR of HHMD was complicated and has considerable overlapping peaks, there was an apparent agreement between the ^{1}H spectrum of HHMD and the summed ^{1}H spectra of HLNL, histidine and lysine (Figures 93 & 94), However, the two peaks at 9.01 and 7.71 ppm are assigned to proton attached to C-5″ and C-4″ of the imidazole ring in the histidine moiety (Figure 93). These two peaks are an excellent match with the peaks observed in the combined ^{13}C spectra of HLNL, histidine and lysine (Figure 94) and confirms the involvement of the nitrogen atom of the imidazole ring in the bond made between the histidine and the norleucine moieties (Figure 88-orange bond).

Table 21: ^{13}C chemical shifts of HHMD. DEPT-135 signals are given for the experimental chemical shift between the brackets. Quaternary carbons (none), tertiary and primary carbons (positive) and secondary carbons (negative).

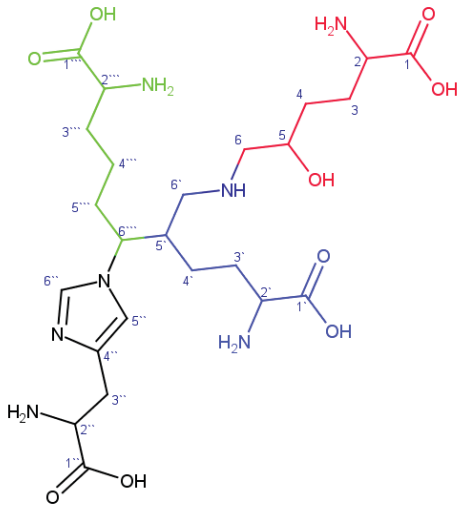

Atom number	**Predicted**	**Tanzer and Hunt *et al.* (1973)[93, 104]**	**Experimental**
4‴	24.11 ppm	22.20	22.38 (negative)
4′	28.27 ppm	24.50	27.41 (negative)
3	29.45 ppm	27.70	27.75 (negative)
3′	30.80 ppm	27.70	30.90 (negative)
3‴	30.99 ppm	29.50	31.00 (negative)
3″	31.14 ppm	30.95	31.10 (negative)
4	32.86 ppm	30.95	31.12 (negative)
4′	35.30 ppm	32.05	31.79 (negative)
5′	43.36 ppm	41.30	41.29 (positive)
6′	46.44 ppm	48.90	48.74 (negative)
6	52.97 ppm	54.00	54.60 (negative)
2‴	55.33 ppm	55.30	54.77 (positive)
2′	55.33 ppm	55.30	54.84 (positive)
2	55.33 ppm	55.50	55.17 (positive)
2″	57.63 ppm	55.70	55.24 (positive)
6‴	59.57 ppm	59.70	62.56 (positive)
5	71.50 ppm	67.05	67.53 (positive)
5″	121.29 ppm	117.60	120.50 (positive)
4″	138.69 ppm	136.00	131.16 (none)
6″	141.12 ppm	138.30	136.70 (positive)
1″	172.52 ppm	173.90	173.56 (none)
1‴	175.33 ppm	173.90	174.91 (none)
1′	175.95 ppm	174.90	174.96 (none)
1	175.95 ppm	175.10	175.08 (none)

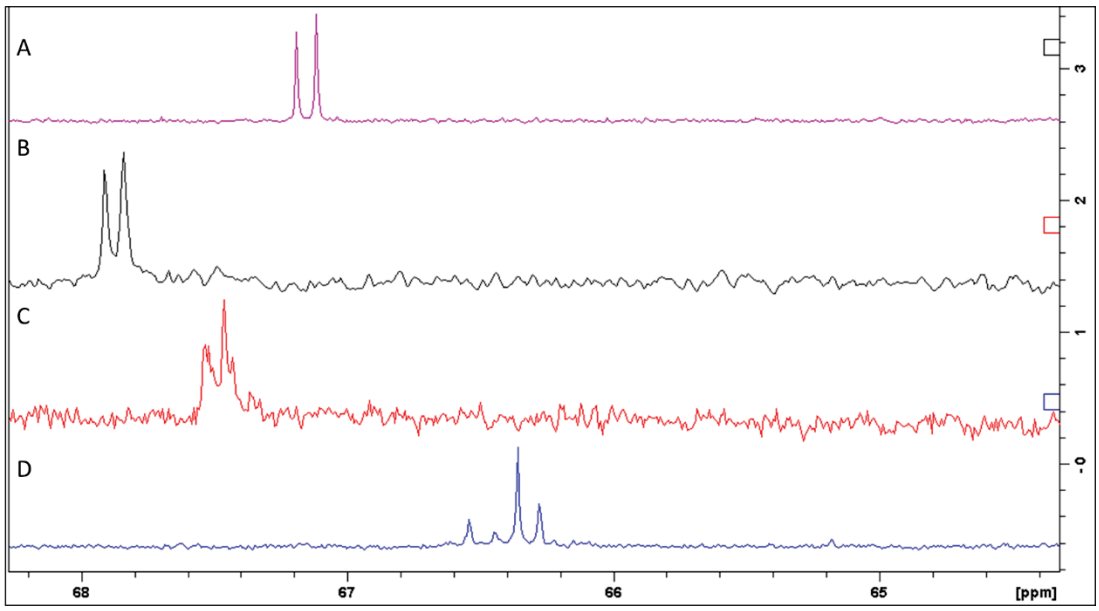

Figure 92: The chemical shift of C-5 which was observed at around 66-68 ppm in (A) hydroxylysine, (B) HLNL, (C) HHMD and (D) HHL. It is similar in hydroxylysine, HLNL and HHMD and different in HHL.

The HSQC 2D spectrum helped to assign ^{1}H spectrum peaks by correlating proton to carbon peaks for each proton attached to a carbon (Figure 95). The peak at 3.94 and 4.54 ppm represent protons that are attached to C-5 and C-6‴, respectively and both peaks are integrated as a single proton. The ^{1}H peaks from 3.7-3.8 ppm were correlated with the protons attached to C-2, C-2′, C-2″ and C-2‴ having chemical shifts of 54.77-55.24 ppm. These are integrated as 4 protons. The ^{1}H peak at 3.15 ppm was for a proton attached to C-6′ with a chemical shift of 48.74 ppm. This peak is shown in red in the 2D spectrum (Figure 95) which suggests a secondary configuration for C-6′. The ^{1}H peak at 2.39 ppm was assigned as a proton attached to C-5′, which has a tertiary configuration. All the remaining ^{1}H peaks observed between 22.38-21.79 ppm are shown in red and all have secondary configurations.

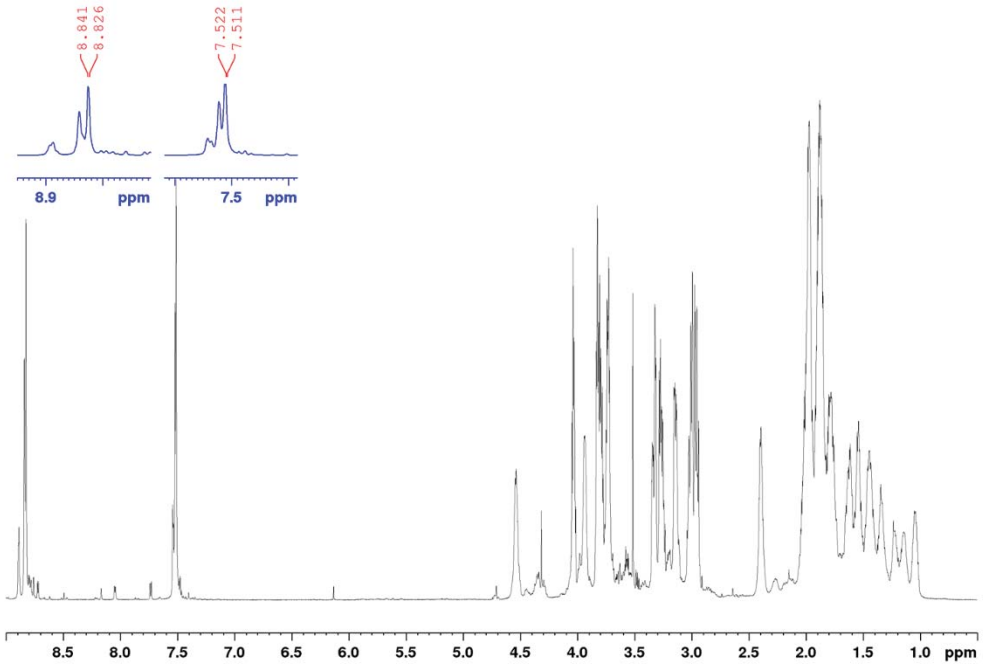

Figure 93: ^{1}H NMR spectrum of HHMD.

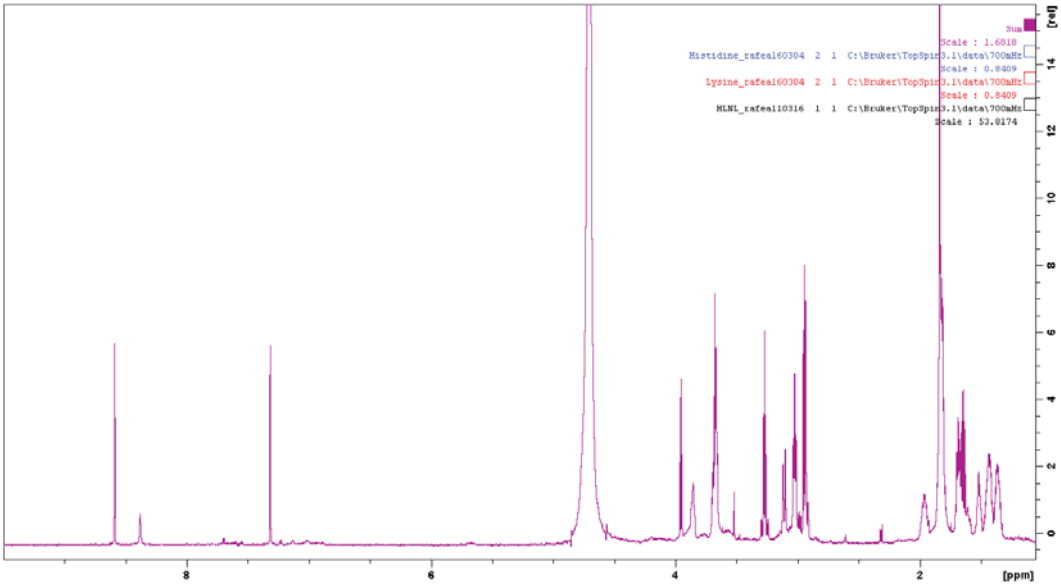

Figure 94: The sum of the ^{1}H NMR spectra of HLNL, histidine and lysine.

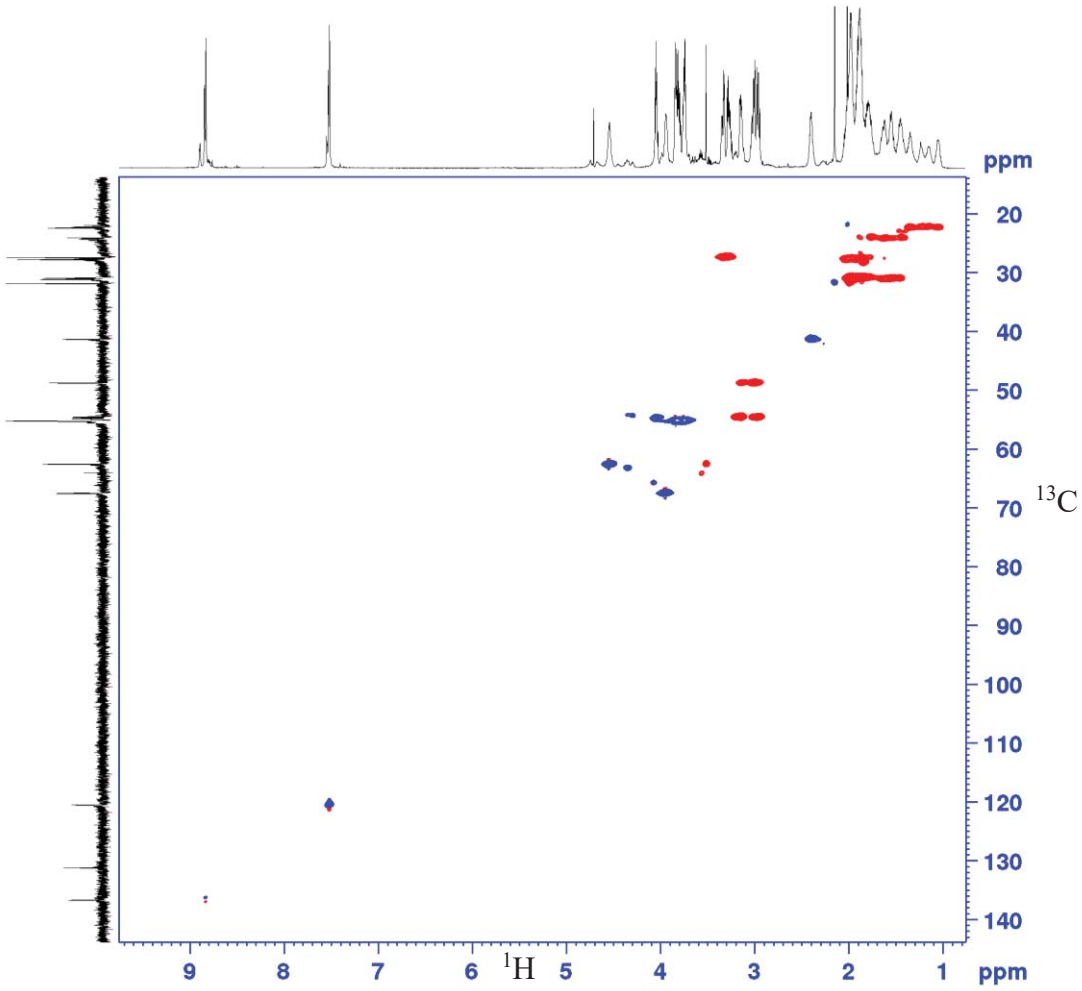

Figure 95: HSQC of HHMD. Blue spots are positive peaks (CH_3 or CH) while red spots are negative peaks (CH_2) in DEPT-135 spectra.

7 CHAPTER SEVEN: Method Development and Crosslink Quantitation

Crosslink analysis of sheep, goat, deer and cow skin

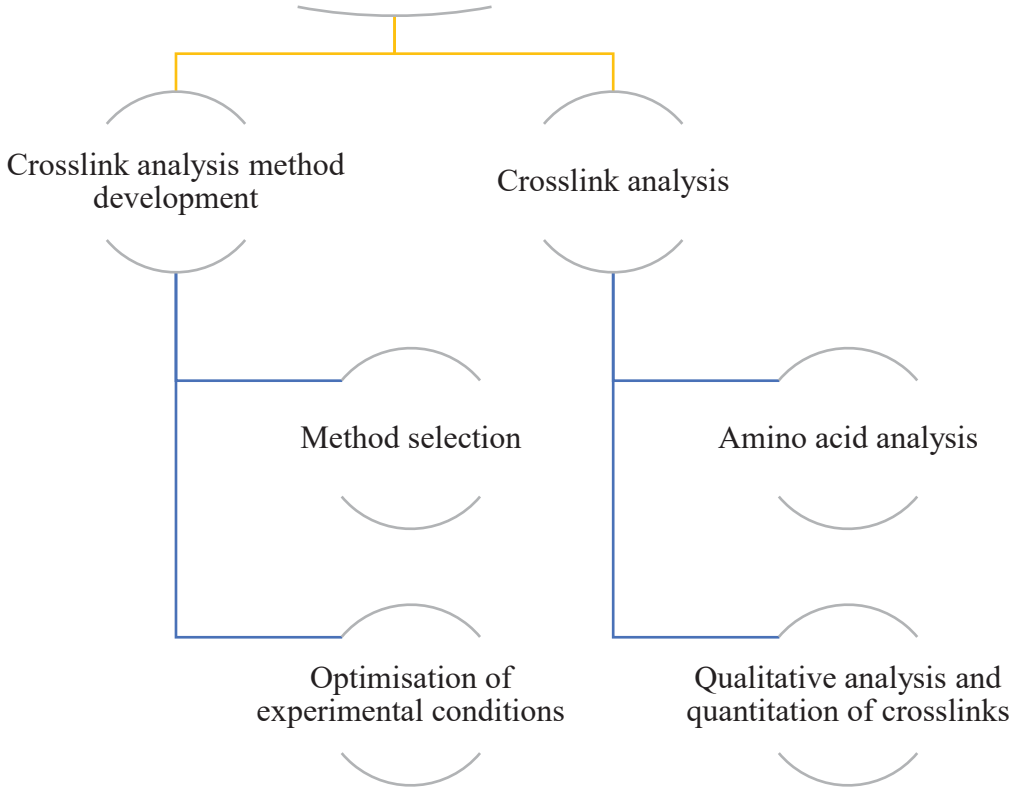

7.1 Introduction

The development of sensitive and accurate quantitative methods for crosslink analysis is essential for evaluating the types and concentrations of crosslinks in collagen. Prior to analysis, the labile crosslinks must first be stabilised by reduction before being isolated from the sample by acid hydrolysis. Upon hydrolysis, both intact crosslinks and free amino acids are released and to separate these the acid hydrolysed mixture is applied to a fibrous cellulose (CF) column to remove the free amino acids. This improves the sensitivity of crosslink detection. Two methods are currently used for the quantitation of crosslinks. These are cation exchange chromatography with UV detection and reversed phase chromatography with mass spectrometry detection [164, 178]. Although, these two methods are commonly used, neither of them has effectively separated and quantified all possible crosslinks in one rapid run without the need for pre- or post-derivatisation of crosslinks. The cation exchange method suffers from low detection sensitivity (~ nmol), broad peaks, long equilibration time and the need for a dedicated instrument. It uses a sodium salt buffer which is unsuitable for mass spectrometry [164, 447]. On the other hand, although the reversed phase C_{18} method uses mass spectrometry for the detection and quantitation of crosslinks, only four crosslinks (HLNL, DHLNL, Pyr and Dpyr) have been identified in this way. Furthermore, the use of ion pairing agents and the long run time (~ 40 min) have limited its use, particularly for the analysis of HHMD and HHL, the major skin crosslinks [178]. Therefore, it became a priory to develop a new sensitive and rapid quantitation method for skin crosslinks.

7.2 Experimental procedure

7.2.1 Chemicals and reagents

Amino acid standards, sodium borohydride (> 99 %), elastin, desmosine and cartilage (from bovine neck ligament) were purchased from Sigma Aldrich (St. Louis, MO, USA). Deionized water was obtained from a Milli-Q Ultra-pure ThermoFisher water system (Dubuque, IA, USA). Mass spectrometry grade water, acetonitrile, methanol and formic acid (> 99 %) were purchased from Fisher Chemical (Fair Lawn, NJ, USA). Hydrochloric acid and acetic acid were purchased from Panreac (Barcelona, Spain). n-butanol (97 %) was purchased from Ajax Finechem, Univar (TarenPoint, NSW, Australia). Fibrous cellulose powder (CF11) was purchased from Whatman (Maidstone, United Kingdom). Dihydroxylysinonorleuince (DHLNL) was purchased from Santa Cruz Biotechnology (Delaware Ave, CA, USA). HLNL, HHL and HHMD were isolated and purified in our laboratory (see Chapter 6 for details).

7.2.2 Instrumentation and analysis

The mass spectrometer used was an Agilent 6520 Accurate-Mass quadrupole time-of-flight (Q-TOF) liquid chromatography mass spectrometry (LC/MS) system (Agilent 6520 Q-TOF, Agilent Technologies, Hanover, Germany) with an electrospray ionization (ESI) source The HPLC was an Agilent 1200 series with a temperature controlled autosampler. Agilent MassHunter Workstation Qualitative Analysis software version B.06.01 SP1 (Agilent Technologies, Santa Clara, CA, USA) was used for qualitative analysis and quantitation was conducted using Agilent MassHunter Workstation Quantitative Analysis Version B.06.00 for QQQ.

7.2.3 Development of the crosslinks separation method

Solvent A was 0.1 % formic acid in water (v/v) and solvent B was 0.1 % formic acid in acetonitrile or methanol (v/v). The flow rate was 400 µL/min and column temperature, 20 ºC. Several isocratic and gradient elutions were tested. The column was a Cogent Diamond Hydride HPLC column (150 mm × 2.1 mm; particle size, 4 µm; pore size 100 Å) with a Cogent diamond hydride guard column (20 mm × 2.1 mm; particle size, 4 µm; pore size, 100 Å) purchased from Microsolv Technology, Leland, NC, USA.

7.2.4 Preparation of skin samples

Small samples were cut from skins obtained as described in chapter 3 section 3.2.2 then lyophilised and kept at – 80 ºC for amino acid and crosslink analysis.

7.2.5 Reduction of skin sample

Lyophilised samples of 100 mg were suspended in 10 volumes of phosphate saline buffer (w/v), containing 0.15 M sodium chloride in 0.1 M sodium phosphate buffer (pH 7.5). Sodium borohydride was dissolved in minimum volume of 1 mM cold sodium hydroxide (~ 4 ºC) then added to the skin solution to give a (1:30) ratio of sodium borohydride to dry skin. The sample mixture was incubated for 2 hours at 37 ºC then reduction was stopped by adjusting pH to 3.0 using glacial acetic acid (pH paper used). After centrifugation at 5000 × g for 10 minutes, the supernatant was discarded and the pellet washed three times with water to remove any excess acetic acid and salt. The reduced skin was then lyophilised and stored at -80 ºC for further analysis.

7.2.6 Hydrolysis of skin samples

Dry reduced skin samples (100 mg) were placed in acid washed 6 x 50 mm screw cap (PTFE) borosilicate glass tubes and 3.0 mL of 6 M HCl containing 3 % phenol was added to the samples. The tubes were sealed and placed in an oven at 110 ^{o}C for 24 hours. The resultant hydrolysate was filtered through plastic syringes plugged with glass-wool, lyophilised, then rehydrated in 1.0 mL water. Ten µL was taken for hydroxyproline analysis to determine the collagen content prior to crosslink enrichment step.

7.2.7 Enrichment of crosslinks

The amino acids were removed from the solution by CF11 column chromatography. First, 5 % of CF11 slurry was prepared by suspending 5 g of CF11 powder in 100 mL of butanol-water-acetic acid (4:1:1, v/v/v). A column was prepared using a 10 mL plastic syringe (0.5 cm × 10 cm), washed with acid followed by water, and plugged with cotton-wool. The column was filled with 5 % CF11 slurry, which was then washed three times with 5 mL of butanol-water-acetic acid (4:1:1, v/v/v). Samples were loaded onto the CF11 column and the initial eluent was discarded. The column was then washed with 10 × 5 mL of fresh butanol-water-acetic acid (4:1:1) to remove most of the amino acids, and the elution monitored by thin layer chromatography (TLC). The crosslinks were then eluted using 25 mL of water, lyophilised then rehydrated in 200 µL of water.

7.2.8 Quantitation of crosslinks

Quantitation of crosslinks was carried out using a previously published method [393]. In summary, the crosslinks were separated on a Cogent Diamond Hydride HPLC column (150 mm × 2.1 mm; particle size, 4 μm; pore size 100 A) using a Cogent diamond hydride guard column (20 mm × 2.1 mm; particle size, 4 μm; pore size, 100 A). Solvent A was 0.1 % formic acid in water (v/v) and solvent B was 0.1 % formic acid in acetonitrile or methanol (v/v). A flow rate of 400 μL/min and a column temperature of 20 °C were used. For gradient elution, the following conditions were used: 0 min 80 % solvent B; 10 min 40 % solvent B; 15 min 10 % solvent B; 20 min 80 % solvent B. The total run time was 20 min, and all samples were filtered through a 0.2 μm ReliaPrep™ syringe filter (Barenstein, Germany) prior to injecting on the column. Sample detection was by mass spectrometry in positive mode and MS scans of 100–1000 m/z were recorded. The fragmentor and skimmer voltages were set at 145 and 55 V, respectively. The nitrogen gas temperature was set to 350 °C with a flow rate of 6 L/min.

7.3 Results and discussion

7.3.1 Silica hydride

As the separation of collagen crosslinks was essential for their detection and reliable quantitation, a method was developed using silica hydride chromatography [393]. Silica hydride is a stable, effective stationary phase and produces reproducible separation. It retains both hydrophobic and hydrophilic compounds depending on the polarity of the mobile phase. A diamond silica hydride column has been previously

reported to separate all standard amino acids including lysine, histidine and arginine [31].

The normal silica hydride surface has polar acidic silanols (Si-OH) on its surface and this has limited its use for separating hydrophobic compounds using organic solvents [448]. For the separation of hydrophilic compounds, the silanols are capped with a long carbon chain such as octadecane (C_{18}) to produce a reverse phase column [449]. Amino acids are not retained on a C_{18} column but eluate within the void column volume. If normal silica HPLC is used with a non-polar solvent, the amino acids are not well resolved and elute as broad peaks [450]. To overcome this problem, post-derivatisation of amino acids has been employed using different reagents such as dabsyl chloride, phenylthiohydantoin, *o*-phthalaldehyde, 9-fluorenylmethyl-chloroformate, and 6-aminoquinolyl-N-hydroxysuccinimydyl carbamate to change the molecular characteristics of the amino acids [451, 452]. However, the formation of multiple derivatives introduces complexity into the separation and analysis [140].

The replacement of the silanol groups in the normal silica with hydride markedly improved the column stability and selectivity (Figure 96) [453]. Pesek *et al.* (2008) showed that non-derivatised amino acids could be fully separated using a diamond hydride column [454] This same stationary phase was then successfully used in this project to separate collagen crosslinks [393].

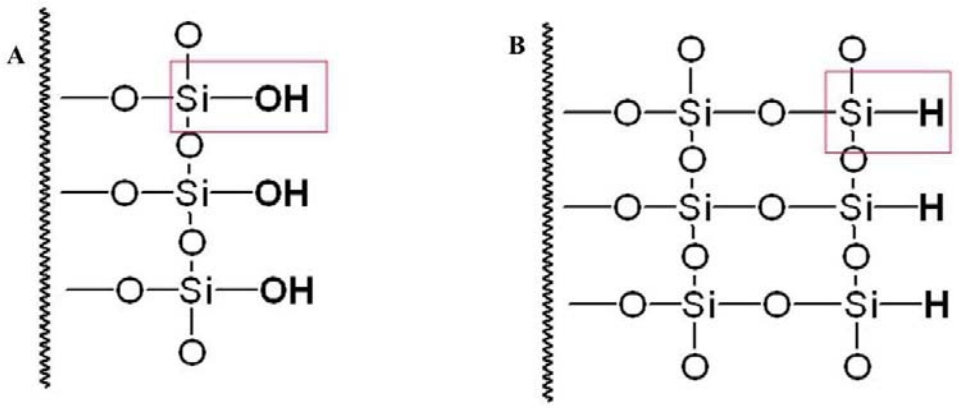

Figure 96: Chemical structure of the surface of (A) Normal silica and (B) Silica hydride.

7.3.2 The effect of solvent on crosslink ionization.

The effect of both an aprotic solvent (acetonitrile) and a protic solvent (methanol) on the crosslink ionisation using positive ion electrospray (ESI) was investigated. The intensity of the singly and doubly charged ions of each crosslink was measured using either 30 % acetonitrile or 30 % methanol in water, both containing 0.1 % formic acid. The response ratio of the doubly charged ions to singly charged ions $[([M+2H]^{2+}/[M+1H]^{+})]$ for the crosslinks was calculated for each crosslink. While the DHLNL, HLNL, LNL, and Pyr response ratios did not significantly change, the ratio was doubled for HHL, Des and HHMD in 30 % methanol (Figure 97). This is due to the fact that the protonation of the analyte during ionisation is enhanced in polar solvents compared to non-polar solvents [455, 456].

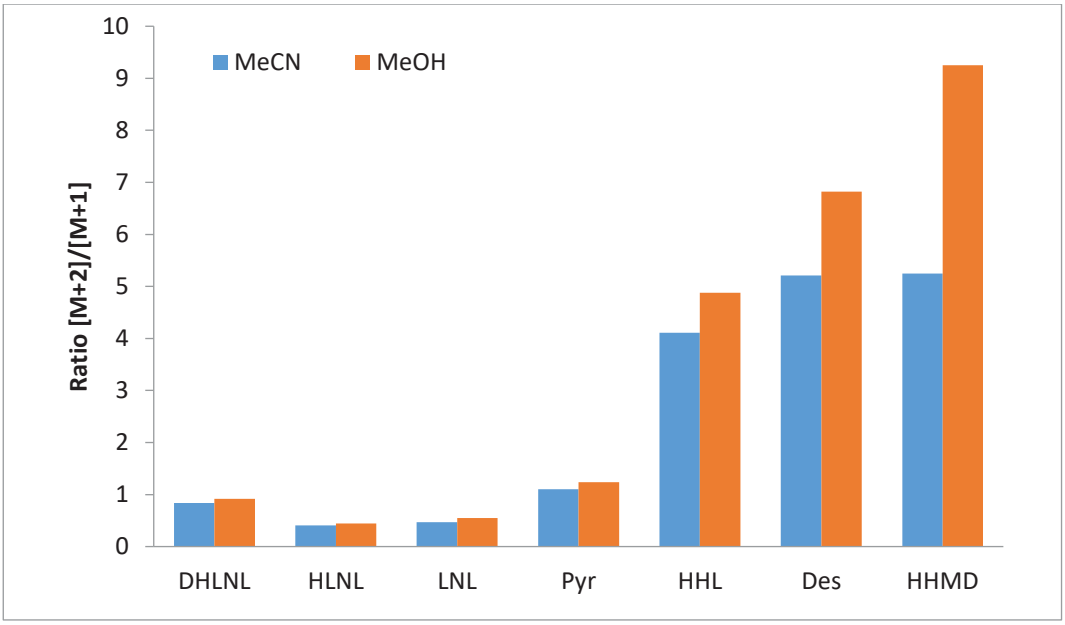

Figure 97: Response ratio ($[M+2H]^{2+}/[M+1H]^{+}$) for different crosslinks. Separation was carried out using isocratic conditions with 30 % acetonitrile or methanol in water containing 0.1 % formic acid, flow rate at 400 µL/min.

7.3.3 Effect of solvent of crosslink retention times

The effect of acetonitrile and methanol on the retention times of crosslinks was then investigated. A range of concentrations of each solvent from 10-90 % (v/v) containing 0.1 % formic acid was prepared. All crosslinks were fully retained on the diamond hydride column at concentrations above 80 % of methanol and 70 % acetonitrile while the basic amino acids and cystine were eluted from the column (Figure 98). This suggests that the diamond hydride column separates the amino acids from the crosslinks with excellent resolution. However, the peaks were broad and the crosslinks poorly resolved. Therefore, gradient conditions were developed.

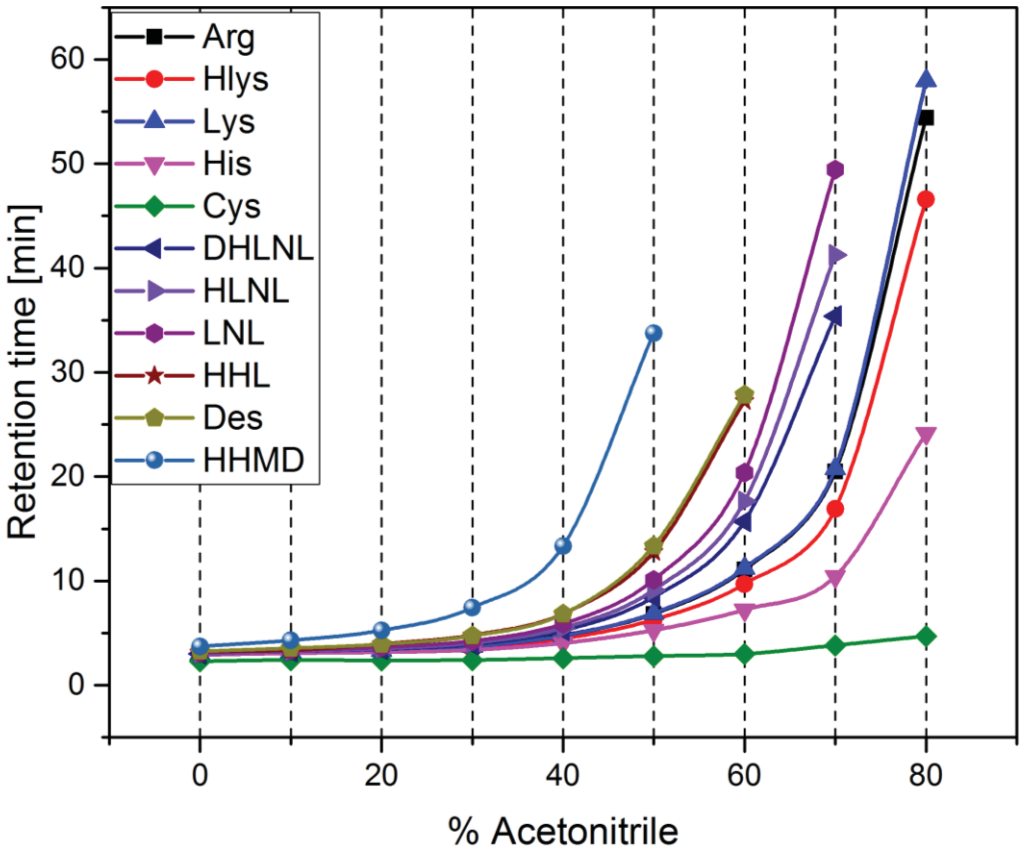

Figure 98: Retention times for basic amino acids arginine (Arg), hydroxylysine (Hlys), lysine (Lys) and histidine (His), cystine (Cys), immature crosslinks (DHLNL, HLNL. LNL) and mature crosslinks (HHL, HHMD and Des).

7.3.4 Effect of ESI source temperature on retention time

To investigate the effect of the ESI source temperature, the positive ion spectra of the crosslinks were measured using different ESI source temperatures (200 ºC, 250 ºC, 275 ºC, 300 ºC and 350 ºC). Although the source temperature caused significant decrease in crosslink retention times as the temperature decreased from 300 ºC to 250 ºC (Figure 99), their resolution did not improve and the response ratio between the doubly charged and singly charged ions did not change.

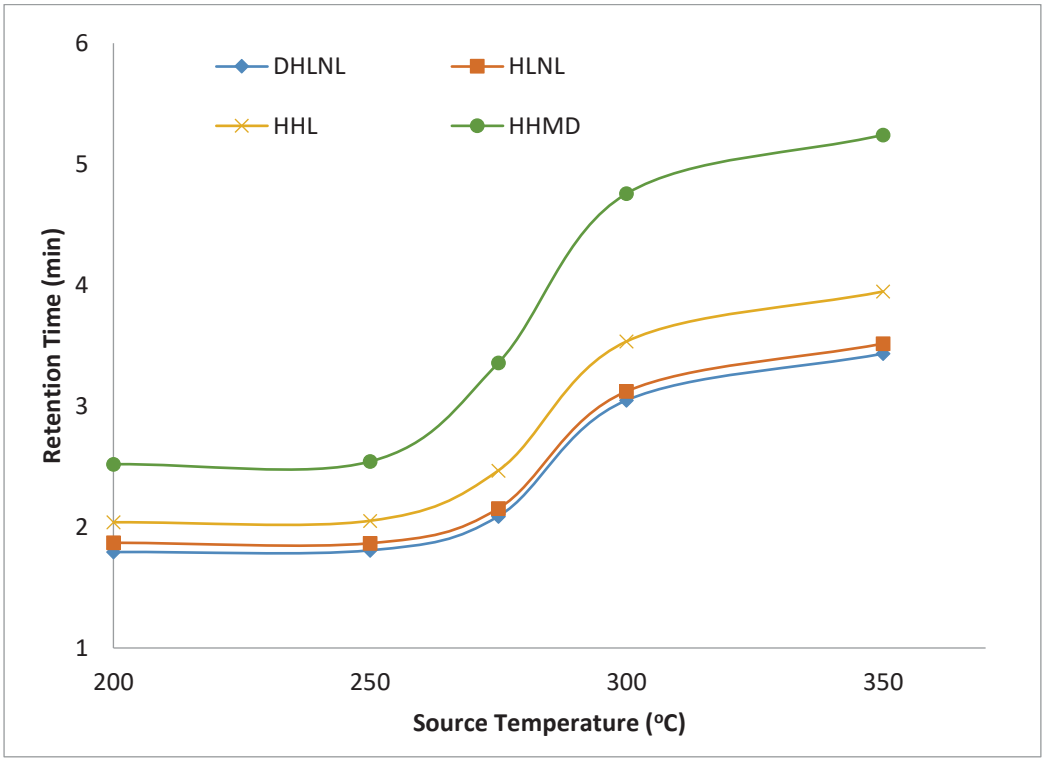

Figure 99: Effect of source temperature (nitrogen gas temperature in ºC) on four crosslink retention times. The crosslinks were eluted isocratically using 80 % acetonitrile with a flow rate of 400 µL/min and total run time of 60 minutes.

7.3.5 Peak resolution and broadening

Seven crosslinks were successfully separated on the silica hydride column using isocratic elution. However, it was observed that in order to elute HHMD with a peak width less than 1 minute, the mobile phase needed to contain at least 80 % water (Figure 100B). When the mobile phase contained less than 60 % water, HHMD eluted as a broad peak (> 3 min wide) and had a long retention time (Figure 100A). It was also observed that Des and HHL were co-eluted from the column when more than 60 % of water was used. In order to address this problem, several gradient elutions were optimised using acetonitrile as the organic solvent in water.

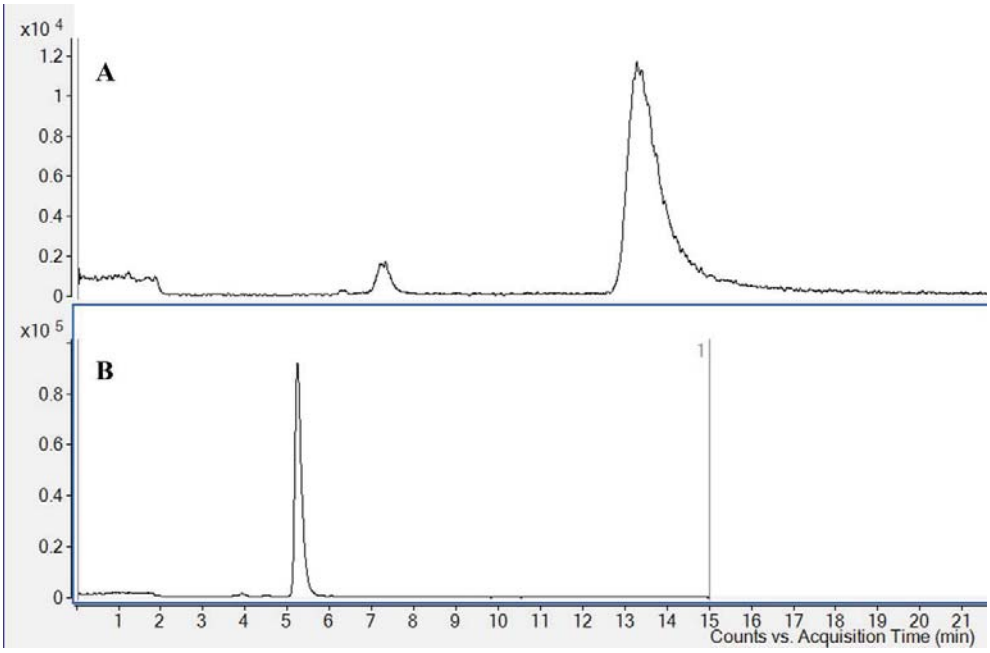

Figure 100: Comparison of the peak width of HHMD using two isocratic conditions: (A) 40 % acetonitrile and (B) 20 % acetonitrile both containing 0.1 % formic acid. Flow rate was 400 µL/min.

7.3.6 Gradient separation

Several gradients were investigated based on a gradual increase of the polarity of the mobile phase using acetonitrile and water. The optimum resolution of all collagen crosslinks was achieved using a binary solvent system consisting of solvent A, (water/0.1 % formic acid (v/v)) and solvent B, (80 % acetonitrile / 0.1 % formic acid (v/v)) at a flow rate of 400 µL/ml over a run time of 20 minutes. These gradients are shown in (Figure 101, inset). All crosslinks were fully resolved and eluted from the column in 10 minutes with a peak width less than 1 minute (Figure 101).

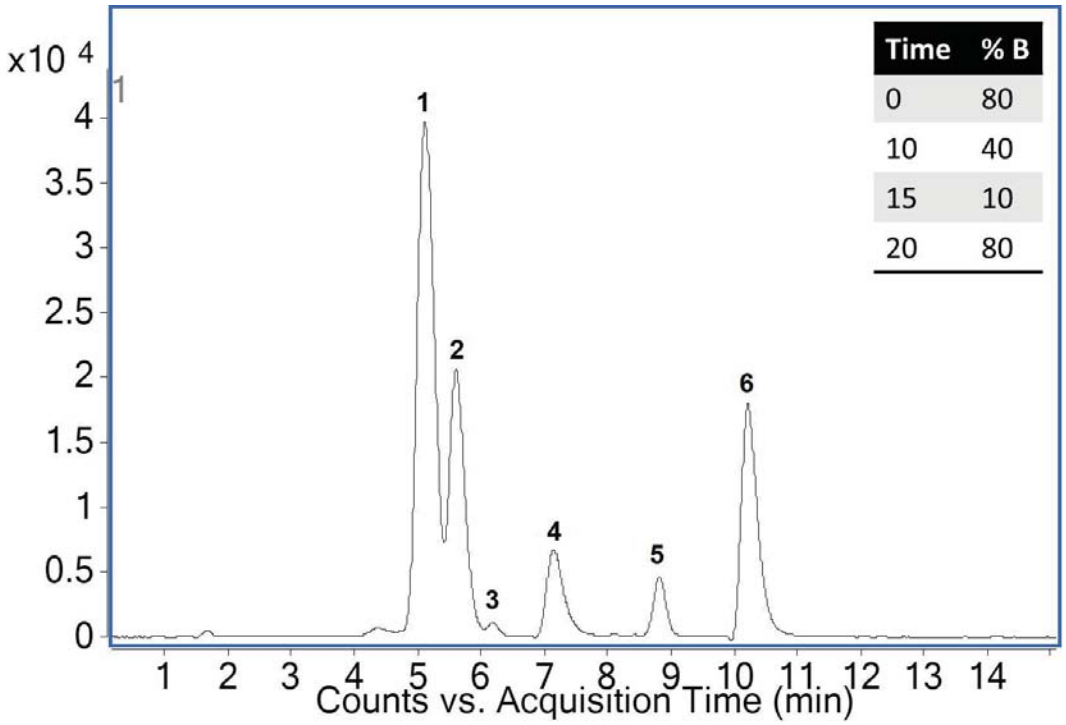

Figure 101: Extracted ion chromatogram (EIC) chromatograms of DHLNL, HLNL, LNL, HHL, Des and HHMD crosslink standards separated on the Cogent Diamond Hydride HPLC column (1) DHLNL, (2) HLNL (3) LNL, (4) HHL, (5) Des and (6) HHMD. Inset table shows gradient used to eluted the crosslinks. Total run time was 20 minutes and flow rate was 400 µL/ml.

7.3.7 Method validation

Retention times, calibration curves, limit of detection (LOD) and limit of quantitation (LOQ) for DHLNL, HLNL, HHL and HHMD were determined as well as the intra- and inter-day precisions (Table 22). LOD and LOQ are defined as concentrations that are 3 and 9 times the signal to noise ratio, respectively. All LOD and LOQ were in sub-pmole range. It should be noted that this is the first report showing HHMD and HHL can be fully separated and detected by mass spectrometry without pre or post-derivatisation.

Correlation coefficients (R^2) for all crosslinks were higher than 0.995 and the coefficient of variation (CV %) of the retention time (R_t) was less than 1 %. The precision values of the measurements within one day (intra-day) and day to day (inter-day), measured over a 3 day time period, were less than 5 % and 10 %, respectively.

Table 22: Results of the method validation

Crosslink	R_t (min) (CV%)	R^2	LOD (pmol)	LOQ (pmol)	CV% Intra-day	CV% Inter-day
DHLNL	5.26 (0.55)	0.9992	0.07	0.2	2.5	6.8
HLNL	5.57 (0.76)	0.9983	0.10	0.3	4.2	7.1
HHL	7.07 (0.53)	0.9961	0.27	0.8	3.6	4.1
Des	8.66 (0.26)	0.9971 0.9931[a]	0.33 0.088 [a]	1.0 0.25 [a]	2.1 -	3.5 -
HHMD	10.17 (0.65)	0.9957 0.9946[a]	1.0 0.13 [a]	3.0 0.38 [a]	4.9 -	9.5 -

[a] Calculated based on the doubly charged ion response.

Surprisingly, the pyridinoline concentration decreased and disappeared after 14 days (Figure 102). It had previously been reported that pyridinoline can be degraded by irradiation with UV [457, 458] which might explain this as no attempt was made to shield the solution from light.

7.3.8 Analysis of crosslinks in animal skins

The optimised method was used to analyse the concentrations of each crosslink in skin samples taken from sheep, goat, deer and cow. Three biological samples of each skin were prepared and the crosslinks were isolated, separated and analysed using both isocratic and gradient elution.

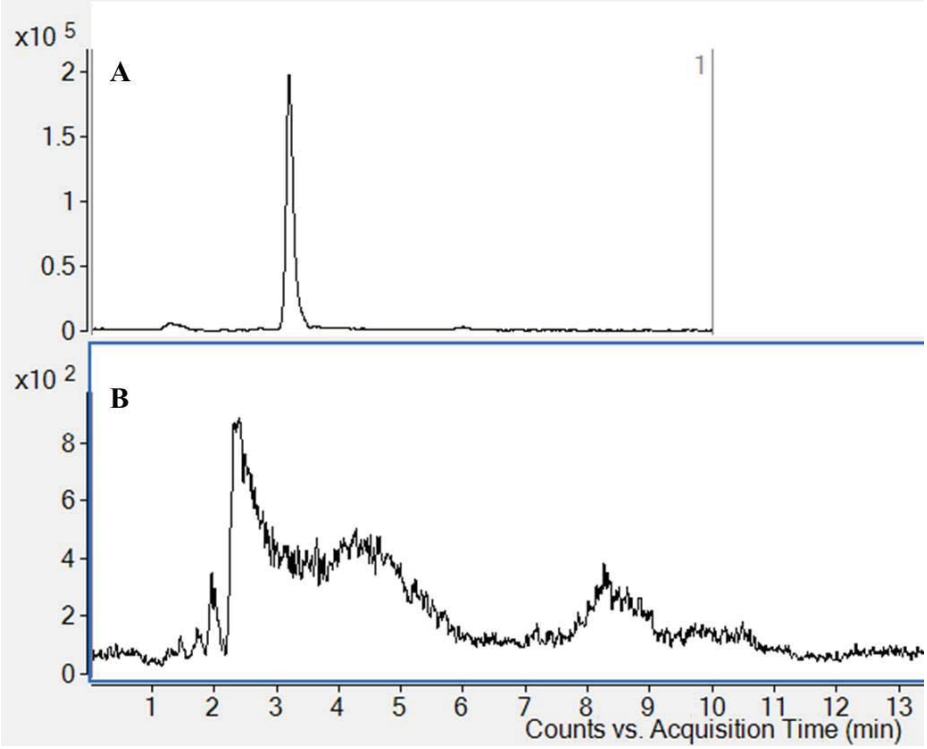

Figure 102: Extracted ion chromatogram (EIC) chromatograms of Pyr (A) day one (B) 14 days. Separation was carried out using 80 % water in acetonitrile. Total run time was 15 minutes and the flow rate was 400 µL/ml.

All skin samples were shown to contain DHLNL, HLNL, LNL, HHL, Des and HHMD, although they were present in different ratios (Figure 103). The total crosslink concentration was highest in cow skin and lowest in sheep skin, while goat and deer skin had similar total crosslink concentrations. In regard to the immature crosslinks, sheep skin contained the highest concentration of DHLNL and cow skin contained the highest HLNL concentration. For the mature crosslinks of HHL and HHMD, cow skin was shown to have the highest concentration of HHMD while deer skin had the highest concentration of HHL.

Using this method, DHLNL, never before detected in skin, was shown to be present in all the skins used in this study. In addition, three extra masses were detected (530.3276 m/z, 427.2439 m/z and 556.2031 m/z), which from preliminary investigations are likely to be crosslinks that have not been previously identified (Figure 105). The 427.2439 m/z crosslink has been previously reported, although there appears to be some controversy about its identity [459, 460]. Unfortunately, there was no time to investigate these within the timeframe of this project, but they will be analysed and characterised in the future.

The ratio between the mature (HHL+HHMD) to immature (DHLNL+HLNL) crosslinks was calculated (Figure 104). It is clear that deer skin has the largest ratio of approximately 30 while sheep skin has the smallest ratio of approximately 5. Goat and cow skins have similar ratios of approximately 12. It has been previously reported that types and concentrations of collagen crosslinks are related to aging [97, 126]. Robins *et al.* (1973) reported a decrease in the concentration of HLNL with ageing and Yamauchi *et al.* (1988) showed that this decrease was associated with an increase in

HHL concentration [97, 126]. The exact age of the goat, deer and cow skins was unknown because the skins were sourced from the meat industry and it was not possible to know the age of each animal. Thus the relationship between crosslink concentrations and age could not be established. However, based on the findings of Yamauchi *et al.* (1988) and this study, it is likely that deer skin was the oldest skin while sheep skin was the youngest. Further studies are required to confirm this by collecting skins of known ages and analysing their crosslinks using the methods reported here. There appears to be some relationship between the total concentration of crosslinks and skin strength. Sheep had the weakest skin and the smallest total concentration of crosslinks while cow had the strongest skin and the largest total concentration of crosslinks.

Initial qualitative results for the pickled skins of sheep, goat, deer and cow showed that the concentration of the HLNL, DHLNL and HHMD crosslinks decreased significantly compared to those in all raw skins tested. Not surprisingly, the concentration of HHL only decreased slightly because it is much more acid stable than the other crosslinks [94, 461]. Further analysis is required to accurately determine the concentration of each crosslink in pickled skins.

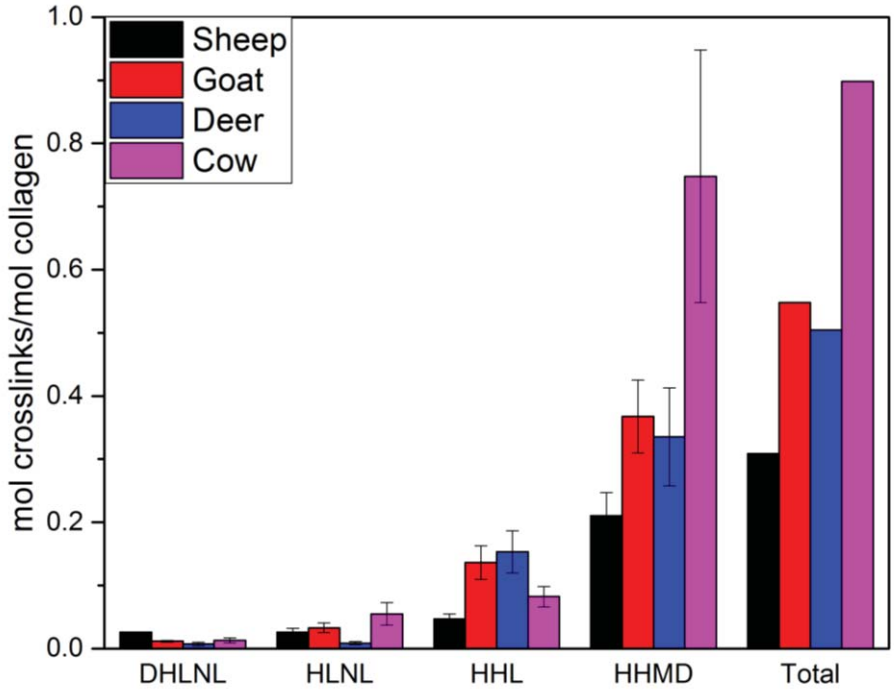

Figure 103: Collagen crosslinks in sheep, goat, deer and cow skins. All values are normalised to the collagen content based on the hydroxyproline concentration in the skins. Average of five biological samples of sheep and goat and four biological replicates of deer and cow.

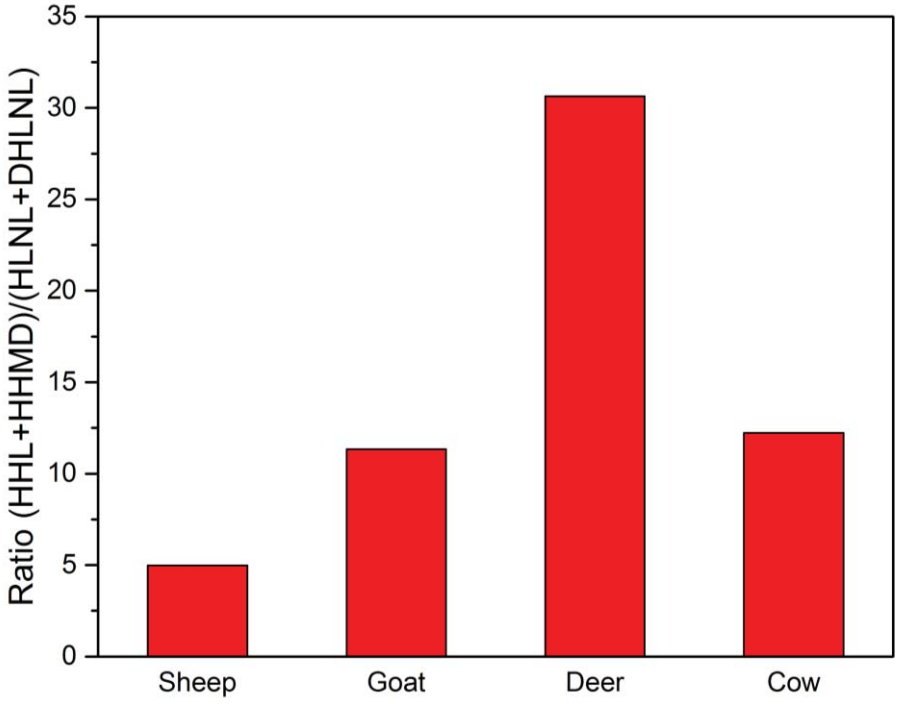

Figure 104: Ratio of mature crosslinks (HHL+HHMD) to immature crosslinks (HLNL+DHLNL).

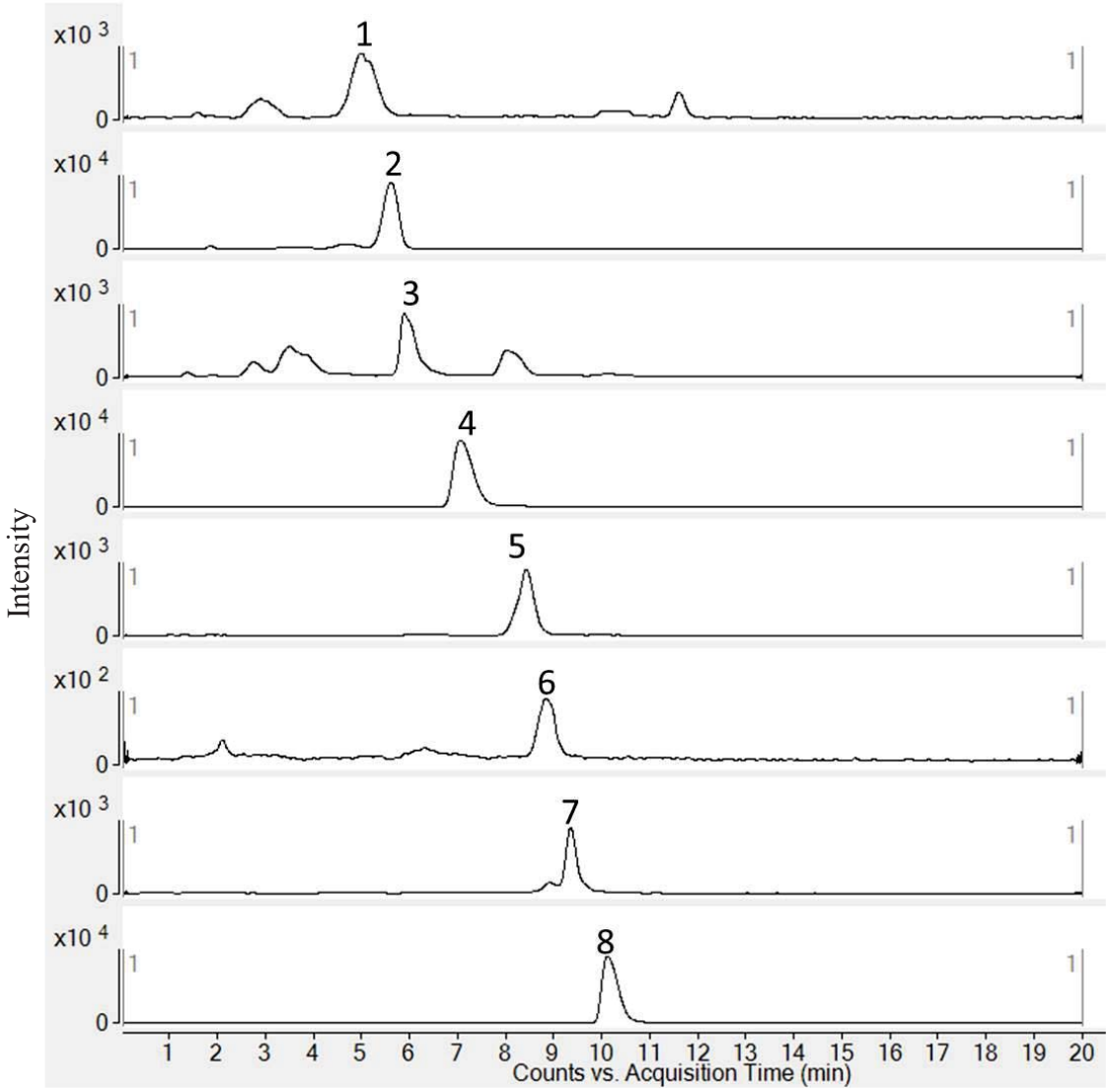

Figure 105: Crosslink chromatogram from one cow skin. Separation by gradient elution. (1) DHLNL (2) HLNL (3) LNL (4) HHL (5) 530.3276 (6) Des (7) 427.2439 (8) HHMD and 556.2031. Separation was carried out with same gradient conditions shown in Figure 95. Total run time was 20 minutes and flow rate was 400 µL/ml.

8 CHAPTER EIGHT: Small Angle X-ray Scattering (SAXS)

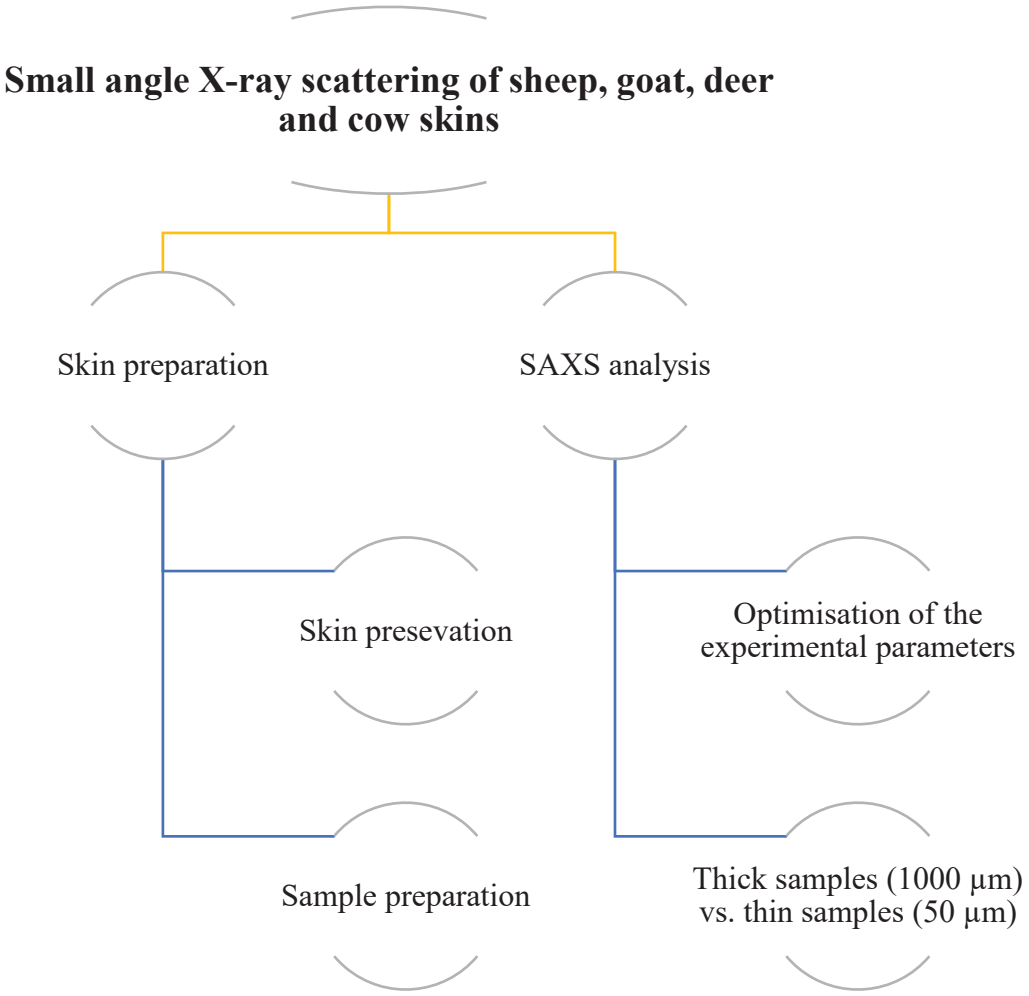

8.1 Introduction

Skin is the largest organ in mammals and has many functions such as regulation of body temperature, protection from the environment and elimination of the waste products. Skin is a non-linear, anisotropic and viscoelastic tissue that is composed of three well defined layers; the epidermis, the dermis and the hypodermis. Each layer is characterised by the specific organisation and distribution of the macromolecular components which defines their biological and mechanical functions [28, 462]. The middle layer or dermis, which accounts for 90% of the weight of the skin, is composed of compact collagen and elastin fibre networks that are responsible for the strength of skin [2].

Collagen is synthesised in the fibroblast then secreted into the extracellular space where it is linked by covalent crosslinks that spontaneously form between collagen molecules as a result of condensation between allysine, hydroxyallysine, lysine, hydroxylysine and histidine residues. The formation of these crosslinks enables the tropocollagen molecules to form microfibrils which are characterised by a parallel staggered arrangement in which every repeat consists of five collagen molecules with a gap and overlap regions creating a periodicity of 67 nm. Microfibrils are further organised into fibrils with diameters of 20–200 nm which then assemble into fibres with diameters of approximately 1 μm [6].

There are several types of covalent crosslinks in skin; lysinonorleucine (LNL) and desmosine (Des) are found in elastin, while hydroxylysinonorleucine (HLNL), dihydroxylysinonorleucine (DHLNL), histidinohydroxylysinonorleucine (HHL), histidinohydroxymerodesmosine (HHMD) are found in collagen [83, 140, 226]. The

development of covalent crosslinks within collagen fibrils is essential for the stabilisation of the tissue structure and therefore critical for the biomechanical properties of specific tissues which are defined by the alignment of their collagen fibrils [6, 12, 82, 365, 375, 376, 463]. For example, the parallel alignment of collagen fibrils in bone enhances its longitudinal strength while the precise organisation of fibrils in the eye provides transparency to the cornea. On the other hand, the anisotropic nature of skin is associated with a random organisation of fibres that is crucial to the superior tear strength of skin [4, 6, 339, 376, 464-467].

Factors that affect the mechanical properties of skin include fibril orientation [339, 468], the types and concentration of crosslinks [375, 376, 469-471], fibril diameter [14, 238, 472, 473] and ageing [96, 474-476]. Using molecular dynamic simulations, Kwansa *et al.* predicted that because the HHL appears to be stronger than either HLNL or DHLNL, the number and position of the different crosslinks is likely to affect the mechanical properties of skin [375]. Although many publications on skin have separately investigated factors that may affect its strength such as fibril orientation, fibril diameter, and crosslink type and concentration, there appears to be no investigation into the relationship between them.

In this work, the key biomolecular components of different animal skins were analysed and related to the physical and structural properties of each type of skin. Four animal skins were selected, each with different physical properties. Sheep skin is weak and thin while cow skin is strong and thick. The skins of goat and deer have moderate strength and while they are thinner than cow, they are stronger than sheep skin [4]. The types and concentrations of crosslinks were measured using a previously published

method [393]. The sample were then examined using small angle X-ray scattering (SAXS) to analyse the fibril orientation and diameter [4, 14, 329, 477] and using transmission electron microscopy (TEM) to visualize the collagen fibrils in each type of skin. As TEM provides only a two dimensional (2D) view of the sample [329, 465], laser confocal microscopy was used to obtain a 3D image of the skin samples which enabled the relationship of the SAXS data to the 3D hierarchical structure of skin to be determined [478]. As a result, a plausible model was proposed that defines skin strength in terms of the correlation between the fibril orientation, fibril diameter and the number and type of crosslinks. The results from this study will be used to gain a better understanding of the factors that are responsible for the physical properties of skin.

8.2 Experimental procedure

8.2.1 Chemicals and materials

See chemicals and materials in chapter 3.

8.2.2 Collection and preparation of skin samples

Skins of sheep, goat, deer and cow were prepared as described in chapter 3 (sections 3.2.2 and 3.2.3). Samples for SAXS analysis were then prepared in two different ways: thicker samples that had been pre-treated to prevent bacterial growth were cut into strips (1.0 mm × 30.0 mm) using a home-made tool which gave a consistent sample thickness (1.0 mm ± 0.1 mm) (See the Appendix for a description of the in house cutting tool under “cutting tool to give skin sections of 1 mm thickness”), then sealed between two pieces of Kapton^{TM} tape to prevent sample dehydration and stored on ice. For thinner samples, 5 mm × 5 mm pieces of skin that had been pre-treated with the

protease cocktail were placed on the sectioning holder of a cryostat microtome (Leica CM 1850 UV cryostat) at -30 °C and sectioned at 50 µm. Three of the best slices were then sealed between two pieces of Kapton^{TM} tape and stored at -30 °C before being transported to the synchrotron on dry ice.

8.2.3 Small-angle X-ray scattering (SAXS) data collection

Skin samples were handled carefully to avoid any stretching or deformation during slicing and preparing samples for SAXS measurements. Sections enclosed in Kapton^{TM} tape were mounted on the sample holder in a transmission geometry (Figure 106), then scattering patterns were recorded at room temperature on the Australian Synchrotron SAXS/WAXS beamline [479]. To test the effect of the beam sampling volume, different beam sizes were used: (200×200), (100×100) and (50×50) µm, with an exposure time of 2 s and an X-ray wavelength of 1.0332 Å. Diffraction patterns were recorded using a Pilatus 1 M detector with a sample to detector distance of 3342 mm, giving a q-range of 0.002 to 0.25 Å^{-1}. Calibration was carried out using a silver behenate standard. An 11×11 map was generated for each sample by recording diffraction patterns as the sample was translated in 0.05 mm steps in the x-y plane (perpendicular to the X-ray beam).

8.2.4 SAXS data analysis

SAXS data from the Australian Synchrotron were visually inspected using ScatterBrain v.2.82 (http://www.synchrotron.org.au/aussyncbeamlines/saxswaxs/ software-saxswaxs). The 2D raw SAXS images recorded in Cartesian coordinates were then

converted into polar coordinates using FIT2D v. 18 (http://www.esrf.eu/computing/scientific/FIT2D/) [480].

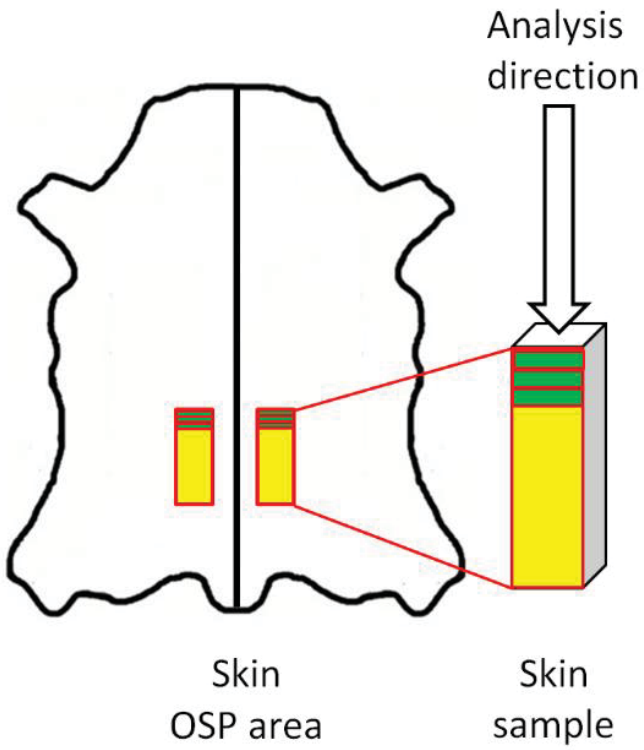

Figure 106: Schematic diagram of skin shows the skin slices in green and the direction of the SAXS analysis.

Three programs written and developed by Dr Bridget Ingham (senior research scientist at Callaghan Innovation, Wellington, New Zealand) were used to generate radial and azimuthal plots from the converted images. See Appendix under "chapter 8 – SAXS" folder for all programs. Also several examples of raw and processed SAXS data are given in the appendix.

8.3 Results and discussion

8.3.1 SAXS data processing

Collagen molecules, fibrils and fibres are the major hierarchical elements of skin and their architecture is influenced by complex interactions with other non-collagenous molecules such as proteoglycans [461]. The tropocollagen molecules spontaneously self-assemble into a parallel staggered arrangement with a D-periodicity of around 67 nm, in which every repeat consists of five collagen helices, resulting in a gap region [(67 nm× 5) – 300 nm = 35 nm] and an overlap [300 nm – (67 nm × 4) = 32 nm]. The resulting fibrils have diameters of approximately 50 nm with a lateral spacing between molecules of 1.5 nm and are then organized into fibres, with diameters of the order of 1 μm, mediated by proteoglycans [461]. Due to this periodicity, collagen shows characteristic equatorial (off-axis) and meridional (on-axis) SAXS scattering (Figure 107). The meridional rings are used to determine the D-periodicity of collagen in the skin sample while the equatorial streak is used to determine the fibril diameter of the collagen. This raw image, however, requires processing before it can be used to measure the collagen D-periodicity and fibril diameter.

8.3.1.1 SAXS image processing

The 2D raw SAXS image obtained in Cartesian co-ordinates (Figure 108) was converted into angular co-ordinates (Figure 109) using the FIT2D program. This image shows the distribution of X-ray scattering intensity of collagen diffraction peak and was used to generate radial and azimuthal plots (see section 8.3.2).

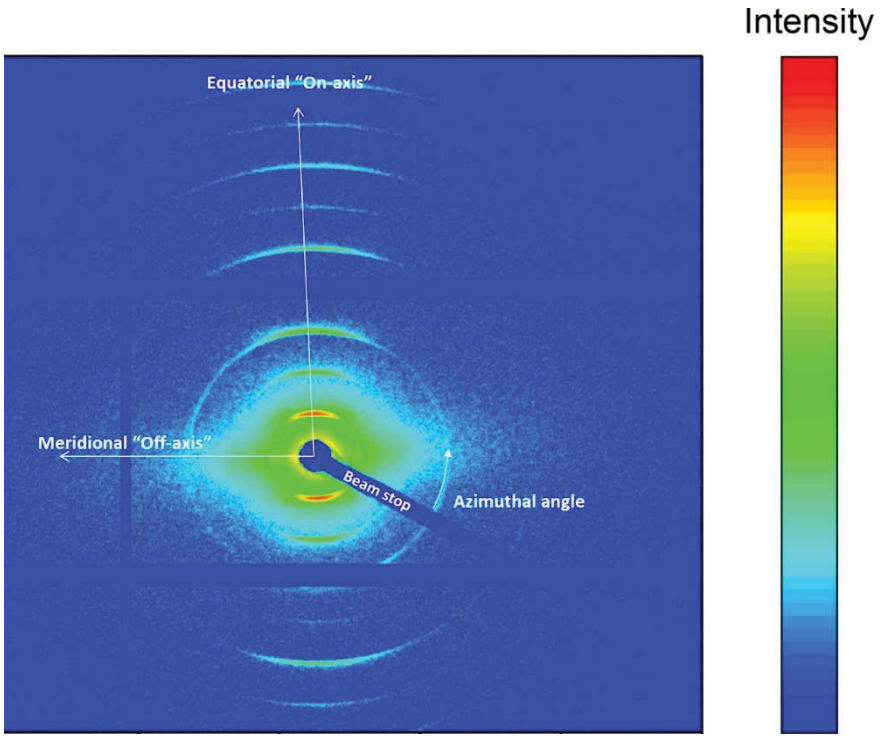

Figure 107: The 2D raw data image in Cartesian co-ordinates showing the on- and off-axis directions according to the position of the collagen diffraction peaks. The azimuthal angle is defined relative to the beamstop. Vertical and horizontal black bars are the gaps between the detector modules.

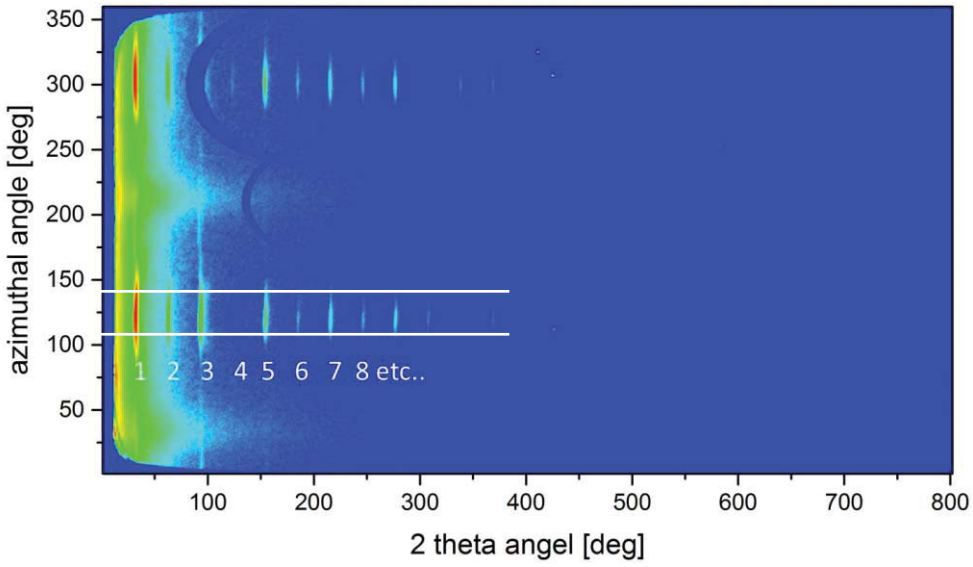

Figure 108: The data in Figure 107 converted into angular co-ordinates using FIT2D. The diffraction peaks (order n as indicated) appear as vertical lines representing the intensity extracted over a 30 degree range around the on- and off-axis directions.

8.3.1.2 Extraction of Diffraction rings

Data processing and analysis was performed using in-house software written and developed by Dr Bridget Ingham from Callaghan Innovation (Wellington, New Zealand) to extract the scattering intensity using cake slice approach as a function of both the radial and azimuthal angle. Radial scattering intensity plots were obtained by integrating the intensity over an azimuthal range of 30 degrees around the on-axis and off-axis directions (where on-axis corresponds to the highest intensity of the collagen diffraction) (Figure 109).

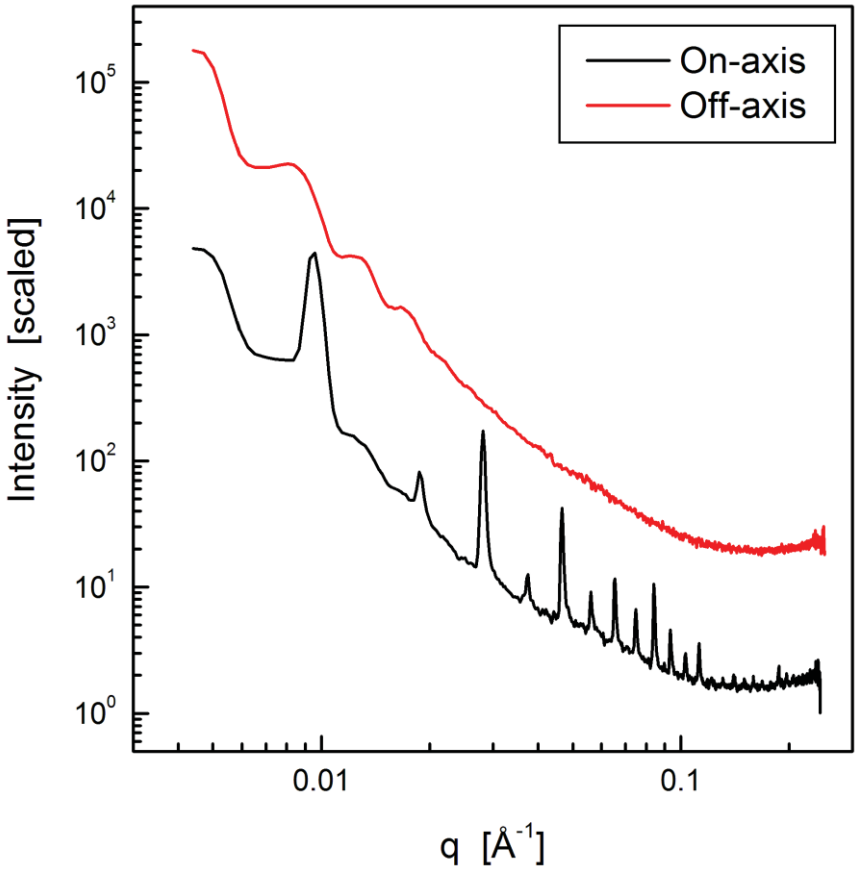

Figure 109: Intensity versus q extracted over 30 degrees around the on- and off-axis directions as indicated in Figure 107. The off-axis data shows form factor scattering from the fibril bundles and no collagen diffraction peaks, while the on-axis data shows strong collagen diffraction peaks superimposed on the (weaker) form factor scattering.

8.3.1.3 Azimuthal angle plot

Azimuthal scattering intensity plots were obtained from the most intense collagen diffraction ring, by converting the data into intensity versus radial angle in 1° azimuthal divisions (Figure 110), then fitting a Gaussian peak with linear background to a narrow range encompassing the peak, and recording the peak area versus azimuthal angle (Figure 111). This method is more accurate than simply extracting the intensity at a fixed point, since it separates the diffraction peak from the background and form factor scattering.

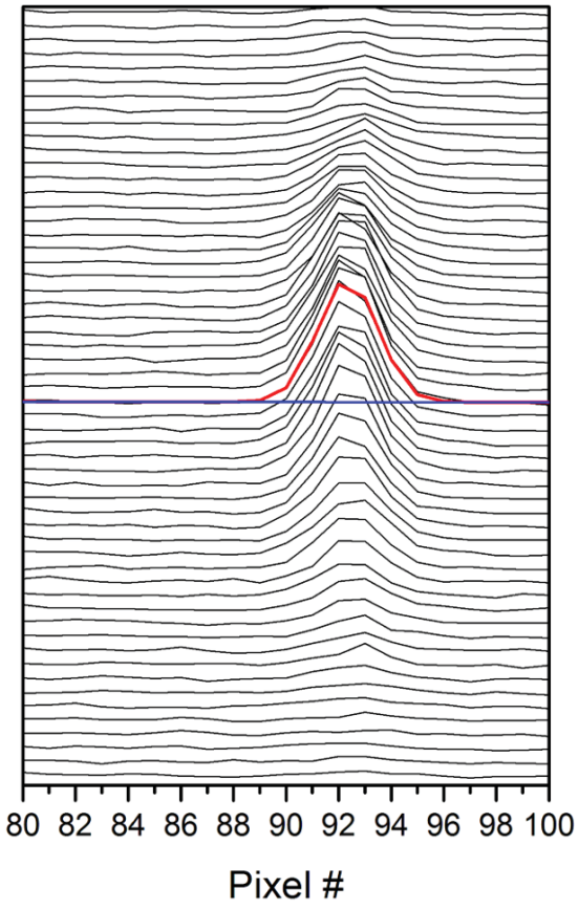

Figure 110: Selected region of processed data from Figure 108, showing how the n = 3 diffraction peak data in each 1° azimuthal slice were fitted using a Gaussian peak (red line) on a linear background (blue line). The peak areas are then plotted versus azimuthal angle to produce Figure 111(a).

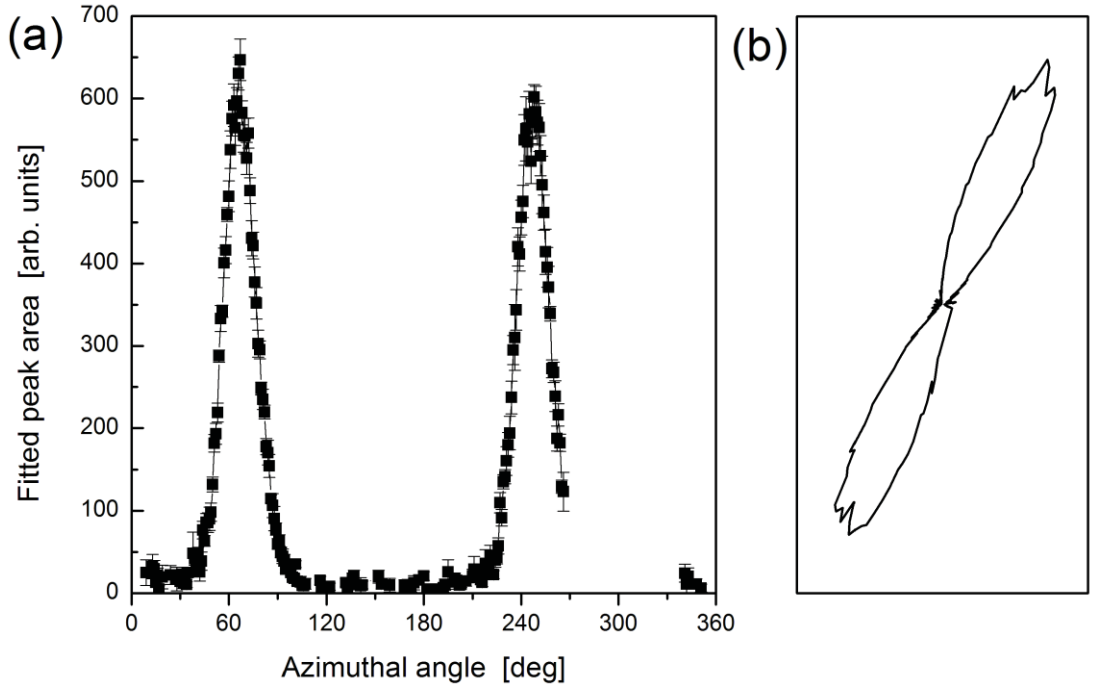

Figure 111: (a) Fitted peak areas of the n = 3 diffraction peak, versus azimuthal angle. (b) The same data, displayed in polar form, clearly demonstrates the directional spread of the fibrils as being 180 degrees.

8.3.1.4 Peak fitting

The intensity versus azimuthal angle plots were fitted using Gaussian peaks to obtain the width, as a direct measure of the spread of distributions of the fibrils. A second in-house computer program was used to fit the scattering intensity versus the magnitude of the scattering vector, q ($q = \frac{4\pi}{\lambda} \sin\theta$, where θ is half of the radial angle), in both the on- and off-axis directions. For a highly oriented region, the off-axis direction shows a series of form factor oscillations and no collagen diffraction peaks (Figure 109). The form factor oscillations were fitted using a spherical form factor (with log-normal size distribution applied to the radius), added to a power-law plus constant background, over a q-range of 0.005 – 0.12 $Å^{-1}$ (full mathematical details are given in section 8.3.1.5). Tests fitting the data to a cylindrical model (the more usual model for

collagen) did not yield results that were significantly different; hence for ease of computation the spherical model was used (see appendix for details-chapter 8). The form factor oscillations are also present in the on-axis direction; since these arise from fibrils of the same size (in a different direction), the size parameters were fixed. Superimposed on the form factor oscillations are the collagen diffraction peaks, which were fitted with Gaussian functions, having their positions determined by the D period as a single parameter (the center of the n^{th} order peak is at $q = \frac{2\pi n}{D}$), their widths defined by two parameters in a Williamson-Hall-type relationship ($w = A.q + B$), and their areas as independently fitted parameters. The on-axis data were fitted over the same q-range (0.005 – 0.12 $Å^{-1}$), which encompassed peaks of order 1 to 12.

8.3.1.5 Full mathematical processing of SAXS results

The SAXS model used consists of three parts: the fibril form factor scattering, the background (arising from the Kapton™ tape, molecular water and other species, and scattering from larger structures), and the collagen diffraction peaks.

$$I(q) = I_{ff}(q) + I_{bkg}(q) + I_{diff}(q)$$

The form factor scattering of a sphere was used, convoluted with a log-normal size distribution:

$$I_{ff}(q) = c\int f(qr)^2 n(r) dr$$

where the form factor of a sphere is $f(qr) = 3\frac{\sin(qr) - qr\cos(qr)}{(qr)^3}$

and the log-normal size distribution has the form $n(r) = \frac{1}{r\sigma\sqrt{2\pi}} \exp\left(\frac{-[\ln(r/r_0)]^2}{2\sigma^2} \right)$

The background scattering consisted of a power law plus constant term:

$$I_{bkg}(q) = aq^{-b} + d$$

The diffraction peaks were modelled as Gaussians,

$$I_{peaks}(q) = \sum_i \frac{A_m}{w(q)\sqrt{\pi/2}} \exp\left(\frac{-2(q - q_{c,m})^2}{w(q)^2} \right)$$

where A_m is the area of peak m, the peak position $q_{c,m} = \frac{2\pi m}{d}$ where d is the D-periodicity (in Å), and $w(q)$ is the width, expressed as $w(q) = a + bq$ where a and b are fitted parameters.

8.3.2 Determining sample and beam parameters

Prior to collecting the SAXS images of skin samples, it was important to establish the experimental conditions to get the optimum X-ray scattering from the oriented collagen fibril bundles with the minimum accumulation of the background. Four parameters were investigated and optimised which included the skin sample thickness, beam size, exposure time (radiation dose) and sample hydration. We addressed the effect of each of these by capturing the diffraction patterns of several skin samples under different conditions.

8.3.2.1 Thick vs thin skin samples

To minimise the spread of distributions observed due to illuminating multiple fibrillar regions having different orientations, samples of two different thicknesses (~1000 and 50 µm) were measured using three different beam sizes (200×200, 100×100 and 50×50 µm). There was virtually no difference in the azimuthal intensity plot for the different beam sizes for the thick samples, but significant differences were observed for the thin samples, with the smallest beam size yielding the narrowest distribution and the absence of other peaks (Figure 112).

In this case the beam is sampling a volume of 50 × 50 × 50 µm. Ideally, this would contain a single fibrillar region (equivalent to a crystallographic 'grain') to give the true spread of orientations within that region. Even with such a small beam size, however, this was not always observed. Multiple fibrillar regions manifest as multiple peaks or asymmetric peaks. Using thin samples minimises the number of fibrils that are oriented parallel to the X-ray beam, which simplifies the orientation distribution equation [330].

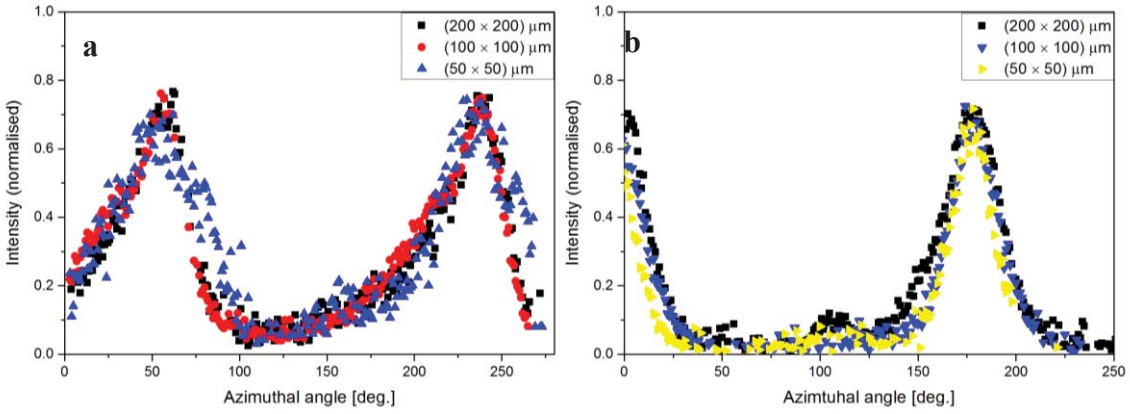

Figure 112: Azimuthal plot of the 3rd diffraction peak of the skin samples. (a) Thick sample (1000 µm). (b) Thin sample (50 µm). Insets show the beam size.

8.3.2.2 Radiation dose

Since these measurements indicated that the thinnest samples appeared to be the most promising for obtaining the orientation distribution, the effect of the radiation dose on a 50 µm sample was investigated by illuminating the same spot for 10 scans and comparing the images collected. No significant change in the scattering pattern was observed indicating that no radiation damage occurred during this time (Figure 113).

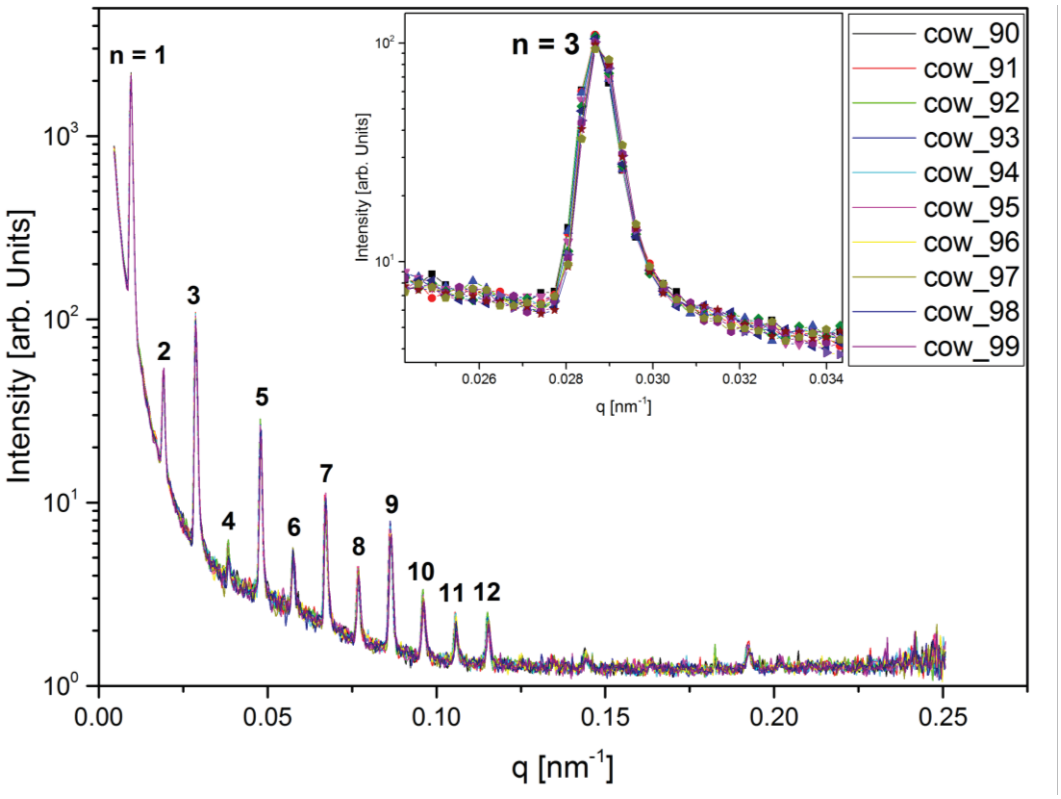

Figure 113: Effect of radiation dose on the q-plot. The same spot was illuminated 10 times with an X-ray that had a beam size of (50×50) µm. The sample thickness was 50 µm and the exposure time was 10 seconds. The inset shows the diffraction peak 3 (n = 3). It is clear that there was no change in the intensity suggesting that no skin damage occurred.

8.3.2.3 Effect of hydration

Sample hydration is essential when collecting SAXS images as water is an integral part of skin because it forms hydrogen bonds between hydroxyproline stabilising the collagen structure [46, 481]. Skin dehydration will therefore result in structural changes to the skin [33]. It has been previously reported that the odd and even diffraction peaks are a good indicator for the degree of hydration of skin [9, 158, 482, 483]. Stinson and Sweeny reported that the intensity of the even diffraction peaks significantly increased while the odd orders appeared to decrease as skin dried out [158]. This fact was used to monitor the SAXS images as they were processed. Any image appearing to have a high intensity of 6^{th} order diffraction peak was rejected because of suspected dehydration. Figure 114 shows the q-plots of dry and hydrated 50 μm skin samples analysed by SAXS. The dry sample shows a large increase in the intensity ratio 3^{rd} to 6^{th} diffraction peaks. The d-spacing has not changed and this is in agreement with Stinson and Sweeny who found that d-spacing did not change on drying [157]. Placing the skin samples between Kapton™ tape appeared to be an effective way to prevent sample dehydration keeping the samples fully hydrated during SAXS data collection.

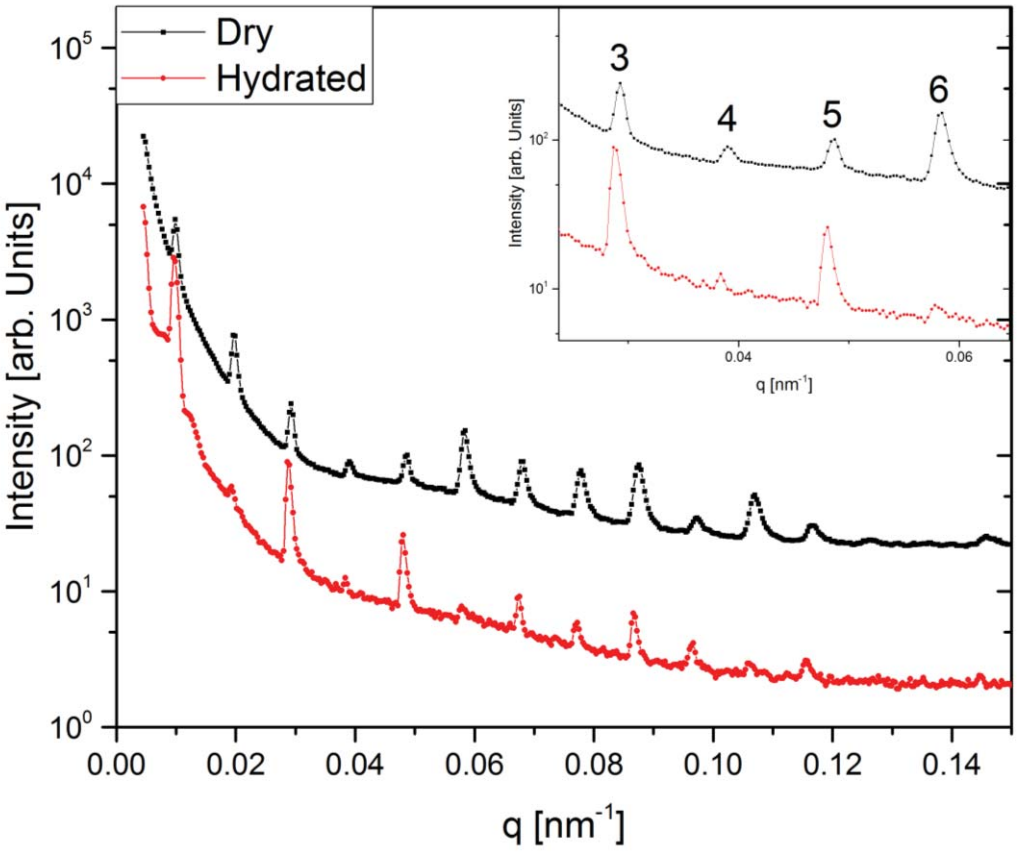

Figure 114: Effect of dehydration on diffraction peaks during SAXS data collection. Dry and fully hydrated 50 µm skin samples were illuminated with an X-ray. Beam size was (50×50) µm and exposure time was 10 seconds. The 6th diffraction ring is barely visibly in hydrated skin sample and when skin dried its intensity increased.

8.3.2.4 Pattern of the X-ray scattering of sheep, goat, deer ad cow skins

The apparent pattern of the diffraction rings in sheep, goat, deer and cow skins was compared. Figure 115 shows 1st to 9th diffraction peaks from the sheep, goat, deer and cow skins. Generally, the odd diffraction peak intensity is much higher than those of even order in all skins. This pattern has been previously correlated to the water content of the collagen fibrils [77, 482]. There were no apparent pattern differences between the skins indicating that they all have similar collagen structures within the collagen fibril.

The pattern of the equatorial (off-axis) scattering, was also analysed by plotting the scattering factor (q in A^{-1}) against the intensity (Figure 116). The shapes of the plots for sheep, goat, deer and cow skins were perfectly matched, however the positions (q value) of the maxima were different. This is related to the differences in the collagen fibril diameter in the different animal skins.

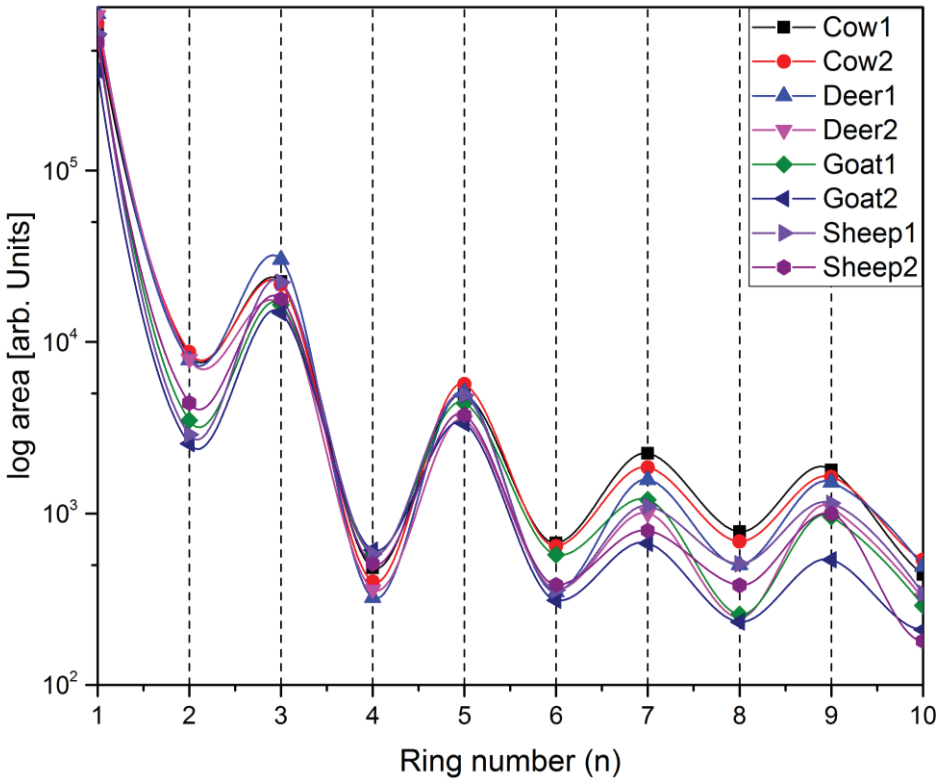

Figure 115: Graph of peak area and the diffraction peak number. This plot was extracted from the meridional (on-axis) data, encompassing the diffraction rings.

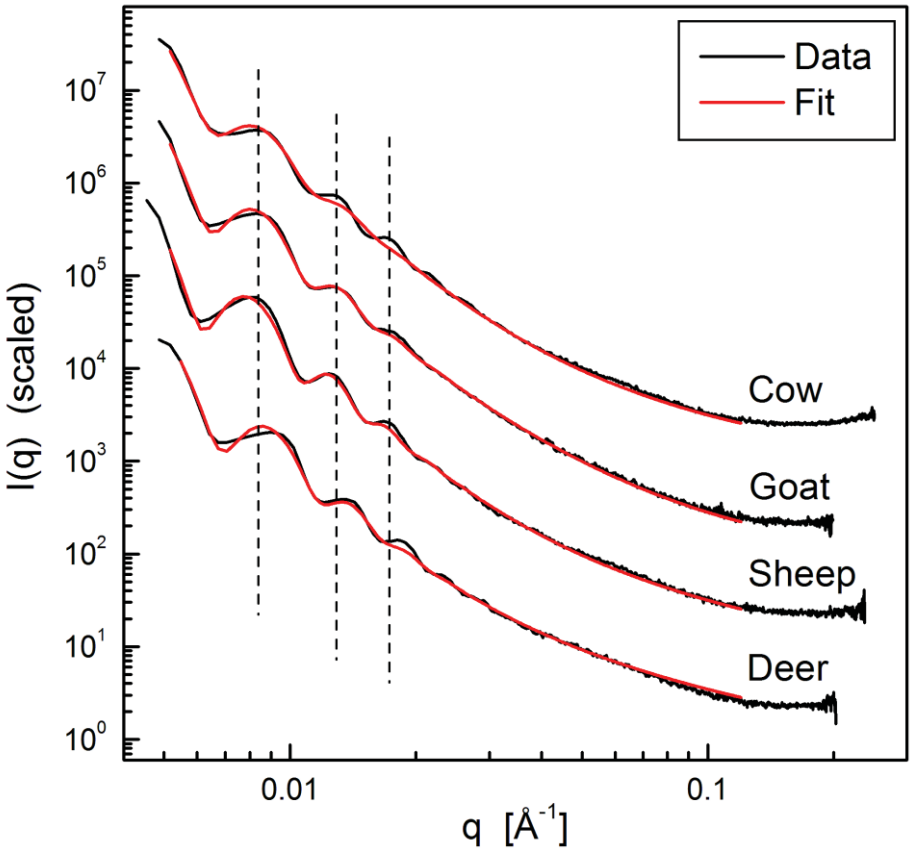

Figure 116: Example of off-axis SAXS data for the sheep, goat, deer and cow skins, showing the form factor oscillations. Dashed lines serve as guides to the eye to illustrate the similarity between cow, goat and sheep, while for deer the oscillations occur at higher q (indicating a smaller fibril diameter).

8.3.3 Fibril radius and D-period of animal skins

Four biological samples of each animal were collected and three replicates from each were analysed with the SAXS. The average fibril radius and D-periodicity of collagen fibrils in thin (50 μm) and thick (1000 μm) skin samples from sheep, goat, deer and cow skins are summarised in Tables 23 and 24. respectively.

The fibril diameter is obtained by fitting the off-axis SAXS patterns to a form factor model. Cow skin had the largest fibril diameter, followed by goat, then sheep, and finally deer, which has the smallest fibril diameter (Table 23). The student t-test gave

significant differences between fibril diameters of sheep, goat, deer and cow skins ($P < 0.05$).

The D-periodicity of collagen in sheep, goat, deer and cow skins was obtained by fitting the diffraction peaks in the on-axis scattering patterns. The relative intensities of these peaks can vary depending on the degree of hydration [157, 484, 485], the presence of ions [486, 487], or changes to the structure due to chemical processing [9]. All skin samples measured had virtually identical patterns in terms of the relative peak intensities, and were consistent with fully hydrated type I collagen. This might suggest that the packing of the collagen molecules inside the fibrils is the same for all skins. The fibrils in cow and deer skins have a slightly larger D-periodicity than those fibrils in goat and sheep skins. However, the student t-test indicated these were insignificant ($P > 0.05$). The same results were obtained from the thick skin samples (table 24), although the differences in the fibril diameters were more significant than those obtained from the thin samples (student t-test, $P < 0.05$).

Table 23: Fibril diameter and d-spacing of raw skin samples of sheep, goat, deer and cow measured with beam size was (50×50) μm, sample thickness 50 μm and exposure time 2 seconds. Average of 4 biological replicates.

Animal	Fibril diameter (nm)	%CV	D-periodicity (nm)	%CV
Sheep	137.5	4.1	64.90	0.12
Goat	141.1	5.2	64.95	0.13
Deer	130.8	2.3	65.02	0.02
Cow	143.8	5.4	65.06	0.16

Table 24: Fibril diameter and d-spacing of raw skin samples of sheep, goat, deer and cow measured with beam size was (200×100) μm, sample thickness 1000 μm and exposure time 10 seconds. Average of 4 biological replicates.

Animal	Fibril diameter (nm)	%CV	D-periodicity (nm)	%CV
Sheep	135.8	2.3	64.96	0.05
Goat	159.3	3.1	64.98	0.14
Deer	131.1	0.8	65.08	0.09
Cow	168.8	11.7	65.11	0.05

8.3.4 Collagen fibril orientation in animal skins

Maps of the fibril orientation at each point (obtained from the plots of the n=3 diffraction ring intensity versus azimuthal angle) are given in Figure 117. These maps show the azimuthal intensity of the n=3 ring normalised to the total integrated intensity for the ring over 30 degrees "cake slice approach", in polar co-ordinates, centred at the real-space co-ordinate where the scan was recorded. For regions where the fibrils are oriented in a single direction (two peaks in the azimuthal plot separated by 180°), the distribution in polar co-ordinates will have a propeller-like shape. Where there are multiple orientations present, these are manifested as additional lobes or distortion of the lobes.

From the maps, it is easy to identify regions in real-space having the same predominant orientation of the fibres. These regions are larger for cow than the other three; many of the 'propellers' in the cow skin map have two narrow lobes and lie in the same direction at adjacent measurement positions. In several places (e.g. x = 0.9, y = 0.1-0.4 in Figure 117-Cow) the 'propellers' have four lobes, two of which are oriented with the direction of an adjacent 'propeller' on either side. In contrast, in the sheep, goat and deer maps, there are relatively few 'propellers' that only have two lobes, and many of the lobes

are asymmetrical, indicating that two regions of similar fibre orientation direction may have been illuminated. There are many polar plots that appear to be quite noisy; for these the intensity of the n=3 diffraction ring was low, making extraction of the azimuthal plot difficult. Nevertheless, a few points were observed where the 'propeller' had two narrow lobes, indicating that a single fibrillar region was illuminated. Generally, the collagen fibrils in cow skin appeared to be mostly of vertical orientation while in sheep and deer skins the orientation of collagen fibrils is predominantly horizontal. On the other hand, goat skin showed a mixture of horizontally and vertically oriented collagen fibrils.

The azimuthal plots with the narrowest distributions were extracted and plotted in Figure 118. These directly show the distribution of fibril orientations. Other researchers have preferred to express the fibril orientation distribution as a single number, such as Herman's orientation factor [334] or the so-called orientation index [4, 330, 488] These measures express the degree of orientation of a sample as a number between zero and one, where zero is isotropic (random orientation) and one is perfectly aligned. (Herman's orientation factor can take on negative numbers up to -0.5, which represents a perfectly aligned sample in the perpendicular direction. In our opinion, reducing the azimuthal intensity curves to a single number involves a removal of information, specifically the shape of the distribution. It is possible for samples with an isotropic component, broad peaks, or multiple peaks, to all have the same value of orientation index (Figure 119, Table 25).

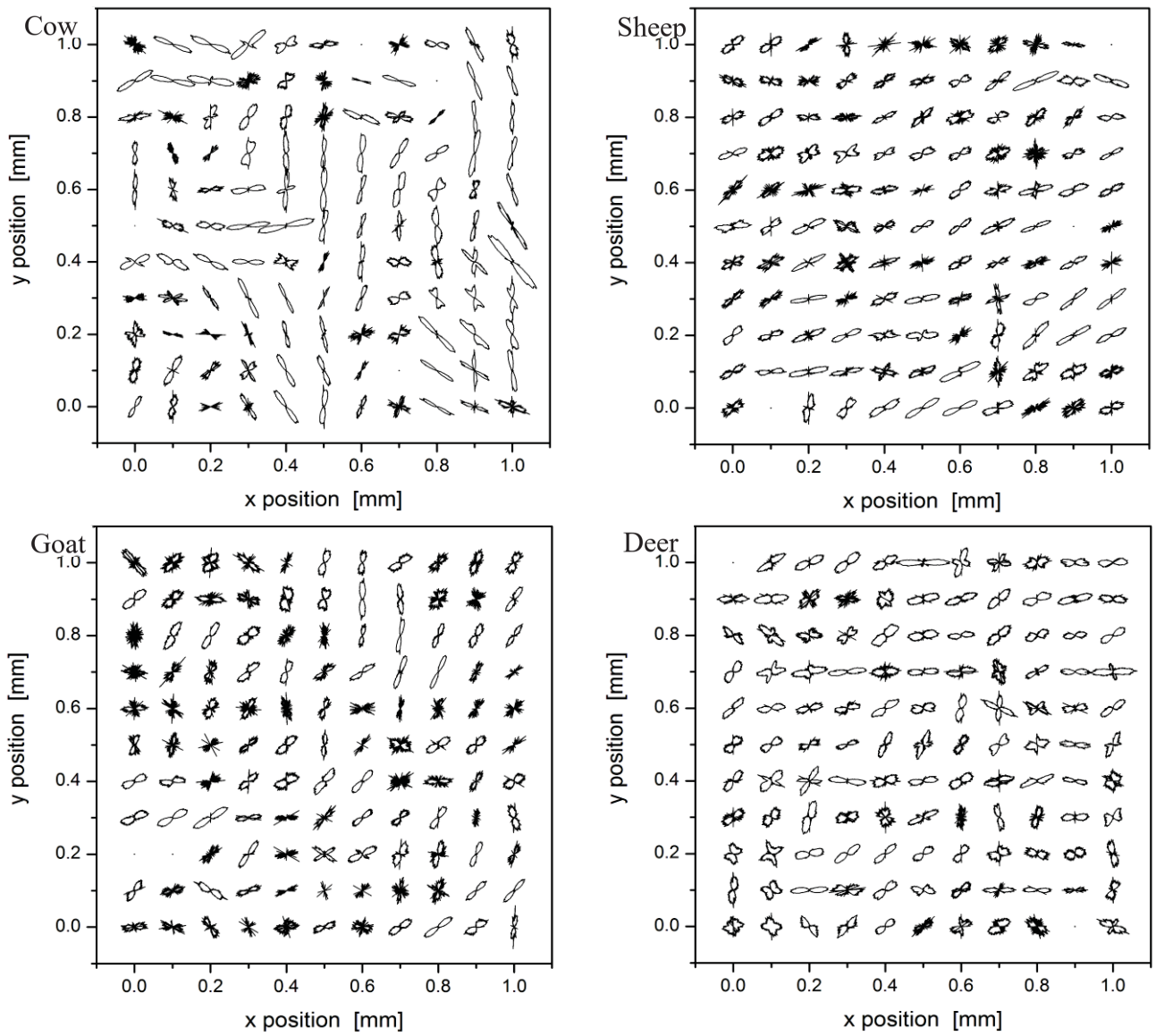

Figure 117: Maps of orientations in different animal skins, obtained from the azimuthal plot of the n = 3 diffraction ring.

.

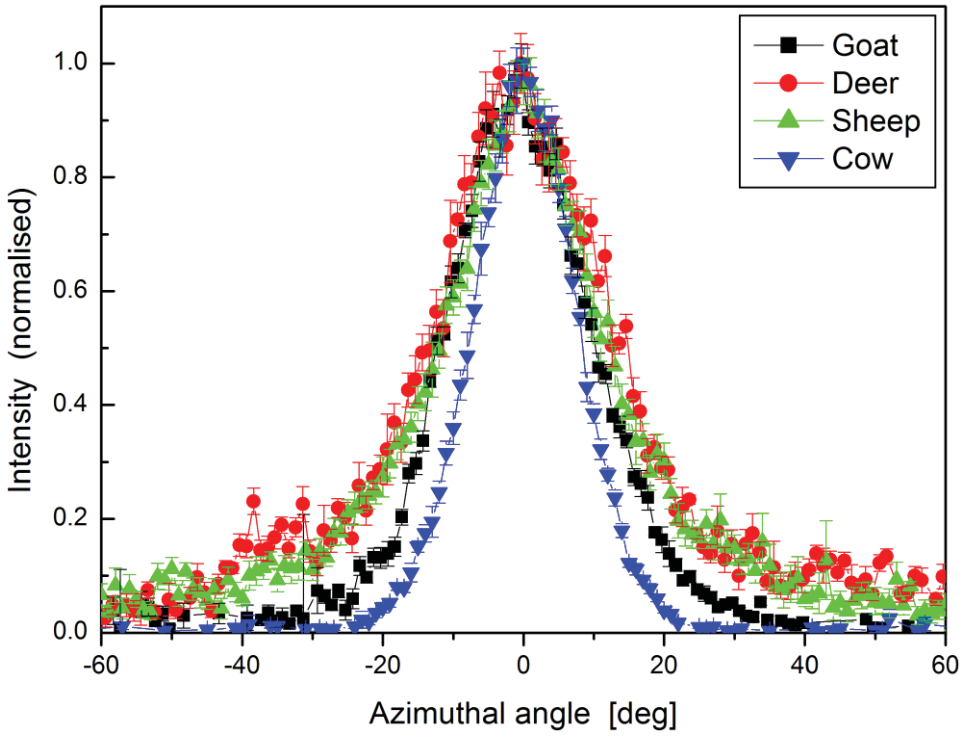

Figure 118: Azimuthal plots corresponding to the narrowest distributions in the maps in Figure 117.

Hence we have elected to present the distribution functions in graphical form. The distributions in Figure 117 were fitted and yielded peak full-widths-at-half-maxima as follows: Cow 15.57 ± 0.04°, goat 21.5 ± 0.1°, sheep 30.2 ± 0.3°, deer 33.4 ± 0.3° (Figure 118).

Recently, Chung-Hao Lee *at al* (2015) has proposed a planar sinusoidally shaped geometric model of collagen fibre kinematics [489]. This model accounted for fibril amplitude and fibre crimp period which has shown to affect the shape of the overall collagen orientation manifested in the azimuthal angle graph (Figure 120).

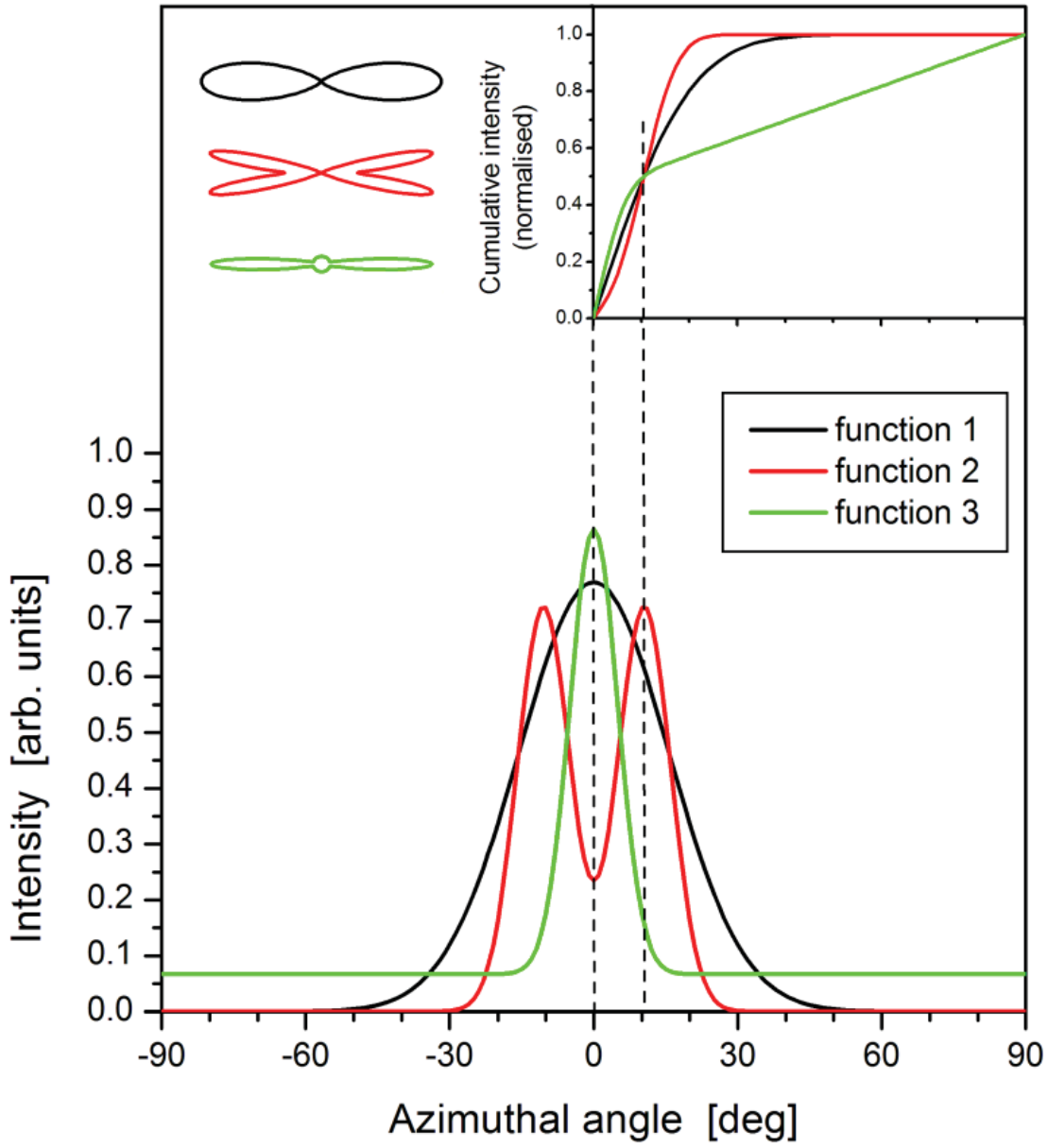

Figure 119: Three example curves with different functions having the same orientation index. The polar plots (top left) clearly show the differences in shape. The parameters are given in Table 25

Since SAXS includes the combined effects of all fibre undulations and orientations, increasing the angle of the collagen crimps will result in the reduction in azimuthal angle width (Figure 120) [489]. This suggests that the collagen fibres in deer skin have the waviest structure while cow skin contains the straightest collagen fibres.

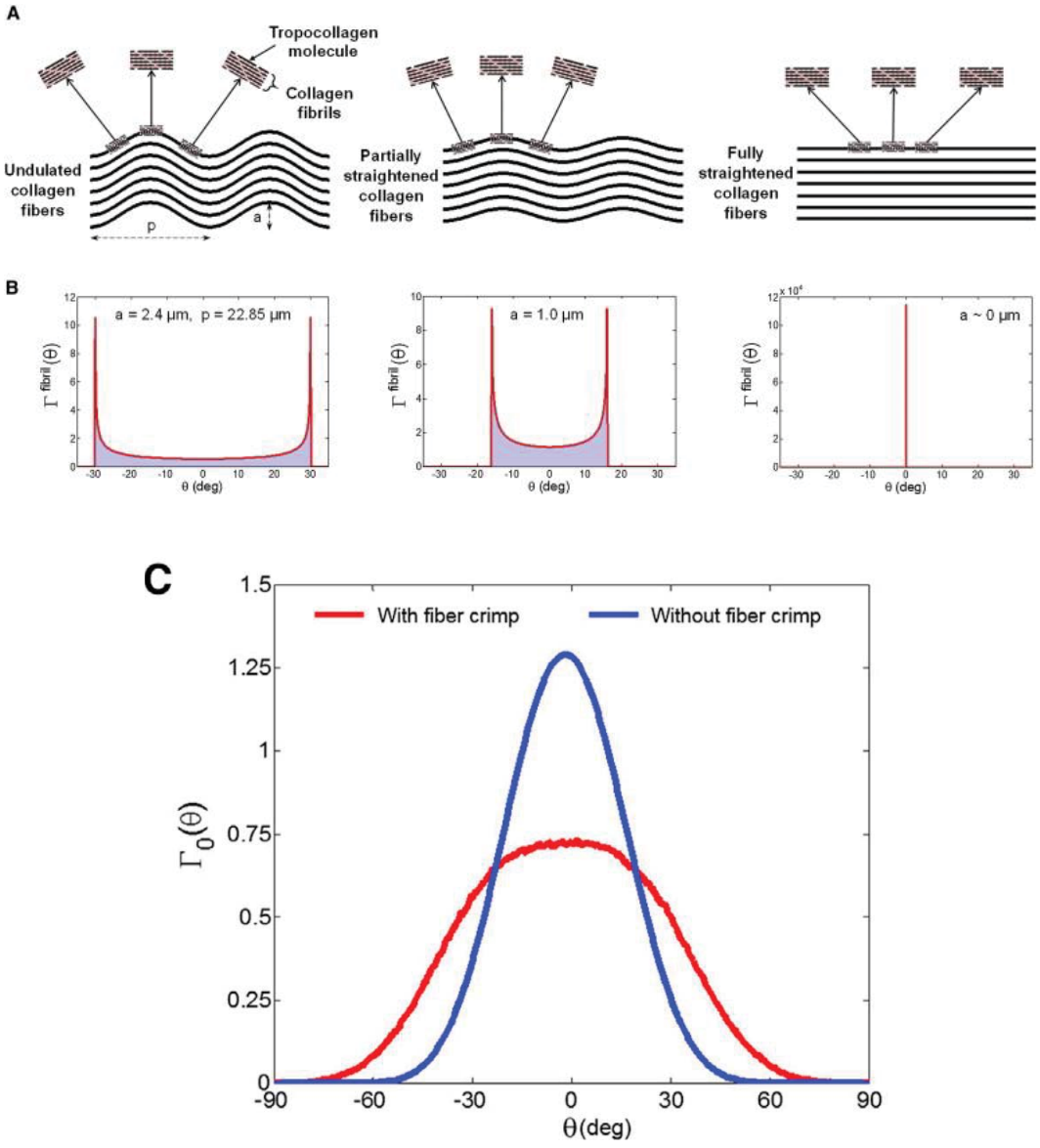

Figure 120: (A) A schematic diagram of the hierarchical structure of the collagen fibre network, from undulated collagen fibres idealized by a sinusoidal geometry, to collagen fibrils composed of tropocollagen molecules under stretch, (B) the corresponding probability density functions of a single fibre at different stretching states and (C)

Predicted fibre orientation distribution function with and without the collagen fibre crimp effect. Taken from [489] with permission from publisher.

Table 25: Parameters for example functions shown in Figure 119: one broad Gaussian peak (function 1), two overlapping Gaussian peaks (function 2), sharp Gaussian peak and isotropic component (function 3).

	Function 1	**Function 2**	**Function 3**
Peak position	0	-10.5, 10.5	0
Peak width	31.1	11, 11	10
Peak area	30	10, 10	10
Isotropic intensity	0	0	0.0671
Orientation angle (OA, at which $\int_0^{OA} I(\omega)d\omega = \int_{OA}^{90°} I(\omega)d\omega$	10.5	10.5	10.5
Orientation index $OI = \frac{90° - OA}{90°}$	0.883	0.883	0.883

9 CHAPTER NINE: Microscopy

Microscopy of sheep. goat, deer and cow skins

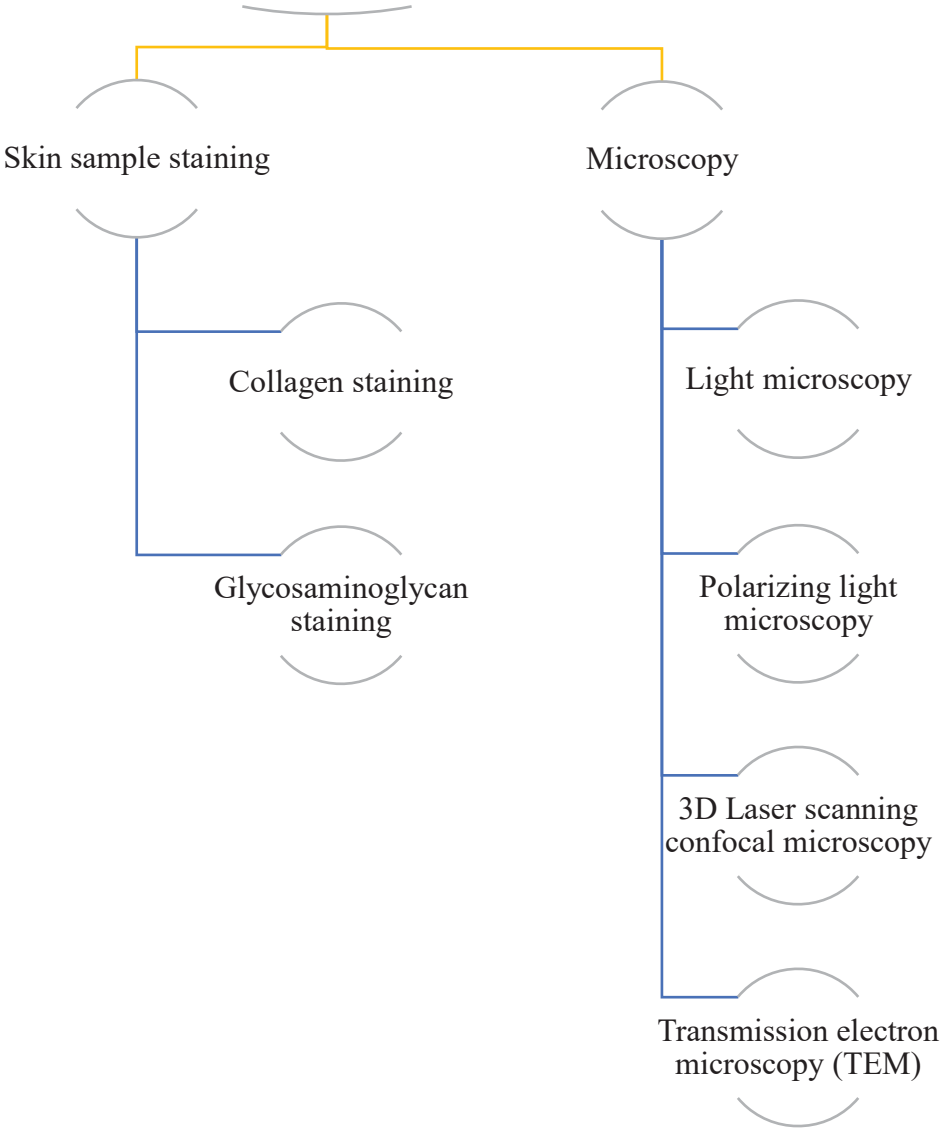

9.1 Experimental procedure

9.1.1 Chemicals and reagents

Potassium permanganate, sodium tungstate, toluidine blue and uranyl acetate were purchased from (BDH, Poole, England). Phosphomolybdic acid was from (Hopkins and Williams, Essex, England). Sirius red was from (F3B spectrum, CA, USA). Picric acid was from (VWR chemicals, PA, USA). Xylene was from (Labscan, Thailand). Glutaraldehyde was from (Merck, NJ, USA). Cuprolinic blue was from (Polysciences, PA, USA).

9.1.2 Laser scanning confocal microscopy

Skin samples were cut into small pieces (2 cm × 2 cm) before being fixed for 24 hours in 40 % formalin made up in 30 mM phosphate buffer (pH 7.2). The fixed samples were rinsed with water then cut into a 40 μm sections using a Leica CM 1850 UV cryostat (Leica Biosystems, Nussloch, Germany) and rinsed again with water. Sections were placed in 1 % (w/v) of potassium permanganate for 5 minutes then removed and rinsed with water before being placed into 1% (w/v) oxalic acid. Once the colour had faded, the sections were washed twice with milliQ water before being placed in 0.2 % (w/v) phosphomolybdic acid for 10 minutes, then rinsed with water. This was followed by staining the sections for 60 minutes with 1 % sirius red dissolved in 1.2 % (w/v) picric acid in water. The pH of the solution was then adjusted with 0.01 M HCl to pH 2.0. The sections were then dehydrated by serial washes in 70 %, 95 % and absolute ethanol. The resulting dehydrated sections were placed in xylene for 5 minutes before being mounted on a glass slide using DPX (Merck, Darmstadt, Germany). Sections

were first examined with light microscope and photographed using a Nikon Eclipse E600WPOL polarising light microscope (Nikon Instruments, Melville, New York, USA) at (1.5X, 5X and 10X) magnification to select the sections to be examined by confocal microscopy. Selected sections were then examined using Leica SP5 DM6000B confocal microscopy (Leica Microsystems Ltd, Knowlhill, Milton Keynes, UK) at 20x, 40x and 63x magnification. 3D scans were generated through a thickness of 40 μm by capturing one image every 0.05-0.3 μm. Standard filters used were FITC with excitation 450-460 nm and emission 500-550 nm, and rhodamine with excitation 538-562 nm and emission 570-640 nm [478].

9.1.3 Glycosaminoglycan-collagen staining and transmission electron microscopy

Skins of sheep, goat, deer and cow were prepared as described in chapter 3 (sections 3.2.2 and section 3.2.3). Skin samples were cut into thin slices (1 mm) using a sterile scalpel blade then fixed in a fixative, containing 2.5 % gluteraldehyde (v/v) and 0.06 % cuprolinic blue in in 0.05 M acetate buffer (pH 5.6) containing 0.3 M $MgCl_2$ for 24 hours [490-492]. The fixed samples were then rinsed three times with the same fixative solution except without cuprolinic blue. Samples were treated with 0.5 % sodium tungstate in acetate buffer for 1 hour then overnight in 0.5 % sodium tungstate in 30 % ethanol.

Samples were then dehydrated in a series of acetone solutions (25%, 50%, 75%, 95% and 100%, twice in each solution), then treated with 50:50 mixture of acetone and Procure 812 resin (ProSciTech, Australia) and allowed to polymerise overnight. They were then placed in 100% Procure 812 resin for 8 hours twice. Finally, samples were

embedded with fresh resin and cured in an oven for 48 hours at 60 ºC. The embedded samples were first trimmed down then cut into 1 µm sections using a glass knife on a Leica EM UC7 ultra-microtome, (Leica Biosystems, Nussloch, Germany) and fixed on glass slides. Sections were quick stained with 0.05% Toluidine Blue then viewed under a light microscope to select suitable areas for TEM. Sample blocks were further trimmed down and selected areas were cut to 100 nm using a diamond knife (Diatome, Swizerland). These cuts were then stretched with chloroform vapour and mounted on grids using a Quick Coat G pen (Daido Sangyo, Japan). Finally, the grids were stained with saturated uranyl acetate in 50% ethanol for 1 hour before being washed with 50% ethanol in water. Samples were then examined with a FEI Technai G2 Spirit BioTWIN Transmission Electron Microscope (Czech Republic). Samples were further stained with lead citrate (Venable and Coggeshall, 1965) for 4 minutes to visualize the collagen fibrils to determine the fibril diameters.

9.2 Results and discussion

9.2.1 Collagen fibril diameters

The fibril diameters were calculated from the transverse section view of each skin by selecting the TEM settings that gave good contrast and high signal to noise ratio. Using ImageJ software (version 1.50i), all selected images were then converted into binary images using a thresholding algorithm which was then processed using the "fill holes" or "remove light/dark outliers" tools. The resulting image was then processed using the "watershed" segmentation algorithm which separated the fibrils in contact with each other. Lastly, "Analyse particles" was used to fit each fibril to a circle, and the area of each circle with a minimum circularity of 0.8 was calculated (Figure 121).

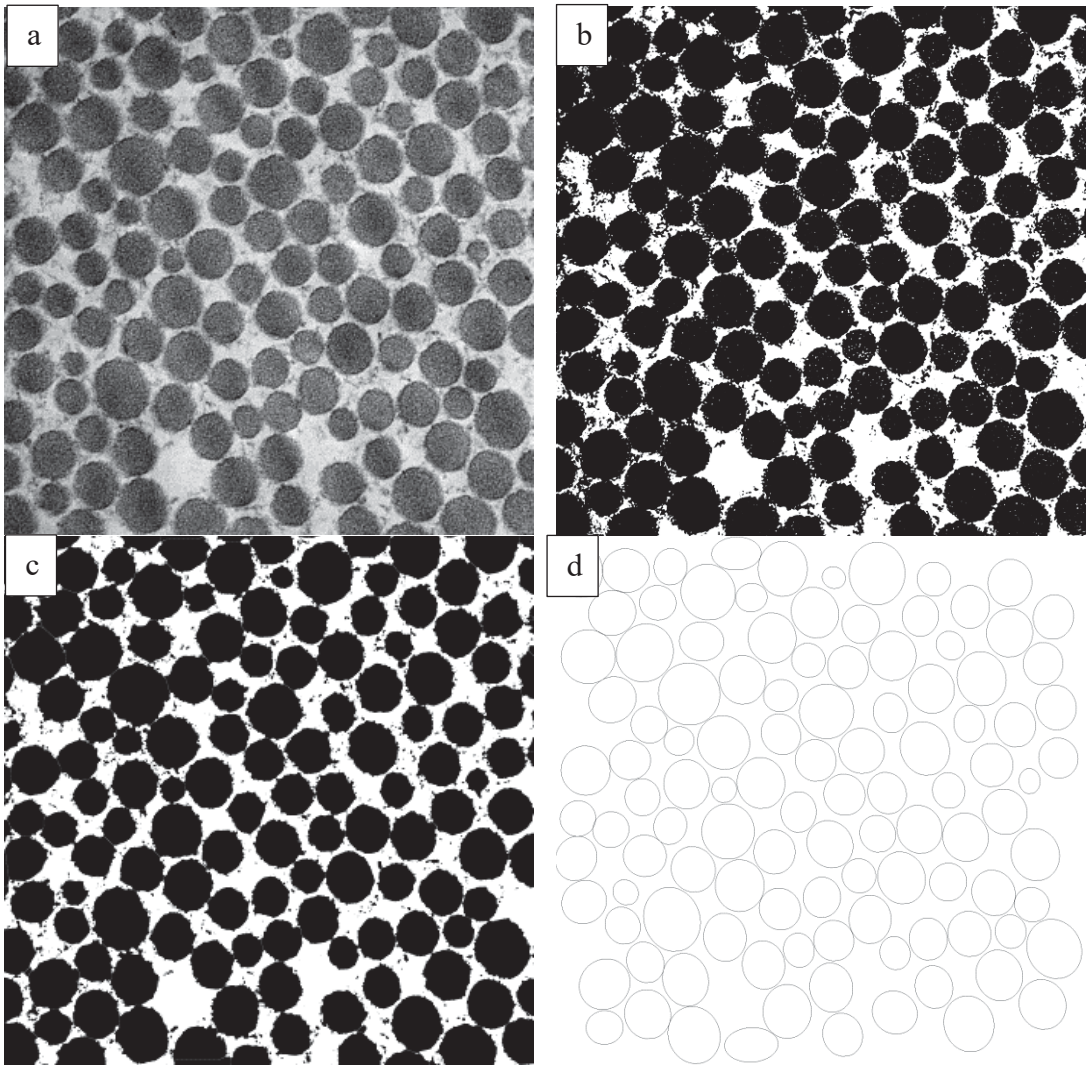

Figure 121: Measurement of collagen fibril diameters using imageJ software v.1.50i. (a) TEM image showing the transverse section view of the collagen fibril. (b) Binary image obtained using the thresholding algorithm. (c) Image b after removal of the light/dark outliers and the "fill holes" tools were applied, followed by application of the "watershed" algorithm. (d) The outline of each fibril after the application of "analyse particles" option in imageJ software.

It has been reported that where there is a narrow distribution of fibril diameters such as in the cornea, a small number of fibril diameter measurements (less than 200) can be used to reliably calculate the distribution. However, a large number of fibril diameter measurements are required in skin and tendon to produce a reliable distribution [493]. In this study as all samples were skins, more than 2000 measurements of the fibril diameters for sheep, goat, deer and cow skins were collected using the transverse sliced TEM images to produce the fibril diameter distribution. These were then used to produce histograms used to calculate the minimum, maximum, mean, standard deviation, range and mass-average diameter of the collagen fibrils in sheep, goat, deer and cow skin samples (Figure 123).

The diameter was calculated from the area of the fibril [d(nm) = 2×sqrt(area/π)]. The range was then calculated from the difference between the minimum and maximum diameters and the mean was calculated by taking the sum of all diameters and dividing this by the total number of measurements. The mass-average diameter was calculated based on the formula below [238, 493].

$$\textbf{Mass-average} = \sum_{i=1}^{N} n_i d_i^3 \Big/ \sum_{i=1}^{N} n_i d_i^2$$

- n_i is the number of measurements made for a fibril diameter d_i.
- N is the number of the increments that make up the fibril diameter.

All skins showed a unimodal fibril distribution with fibril diameters ranging from 33 to 157 nm, which in good agreement with the previously published results for skin [238, 465, 493, 494]. Using a pairwise multiple comparison (Tukey test, $P < 0.05$), the mean fibril diameters of all skins were significantly different to each other (Figure 122).

Cow skin had the largest mean fibril diameter at 96 nm followed by goat skin at 86 nm then sheep skin at 80 nm. Deer skin had the smallest mean fibril diameter at 72 nm. Figure 123 shows also that the distribution of the fibril diameters in sheep skin is much narrower than that in cow and goat skins but similar to that in deer skin.

The standard deviation of the mean (Figure 123) quantifies the amount by which every fibril diameter within a skin sample varies from the mean. It effectively indicates how tightly the fibril diameters in the skin sample are spread around the mean. Thus, cow skin showed the largest standard deviation which was equated to the largest range of fibril diameters, 122 nm, within the cow skin samples. This was followed by goat skin with a 107 nm spread of fibril diameters. Sheep and deer skins had the narrowest spread of fibril diameters, 59 nm and 70 nm, respectively.

In a normal unimodal distribution, the increase in the mean diameter is associated with an increase in the mass-average [325]. This was valid for all skins in that cow skin with the largest mean had the largest mass-average of 102 nm and deer skin with the smallest mean had the smallest mass-average of 75 nm. The difference between the mean and the mass-average was directly correlated to the standard deviation which was the largest in cow skin and the smallest in deer skins.

Strikingly, sheep skin contained the largest minimum fibril diameters of 48 nm, although it had the second smallest mean fibril diameter after deer skin. This was the major influence on sheep skin having the narrowest spread of diameters. In contrast, cow skin had the largest spread of fibril diameter, a reflection of it containing fibrils with the largest maximum diameter of 169 nm.

The void volume (not occupied by fibrils) from the TEM images of sheep, goat, deer and cow was also examined by ImageJ software, but although no apparent differences were found between sheep, goat and deer skins, cow skin appeared to have a smaller interspacing between fibrils (Figure 123).

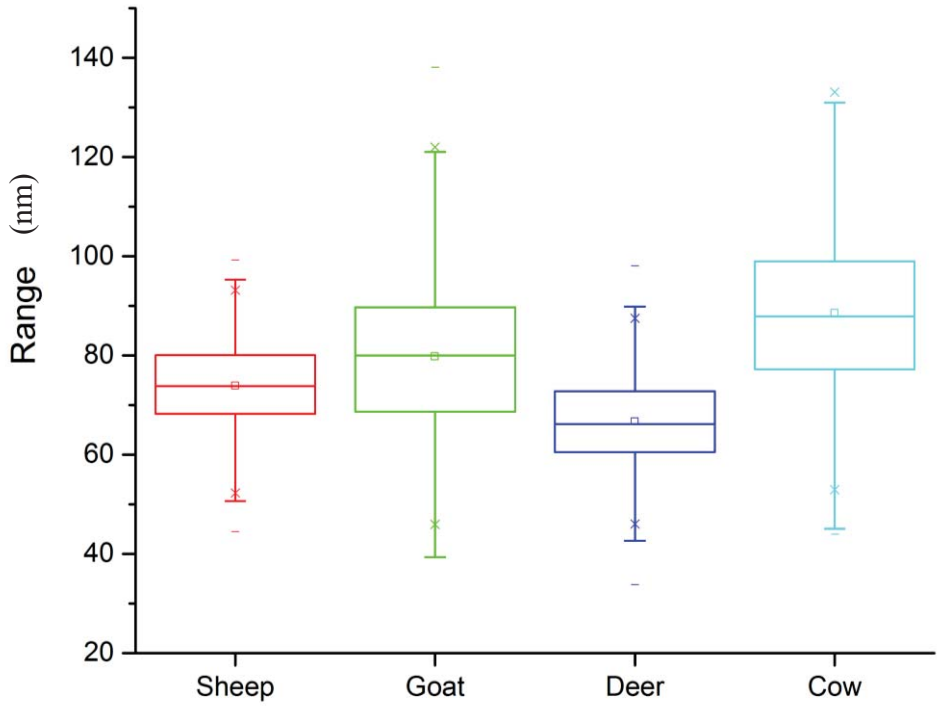

Figure 122: A pairwise multiple comparison (Tukey test) ($P < 0.05$) of the mean fibril diameter in sheep, goat, deer and cow skins.

9.2.2 Localization and visualisation of glycosaminoglycans by cuprolinic blue

Several methods have been developed to visualise glycosaminoglycans in biological tissues including the use of the cationic stain alcian blue (Figure 124A) [495, 496], ruthenium red [497], cationic ferritin [498] and cuprolinic blue [499]. Although alcian blue is the most common method used, it is not specific for glycosaminoglycan chains, staining DNA and RNA as well [499].

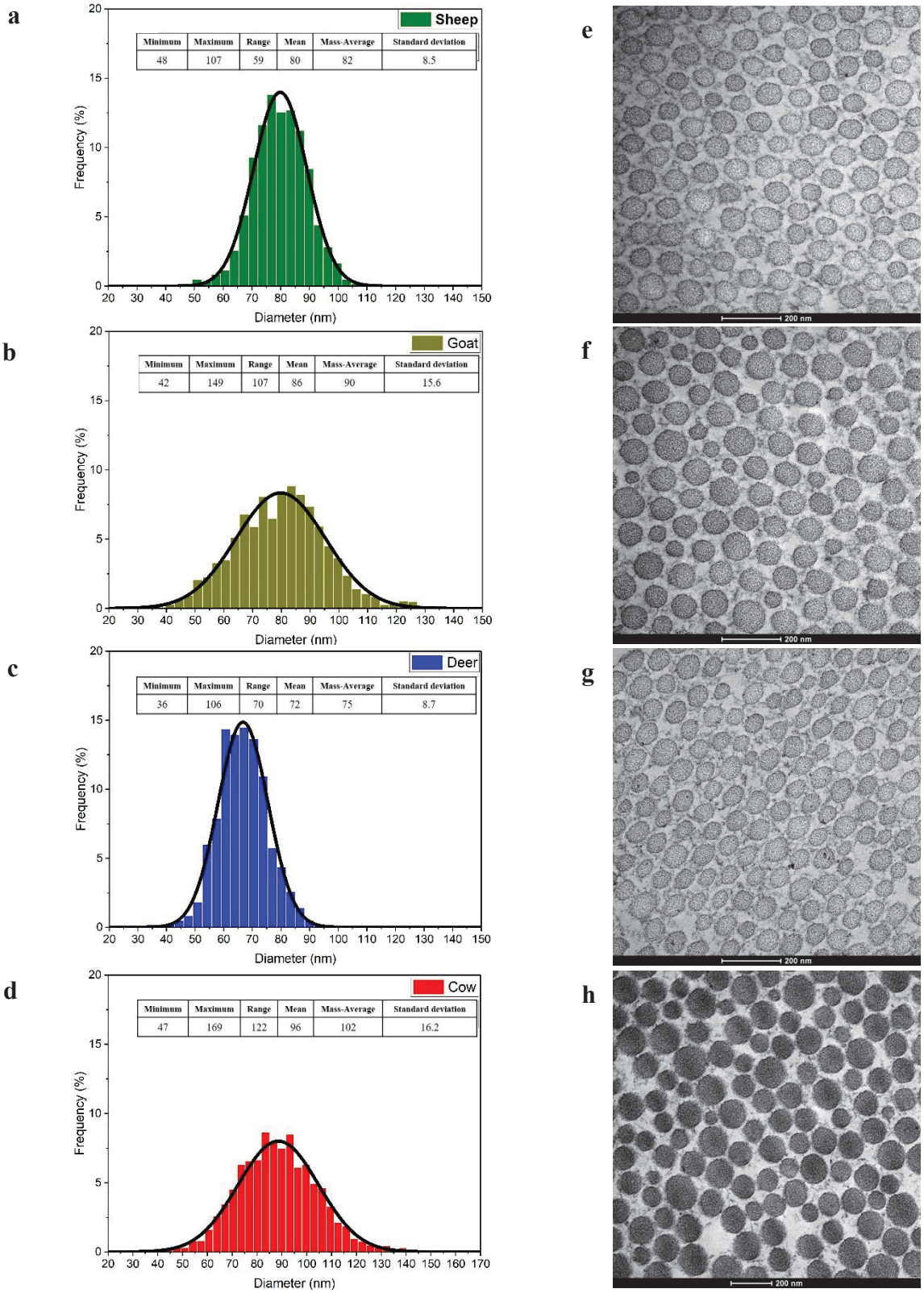

Figure 123: Fibril diameter histograms and transverse sections (a-d) Histograms of percentage frequency of fibril diameters of sheep, goat, deer and cow. (e-h) Transverse sections of collagen fibrils of sheep, goat, deer and cow skins (corium side).

In 1972, Scott synthesized two cation copper phthalocyanins which are named as cuprolinic and cupromeronic blue (Figure 124 B&C) which selectively bind to the negatively charged, sulfated residues of the glycosaminoglycan chains of proteoglycans [500, 501]. The use of a critical electrolyte concentration of 0.1-0.3 M of Mg^{+2} is crucial to block the stain uptake by the carboxyl and phosphate groups [492, 502, 503]. According to Scott (1985) and Toin *et al.* (1987) the glycosaminoglycan chains collapse onto the protein core, but the proteoglycans retain their shape to produce electron-dense structures that can be seen with electron microscopy [491, 504]. This method has been used to determine the shape and location of sulfated glycosaminoglycans in many biological tissues [491, 502, 504-509].

Two biological replicates of sheep, goat, deer and cow skins were prepared as follows: a control sample was stained only with uranyl acetate to examine the collagen fibril while a second sample of the same skin was stained first with cuprolinic blue (to reveal the sulfated glycosaminoglycans) then uranyl acetate. The controls showed the organisation of the collagen fibrils with clear D-periodicity, but no proteoglycans (Figure 118a-118d). The cuprolinic blue showed the collagen organisation with additional black dense structures representing the sulfated glycosaminoglycans (Figure 118e-118g). It had previously been shown that the glycosaminoglycans could appear as small or long filaments, dot-like structures or large aggregates preferentially localized around the collagen fibrils [491, 510]. They run both perpendicular and parallel to the collagen fibrils and appear to interact with the fibrils at the positions of D-periodicity [491, 507, 509, 511].

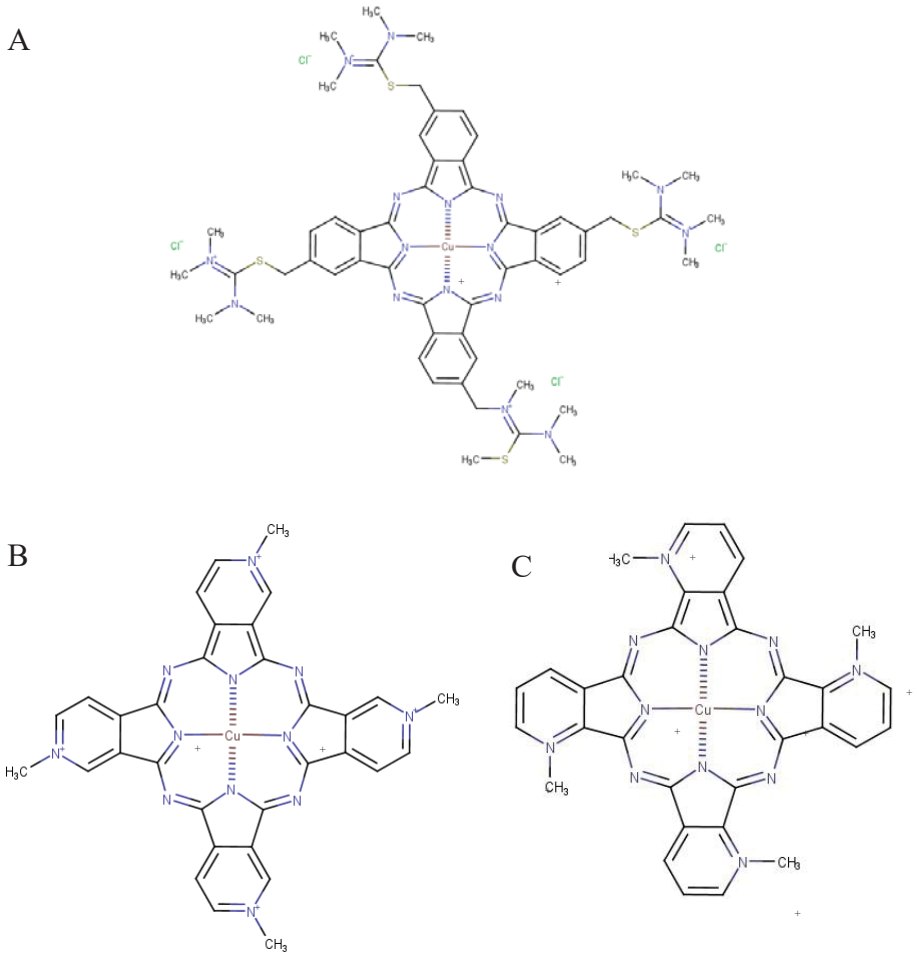

Figure 124: Chemical structures of (A) alcian blue (B) cupromeronic blue (C) cuprolinic blue.

Generally, all skin (corium side) samples of sheep, goat, deer and cow contained black dense filaments that were mainly associated with the D-periodicity of collagen. Dermatan sulfate is the major glycosaminoglycan in skin and has been previously visualised using cuprolinic blue as small and thin filaments with a maximum length of 60 nm [491]. These previous results are in good agreement with the results obtained in this study which show small and thin filaments oriented perpendicularly to the collagen fibrils and in close proximity to the gap zone periodicity and mainly at the ‘d’ band

[285, 512]. The shape, amount and length of those filaments are, however, significantly different in sheep, goat, deer and cow skins (Figure 125).

The filaments of deer skin appeared as regular shapes and structures with a length ranging from 20-50 nm (Figure 125g). They are highly organised with respect to the collagen fibrils and appear to be associated with their D-periodicity. Looking at a group of filaments associated with one collagen fibril, it appears that they are commonly separated by a regular distance and that they are linking the fibrils. Smaller aggregates are occasionally seen suggesting that in deer skin dermatan sulfate is the predominant glycosaminoglycan and is found in regular arrays within the collagen fibrils. Goat skin on the other hand, exhibited a less regular arrangement of glycosaminoglycans ranging from large aggregates to dot-like structures (Figure 125f). It did contain some rods similar to those seen in deer (Figure 125g) linking the collagen fibrils but they were less common. Cow and sheep skins appeared to contain lower concentrations of glycosaminoglycans compared to deer and goat skins (Figure 125e-h). The rod-shaped structures were either not observed or rare.

Generally, deer and goat skins contained a higher amount of the apparent glycosaminoglycans while the apparent amount in sheep and cow skins was less and more alike (Figure 125e-h). Also the amount of glycosaminoglycans appeared to be higher in deer and goat skins compared to sheep and cow skins. Furthermore, the sizes of glycosaminoglycans were significantly diverse ranging from dot-like structures commonly seen in cow, goat and sheep skins to rod-like structures commonly seen in deer skins.

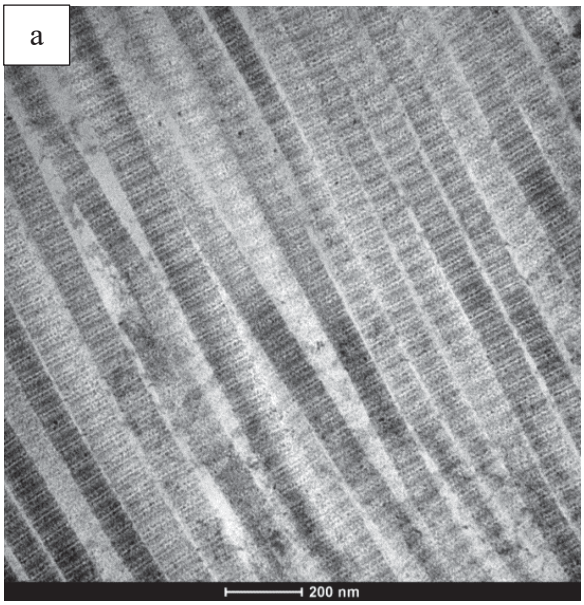

Sheep skin stained with uranyl acetate

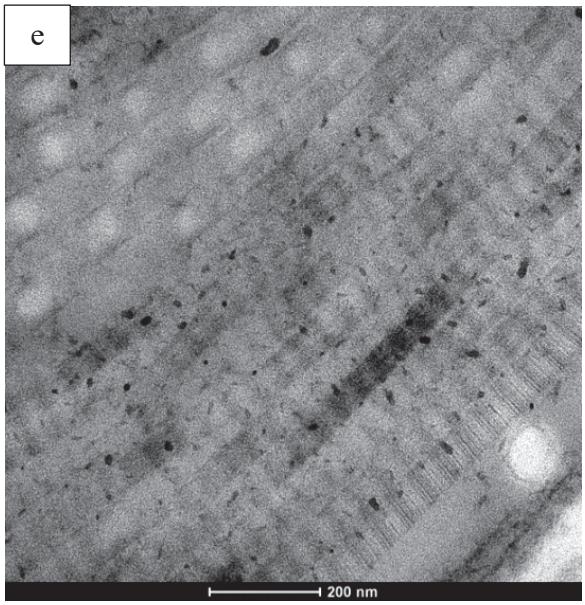

Sheep stained with uranyl acetate and cuprolinic blue

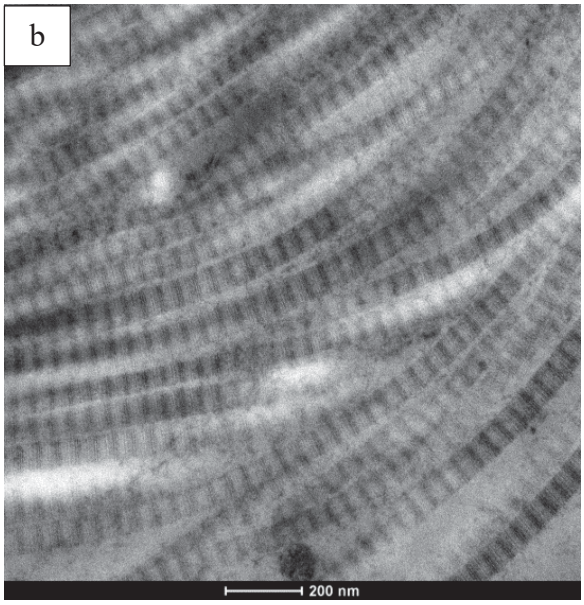

Goat stained with uranyl acetate

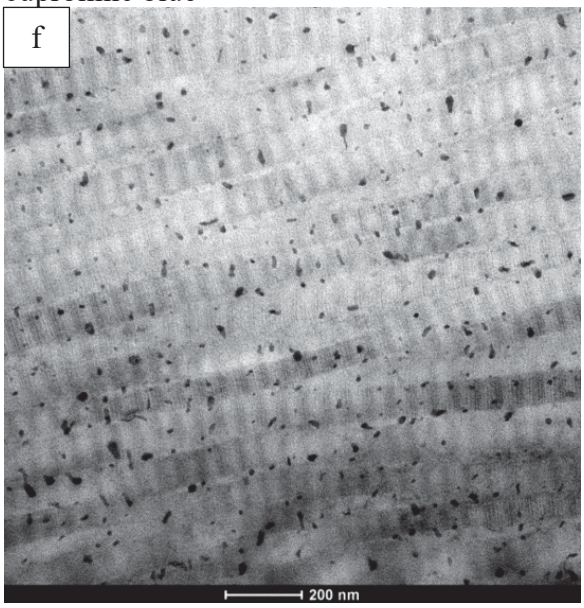

Goat stained with uranyl acetate and cuprolinic blue

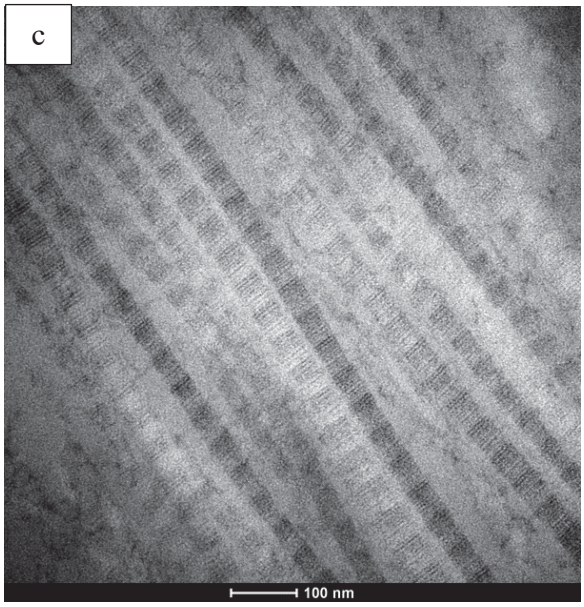

Deer stained with uranyl acetate

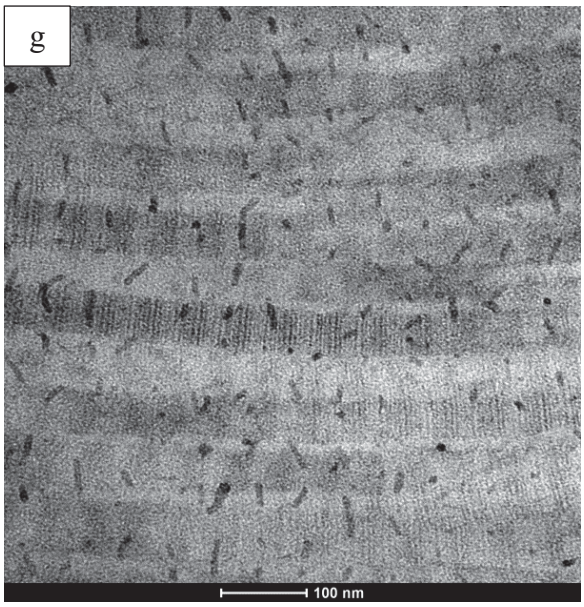

Deer stained with uranyl acetate and cuprolinic blue

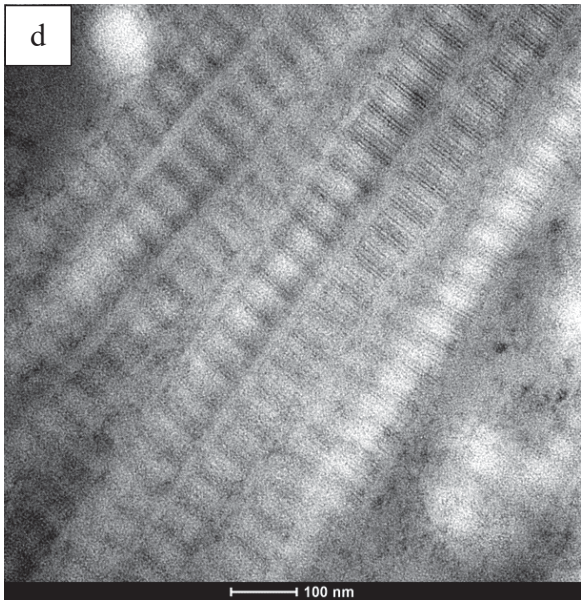

Cow stained with uranyl

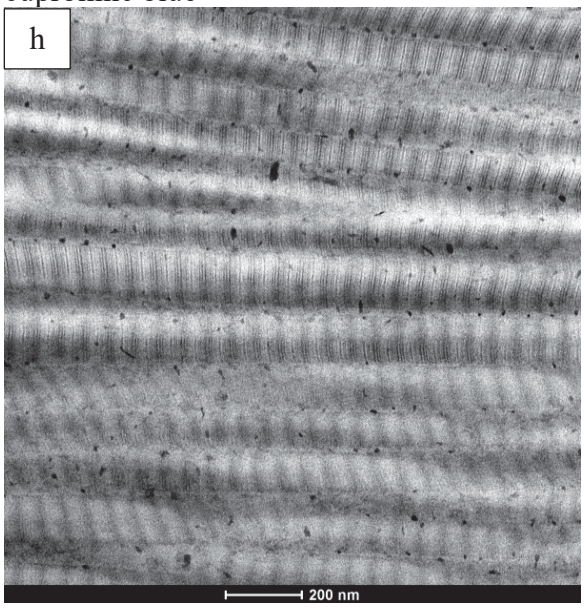

Cow stained with uranyl acetate and cuprolinic blue

Figure 125: TEM images of the longitudinal sections of sheep, goat, deer and cow skins (corium side). (a-d) skin sections are not stained with cuprolinic blue. (e-h) skin sections are stained with cuprolinic blue.

9.2.3 Laser scanning confocal microscopy

9.2.3.1 Introduction

Collagen fibres are the building blocks of collagenous tissues including skin, bone, tendon and cartilage in that their size, organisation and orientation largely influence the mechanical properties of the tissue such as strength, flexibility and compressibility [6, 398, 466, 513]. Several methods have been developed to visualise collagen fibres, the most common histological technique being picrosirius red staining [478, 514, 515]. A combination of picrosirius red and microscopy is a powerful method to detect and analyse collagen fibre density and orientation [478, 514, 516, 517]. Collagen is intrinsically birefringent and so polarizing light microscopy has been utilized to investigate the qualitative structural organisation of picrosirius red stained collagen fibres in several biological tissues [518-521]. Recently, laser scanning confocal microscopy has been developed to visualize and study the collagen content and fibre orientation in tissues [478, 522, 523].

A comparison of the organisation of collagen fibre organisation in sheep, goat, deer and cow skins and correlation with their mechanical properties has not been previously reported. It is important to bridge this gap by trying to understand how macromolecules including collagen and glycosaminoglycans combine together to produce a biomaterial with specific mechanical characteristics such as tensile and tear strength [6, 398].

9.2.3.2 Results and discussion

All skin samples were first examined using a light microscope and polarising light microscope to select the areas to be visualised using laser scanning confocal microscopy. It was clearly observed that skin samples have significant differences in their total thickness and in the relative thicknesses of the grain and corium layers. Cow skin had the largest total skin thickness followed by sheep, then goat and finally deer skin. Sheep skin had the largest grain layer which made up more than 50% of the total skin thickness and deer skin had the smallest grain layer making up to 10% of the total skin thickness. Goat and cow skins are made up of about 35% and 20% of grain layer, respectively. As a result, sheep skin contained the smallest corium layer which is the layer of the skin that is responsible for skin strength. On the other hand, deer skin had the largest corium layer making about 90% of the skin.

In polarising light microscopy, linearly polarized light passes through a sample and is resolved into two rays, the ordinary and extraordinary which are polarised at right angles to each other. These rays travel at unequal velocities through birefringent samples because of the anisotropic organisation of molecules such as collagen [524]. The intensity of the light depends on the anisotropic properties of the sample where the magnitude of the phase difference generates contrast with the background appearing as bright and dark fields [525]. The brightest position occurs at a phase difference of 45^{o} while the darkest occurs at 0^{o} and 90^{o} [525]. This is known as intrinsic birefringence and is a characteristic property of the tissue that is dependent on the alignment, orientation and nature of the molecular organisation [524, 526, 527].

Collagen stained with picrosirius red is observed under a polarising light microscope in different interference colors ranging from green, yellow to red [514, 516, 517]. It has been reported that the increasing thickness of collagen fibrils shifts the color from green to red: the thin collagen fibril bundles appear in green while the thicker bundles appear in orange to red [514, 526, 527]. Also more highly oriented collagen fibres result in regions with a high intensity of bright areas [514, 516].

Figures from 126a-126d show clearly that the grain layer is greener than the corium layer suggesting that grain contains thinner collagen fibres than the corium. It is known that the grain layer consists of thin and poorly organised fibres composed of collagen types I and III while the corium contains mainly thick and more oriented fibre bundles of collagen I [37, 278]. This study showed there were no significant differences in the apparent organisation of the grain layers of sheep, goat, deer and cow skins.

Looking at the corium layers of sheep, goat, deer and cow skins, it was clear that in all skins, the collagen fibre bundles are interwoven and run in all directions. However significant differences are observed in the birefringence intensities. Sheep and cow skins show more uniformity in the birefringence intensities suggesting that the collagen fibre bundles in the corium layer do not change direction. In contrast, goat and deer skins show much lower uniformity in the birefringence intensities which implies that the collagen bundles are constantly changing their direction. Deer skin, the densest structure of all the skin samples tested, has the most variation in birefringence intensity. On the other hand, cow skin, with the largest fibre bundles, has the most highly consistent birefringence intensity followed by sheep then goat skins.

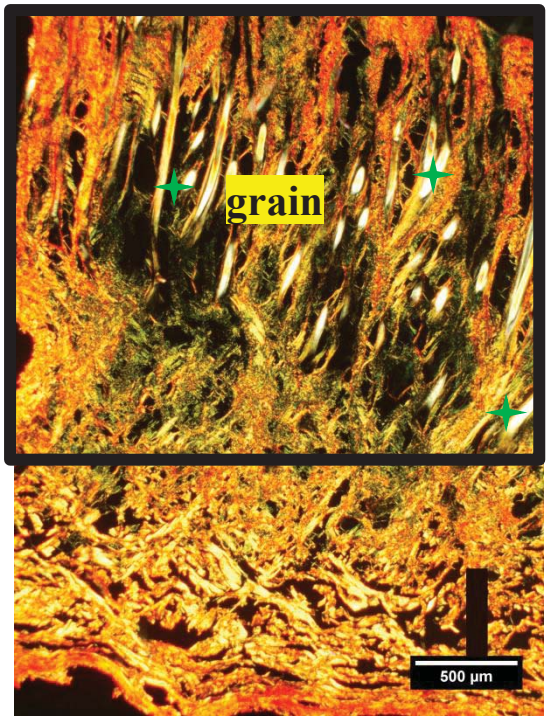

Grain layer of sheep skin

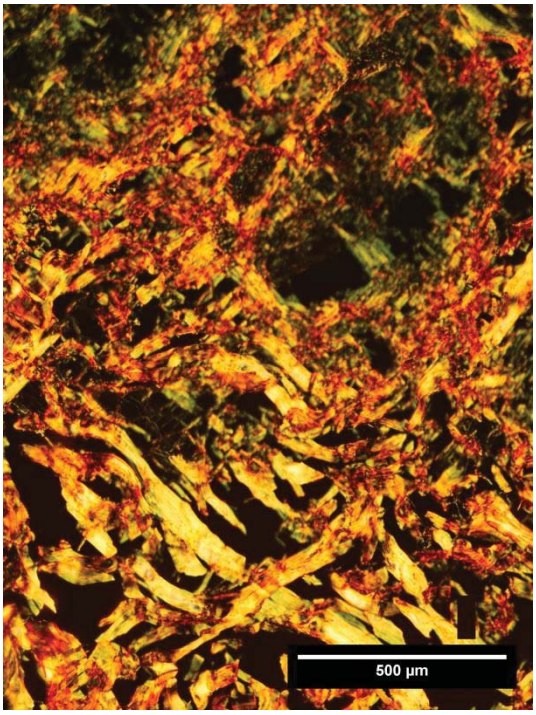

Corium layer of sheep skin

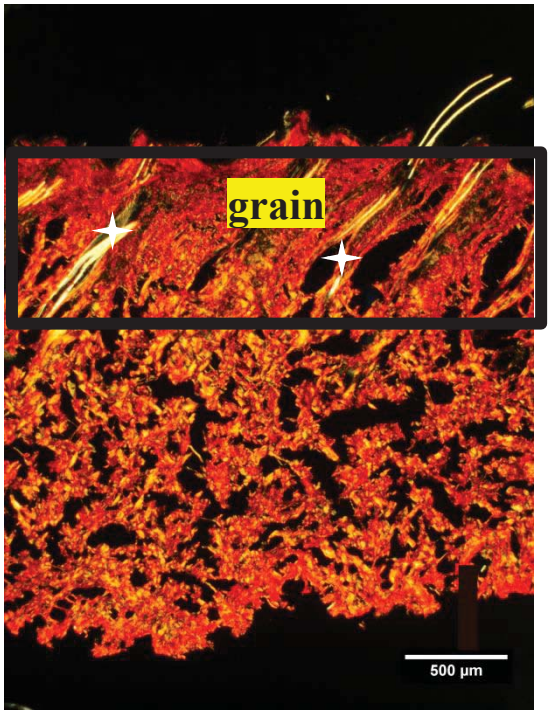

Grain layer of goat skin

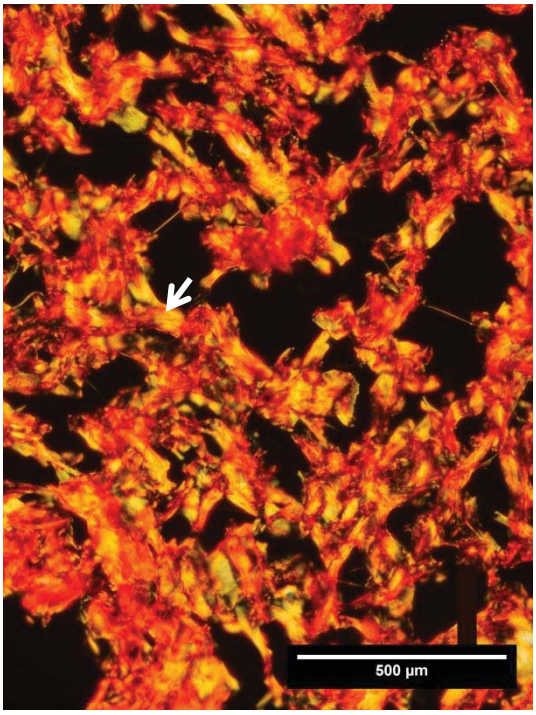

Corium layer of goat skin

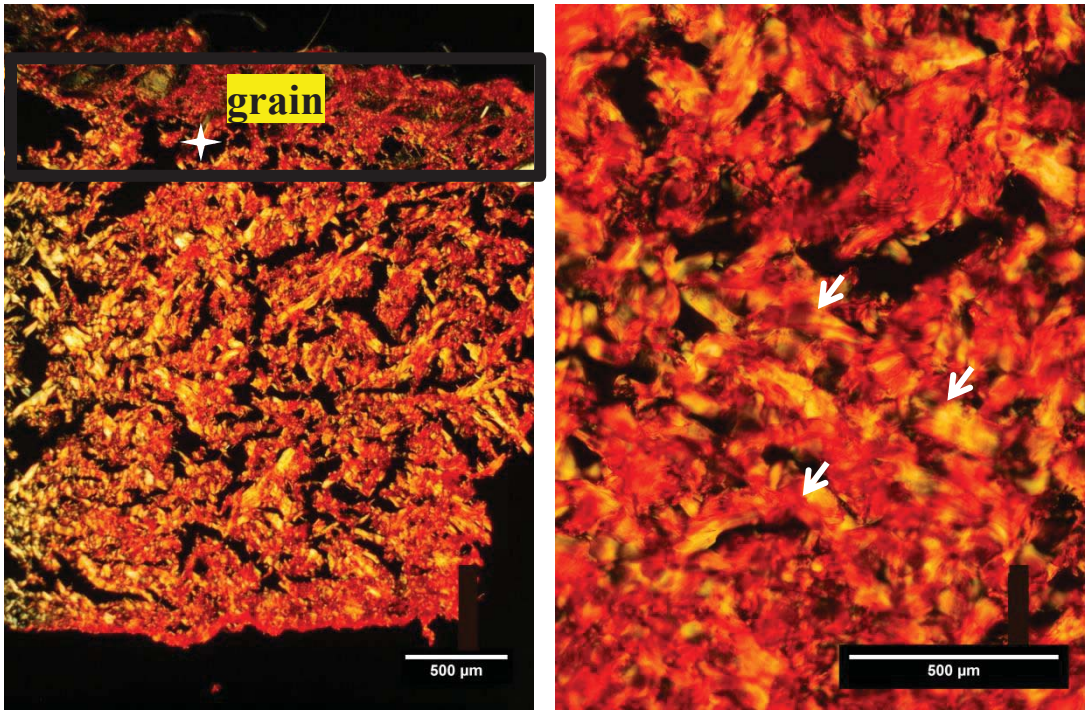

Grain layer of deer skin

Corium layer of deer skin

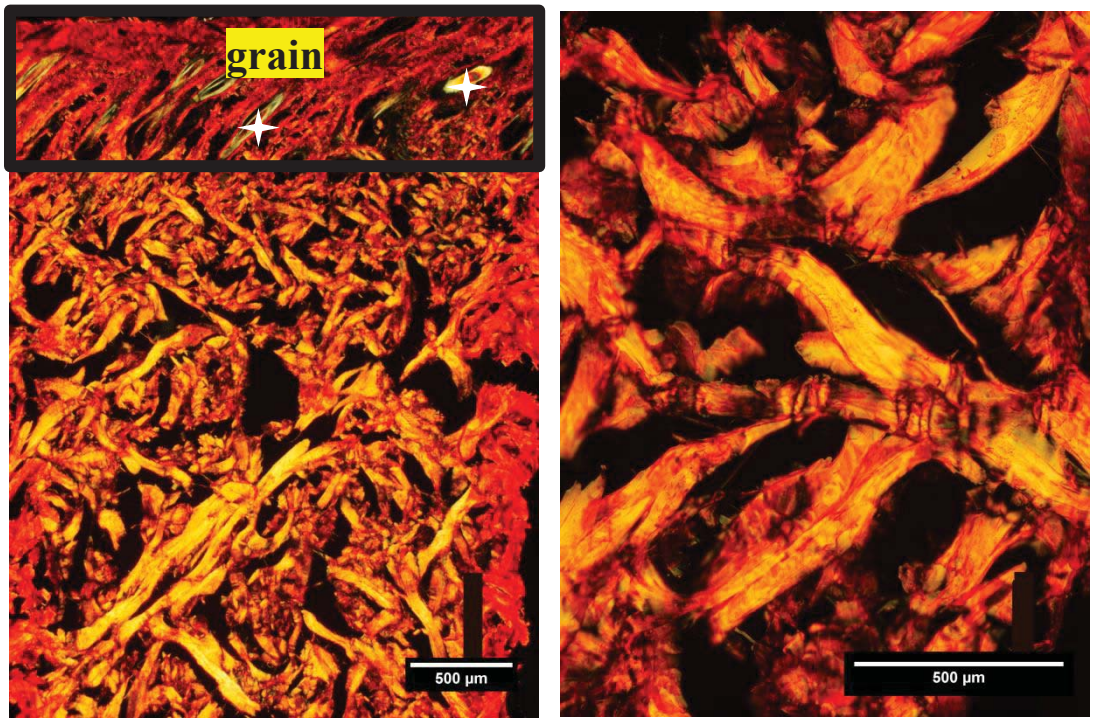

Grain layer of cow skin

Corium layer of cow skin

Figure 126: Polarizing light microscopy images of skins of sheep, goat, deer and cow. Two different magnifications are shown. Arrows represent positions where the fibre bundles change direction. Stars show the hair follicles.

The results of the polarising light microscope are in line with the laser scanning confocal microscopy results. Figures from 127a to 127d show the grain layers of sheep, goat, deer and cow skins, respectively. It is clear that there are few differences between the skin samples. They all appear to be composed of thin and randomly oriented collagen fibre bundles.

Looking at the corium layer of the skins (Figures 127e-127h), the size and organisation of the collagen fibre bundles are significantly different. Cow and sheep skins have straight fibre bundles with no kinks or direction change while goat and deer skins contain fibre bundles with many bends and kinks. Deer skins appeared to have a fibre bundle structure that zig-zags. The fibril bundles making up each fibre are very distinct and clearly different to those in all other skins. On the other hand, the fibre bundles in the sheep skin appeared to contain fibril bundles that are merged together resulting in a featureless fibre.

Figure 128 clearly shows the significant differences in the waviness of the fibre bundles in deer and cow skins. The fibre in the deer skin appears to change its direction with a sharp angle while in cow skin, the fibres run mainly straight.

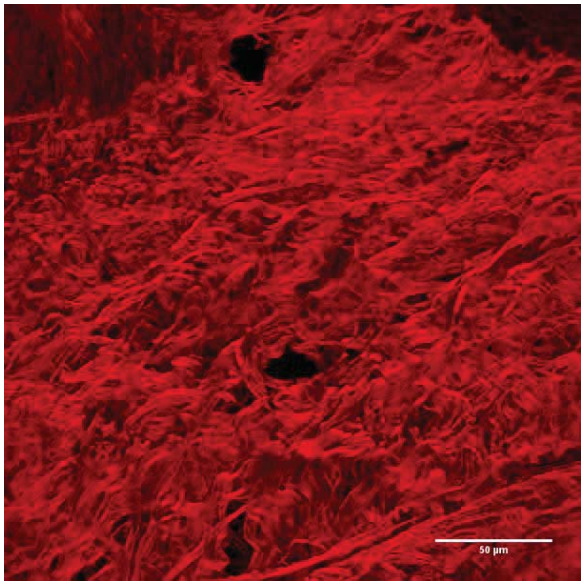

Grain layer of sheep skin

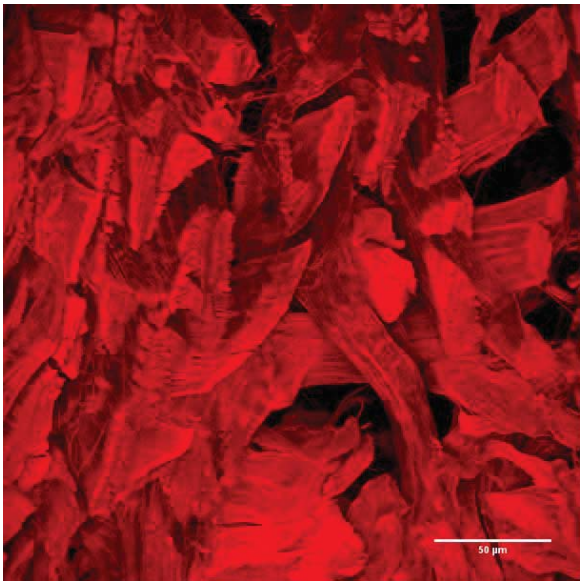

Corium layer of sheep skin

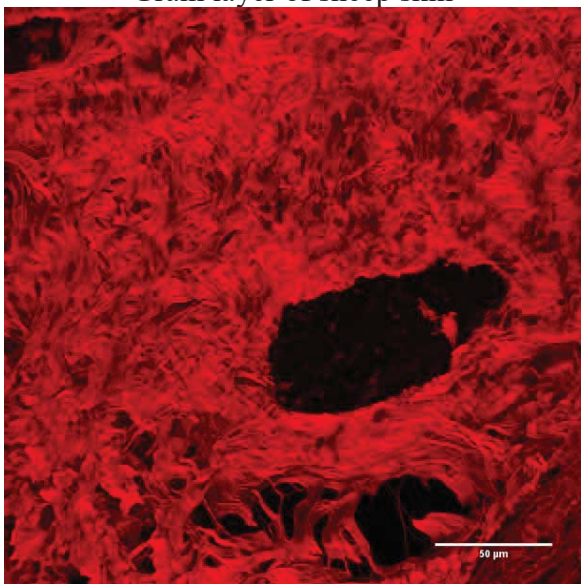

Grain layer of goat skin

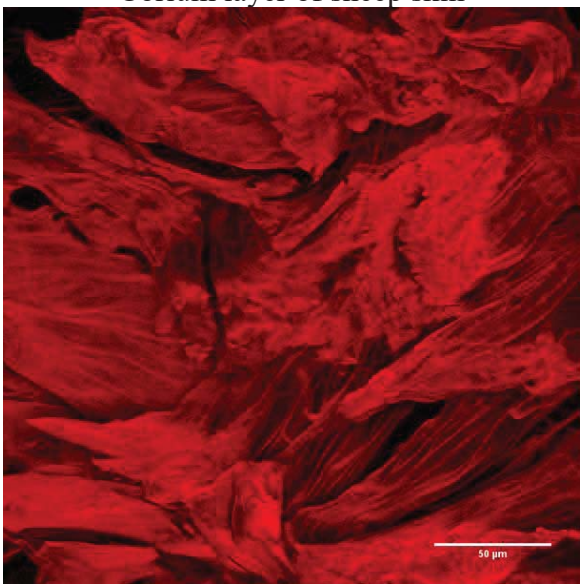

Corium layer of goat skin

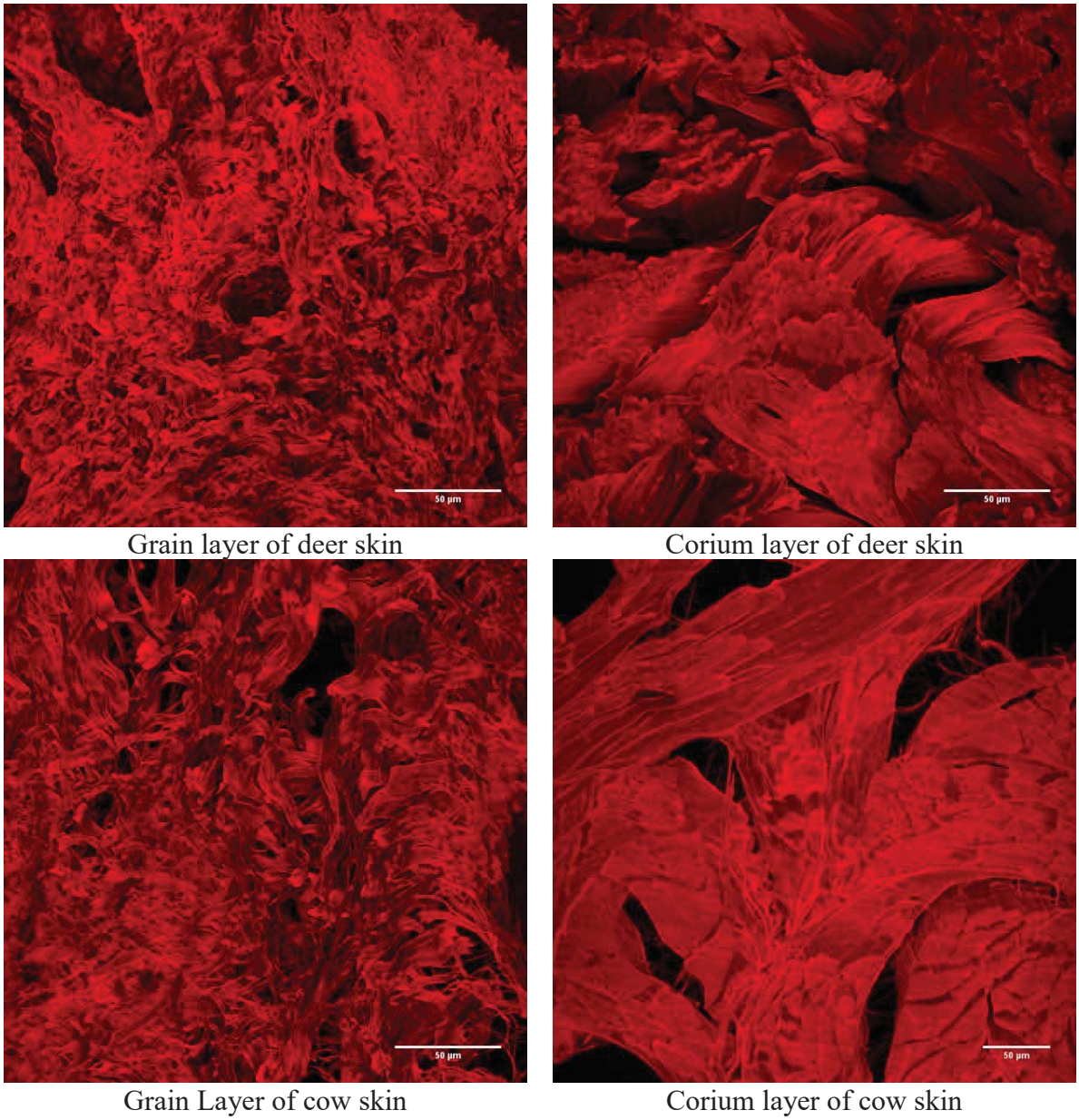

Grain layer of deer skin | Corium layer of deer skin

Grain Layer of cow skin | Corium layer of cow skin

Figure 127: Laser scanning confocal images of sheep, goat, deer and cow skins stained with picrosirius red.

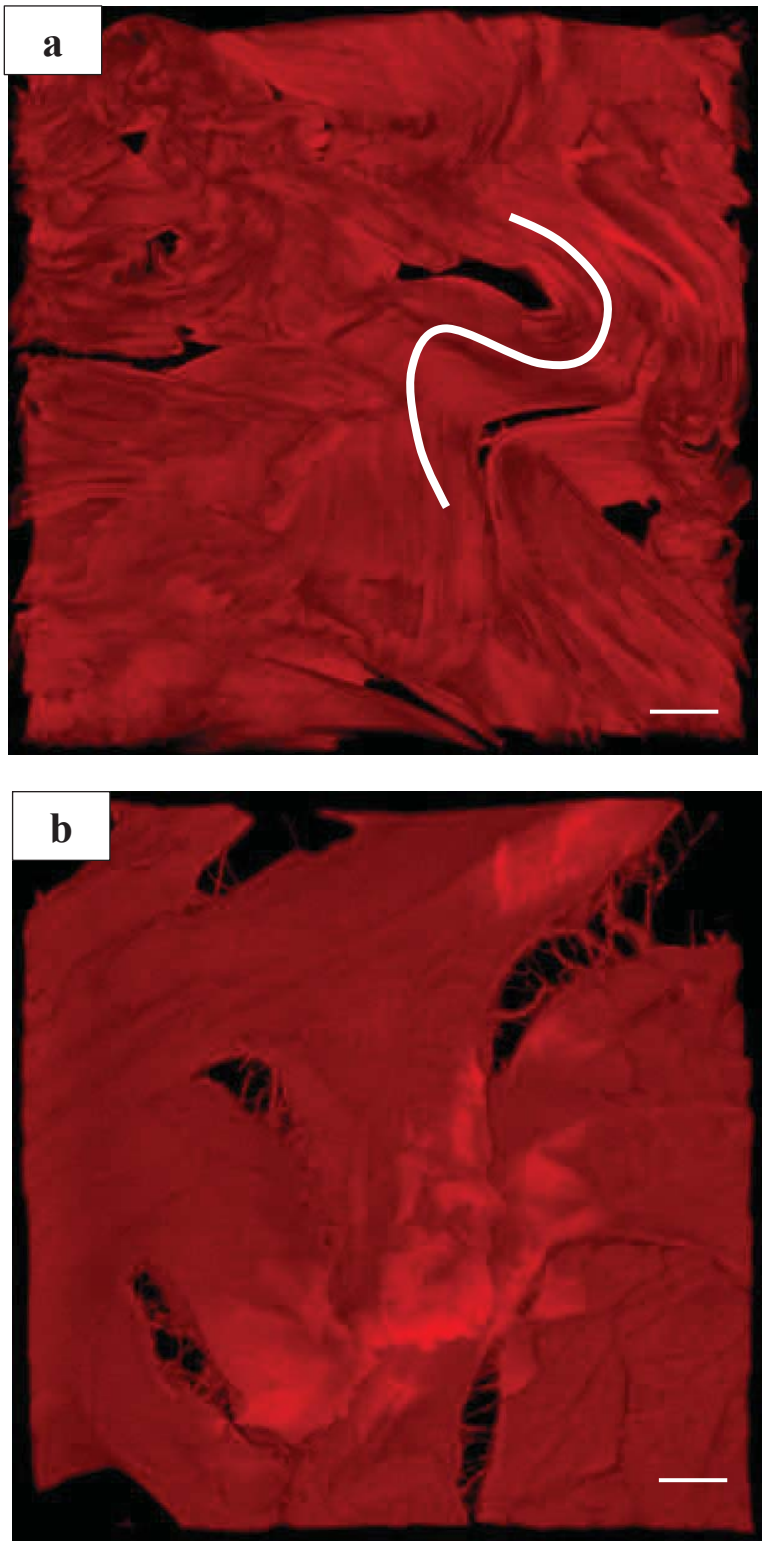

Figure 128: The top view of the 3D-images of the laser confocal scanning microscopy of (a) deer and (b) cow skins showing the waviness pattern in each skin. The curved and straight white lines show the waviness pattern of the fibre bundle in deer and cow skins, respectively. Scale bar is 50 μm.

10 **CHAPTER TEN:** Conclusion

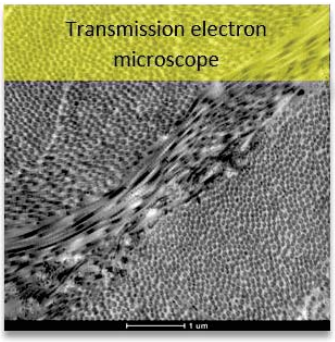

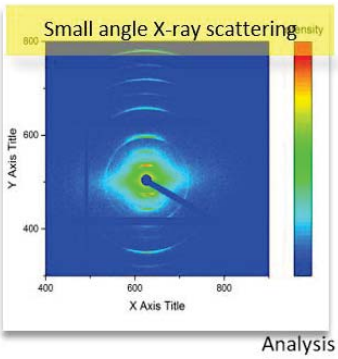

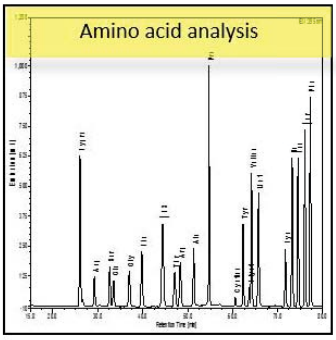

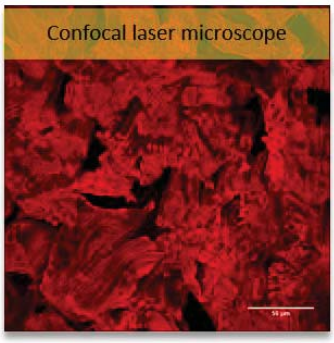

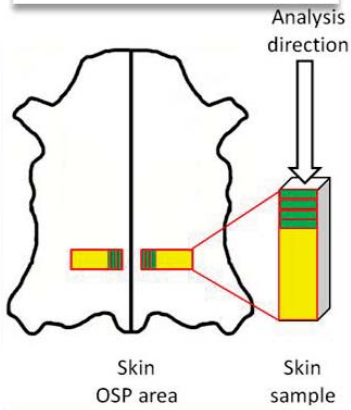

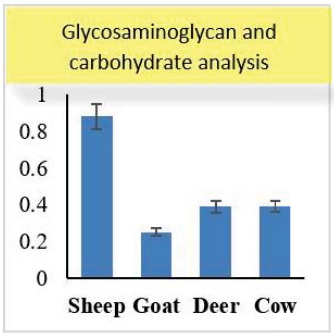

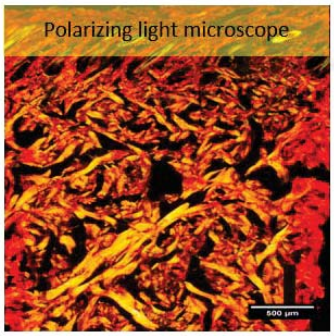

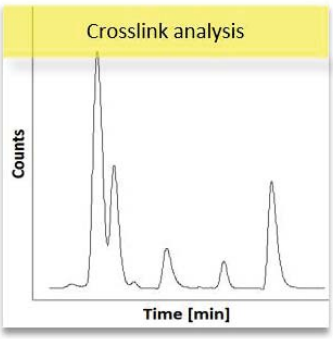

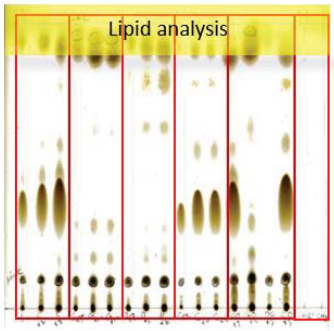

Table 26: Summary of the results of sheep, goat, deer and cow skins.

Skin	Sheep	Goat	Deer	Cow
Thickness (mm)	2.35	1.80	1.62	5.60
Tear Strength (N/mm)	29.7	60.7	84.4	160.0
Tensile Strength (N/mm^2)	7.3	17.2	28.3	29.2
DSC (^oC)	64.2	64.9	66.8	66.5
Collagen content % *	36.0	58.8	61.9	70.9
Lipid content % *	17.0	3.0	4.5	6.5
Total Glycosaminoglycans (mg/mg skin) *	0.88	0.25	0.41	0.42
Mean Fibril Diameters (nm)	80	86	72	96
Total collagen crosslinks (mol crosslinks/mol collagen)	0.32	0.57	0.56	0.88
Glycosaminoglycans in TEM	Very low	High with different shapes	High with consistent shapes	Low
Collagen architecture under confocal laser microscope	Not wavy	Wavy	Too wavy	Least wavy

* in dry skin.

The most common skins used in leather manufacture are sourced from sheep, goat, deer and cow. Each skin has different biomechanical properties, although they are made up of the same macromolecules that include collagen, elastin and proteoglycans. The detailed molecular drivers of these differences are however, not known. Much is known about collagen structure; its biosynthesis, primary, secondary, tertiary and quaternary structure, its types and its organisation into fibrils then fibres. There are, however, notable differences in the way fibrils are incorporated into fibres, and in the way the fibres themselves are arranged in different animal skins. This study investigated whether there is a link between the unique biomechanical functions of each skin and the molecules making up this complex material. Are there molecular differences that could be correlated with these different skin architectures? The reason for carrying out this study was to understand the molecular determinants of skin strength; such knowledge could result in the development or modifications to skin processing methods to produce leather with improved quality and strength. For example, sheep skin is supple and soft but has a low tensile strength, and with current technologies, cannot be used to make shoes or bags. Improving its tensile strength would be of enormous economic value to New Zealand.

The first part of this study required detailed and accurate measurements of the physical properties of sheep, goat, deer and cow skins in order to gain some understanding of the differences between them. Thus the thickness, shrinkage temperature, tear and tensile strengths of a minimum of five biological replicates of each animal skin were measured (Table 26). Because the skins were sourced from the meat industry it was not possible to know the exact age of each animal, which may have had an influence on

the results obtained. On the other hand, as it is not possible for the leather industry to choose hides on the basis of age, it was not considered to be an issue for this study which was aimed at investigating bulk differences in skins regardless of age or other environmental influences. Each collection of skin was limited to five biological replicates because of the difficulty in obtaining goat and deer skins, and because five was considered a compromise to the number of samples ideally required to obtain statistical significance.

It was found that in the skin raw state, when normalized for thickness, cow had the highest tensile strength skin followed by deer, goat and sheep skins. Generally, the shrinkage temperature had a positive correlation with tensile strength, although the differences in shrinkage temperature were small; for example, although cow skin had a much higher tensile strength than the other three skins the difference in its shrinkage temperature from the other skins while significant, was small. After much investigation, it was decided to measure the thickness of each skin using standard reference methods. This is done by placing the skin on a hard, flat surface and determining the distance from the base using a presser foot that is parallel to the base and applied to the top surface of the material. The pressure applied to the presser foot depends on the material being measured The results clearly showed that deer skin was thinnest at 1.60 mm followed by goat, sheep and cow skins at 1.80, 2.35 and 5.60 mm, respectively. There was no obvious relationship between the skin total thickness and its tensile strength. Interestingly when the percentage contribution of grain and corium layers to skin total thickness was considered, a positive correlation with tensile strength could be seen. It is worthwhile remembering that the corium is where most of the type

I collagen is found and where the collagen is tightly packed and structured. Sheep skin has about 50% of corium and 50% grain while cow, deer and goat skins are made up from approximately 81%, 88% and 67% corium respectively. Thus despite cow skin having slightly less corium its thickness provides it with greater strength than deer skin which has the greatest proportion of corium.

As sample preparation has a profound effect on the final outcome of many molecular analyses, skin samples were treated immediately after collection by dipping in a mixture of protease inhibitors to minimise any bacterial activity leading to skin degradation prior to analysis. Such treatment had been experimentally shown to effect suitable protection without any significant loss of protein, collagen, carbohydrate or glycosaminoglycans from the depilated skins.

In this study skin structure was investigated at several levels of magnification from μm to Å. Firstly, confocal laser microscopy allowed the visualisation of collagen fibres (μm in diameter) in the skin when the skin samples were stained with picrosirius red, a stain specific for collagen. These showed that deer skin was more "crimped" than sheep, goat and cow skins with well-organised fibres weaving in and out of the plane and changing direction often. Although cow skin also contained well organised bunches of large fibres, they were more likely to be aligned in one direction with little crimping and few gaps. While these two skins have the greatest tensile strength of the four skins examined, they have very different thickness (cow the thickest and deer the thinnest skin) and display different stretching profiles when placed under stress. Cow skin has the highest tensile strength, but is not as flexible as deer skin, a direct result of the "crimping" seen in the deer skin fibres when examined with confocal laser

microscopy. When subjected to stress, the crimped fibres are able to straighten out before the individual tropocollagen molecules have to slide against one another within the fibrils in order to accommodate the stress. Sheep skin, the weakest skin with the smallest percentage of corium, contained fibres that had a more regular arrangement like those in cow skin but were much smaller and more widely spaced. On the other hand, the fibres in goat skin were arranged in a way that was intermediate between those in cow and deer skins *i.e.* there was some "crimping" but not as much as seen in deer skin and the fibres were approximately the same size as those in deer skin but more widely spaced like those in sheep skin. These observations are consistent with results obtained from amino acid analyses which showed that sheep skin had the lowest total protein as well as the lowest collagen content (36%) while cow, the thickest of the skins, contained the highest protein concentration and not surprisingly the highest proportion of collagen (76%) per unit of mass. Deer skin is an anomaly. It contains less collagen (62%) than cow skin yet it is almost as strong and much more flexible. Clearly this is due to the fibre architecture, which counteracts the lower collagen content allowing the skin to stretch more before it breaks. It is not surprising that sheep skin with its thin corium layer, lower collagen content and featureless fibres is the weakest of the four skins examined. Goat skin which contains less collagen (59%) than deerskin, has a lower tensile strength than deer skin, with a fibre architecture intermediate between those of sheep and deer.

Other interactions that influence fibril architecture are those between proteoglycans and collagen fibrils. These have been examined in many collagenous materials and it has been shown that both moieties making up the proteoglycan, the core protein and

the glycosaminoglycan polysaccharides, influence fibril spacing and contribute to the mechanical strength of the skin [272, 286, 507-509] Previous studies of glycosaminoglycans in connective tissue have identified two different types; large aggregated proteoglycans (LAPs) and small leucine rich proteoglycans (SLRPs) [233, 508]. The protein moieties of the latter are known to bind to specific sites on the surface of type I collagen fibrils, the binding being stabilised by electrostatic interactions between the glycosaminoglycan sidechains and the fibrils. Decorin is one of the most common SLRPs found in animal skins and has been shown to play an essential role in correct fibril assembly as well as inhibiting cleavage of collagen fibrils by matrix metalloproteases [271, 282, 284, 285, 288]. The LAPS are more commonly found filling up the gaps between collagen fibres and fibrils, acting as glue to hold them together. Transmission electron microscopy (TEM) was used to examine the skin samples at nm resolution and to visualise the proteoglycans. Measurement of mass-average diameters and diameter distribution of collagen fibrils in these dehydrated samples showed that the mass-average diameter of cow skin was the largest, followed by goat then sheep skin, while unexpectedly, that of deer skin was the smallest. As deer skin is the second strongest skin, the relationship between the mass average diameter and skin strength reported by previous researchers is questionable.

In order to visualise the proteoglycans, skin slices were stained using cuprolinic blue in the presence of critical electrolyte concentration concentrations of $MgCl_2$ with tungstate as an intensifier. This dye preferentially binds to highly negatively charged sulfated glycosaminoglycans, and is thought to prevent the sugar chains from collapsing during sample preparation [499]. Comparison of the four skins showed there

were significant differences in proteoglycan apparent size and position between collagen fibrils in the four skins. Only the corium of the four skins was examined using this stain because grain layer contained much smaller and unorganized collagen fibrils in all animal skins making the visualization of glycosaminoglycans with respect to the collagen fibrils impossible. In deer skin the individual micro fibrils clearly appeared to be linked by regular arrays of filaments. Not only were they regularly spaced, but they had the appearance of small cylinders of the same size implying that the glycosaminoglycan chains were reasonably large (30-40 nm) and of the same type. The arrangement in cow skin was not so regular, often being visualised as intense dark splotches implying that these may be due to larger local concentrations of different proteoglycans. The fact that the two strongest skins appeared to have different arrangements and concentrations of proteoglycans raises interesting questions. It seems that the higher concentrations of proteoglycans resulted in a smaller collagen fibril diameter in deer skin. On the other hand, in cow skin the larger and aggregated proteoglycans resulted in a larger fibril diameter. As the higher concentrations of SLRPs such as decorin should be reflected in higher leucine concentrations, amino acid analyses of deer and cow skins were done on the whole skin rather than the corium alone which did not allow an accurate estimation of SLRPs in each skin layer. Nevertheless, the concentrations of aspartic acid, glutamic acid, lysine and leucine, the major amino acids in decorin, were higher in deer skin than those in cow skin. This supports the higher decorin concentrations in deer skin than cow skin. On the other hand, the total glycosaminoglycan concentration was slightly lower in deer skin than cow skin suggesting that deer skin contains shorter and less glycosaminoglycan chains linked to decorin core protein. In contrast, cow skin contains longer and more

glycosaminoglycan chains making them more susceptible to aggregation when stained with cuprolinic blue and therefore they were seen as intense dark splotches with TEM.

TEM images of goat skin, one of the weaker skins, showed the fibrils were linked by fewer proteoglycan filaments and these appeared to be less well ordered. Sheep skin on the other hand seemed to have no proteoglycans amongst the fibrils, which was at odds with sheep skin containing the highest concentration of glycosaminoglycans when these were measured in whole skin samples. One possible explanation for this is that most of the glycosaminoglycans are located in the grain rather than the corium as sheep skin is almost 50% grain in marked contrast to the other skins, all of which have a much smaller grain layer. Another possible explanation is that there are more LAPs filling up the gaps between the collagen fibrils in sheep skin, as confocal microscopy showed the fibres in sheep skin were not as closely packed. The lack of SLRPs would have the effect of reducing restraints on fibril packing, allowing them to be further apart and form smaller fibres, the arrangement observed for sheep skin. This hypothesis is supported by amino acid analysis, as sheep skin has a higher leucine content than the goat, deer and cow skins

In order to look at the microfibril organisation within individual fibrils, small angle X-ray scattering (SAXS) was used. The diameters and D-periodicity of collagen fibrils in all raw skins were measured while the skins were in their hydrated state in contrast to the measurements made using TEM where the skin samples were dehydrated. While there were no significant differences in D-periodicity between skins, the collagen fibril diameters were significantly different with cow skin having the largest diameter and deer skin the smallest. While the order in size remained the same for each of the four

skins, the actual diameters of the hydrated samples were larger than those measured by TEM as expected. Careful preparation of 50 μm thick samples enabled a small envelope of fibres to be exposed to the X-rays resulting in a more accurate assessment of the angular distribution of fibrils compared to what had been previously reported. Orientation maps generated from the data allowed visualisation of the 3-dimensional organisation of the collagen fibrils in each skin sample. Deer and goat skins appeared to have multiple fibrils running in many different directions in contrast to the fibrils in sheep and cow skins in which the collagen fibrils appeared to be oriented in two main directions approximately 60 and 90 degrees apart. These results again show that the two strongest skins have a totally different arrangements of fibrils within each fibre indicating that fibril organisation is not correlated with skin strength.

Lastly, can the analyses of the molecules that make up skin be related to the physical characteristics discussed above? It has long been recognized that the crosslinks between tropocollagen molecules are extremely important for the integrity and strength of skin, [11, 63] but while much is known about the crosslinks found in cartilage and bone, little research has been done on those in animal skins. Analysis of the crosslinks in the four skins showed that not surprisingly, cow skin contained the highest concentration of crosslinks while sheep skin showed the lowest. Interestingly, goat and deer skins had similar concentrations of crosslinks despite having different concentrations of collagen. For crosslinks to form, lysine and hydroxylysine residues need to be oxidatively deaminated by the enzyme lysyl oxidase. The hydroxyl group of hydroxylysine can also be glycosylated, yet the function of this glycosylation in skin is not yet clear. Whether the two modifications are mutually exclusive is not known. If

they were, it is possible that the amount of glycosylation of hydroxylysine may influence the number of crosslinks that are able to form. Analysis of total carbohydrate in the four skin samples showed that sheep skin had twice as much total carbohydrate as the goat, deer and cow skins. The main source of these carbohydrates is most likely to be from the glycosaminoglycans and from glycosylated collagen. Sheep skin has twice the concentration of glycosaminoglycans implying the source of the carbohydrates in sheep skin is the glycosaminoglycans. However, analysis of pickled skin which has lost most of its proteoglycans and contains mainly collagen showed that it contains a significantly higher proportion of carbohydrate than that in deer, goat and cow skins. It is thus possible that sheep skin collagen is more highly glycosylated and this has a detrimental effect on the activity of lysyl oxidase, decreasing the number of crosslinks being formed. Strikingly, the ratio between the mature to immature crosslinks was significantly higher in deer skin relative to sheep, goat and cow skins. Examination of pickled skin gave interesting and unexpected results. Total protein, total carbohydrate and glycosaminoglycan concentrations were barely significantly different between the skins, implying that the pretanning process removed a greater proportion of non-collagenous proteins such as proteoglycans from sheep skin compared to the other animal skins. This is not surprising bearing in mind the more open structure of sheep skin corium, and the greater proportion of grain. But when the tensile strength of the animal leathers was measured the order of strength changed at the top of the table, and deer skin became the strongest [4]. Remember that deer skin was always an anomaly. It had the smallest fibre diameter, a very distinct arrangement of proteoglycan, crimped fibres and a high angle of weave, or meshed arrangement of fibres. Another pertinent difference is the proportion of trivalent crosslinks and the high

ratio of mature to immature crosslinks it contains. Although cow skin has the highest number of mature crosslinks, it has a lower proportion of trivalent compared to tetravalent crosslinks. Deer skin has a significantly higher proportion of trivalent crosslinks, the only crosslink that is acid-stable. Destruction of crosslinks and loss of proteoglycan that is a result of exposure of the skins to sulfide during depilation removes all restraints on fibril organisation; the fibrils become more widely spaced and as a result, the skins lose strength. Because deer skin has the greatest concentration of acid stable crosslinks the original arrangement of fibrils is less likely to be changed, resulting in less swelling of the skin and retention of more tensile strength.

When the HLNL, HHL and HHMD crosslinks were isolated and purified from skin, NMR results strongly suggested the existence of two diastereomers of HLNL and HHMD but not HHL. Although, the presence of these diastereomers is still controversial, they could provide a plausible explanation for why tissues containing collagen I produced different crosslink concentrations and types. It has been recently reported that specific lysylhydroxylases catalyse lysyl hydroxylation of C-5 of lysine to produce hydroxylysine with specific stereochemistry of 5S or 5R and the latter is the known configuration in collagen [528]. This may explain why the proportion of 5S to 5R of hydroxylysine, the main residue involving in crosslinks formation, may have an effect on the glycosylation patterns and crosslink types and concentrations in collagen.

In summary, this study shed light on the skin structure organisation and the multiple factors contributing to its strength. Previous studies reported an individual correlation between skin strength and collagen fibres and fibrils orientation [4, 339] and collagen fibril diameter [14, 325]. However, in this study, smaller collagen fibrils in the strong

deer skin was associated with higher concentrations of the mature crosslinks and higher collagen “crimps”. Cow skin in contrast to deer skin is made up from large collagen fibre that are more arranged and contained lower concentration of mature crosslinks than deer skins. This does not agree with the previous reports of Siegel *et al*. (1976) [74], Parry *et al.* (1978) [529], Ono *et al*. (1993) [530] and Bailey *et al.* (1998) [76] which all demonstrated a positive correlation between the mature crosslink concentrations and fibril diameters thus the skin strength. Also this does not agree with the reports that showed a strong positive correlation between the collagen fibril orientation and strength [4, 339]. This study shows that a combination of the organisation of collagen fibres, diameters of collagen fibril, types and concentrations of proteoglycans and crosslinks is needed to study the skin strength. This would provide a deeper understanding of the skin structure and its strength. Finally, the ultimate goal of this study was to understand the basis of these factors which will allow informed changes to age old processing regimes that will help leather manufacturers to develop processes that will enhance the desirable properties of individual hides and skins rather than attenuating them. While the results have answered some questions, they have raised many more for future work.

11 Directions for Future Research

1. In this study, amino acid analysis was carried out on the whole animal skin and included both the grain and corium layers. To obtain a better understanding of the collagen structure in skin, the grain and corium of the animal skins should be separated and the collagen extracted from them before any analyses are done. This will allow the precise amount of hydroxyproline in each animal's corium and grain to be measured which will allow accurate estimations of the collagen and non-collagenous protein contents. Care should also be taken to separate the non-soluble from the soluble collagen as such a measurement is relevant to the amount of collagen that is crosslinked and therefore likely to be type 1 collagen.
2. During this study, mounting evidence suggested that hydroxylysine, HLNL and HHMD diastereomers occur in collagen. This evidence needs to be verified. To do this, acid hydrolysis of collagen will be replaced with complete enzymatic digestion of collagen into amino acids and followed by the quantitation of amino acids and crosslinks using the methods developed in this study. At the same time a bioinformatics study of sheep, cow, deer and goat genomes (where available) should be made to identify lysyl hydroxylase enzymes and to characterise their substrates. If different diastereomers do occur naturally, there could be more than one gene for this enzyme.
3. In this study, a novel, rapid and sensitive method has been developed for collagen and elastin crosslink analysis therefore more specific analyses should be explored using this method:

A. The types and concentrations of collagen and elastin crosslinks should be measured separately in the grain and corium of the different skins.
B. Changes in the types and concentrations of collagen and elastin crosslinks during leather processing should be monitored after liming, deliming, bating and pickling.
C. The putative crosslinks observed during this study should be isolated, purified and characterised.
D. If possible, changes in crosslink types and concentrations with animal age should be analysed because in this study the age of the animal skins was unknown, and age is known to change the crosslinking profile in tissues like tendon and bone.

4. In this study to obtain high quality SAXS data, it was important to optimise the preparation of skin samples and to develop programs to process the large number of SAXS images recorded. These programs can be used in future to study SAXS data collected on different skins at various stages of leather processing which will provide valuable information about the changes occurring in collagen fibril organisation. The information about the changes in fibril architecture should then be correlated to the changes occurring at the molecular level in skin.
5. In this study, cuprolinic blue was successfully used to specifically stain the glycosaminoglycans in the skin. The glycosaminoglycan organisation within collagen fibrils and their amount were obvious but their identities were not determined. Such information on proteoglycan type, specifically the type of glycosaminoglycan chain is valuable information when trying to understand the influence of proteoglycans on fibril organisation. The use of enzymes that digest

specific glycosaminoglycans will facilitate the identification of glycosaminoglycan types and their effect on fibril organisation and elucidate the roles these molecules play in stabilising skin structure.

12 APPENDICES

See CD-ROM attached!

Contents

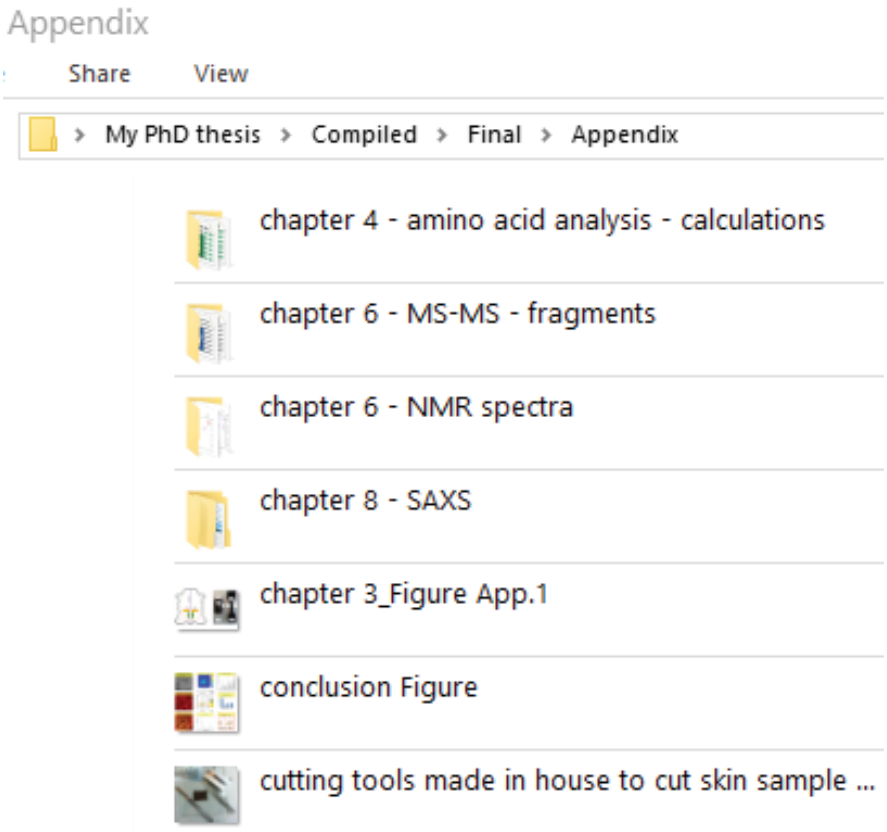

13 References

[1] World statistical compendium for raw hides and skins, leather and leather footwear 1993-2012, Food and Agriculture Organization of the United Nation, 2012.
[2] A. D. Covington, Tanning Chemistry: The Science of Leather, The Royal Society of Chemistry, Cambridge, UK, 2009.
[3] K. H. Sizeland, R. L. Edmonds, M. M. Basil-Jones, N. Kirby, A. Hawley, S. Mudie, R. G. Haverkamp, Changes to collagen structure during leather processing, J. Agric. Food. Chem., (2015), 2499-2505.
[4] K. H. Sizeland, M. M. Basil-Jones, R. L. Edmonds, S. M. Cooper, N. Kirby, A. Hawley, R. G. Haverkamp, Collagen orientation and leather strength for selected mammals, J. Agric. Food. Chem., 61 (2013), 887-892.
[5] Y. Chan, G. M. Cox, R. G. Haverkamp, J. M. Hill, Mechanical model for a collagen fibril pair in extracellular matrix, Eur. Biophys. J., 38 (2009), 487-493.
[6] P. Fratzl, Collagen: structure and mechanics, Springer, New York, USA, 2008.
[7] R. C. Picu, Mechanics of random fibre networks—a review, Soft Matter, 7 (2011), 6768-6785.
[8] A. J. van der Slot-Verhoeven, E. A. van Dura, J. Attema, B. Blauw, J. DeGroot, T. W. Huizinga, A. Zuurmond, R. A. Bank, The type of collagen cross-link determines the reversibility of experimental skin fibrosis, Biochimica et Biophysica Acta (BBA)-Molecular Basis of Disease, 1740 (2005), 60-67.
[9] C. A. Maxwell, T. J. Wess, C. J. Kennedy, X-ray diffraction study into the effects of liming on the structure of collagen, Biomacromolecules, 7 (2006), 2321-2326.
[10] R. E. Bulo, L. Siggel, F. Molnar, H. Weiss, Modeling of bovine type-I collagen fibrils: Interaction with pickling and retanning agents, Macromol. Biosci., 7 (2007), 234-240.
[11] D. J. S. Hulmes, Collagen: Diversity, Synthesis and Assembly, in: P. Fratzl (Ed.) Collagen, Springer, New York, USA, (2008), 15-47.
[12] D. R. Eyre, M. A. Weis, J. J. Wu, Advances in collagen cross-link analysis, Methods, 45 (2008), 65-74.
[13] R. P. Mecham, D. E. Birk, P. D. Yurchenco, Extracellular Matrix Assembly and Structure, Academic Press, Massachusetts, USA, (2013).
[14] H. C. Wells, R. L. Edmonds, N. Kirby, A. Hawley, S. T. Mudie, R. G. Haverkamp, Collagen fibril diameter and leather strength, J. Agric. Food. Chem., 61 (2013), 11524-11531.
[15] C. K. Liu, N. P. Latona, J. Lee, P. H. Cooke, Microscopic observations of leather looseness and its effects on mechanical properties, JALCA, 104 (2009), 230-236.
[16] M. P. E. Wenger, L. Bozec, M. A. Horton, P. Mesquida, Mechanical properties of collagen fibrils, Biophys. J., 93 (2007), 1255-1263.
[17] P. P. Purslow, T. J. Wess, D. W. Hukins, Collagen orientation and molecular spacing during creep and stress-relaxation in soft connective tissues, J. Exp. Biol, 201 (1998), 135-142.
[18] M. Fang, Type I Collagen Nanomorphology in Relation to Disease, Tissue Hierarchy, and Fibrillogenesis, PhD. Thesis, University of Michigan, (2013).

[19] E. Mosler, W. Folkhard, E. Knörzer, H. Nemetschek-Gansler, T. Nemetschek, M. Koch, Stress-induced molecular rearrangement in tendon collagen, J. Mol. Biol., 182 (1985), 589-596.
[20] M. M. Basil-Jones, R. L. Edmonds, G. E. Norris, R. G. Haverkamp, Collagen fibril alignment and deformation during tensile strain of leather: A small-angle X-ray scattering study, J. Agric. Food. Chem., 60 (2012), 1201-1208.
[21] M. M. Basil-Jones, R. L. Edmonds, T. F. Allsop, S. M. Cooper, G. Holmes, G. E. Norris, D. J. Cookson, N. Kirby, R. G. Haverkamp, Leather structure determination by small-angle X-ray scattering (SAXS): cross sections of ovine and bovine leather, J. Agric. Food. Chem., 58 (2010), 5286-5291.
[22] L. Yang, K. O. van der Werf, C. F. C. Fitié, M. L. Bennink, P. J. Dijkstra, J. Feijen, Mechanical properties of native and cross-linked type I collagen fibrils, Biophys. J., 94 (2008), 2204-2211.
[23] D. Rabinovich, Seeking soft leathers with a tight grain, World Leather, 14 (2001), 27-32.
[24] M. Zhang, G. Li, Partial characterization of fish skin collagen cross-linked by N-hydroxysuccinimide activated adipic acid, J. Aquat. Food Prod. Technol., 23 (2014), 44-58.
[25] N. Usharani, G. C. Jayakumar, S. V. Kanth, J. R. Rao, B. Chandrasekaran, Molecular understanding of collagen stabilization: interaction of valeraldehyde with collagen, J. Macromol. Sci. A, 49 (2012), 666-673.
[26] J. Churchill, The Complete Book of Tanning Skins and Furs, Stackpole Books, New York, USA, (1983).
[27] C. Bonnans, J. Chou, Z. Werb, Remodelling the extracellular matrix in development and disease, Nat. Rev. Mol. Cell Biol., 15 (2014), 786-801.
[28] A. Pappas, Skin Lipids: An Introduction and Their Importance, in: A. Pappas (Ed.) Lipids and Skin Health, Springer, New Jersey, USA, (2015), 3-5.
[29] C. M. Chuong, B. J. Nickoloff, P. M. Elias, L. A. Goldsmith, E. Macher, P. A. Maderson, J. P. Sundberg, H. Tagami, P. M. Plonka, K. Thestrup-Pederson, What is the 'true' function of skin?, Exp. Dermatol., 11 (2002), 159-187.
[30] M. Kite, R. Thomson, Conservation of Leather and Related Materials, Routledge, Abingdon, UK, (2006).
[31] J.H. Sharphouse, Leather Technician's Handbook, Leather Producers' Association, UK, (1983).
[32] R. Maynes, Structure and Function of Collagen Types, Elsevier, The Netherland, (2012).
[33] G. Reich, From Collagen to Leather - The Theoretical Background, BASF Service center, Ludwigshafen, Germany, (2007).
[34] W. Montagna, The Structure and Function of Skin, Third ed., Academic Press, UK, (1974).
[35] A. D. Covington, Modern tanning chemistry, Chem. Soc. Rev., 26 (1997) 111-126.
[36] J. A. Ramshaw, Distribution of type III collagen in bovine skin of various ages, Connect. Tissue Res., 14 (1986), 307-314.

[37] R. R. Driskell, F. M. Watt, Understanding fibroblast heterogeneity in the skin, Trends Cell Biol., 25 (2015), 92-99.
[38] E. H. Nashy, O. Osman, A. A. Mahmoud, M. Ibrahim, Molecular spectroscopic study for suggested mechanism of chrome tanned leather, Spectrochim. Acta, Pt. A: Mol. Biomol. Spectrosc., 88 (2012), 171-176.
[39] B. Madhan, V. Subramanian, J. R. Rao, B. U. Nair, T. Ramasami, Stabilization of collagen using plant polyphenol: Role of catechin, Int. J. Biol. Macromol., 37 (2005), 47-53.
[40] P. Ghosh, Adhesive And Coating Technology, Tata McGraw-Hill Education, New Delhi, India, (2008).
[41] K. E. Kadler, D. F. Holmes, J. A. Trotter, J. A. Chapman, Collagen fibril formation, Biochem. J, 316 (1996), 1-11.
[42] E. M. Culav, C. H. Clark, M. J. Merrilees, Connective tissues: matrix composition and its relevance to physical therapy, Phys. Ther., 79 (1999), 308-319.
[43] C. Illidge, C. Kielty, A. Shuttleworth, Type VIII collagen: heterotrimeric chain association, Int. J. Biochem. Cell Biol., 33 (2001), 521-529.
[44] M. Yamauchi, M. Sricholpech, Lysine post-translational modifications of collagen, Essays Biochem., 52 (2012), 113-133.
[45] G. Bou-Gharios, B. de Crombrugghe, Type I Collagen Structure, Synthesis, and Regulation in: L.G. Raisz, T.J. Martin (Eds.) Principles of Bone Biology, Academic Press, Massachusetts, USA, (2008), 285-318.
[46] G. Ramachandran, M. Bansal, R. Bhatnagar, A hypothesis on the role of hydroxyproline in stabilizing collagen structure, BBA-Protein Structure, 322 (1973), 166-171.
[47] C. M. Kielty, M. E. Grant, The Collagen Family: Structure, Assembly, and Organization in the Extracellular Matrix, in: P.M. Royce, B. Steinmann (Eds.) Connective Tissue and Its Heritable Disorders: Molecular, Genetic, and Medical Aspects, Second Edition, John Wiley & Son, New Jersey, USA, (2003), 159-221.
[48] K. Gelse, E. Pöschl, T. Aigner, Collagens-Structure, function, and biosynthesis, Adv. Drug Del. Rev., 55 (2003), 1531-1546.
[49] D. J. Prockop, Mutations that alter the primary structure of type I collagen. The perils of a system for generating large structures by the principle of nucleated growth, J. Biol. Chem., 265 (1990), 15349-15352.
[50] P. Fratzl, R. Weinkamer, Nature's hierarchical materials, Prog. Mater Sci., 52 (2007), 1263-1334.
[51] M. A. Meyers, P. Y. Chen, A. Y. M. Lin, Y. Seki, Biological materials: structure and mechanical properties, Prog. Mater Sci., 53 (2008), 1-206.
[52] J. Myllyharju, K. I. Kivirikko, Collagens, modifying enzymes and their mutations in humans, flies and worms, Trends Genet., 20 (2004), 33-43.
[53] M. D. Shoulders, R. T. Raines, Collagen structure and stability, Annu. Rev. Biochem, 78 (2009), 929-958.
[54] J. Eastoe, The amino acid composition of mammalian collagen and gelatin, Biochem. J, 61 (1955), 589-600.

[55] J. P. Malone, A. George, A. Veis, Type I collagen N-telopeptides adopt an ordered structure when docked to their helix receptor during fibrillogenesis, Proteins: Structure, Function, and Bioinformatics, 54 (2004), 206-215.
[56] A. Viidik, J. Vuust, Biology of Collagen, Academic Press, Massachusetts, USA, 1980.
[57] R. E. Burgeson, R. Mayne, Structure and Function of Collagen Types, Elsevier, Amsterdam, The Netherland, (2012).
[58] D. Villone, A. Fritsch, M. Koch, L. Bruckner-Tuderman, U. Hansen, P. Bruckner, Supramolecular interactions in the dermo-epidermal junction zone anchoring fibril - collagen VII tightly binds to banded collagen fibrils, J. Biol. Chem., 283 (2008), 24506-24513.
[59] P. Agarwal, D. Zwolanek, D. R. Keene, J. N. Schulz, K. Blumbach, D. Heinegård, F. Zaucke, M. Paulsson, T. Krieg, M. Koch, Collagen XII and XIV, new partners of cartilage oligomeric matrix protein in the skin extracellular matrix suprastructure, J. Biol. Chem., 287 (2012), 22549-22559.
[60] S. Grässel, C. Unsöld, H. Schäcke, L. Bruckner-Tuderman, P. Bruckner, Collagen XVI is expressed by human dermal fibroblasts and keratinocytes and is associated with the microfibrillar apparatus in the upper papillary dermis, Matrix Biol., 18 (1999), 309-317.
[61] L. Knott, A. J. Bailey, Collagen cross-links in mineralizing tissues: a review of their chemistry, function, and clinical relevance, Bone, 22 (1998), 181-187.
[62] D. R. Eyre, M. J. Glimcher, Comparative biochemistry of collagen crosslinks: reducible bonds in invertebrate collagens, Biochim. Biophys. Acta, 243 (1971), 525-529.
[63] N. C. Avery, A. J. Bailey, Restraining Cross-Links Responsible for the Mechanical Properties of Collagen Fibres: Natural and Artificial, in: P. Fratzl (Ed.) Collagen, Springer, New York, USA, (2008), 81-110.
[64] Y. Li, G. Fessel, M. Georgiadis, J. G. Snedeker, Advanced glycation end-products diminish tendon collagen fibre sliding, Matrix Biol., 32 (2013), 169-177.
[65] G. Fessel, Y. Li, V. Diederich, M. Guizar-Sicairos, P. Schneider, D.R. Sell, V.M. Monnier, J.G. Snedeker, Advanced glycation end-products reduce collagen molecular sliding to affect collagen fibril damage mechanisms but not stiffness, PloS one, 9 (2014), e110948.
[66] K. Reiser, R. J. McCormick, R. B. Rucker, Enzymatic and nonenzymatic cross-linking of collagen and elastin, The FASEB Journal, 6 (1992), 2439-2449.
[67] N.C. Avery, A. J. Bailey, Enzymic and non-enzymic cross-linking mechanisms in relation to turnover of collagen: Relevance to aging and exercise, Scand. J. Med. Sci. Sports, 15 (2005), 231-240.
[68] K. Uzawa, H. N. Yeowell, K. Yamamoto, Y. Mochida, H. Tanzawa, M. Yamauchi, Lysine hydroxylation of collagen in a fibroblast cell culture system, Biochem. Biophys. Res. Commun., 305 (2003), 484-487.
[69] K. I. Kivirikko, R. Myllylä, Posttranslational Enzymes in the Biosynthesis of Collagen: Intracellular Enzymes, in: L.W. Cunningham, D.W. Frederiksen (Eds.) Methods Enzymol., Elsevier, Amsterdam, The Netherlands, (1982), 245-304.

[70] M. Terajima, I. Perdivara, M. Sricholpech, Y. Deguchi, N. Pleshko, K.B. Tomer, M. Yamauchi, Glycosylation and cross-linking in bone type I collagen, J. Biol. Chem., 289 (2014), 22636-22647.
[71] S. R. Pinnell, G. R. Martin, The cross-linking of collagen and elastin: enzymatic conversion of lysine in peptide linkage to alpha-aminoadipic-delta-semialdehyde (allysine) by an extract from bone, PNAS, 61 (1968), 708.
[72] H. A. Lucero, H. M. Kagan, Lysyl oxidase: an oxidative enzyme and effector of cell function, Cell. Mol. Life Sci., 63 (2006), 2304-2316.
[73] L. I. Smith-Mungo, H. M. Kagan, Lysyl oxidase: Properties, regulation and multiple functions in biology, Matrix Biol., 16 (1998), 387-398.
[74] R.C. Siegel, Collagen cross-linking. Synthesis of collagen cross-links in vitro with highly purified lysyl oxidase, J. Biol. Chem., 251 (1976), 5786-5792.
[75] A. Viidik, Connective tissues—possible implications of the temporal changes for the aging process, Mechanisms of ageing and development, 9 (1979), 267-285.
[76] A. J. Bailey, R. G. Paul, L. Knott, Mechanisms of maturation and ageing of collagen, Mech. Ageing Dev., 106 (1998), 1-56.
[77] P. Fratzl, K. Misof, I. Zizak, G. Rapp, H. Amenitsch, S. Bernstorff, Fibrillar structure and mechanical properties of collagen, J. Struct. Biol., 122 (1998), 119-122.
[78] A. J. Bailey, C. M. Peach, Isolation and structural identification of a labile intermolecular crosslink in collagen, Biochem. Biophys. Res. Commun., 33 (1968), 812-819.
[79] J. A. Last, L. G. Armstrong, K. M. Reiser, Biosynthesis of collagen crosslinks, Int. J. Biochem., 22 (1990), 559-564.
[80] M. L. Tanzer, G. Mechanic, Collagen reduction by sodium borohydride: effects of reconstitution, maturation and lathyrism, Biochem. Biophys. Res. Commun., 32 (1968), 885-892.
[81] M. L. Tanzer, Collagen crosslinks: Stabilization by borohydride reduction, Biochimica et Biophysica Acta (BBA) - Protein Structure, 133 (1967), 584-587.
[82] E. G. Canty, K. E. Kadler, Collagen fibril biosynthesis in tendon: a review and recent insights, Comp. Biochem. Physiol., A: Mol. Integr. Physiol., 133 (2002), 979-985.
[83] D. R. Eyre, M. A. Paz, P. M. Gallop, Cross-linking in collagen and elastin, Annu. Rev. Biochem, 53 (1984), 717-748.
[84] G. Mechanic, P. M. Gallop, M. L. Tanzer, The nature of crosslinking in collagens from mineralized tissues, Biochem. Biophys. Res. Commun., 45 (1971), 644-653.
[85] A. J. Bailey, M. S. Shimokomaki, Age related changes in the reducible cross-links of collagen, FEBS Lett., 16 (1971), 86-88.
[86] R. B. Fairweather, M. L. Tanzer, P. M. Gallop, Aldol-histidine, a new trifunctional collagen crosslink, Biochem. Biophys. Res. Commun., 48 (1972), 1311-1315.
[87] A. J. Bailey, C. M. Peach, The chemistry of the collagen cross-links. The absence of reduction of dehydrolysinonorleucine and dehydrohydroxylysinonorleucine in vivo, Biochem. J, 121 (1971), 257-259.
[88] R. Lent, C. Franzblau, Studies on the reduction of bovine elastin: Evidence for the presence of Δ6,7-dehydrolysinonorleucine, Biochem. Biophys. Res. Commun., 26 (1967), 43-50.

[89] K. A. Smolenski, N. C. Avery, N. D. Light, A new rapid method for the identification of reducible collagen cross-links in small tissue samples, Biochem. J, 213 (1983) 525-532.
[90] N. R. Davis, Stable crosslinks of collagen, Biochem. Biophys. Res. Commun., 54 (1973), 914-922.
[91] A. J. Bailey, L. J. Fowler, C. M. Peach, Identification of two interchain crosslinks of bone and dentine collagen, Biochem. Biophys. Res. Commun., 35 (1969), 663-671.
[92] G. L. Mechanic, Collagen crosslinks: Direct evidence of a reducible stable form of the Schiff base Δ6dehydro-5,5′-dihydroxylysinonorleucine as 5-keto-5′-hydroxylysinonorleucine in bone collagen, Biochem. Biophys. Res. Commun., 56 (1974), 923-927.
[93] M. L. Tanzer, T. Housley, L. Berube, R. Fairweather, C. Franzblau, P.M. Gallop, Structure of two histidine-containing cross-links from collagen, J. Biol. Chem., 248 (1973), 393-402.
[94] M. Yamauchi, R. London, C. Guenat, F. Hashimoto, G. Mechanic, Structure and formation of a stable histidine-based trifunctional cross-link in skin collagen, J. Biol. Chem., 262 (1987), 11428-11434.
[95] D. R. Eyre, T. J. Koob, K. P. Van Ness, Quantitation of hydroxypyridinium crosslinks in collagen by high-performance liquid chromatography, Anal. Biochem., 137 (1984), 380-388.
[96] E. C. Naylor, R. E. B. Watson, M. J. Sherratt, Molecular aspects of skin ageing, Maturitas, 69 (2011), 249-256.
[97] M. Yamauchi, D. T. Woodley, G. L. Mechanic, Aging and cross-linking of skin collagen, Biochem. Biophys. Res. Commun., 152 (1988), 898-903.
[98] A. J. Bailey, R. G. Paul, The Mechanisms and Consequences of the Maturation and Ageing of Collagen, P. Indian Acad. Sci. - Chem Sci., Springer, (1999), 57-69.
[99] M. Yamauchi, P. Prisayanh, Z. Haque, D.T. Woodley, Collagen cross-linking in sun-exposed and unexposed sites of aged human skin, J. Invest. Dermatol., 97 (1991), 937-941.
[100] S. P. Robins, A. J. Bailey, The chemistry of the collagen cross links. The characterization of fraction C, a possible artifact produced during the reduction of collagen fibres with borohydride, Biochem. J, 135 (1973), 657-665.
[101] R. C. Siegel, J. B. Lian, Lysyl oxidase dependent synthesis of a collagen cross-link containing histidine, Biochem. Biophys. Res. Commun., 67 (1975), 1353-1359.
[102] K. M. Reiser, S. M. Hennessy, J. A. Last, Analysis of age-associated changes in collagen crosslinking in the skin and lung in monkeys and rats, BBA - General Subjects, 926 (1987), 339-348.
[103] M. L. Tanzer, R. Fairweather, P. M. Gallop, Isolation of the crosslink, hydroxymerodesmosine, from borohydride-reduced collagen, BBA-Protein Structure, 310 (1973), 130-136.
[104] E. Hunt, H. R. Morris, Collagen cross-links. A mass-spectrometric and 1H-and 13C-nuclear-magnetic-resonance study, Biochem. J, 135 (1973), 833-843.
[105] L. Knott, C. C. Whitehead, R. Fleming, A. J. Bailey, Biochemical changes in the collagenous matrix of osteoporotic avian bone, Biochem. J, 310 (1995), 1045-1051.

[106] R. Kuypers, M. Tyler, L. Kurth, I. D. Jenkins, D. J. Horgan, Identification of the loci of the collagen-associated Ehrlich chromogen in type I collagen confirms its role as a trivalent cross-link, Biochem. J, 283 (1992), 129-136.
[107] D. A. Slatter, N. C. Avery, A. J. Bailey, Identification of a new cross-link and unique histidine adduct from bovine serum albumin incubated with malondialdehyde, J. Biol. Chem., 279 (2004), 61-69.
[108] J. E. Scott, E. Hughes, A. Shuttleworth, A collagen-associated Ehrlich chromogen: a pyrrolic cross-link?, Biosci. Rep., 1 (1981), 611-618.
[109] T. J. Koob, D. R. Eyre, K. P. Van Ness, Defection and photolysis of hydroxypyridinium cross-links in cartilage collagen in situ, Trans Ortho Res Soc, 8 (1983), 23-25.
[110] J. D. Brady, S. P. Robins, Structural characterization of pyrrolic cross-links in collagen using a biotinylated Ehrlich's reagent, J. Biol. Chem., 276 (2001), 18812-18818.
[111] D. A. Hanson, D. R. Eyre, Molecular site specificity of pyridinoline and pyrrole cross-links in type I collagen of human bone, J. Biol. Chem., 271 (1996), 26508-26516.
[112] D. Fujimoto, K. Akiba, N. Nakamura, Isolation and characterization of a fluorescent material in bovine achilles tendon collagen, Biochem. Biophys. Res. Commun., 76 (1977), 1124-1129.
[113] D. F. Elsden, N. D. Light, A. J. Bailey, An investigation of pyridinoline, a putative collagen cross-link, Biochem. J, 185 (1980), 531-534.
[114] S. Sakura, D. Fujimoto, Electrochemical Behaviour of Pyridinoline, a Crosslinking Amino Acid of Collagen, J. Biochem., 89 (1981), 1541-1546.
[115] T. Ogawa, T. Ono, M. Tsuda, Y. Kawanishi, A novel fluor in insoluble collagen: a crosslinking moiety in collagen molecule, Biochem. Biophys. Res. Commun., 107 (1982), 1252-1257.
[116] D. R. Eyre, H. Oguchi, The hydroxypyridinium crosslinks of skeletal collagens: their measurement, properties and a proposed pathway of formation, Biochem. Biophys. Res. Commun., 92 (1980), 403-410.
[117] S. Robins, A. Duncan, Cross-linking of collagen. Location of pyridinoline in bovine articular cartilage at two sites of the molecule, Biochem. J, 215 (1983), 175-182.
[118] N. Light, A. J. Bailey, Collagen cross-links: Location of pyridinoline in type I collagen, FEBS Lett., 182 (1985), 503-508.
[119] M. P. Cohen, Diabetes and Protein Glycosylation: Measurement and Biological Relevance, Springer Science & Business Media, New York, USA, (2002).
[120] W. G. John, E. J. Lamb, The Maillard or browning reaction in diabetes, Eye, 7 (1993), 230-237.
[121] R. Singh, A. Barden, T. Mori, L. Beilin, Advanced glycation end-products: a review, Diabetologia, 44 (2001), 129-146.
[122] N. Avery, A. J. Bailey, The effects of the Maillard reaction on the physical properties and cell interactions of collagen, Pathol. Biol., 54 (2006), 387-395.
[123] P. Gkogkolou, M. Böhm, Advanced glycation end products: Key players in skin aging?, Dermato-endocrinology, 4 (2012), 259-270.

[124] K. M. Biemel, O. Reihl, J. Conrad, M.O. Lederer, Formation pathways for lysine-arginine cross-links derived from hexoses and pentoses by maillard processes: unraveling the structure of a pentosidine precursor, J. Biol. Chem., 276 (2001), 23405-23412.
[125] D. R. Sell, V. M. Monnier, Structure elucidation of a senescence cross-link from human extracellular matrix. Implication of pentoses in the aging process, J. Biol. Chem., 264 (1989), 21597-21602.
[126] S. Robins, A. J. Bailey, Age-related changes in collagen: the identification of reducible lysine-carbohydrate condensation products, Biochem. Biophys. Res. Commun., 48 (1972), 76-84.
[127] D. R. Eyre, M. A. Weis, J.J. Wu, Maturation of collagen ketoimine cross-links by an alternative mechanism to pyridinoline formation in cartilage, J. Biol. Chem., 285 (2010), 16675-16682.
[128] J. Folk, J. Finlayson, The ε-(γ-glutamyl) lysine crosslink and the catalytic role of transglutaminases, Adv. Protein Chem., 31 (1977), 1-133.
[129] C. S. Greenberg, P. J. Birckbichler, R. H. Rice, Transglutaminases: multifunctional cross-linking enzymes that stabilize tissues, The FASEB Journal, 5 (1991), 3071-3077.
[130] M. W. Mosesson, Fibrinogen and fibrin structure and functions, J. Thromb. Haemost., 3 (2005), 1894-1904.
[131] R. N. Chen, H. O. Ho, M. T. Sheu, Characterization of collagen matrices crosslinked using microbial transglutaminase, Biomaterials, 26 (2005), 4229-4235.
[132] J. M. Orban, L. B. Wilson, J. A. Kofroth, M. S. El-Kurdi, T. M. Maul, D. A. Vorp, Crosslinking of collagen gels by transglutaminase, J. Biomed. Mater. Res. A, 68 (2004), 756-762.
[133] M. Yu, J. Hwang, T. J. Deming, Role of L-3, 4-dihydroxyphenylalanine in mussel adhesive proteins, JACS, 121 (1999), 5825-5826.
[134] J. H. Waite, M. L. Tanzer, Polyphenolic substance of Mytilus edulis: novel adhesive containing L-dopa and hydroxyproline, Science, 212 (1981), 1038-1040.
[135] J. H. Waite, X. X. Qin, K. J. Coyne, The peculiar collagens of mussel byssus, Matrix Biol., 17 (1998), 93-106.
[136] J. H. Waite, T. J. Housley, M. L. Tanzer, Peptide repeats in a mussel glue protein: theme and variations, Biochemistry, 24 (1985), 5010-5014.
[137] H. G. Silverman, F. F. Roberto, Understanding marine mussel adhesion, Mar. Biotechnol., 9 (2007), 661-681.
[138] S. O. Andersen, The cross-links in resilin identified as dityrosine and trityrosine, Biochimica et biophysica acta (BBA)-general subjects, 93 (1964), 213-215.
[139] D. Fujimoto, K. Horiuchi, M. Hirama, Isotrityrosine, a new crosslinking amino acid isolated from Ascaris cuticle collagen, Biochem. Biophys. Res. Commun., 99 (1981), 637-643.
[140] N. C. Avery, T. J. Sims, A. J. Bailey, Quantitative Determination of Collagen Cross-links, Extracellular Matrix Protocols, Springer, New York, USA, (2009), 103-121.
[141] K. von der Mark, Structure, Biosynthesis and Gene Regulation of Collagens in Cartilage and Bone, Academic Press, Massachusetts, USA, (1999).

[142] P. M. Gallop, O. O. Blumenfeld, S. Seifter, Structure and metabolism of connective tissue proteins, Annu. Rev. Biochem, 41 (1972), 617-672.
[143] J. H. Fessler, K. J. Doege, K. G. Duncan, L. I. Fessler, Biosynthesis of collagen, J. Cell. Biochem., 28 (1985), 31-37.
[144] C. A. Miles, N. C. Avery, V. V. Rodin, A. J. Bailey, The increase in denaturation temperature following cross-linking of collagen is caused by dehydration of the fibres, J. Mol. Biol., 346 (2005), 551-556.
[145] M. Diab, J. Wu, D. Eyre, Collagen type IX from human cartilage: a structural profile of intermolecular cross-linking sites, Biochem. J, 314 (1996), 327-332.
[146] D. R. Eyre, T. Pietka, M. A. Weis, J. J. Wu, Covalent cross-linking of the NC1 domain of collagen type IX to collagen type II in cartilage, J. Biol. Chem., 279 (2004), 2568-2574.
[147] W. Henkel, R. W. Glanville, Covalent crosslinking between molecules of type I and type III collagen, Eur. J. Biochem., 122 (1982), 205-213.
[148] A. J. Bailey, C. M. Lapière, Effect of an additional peptide extension of the N-terminus of collagen from dermatosparactic calves on the cross-linking of the collagen fibres, Eur. J. Biochem., 34 (1973), 91-96.
[149] C. M. Lapiere, B. Nusgens, G. Pierard, Interaction between collagen type I and type III in conditioning bundles organization, Connect. Tissue Res., 5 (1977), 21-29.
[150] R. Fleischmajer, J. Perlish, R. Burgeson, F. Shaikh-Bahai, R. Timpl, Type I and Type III Collagen Interactions during Fibrillogenesisa, Ann. N.Y. Acad. Sci., 580 (1990), 161-175.
[151] M. Barnes, B. Constable, L. Morton, P. Royce, Age-related variations in hydroxylation of lysine and proline in collagen, Biochem. J, 139 (1974), 461-468.
[152] J. J. Wu, P. E. Woods, D. R. Eyre, Identification of cross-linking sites in bovine cartilage type IX collagen reveals an antiparallel type II-type IX molecular relationship and type IX to type IX bonding, J. Biol. Chem., 267 (1992), 23007-23014.
[153] A. Mhaske, D. Raut, R. Singh, A. Mani, J. Patel, S. Quereshi, Extraction and partial characterization of collagen from different animal skins, Rec. Res. Sci. and Tech., 2 (2010), 28-31.
[154] A. J. Bailey, C. M. Peach, L. Fowler, Chemistry of the collagen cross-links. Isolation and characterization of two intermediate intermolecular cross-links in collagen, Biochem. J, 117 (1970), 819-831.
[155] A. J. Bailey, S. P. Robins, Embryonic skin collagen. Replacement of the type of aldimine crosslinks during the early growth period, FEBS Lett., 21 (1972), 330-334.
[156] G. L. Mechanic, E. P. Katz, M. Henmi, C. Noyes, M. Yamauchi, Locus of a histidine-based, stable trifunctional, helix to helix collagen cross-link: stereospecific collagen structure of type I skin fibrils, Biochemistry, 26 (1987), 3500-3509.
[157] R. H. Stinson, P. R. Sweeny, Skin collagen has an unusual d-spacing, BBA-Protein Structure, 621 (1980), 158-161.
[158] B. Brodsky, E. F. Eikenberry, K. Cassidy, An unusual collagen periodicity in skin, BBA-Protein Structure, 621 (1980), 162-166.
[159] P. H. Bernstein, G. Mechanic, A natural histidine-based imminium cross-link in collagen and its location, J. Biol. Chem., 255 (1980), 10414-10422.

[160] A. Veis, A. Perry, The Phosphoprotein of the dentin matrix, Biochemistry, 6 (1967), 2409-2416.
[161] L. J. Fowler, A. J. Bailey, Current concepts of the crosslinking in bone collagen, Clin. Orthop. Relat. Res., 85 (1972), 193-206.
[162] C. A. Miles, L. Knott, I. G. Sumner, A. J. Bailey, Differences between the thermal stabilities of the three triple-helical domains of type IX collagen, J. Mol. Biol., 277 (1998), 135-144.
[163] M. Takahashi, K. Kushida, H. Hoshino, M. Suzuki, M. Sano, S. Miyamoto, T. Inoue, Concentrations of pyridinoline and deoxypyridinoline in joint tissues from patients with osteoarthritis or rheumatoid arthritis, Ann. Rheum. Dis., 55 (1996), 324-327.
[164] T. J. Sims, A. J. Bailey, Quantitative analysis of collagen and elastin cross-links using a single-column system, J. Chromatogr. B: Biomed.Sci. App., 582 (1992), 49-55.
[165] M. Fountoulakis, H. W. Lahm, Hydrolysis and amino acid composition analysis of proteins, J. Chromatogr. A, 826 (1998), 109-134.
[166] W. Ames, The preparation of gelatin. Parts I-III, J. Soc. Chem. Ind., London, 63 (1944), 200.
[167] P. M. Gallop, S. Seifter, E. Meilman, Occurrence of Ester-Like Linkages in Collagen, Nature, 183 (1959), 1659-1661.
[168] K. H. Gustavson, The Chemistry and Reactivity of Collagen, Academic Press, NY, USA, (1956).
[169] S. Partridge, D. Elsden, J. Thomas, Constitution of the cross-linkages in elastin, Nature, (1963), 1297-1298.
[170] M. L. Tanzer, G. Mechanic, Isolation of lysinonorleucine from collagen, Biochem. Biophys. Res. Commun., 39 (1970), 183-189.
[171] P. M. Gallop, S. Seifter, Features of Primary Structure and Unusual Linkages in the Collagen Molecule, Collagen, (N. Ramanathan, editor), New York, Interscience Press Inc, (1962).
[172] O. O. Blumenfeld, P.M. Gallop, Amino aldehydes in tropocollagen: the nature of a probable cross-link, PNAS, 56 (1966), 1260-1267.
[173] M. Rojkind, O. O. Blumenfeld, P. M. Gallop, Localization and partial characterization of an aldehydic component in tropocollagen, J. Biol. Chem., 241 (1966), 1530-1536.
[174] A. J. Bailey, Intermediate labile intermolecular crosslinks in collagen fibres, BBA - Protein Structure, 160 (1968), 447-453.
[175] M. Rojkind, A. M. Gutierrez, M. Zeichner, R. W. Lent, The nature of the intramolecular cross-link in collagen, Biochem. Biophys. Res. Commun., 36 (1969), 350-356.
[176] S. J. M. Skinner, Rapid method for the purification of the elastin cross-links, desmosine and isodesmosine, J. Chromatogr. B: Biomed.Sci. App., 229 (1982), 200-204.
[177] B. C. Starcher, Determination of the elastin content of tissues by measuring desmosine and isodesmosine, Anal. Biochem., 79 (1977), 11-15.

[178] E. Gineyts, O. Borel, R. Chapurlat, P. Garnero, Quantification of immature and mature collagen crosslinks by liquid chromatography–electrospray ionization mass spectrometry in connective tissues, J. Chromatogr. B, 878 (2010), 1449-1454.
[179] F. Nakamura, K. Suyama, Silica gel high-performance liquid chromatography for the determination of cross-links in elastin, J. Chromatogr. Sci., 29 (1991), 217-220.
[180] F. Nakamura, K. Yamazaki, K. Suyama, Isolation and structural characterization of a new crosslinking amino acid, cyclopentenosine, from the acid hydrolysate of elastin, Biochem. Biophys. Res. Commun., 186 (1992), 1533-1538.
[181] M. Saito, K. Marumo, K. Fujii, N. Ishioka, Single-column high-performance liquid chromatographic–fluorescence detection of immature, mature, and senescent cross-Links of collagen, Anal. Biochem., 253 (1997), 26-32.
[182] D. Black, A. Duncan, S.P. Robins, Quantitative analysis of the pyridinium crosslinks of collagen in urine using ion-paired reversed-phase high-performance liquid chromatography, Anal. Biochem., 169 (1988), 197-203.
[183] W. R. Cumiskey, E. D. Pagani, D. C. Bode, Enrichment and analysis of desmosine and isodesmosine in biological fluids, J. Chromatogr. B: Biomed.Sci. App., 668 (1995), 199-207.
[184] C. P. Winlove, K. H. Parker, N. C. Avery, A. J. Bailey, Interactions of elastin and aorta with sugars in vitro and their effects on biochemical and physical properties, Diabetologia, 39 (1996), 1131-1139.
[185] D. A. Pratt, Y. Daniloff, A. Duncan, S. P. Robins, Automated analysis of the pyridinium crosslinks of collagen in tissue and urine using solid-phase extraction and reversed-phase high-performance liquid chromatography, Anal. Biochem., 207 (1992), 168-175.
[186] M. Takahashi, T. Ohishi, H. Aoshima, K. Kushida, T. Inoue, K. Horiuchi, Pre-fractionation with cation exchanger for determination of intermolecular crosslinks, pyridinoline, and pentosidine, in hydrolysate, J. Liq. Chromatogr. Rel. Technol., 16 (1993), 1355-1370.
[187] T. J. Sims, N. C. Avery, A. J. Bailey, Quantitative determination of collagen crosslinks, Extracellular Matrix Protocols, 139 (2000), 11-26.
[188] S. P. Robins, M. Shimokomaki, A. J. Bailey, The chemistry of the collagen cross-links. Age-related changes in the reducible components of intact bovine collagen fibres, Biochem. J, 131 (1973), 771-780.
[189] E. Kindt, D. T. Rossi, K. Gueneva-Boucheva, H. Hallak, Quantitative method for biomarkers of collagen degradation using liquid chromatography tandem mass spectrometry, Anal. Biochem., 283 (2000), 71-76.
[190] G. E. Sroga, D. Vashishth, UPLC methodology for identification and quantitation of naturally fluorescent crosslinks in proteins: A study of bone collagen, J. Chromatogr. B, 879 (2011), 379-385.
[191] S. Ma, G. M. Turino, Y. Y. Lin, Quantitation of desmosine and isodesmosine in urine, plasma, and sputum by LC–MS/MS as biomarkers for elastin degradation, J. Chromatogr. B, 879 (2011), 1893-1898.
[192] J. R. Chen, M. Takahashi, K. Kushida, M. Suzuki, K. Suzuki, K. Horiuchi, A. Nagano, Direct detection of crosslinks of collagen and elastin in the hydrolysates of human

yellow ligament using single-column high performance liquid chromatography, Anal. Biochem., 278 (2000), 99-105.
[193] S. Viguet-Carrin, E. Gineyts, C. Bertholon, P. D. Delmas, Simple and sensitive method for quantification of fluorescent enzymatic mature and senescent crosslinks of collagen in bone hydrolysate using single-column high performance liquid chromatography, J. Chromatogr. B, 877 (2009), 1-7.
[194] B. Valeur, M. N. Berberan-Santos, Molecular Fluorescence: Principles and Applications, 2nd ed., John Wiley & Sons, Weinheim, Germany, (2012).
[195] E. Paschalis, K. Verdelis, S. Doty, A. Boskey, R. Mendelsohn, M. Yamauchi, Spectroscopic characterization of collagen cross-Links in bone, J. Bone Miner. Res., 16 (2001), 1821-1828.
[196] B. B. Doyle, E. Bendit, E. R. Blout, Infrared spectroscopy of collagen and collagen-like polypeptides, Biopolymers, 14 (1975), 937-957.
[197] Y. A. Lazarev, B. Grishkovsky, T. Khromova, Amide I band of IR spectrum and structure of collagen and related polypeptides, Biopolymers, 24 (1985), 1449-1478.
[198] B. de Campos Vidal, M. L. S. Mello, Collagen type I amide I band infrared spectroscopy, Micron, 42 (2011), 283-289.
[199] L. Debelle, A. Tamburro, Elastin: molecular description and function, Int. J. Biochem. Cell Biol., 31 (1999), 261-272.
[200] J. Rosenbloom, W. Abrams, R. Mecham, Extracellular matrix 4: the elastic fibre, The FASEB Journal, 7 (1993), 1208-1218.
[201] B. Starcher, R. L. Aycock, C. H. Hill, Multiple roles for elastic fibres in the skin, J. Histochem. Cytochem., 53 (2005), 431-443.
[202] J. A. Foster, E. Bruenger, W. R. Gray, L. B. Sandberg, Isolation and amino acid sequences of tropoelastin peptides, J. Biol. Chem., 248 (1973), 2876-2879.
[203] J.G. Bieth, Elastases: Catalytic and Biological Properties, in: R.P. Mecham (Ed.) Regulation of Matrix Accumalation, Academic Press, London, UK, (1986).
[204] D. Wender, L. Treiber, H. Bensusan, A. Walton, Synthesis and characterization of poly (LysAla3), Biopolymers, 13 (1974), 1929-1941.
[205] W. Gray, Molecular model for elastin structure and function, Nature, 246 (1973), 461-466.
[206] W. Gray, Some Kinetic Aspects of Crosslink Biosynthesis, in: W.R. Gray, C. Franzblau (Eds.) Elastin and Elastic Tissue, Springer (1977), 285-290.
[207] A. Tamburro, B. Bochicchio, A. Pepe, The dissection of human tropoelastin: from the molecular structure to the self-assembly to the elasticity mechanism, Pathol. Biol., 53 (2005), 383-389.
[208] F. Antonicelli, G. Bellon, L. Debelle, W. Hornebeck, Elastin-Elastases and Inflamm-Aging, Curr. Top. Dev. Biol., 79 (2007), 99-155.
[209] B. Alberts, D. Bray, K. Hopkin, A. Johnson, J. Lewis, M. Raff, K. Roberts, P. Walter, Essential Cell Biology, 4th ed., Garland Science, New York, USA, (2013).
[210] S. G. Wise, S. M. Mithieux, M. J. Raftery, A. S. Weiss, Specificity in the coacervation of tropoelastin: solvent exposed lysines, J. Struct. Biol., 149 (2005), 273-281.

[211] T. J. Broekelmann, B. A. Kozel, H. Ishibashi, C. C. Werneck, F. W. Keeley, L. Zhang, R. P. Mecham, Tropoelastin interacts with cell-surface glycosaminoglycans via its COOH-terminal domain, J. Biol. Chem., 280 (2005), 40939-40947.
[212] B. Vrhovski, S. Jensen, A.S. Weiss, Coacervation characteristics of recombinant human tropoelastin, Eur. J. Biochem., 250 (1997), 92-98.
[213] C. Franzblau, B. Faris, R. W. Lent, L. L. Salcedo, B. Smith, R. Jaffe, and G. Crombie. Chemistry and biosynthesis of crosslinks in elastin, Chemistry and molecular biology of the intracellular matrix 1, (1970): 617-639.
[214] A. Czirok, J. Zach, B. A. Kozel, R. P. Mecham, E. C. Davis, B. J. Rongish, Elastic fibre macro-assembly is a hierarchical, cell motion-mediated process, J. Cell. Physiol., 207 (2006), 97-106.
[215] M. Akagawa, K. Suyama, Mechanism of formation of elastin crosslinks, Connect. Tissue Res., 41 (2000), 131-141.
[216] S. Partridge, D. Elsden, J. Thomas, A. Dorfman, A. Telser, P. L. Ho, Biosynthesis of the desmosine and isodesmosine cross-bridges in elastin, Biochem. J., 93 (1964), 30C-33C.
[217] K. A. Piez, Cross-linking of collagen and elastin, Annu. Rev. Biochem, 37 (1968), 547-570.
[218] M. A. Paz, E. Henson, O. O. Blumenfeld, S. Seifter, P. M. Gallop, Dehydromerodesmosine and merodesmosine in elastin, Biochem. Biophys. Res. Commun., 44 (1971), 1518-1523.
[219] S. G. Wise, A. S. Weiss, Tropoelastin, Int. J. Biochem. Cell Biol., 41 (2009) 494-497.
[220] S. Shapiro, S. Endicott, M. Province, J. Pierce, E. Campbell, Marked longevity of human lung parenchymal elastic fibres deduced from prevalence of D-aspartate and nuclear weapons-related radiocarbon, J. Clin. Invest., 87 (1991), 1828-1834.
[221] B. C. Starcher, Elastin and the lung, Thorax, 41 (1986), 577-585.
[222] R. B. Rucker, M. A. Dubick, Elastin metabolism and chemistry: potential roles in lung development and structure, Environ. Health Perspect., 55 (1984), 179-191.
[223] O. H. Lowry, D. R. Gilligan, E. M. Katersky, The determination of collagen and elastin in tissues, with results obtained in various normal tissues from different species, J. Biol. Chem., 139 (1941), 795-804.
[224] V. D. Hospelhorn, M. J. FitzPatrick, The isolation of elastic tissue from lung, Biochem. Biophys. Res. Commun., 6 (1961), 191-195.
[225] R. P. Mecham, Methods in elastic tissue biology: Elastin isolation and purification, Methods, 45 (2008), 32-41.
[226] N. Kaga, S. Soma, T. Fujimura, K. Seyama, Y. Fukuchi, K. Murayama, Quantification of elastin cross-linking amino acids, desmosine and isodesmosine, in hydrolysates of rat lung by ion-pair liquid chromatography–mass spectrometry, Anal. Biochem., 318 (2003), 25-29.
[227] N. A. Devenport, J. C. Reynolds, V. Parkash, J. Cook, D. J. Weston, C. S. Creaser, Determination of free desmosine and isodesmosine as urinary biomarkers of lung disorder using ultra performance liquid chromatography–ion mobility-mass spectrometry, J. Chromatogr. B, 879 (2011), 3797-3801.

[228] N. T. Soskel, High-performance liquid chromatographic quantitation of desmosine plus isodesmosine in elastin and whole tissue hydrolysates, Anal. Biochem., 160 (1987), 98-104.
[229] P. Laurent, L. Magne, J. De Palmas, J. Bignon, M. C. Jaurand, Quantitation of elastin in human urine and rat pleural mesothelial cell matrix by a sensitive avidin-biotin ELISA for desmosine, J. Immunol. Methods, 107 (1988), 1-11.
[230] Y. Yamaguchi, J. Haginaka, M. Kunitomo, H. Yasuda, Y. Bandô, High-performance liquid chromatographic determination of desmosine and isodesmosine in tissues and its application to studies of alteration of elastin induced by atherosclerosis, J. Chromatogr. B: Biomed.Sci. App., 422 (1987), 53-59.
[231] S. D. Choudhury, T. Allsop, A. Passman, G. Norris, Use of a proteomics approach to identify favourable conditions for production of good quality lambskin leather, Anal. Bioanal. Chem., 384 (2006), 723-735.
[232] J. D. San Antonio, R. V. Iozzo, Glycosaminoglycans: structure and biological functions, eLS, (2001), 1-8.
[233] L. Schaefer, R. M. Schaefer, Proteoglycans: from structural compounds to signaling molecules, Cell Tissue Res., 339 (2010), 237-246.
[234] A. J. Fosang, T. E. Hardingham, Matrix Proteoglycans, in: W.D. Comper (Ed.) Extracellular Matrix, Harwood Academic, Amsterdam, The Netherlands, (1996), 200-230.
[235] M. J. Seibel, S. P. Robins, J. P. Bilezikian, Dynamics of Bone and Cartilage Metabolism: Principles and Clinical Applications, Academic Press, Massachusetts, USA, (2006).
[236] D. P. Gamblin, E. M. Scanlan, B. G. Davis, Glycoprotein synthesis: an update, Chem. Rev., 109 (2008), 131-163.
[237] L. A. Goldsmith, Biochemistry and Physiology of the Skin: Volumes I and II, Oxford University Press, New York, USA, (1983).
[238] M. H. Flint, A. S. Craig, H. C. Reilly, G. C. Gillard, D. A. D. Parry, Collagen fibril diameters and glycosaminoglycan content of skins-indices of tissue maturity and function, Connect. Tissue Res., 13 (1984), 69-81.
[239] B. ÖBrink, The influence of glycosaminoglycans on the formation of fibres from monomeric tropocollagen in vitro, Eur. J. Biochem., 34 (1973), 129-137.
[240] G. D. Pins, D. L. Christiansen, R. Patel, F. H. Silver, Self-assembly of collagen fibres. Influence of fibrillar alignment and decorin on mechanical properties, Biophys. J., 73 (1997), 2164-2172.
[241] U. F. Gruber, Dextran and the prevention of postoperative thromboembolic complications, Surgical Clinics of North America, (1975), 679-696.
[242] J. Shatton, M. Schubert, Isolation of a mucoprotein from cartilage, J. Biol. Chem., 211 (1954), 565-573.
[243] W. D. Comper, Extracellular Matrix Vol (1): Tissue Function, CRC Press, London, UK, (1996).
[244] N. S. Gandhi, R. L. Mancera, The structure of glycosaminoglycans and their interactions with proteins, Chem. Biol. Drug Des., 72 (2008), 455-482.

[245] N. Volpi, Disaccharide mapping of chondroitin sulfate of different origins by high-performance capillary electrophoresis and high-performance liquid chromatography, Carbohydr. Polym., 55 (2004), 273-281.
[246] O. Habuchi, Diversity and functions of glycosaminoglycan sulfotransferases, BBA - General Subjects, 1474 (2000), 115-127.
[247] J. L. van Susante, J. Pieper, P. Buma, T. H. van Kuppevelt, H. van Beuningen, P. M. van der Kraan, J. H. Veerkamp, W. B. van den Berg, R. P. Veth, Linkage of chondroitin-sulfate to type I collagen scaffolds stimulates the bioactivity of seeded chondrocytes in vitro, Biomaterials, 22 (2001), 2359-2369.
[248] C. M. Tierney, M. G. Haugh, J. Liedl, F. Mulcahy, B. Hayes, F. J. O'Brien, The effects of collagen concentration and crosslink density on the biological, structural and mechanical properties of collagen-GAG scaffolds for bone tissue engineering, J. Mech. Behav. Biomed. Mater., 2 (2009), 202-209.
[249] R. Reed, K. Lilja, T. Laurent, Hyaluronan in the rat with special reference to the skin, Acta Physiol. Scand., 134 (1988), 405-411.
[250] B. B. Werth, M. Bashir, L. Chang, V. P. Werth, Ultraviolet irradiation induces the accumulation of chondroitin sulfate, but not other glycosaminoglycans, in human skin, PloS one, 6 (2011), e14830.
[251] J. M. Trowbridge, R. L. Gallo, Dermatan sulfate: new functions from an old glycosaminoglycan, Glycobiology, 12 (2002), 117R-125R.
[252] D. Rabenstein, Heparin and heparan sulfate: structure and function, Nat. Prod. Rep., 19 (2002), 312-331.
[253] M. Bernfield, M. Götte, P. W. Park, O. Reizes, M. L. Fitzgerald, J. Lincecum, M. Zako, Functions of cell surface heparan sulfate proteoglycans, Annu. Rev. Biochem, 68 (1999), 729-777.
[254] P. Gavriel, H. M. Kagan, Inhibition by heparin of the oxidation of lysine in collagen by lysyl oxidase, Biochemistry, 27 (1988), 2811-2815.
[255] N. Parthasarathy, I. J. Goldberg, P. Sivaram, B. Mulloy, D. M. Flory, W. D. Wagner, Oligosaccharide sequences of endothelial cell surface heparan sulfate proteoglycan with affinity for lipoprotein lipase, J. Biol. Chem., 269 (1994), 22391-22396.
[256] S. Chakravarti, T. Magnuson, J. H. Lass, K. J. Jepsen, C. LaMantia, H. Carroll, Lumican regulates collagen fibril assembly: skin fragility and corneal opacity in the absence of lumican, J. Cell Biol., 141 (1998), 1277-1286.
[257] T. Hardingham, A. Fosang, Proteoglycans: many forms and many functions, The FASEB Journal, 6 (1992), 861-870.
[258] T. C. Laurent, U. Laurent, J. Fraser, Functions of hyaluronan, Ann. Rheum. Dis., 54 (1995), 429-432.
[259] J. Necas, L. Bartosikova, P. Brauner, J. Kolar, Hyaluronic acid (hyaluronan): a review, Vet. Med., 53 (2008), 397-411.
[260] L. J. Meyer, R. Stern, Age-dependent changes of hyaluronan in human skin, J. Invest. Dermatol., 102 (1994), 385-389.
[261] E. Papakonstantinou, M. Roth, G. Karakiulakis, Hyaluronic acid: a key molecule in skin aging, Dermato-endocrinology, 4 (2012), 253-258.

[262] S. N. Park, J. C. Park, H. O. Kim, M. J. Song, H. Suh, Characterization of porous collagen/hyaluronic acid scaffold modified by 1-ethyl-3-(3-dimethylaminopropyl)carbodiimide cross-linking, Biomaterials, 23 (2002), 1205-1212.
[263] M. Reháková, D. Bakoš, K. Vizárová, M. Soldán, M. Juríc˘ková, Properties of collagen and hyaluronic acid composite materials and their modification by chemical crosslinking, J. Biomed. Mater. Res., 30 (1996), 369-372.
[264] W. Manuskiatti, H.I. Maibach, Hyaluronic acid and skin: wound healing and aging, Int. J. Dermatol., 35 (1996), 539-544.
[265] I. Ghersetich, T. Lotti, G. Campanile, C. Grappone, G. Dini, Hyaluronic acid in cutaneous intrinsic aging, Int. J. Dermatol., 33 (1994), 119-122.
[266] K. B. Lee, D. Loganathan, Z. M. Merchant, R. Linhardt, Carbohydrate analysis of glycoproteins A review, Appl. Biochem. Biotechnol., 23 (1990), 53-80.
[267] J. Stepper, S. Shastri, T. S. Loo, J. C. Preston, P. Novak, P. Man, C.H. Moore, V. Havlíček, M.L. Patchett, G.E. Norris, Cysteine S-glycosylation, a new post-translational modification found in glycopeptide bacteriocins, FEBS Lett., 585 (2011), 645-650.
[268] R. Kornfeld, S. Kornfeld, Structure of Glycoproteins and Their Oligosaccharide Units, in: J.L. William (Ed.) The Biochemistry of Glycoproteins and Proteoglycans, Springer, New Jersey, USA, (1980), 1-34.
[269] J. T. Gallagher, The extended family of proteoglycans: social residents of the pericellular zone, Curr. Opin. Cell Biol., 1 (1989), 1201-1218.
[270] T. R. Oegema, J. Laidlaw, V. C. Hascall, D. D. Dziewiatkowski, The effect of proteoglycans on the formation of fibrils from collagen solutions, Arch. Biochem. Biophys., 170 (1954), 698-709.
[271] D. R. Stamov, A. Müller, Y. Wegrowski, S. Brezillon, C.M. Franz, Quantitative analysis of type I collagen fibril regulation by lumican and decorin using AFM, J. Struct. Biol., 183 (2013), 394-403.
[272] Y. Li, Y. Liu, W. Xia, D. Lei, J.J. Voorhees, G.J. Fisher, Age-dependent alterations of decorin glycosaminoglycans in human skin, Sci. Rep., 3 (2013), 1-8.
[273] C. Malavaki, S. Mizumoto, N. Karamanos, K. Sugahara, Recent advances in the structural study of functional chondroitin sulfate and dermatan sulfate in health and disease, Connect. Tissue Res., 49 (2008), 133-139.
[274] K. G. Danielson, H. Baribault, D. F. Holmes, H. Graham, K. E. Kadler, R. V. Iozzo, Targeted disruption of decorin leads to abnormal collagen fibril morphology and skin fragility, J. Cell Biol., 136 (1997), 729-743.
[275] P. G. Scott, P. A. McEwan, C. M. Dodd, E. M. Bergmann, P. N. Bishop, J. Bella, Crystal structure of the dimeric protein core of decorin, the archetypal small leucine-rich repeat proteoglycan, PNAS, 101 (2004), 15633-15638.
[276] S. P. Henry, M. Takanosu, T. C. Boyd, P. M. Mayne, H. Eberspaecher, W. Zhou, B. De Crombrugghe, M. Höök, R. Mayne, Expression pattern and gene characterization of asporin: A newly discovered member of the leucine-rich repeat protein family, J. Biol. Chem., 276 (2001), 12212-12221.
[277] C. C. Reed, R. V. Iozzo, The role of decorin in collagen fibrillogenesis and skin homeostasis, Glycoconjugate J., 19 (2002), 249-255.

[278] J. M. Sorrell, A. I. Caplan, Fibroblast heterogeneity: more than skin deep, J. Cell Sci., 117 (2004), 667-675.
[279] C. T. Thorpe, H. L. Birch, P. D. Clegg, H. R. Screen, The role of the non-collagenous matrix in tendon function, Int. J. Exp. Pathol., 94 (2013), 248-259.
[280] Y. Nomura, Structural change in decorin with skin aging, Connect. Tissue Res., 47 (2006), 249-255.
[281] P. Neame, H. Choi, L. Rosenberg, The primary structure of the core protein of the small, leucine-rich proteoglycan (PG I) from bovine articular cartilage, J. Biol. Chem., 264 (1989), 8653-8661.
[282] D. R. Keene, J. D. San Antonio, R. Mayne, D. J. McQuillan, G. Sarris, S. A. Santoro, R. V. Iozzo, Decorin binds near the C terminus of type I collagen, J. Biol. Chem., 275 (2000), 21801-21804.
[283] R. J. McCormick, Extracellular modifications to muscle collagen: implications for meat quality, Poultry Science, 78 (1999), 785-791.
[284] D. A. Carrino, J. M. Sorrell, A. I. Caplan, Age-related Changes in the proteoglycans of human skin, Arch. Biochem. Biophys., 373 (2000), 91-101.
[285] R. Fleischmajer, L. W. Fisher, E. D. MacDonald, L. Jacobs, J.S. Perlish, J. D. Termine, Decorin interacts with fibrillar collagen of embryonic and adult human skin, J. Struct. Biol., 106 (1991), 82-90.
[286] S. Rigozzi, R. Müller, A. Stemmer, J. Snedeker, Tendon glycosaminoglycan proteoglycan sidechains promote collagen fibril sliding—AFM observations at the nanoscale, J. Biomech., 46 (2013), 813-818.
[287] R. Fleischmajer, L.W. Fisher, E.D. MacDonald, L. Jacobs Jr, J.S. Perlish, J.D. Termine, Decorin interacts with fibrillar collagen of embryonic and adult human skin, J. Struct. Biol., 106 (1991), 82-90.
[288] L. Svensson, D. Heineg, Decorin-binding sites for collagen type I are mainly located in leucine-rich repeats 4-5, J. Biol. Chem., 270 (1995), 20712-20716.
[289] C. Wiberg, E. Hedbom, A. Khairullina, S. R. Lamandé, Å. Oldberg, R. Timpl, M. Mörgelin, D. Heinegård, Biglycan and decorin bind close to the n-terminal region of the collagen VI triple helix, J. Biol. Chem., 276 (2001), 18947-18952.
[290] P. M. Royce, B. Steinmann, Connective Tissue and Its Heritable Disorders: Molecular, Genetic, and Medical Aspects, John Wiley & Sons, NJ, USA, (2003).
[291] S. Chakravarti, R. L. Stallings, N. SundarRaj, P.K. Cornuet, J.R. Hassell, Primary structure of human lumican (keratan sulfate proteoglycan) and localization of the gene (LUM) to chromosome 12q21.3-q22, Genomics, 27 (1995), 481-488.
[292] J. R. Dunlevy, P. J. Neame, J. P. Vergnes, J. R. Hassell, Identification of the N-linked oligosaccharide sites in chick corneal lumican and keratocan that receive keratan sulfate, J. Biol. Chem., 273 (1998), 9615-9621.
[293] J. M. Sorrell, D. A. Carrino, M. A. Baber, A. I. Caplan, Versican in human fetal skin development, Anat. Embryol., 199 (1999), 45-56.
[294] H. P. Erickson, V. A. Lightner, Hexabrachion protein (tenascin, cytotactin, brachionectin) in connective tissues, embryonic brain, and tumors, Adv. Mol. Cell Biol., 2 (1988), 55-90.

[295] H. P. Erickson, Tenascin-C, tenascin-R and tenascin-X: a family of talented proteins in search of functions, Curr. Opin. Cell Biol., 5 (1993), 869-876.
[296] D. R. Zimmermann, E. Ruoslahti, Multiple domains of the large fibroblast proteoglycan, versican, The EMBO journal, 8 (1989), 2975.
[297] M. Yamagata, K. Yamada, M. Yoneda, S. Suzuki, K. Kimata, Chondroitin sulfate proteoglycan (PG-M-like proteoglycan) is involved in the binding of hyaluronic acid to cellular fibronectin, J. Biol. Chem., 261 (1986), 13526-13535.
[298] T. N. Wight, Versican: a versatile extracellular matrix proteoglycan in cell biology, Curr. Opin. Cell Biol., 14 (2002), 617-623.
[299] B. Bode-Lesniewska, M. T. Dours-Zimmermann, B. F. Odermatt, J. Briner, P. U. Heitz, D. R. Zimmermann, Distribution of the large aggregating proteoglycan versican in adult human tissues, J. Histochem. Cytochem., 44 (1996), 303-312.
[300] E. F. Bernstein, L. W. Fisher, K. Li, R. G. LeBaron, E. Tan, J. Uitto, Differential expression of the versican and decorin genes in photoaged and sun-protected skin. Comparison by immunohistochemical and northern analyses, Laboratory investigation; J. Tech. Meth. Pathol., 72 (1995), 662-669.
[301] V. A. Lightner, F. Gumkowski, D. D. Bigner, H. P. Erickson, Tenascin/hexabrachion in human skin: biochemical identification and localization by light and electron microscopy, J. Cell Biol., 108 (1989), 2483-2493.
[302] E. Aufderheide, R. Chiquet-Ehrismann, P. Ekblom, Epithelial-mesenchymal interactions in the developing kidney lead to expression of tenascin in the mesenchyme, J. Cell Biol., 105 (1987), 599-608.
[303] V. Lightner, C. Slemp, H. Erickson, Localization and quantitation of hexabrachion (tenascin) in skin, embryonic brain, tumors, and plasma, Ann. N.Y. Acad. Sci., 580 (1990), 260-275.
[304] S. Rees, C. Dent, B. Caterson, Metabolism of proteoglycans in tendon, Scand. J. Med. Sci. Sports, 19 (2009), 470-478.
[305] J. H. Yoon, J. Halper, Tendon proteoglycans: biochemistry and function, J Musculoskelet. Neuronal. Interact., 5 (2005), 22-34.
[306] T. Nikkari, Comparative chemistry of sebum, J. Invest. Dermatol., 62 (1974), 257-267.
[307] V. A. Ziboh, R. S. Chapkin, Metabolism and function of skin lipids, Prog. Lipid Res., 27 (1988), 81-105.
[308] P. M. Elias, Advances in Lipid Research: Skin Lipids, Elsevier, Amsterdam, The Netherland, 2016.
[309] D. R. Drake, K. A. Brogden, D. V. Dawson, P. W. Wertz, Thematic review series: skin lipids. Antimicrobial lipids at the skin surface, J. Lipid Res., 49 (2008), 4-11.
[310] K. Uchimura, Keratan Sulfate: Biosynthesis, Structures, and Biological Functions, in: H. Nakato, U.R. Desai (Eds.) Glycosaminoglycans, Springer, New Jersey, USA, (2015), 389-400.
[311] K. Ohsawa, T. Watanabe, R. Matsukawa, Y. Yoshimura, K. Imaeda, The possible role of squalene and its peroxide of the sebum in the occurrence of sunburn and protection from the damage caused by UV irradiation, J. Toxicol. Sci., 9 (1984), 151-159.

[312] J. S. Lindholm, J. M. McCormick, S. W. Colton Vi, D. T. Downing, Variation of skin surface lipid composition among mammals, Comparative Biochemistry and Physiology Part B: Comparative Biochemistry, 69 (1981), 75-78.
[313] D. T. Downing, J. S. Lindholm, Skin surface lipids of the cow, Comparative Biochemistry and Physiology Part B: Comparative Biochemistry, 73 (1982), 327-330.
[314] M. E. Stewart, D. T. Downing, Chemistry and function of mammalian sebaceous lipids, Skin Lipids: Adv. Lipid Res., 24 (1991), 263-302.
[315] N. Nicolaides, H. C. Fu, G. R. Rice, The Skin surface lipids of man compared with those of eighteen species of animals, J. Invest. Dermatol., 51 (1968), 83-89.
[316] W. W. Christie, The composition, structure and function of lipids in the tissues of ruminant animals, Prog. Lipid Res., 17 (1978), 111-205.
[317] A. M. Del Pozo, M. Oñaderra, J. Laynez, J. G. Gavilanes, Interaction of type I collagen fibrils with phospholipid vesicles, Matrix, 9 (1989), 405-410.
[318] M. Ghannam, M. M. Mady, W. Khalil, Interaction of type-I collagen with phospholipid monolayer, Biophys. Chem., 80 (1999), 31-40.
[319] M. M. Mady, Biophysical studies on collagen-lipid interaction, J. Biosci. Bioeng., 104 (2007), 144-148.
[320] M. Pajean, A. Huc, D. Herbage, Stabilization of liposomes with collagen, Int. J. Pharm., 77 (1991), 31-40.
[321] B. E. Warren, X-ray Diffraction, Dover Publications, New York, USA, (1990).
[322] L. Feigin, D. Svergun, Structure Analysis by Small-Angle X-ray and Neutron Scattering, Plenum Press, New York, USA, (1987).
[323] O. Glatter, O. Kratky, Small-Angle X-ray Scattering, Academic Press, London, UK, (1982).
[324] D. J. S. Hulmes, A. Miller, S. W. White, B. B. Doyle, Interpretation of the meridional X-ray diffraction pattern from collagen fibres in terms of the known amino acid sequence, J. Mol. Biol., 110 (1977), 643-666.
[325] D. A. D. Parry, G. R. G. Barnes, A. S. Craig, A comparison of the size distribution of collagen fibrils in connective tissues as a function of age and a possible relation between fibril size distribution and mechanical properties, Proceedings of the Royal Society of London. Series B. Biological Sciences, 203 (1978), 305-321.
[326] N. Sasaki, S. Odajima, Elongation mechanism of collagen fibrils and force-strain relations of tendon at each level of structural hierarchy, J. Biomech., 29 (1996), 1131-1136.
[327] S. Skou, R. E. Gillilan, N. Ando, Synchrotron-based small-angle X-ray scattering of proteins in solution, Nat. Protocols, 9 (2014), 1727-1739.
[328] C. Giannini, D. Siliqi, M. Ladisa, D. Altamura, A. Diaz, A. Beraudi, T. Sibillano, L. De Caro, S. Stea, F. Baruffaldi, Scanning SAXS–WAXS microscopy on osteoarthritis-affected bone–an age-related study, J. Appl. Crystallogr., 47 (2014), 110-117.
[329] K. L. Goh, J. Hiller, J. L. Haston, D. F. Holmes, K. E. Kadler, A. Murdoch, J. R. Meakin, T. J. Wess, Analysis of collagen fibril diameter distribution in connective tissues using small-angle X-ray scattering, BBA - General Subjects, 1722 (2005), 183-188.

[330] P. L. Kronick, M. S. Sacks, Quantification of vertical-fibre defect in cattle hide by small-angle light scattering, Connect. Tissue Res., 27 (1991), 1-13.
[331] J. Kinney, J. Pople, G. Marshall, S. Marshall, Collagen orientation and crystallite size in human dentin: a small angle X-ray scattering study, Calcif. Tissue Int., 69 (2001), 31-37.
[332] M. S. Sacks, D. B. Smith, E. D. Hiester, A small angle light scattering device for planar connective tissue microstructural analysis, Ann. Biomed. Eng., 25 (1997), 678-689.
[333] S. L. Hilbert, V. J. Ferrans, W. M. Swanson, Optical methods for the nondestructive evaluation of collagen morphology in bioprosthetic heart valves, J. Biomed. Mater. Res., 20 (1986), 1411-1421.
[334] W. Yang, V. Sherman, B. Gludovatz, E. Schaible, P. Stewart, R. Ritchie, M. Meyers, On the tear resistance of skin, Nat. Comm., 6 (2015), 1-10.
[335] W. Claffey, Interpretation of the small-angle X-ray diffraction of collagen in view of the primary structure of the alpha1 chain, Biophys. J., 19 (1977), 63-70.
[336] H. Suhonen, M. Fernández, R. Serimaa, P. Suortti, Simulation of small-angle X-ray scattering from collagen fibrils and comparison with experimental patterns, Phys. Med. Biol., 50 (2005), 5401-5416.
[337] W. H. Bragg, W. L. Bragg, The reflection of X-rays by crystals, Proc. Royal Soc. A., 88 (1913), 428-438.
[338] P. Kronick, M. Sacks, Matrix macromolecules that affect the viscoelasticity of calfskin, J. Biomech. Eng., 116 (1994), 140-145.
[339] M. M. Basil-Jones, R. L. Edmonds, S. M. Cooper, N. Kirby, A. Hawley, R. G. Haverkamp, Collagen fibril orientation and tear strength across ovine skins, J. Agric. Food. Chem., 61 (2013), 12327-12332.
[340] H. C. Wells, K. H. Sizeland, N. Kirby, A. Hawley, S. Mudie, R. G. Haverkamp, Collagen fibril structure and strength in acellular dermal matrix materials of bovine, porcine, and human origin, ACS Biomater. Sci. Eng., 1 (2015), 1026-1038.
[341] S. Tomlin, C. Worthington, Low-angle X-ray diffraction patterns of collagen, Proc. Royal Soc. A., 235 (1956), 189-201.
[342] T. Bitter, H. M. Muir, A modified uronic acid carbazole reaction, Anal. Biochem., 4 (1962), 330-334.
[343] T. Masuko, A. Minami, N. Iwasaki, T. Majima, S.-I. Nishimura, Y. C. Lee, Carbohydrate analysis by a phenol–sulfuric acid method in microplate format, Anal. Biochem., 339 (2005), 69-72.
[344] M. Cesaretti, E. Luppi, F. Maccari, N. Volpi, A 96-well assay for uronic acid carbazole reaction, Carbohydr. Polym., 54 (2003), 59-61.
[345] M. Wodzicka, Studies on the thickness and chemical composition of the skin of sheep: Development techniques, N. Z. J. Agric. Res., 1 (1958), 582-591.
[346] J. M. V. Williams, IULTCS (IUP) test methods-measurement of tear load-double edge tear, J. Soc. Leather Technol. Chem., 84 (2000), 327-329.
[347] P. Millington, R. Wilkinson, Skin. Biological Structure and Function, Cambridge University Press, Cambridge, UK, (1983).

[348] P. Muthiah, N. Ramanathan, Y. Nayudamma, Mechanical properties of skins, hides and constituent fibres, Biorheology, 4 (1967), 185-191.
[349] D. Bailey, M. Birbir, The impact of halophilic organisms on the grain quality of brine cured hides, JALCA, (1996), 47-51.
[350] A. Orlita, Microbial biodeterioration of leather and its control: a review, Int. Biodeterior. Biodegrad., 53 (2004), 157-163.
[351] H. Abasher, Effect of aerobic bacteria on hides and skins and leather quality, MSc. thesis, University of Khartoum, 2015.
[352] D. O'leary, G. Attenburrow, Differences in strength between the grain and corium layers of leather, J. Mater. Sci., 31 (1996), 5677-5682.
[353] A. Finch, D. Ledward, Shrinkage of collagen fibres: A differential scanning calorimetric study, BBA-Protein Structure, 278 (1972), 433-439.
[354] W. K. Loke, E. Khor, Validation of the shrinkage temperature of animal tissue for bioprosthetic heart valve application by differential scanning calorimetry, Biomaterials, 16 (1995), 251-258.
[355] P. E. McClain, E. R. Wiley, Differential scanning calorimeter studies of the thermal transitions of collagen implications on structure and stability J. Biol. Chem., 247 (1972), 692-697.
[356] K. A. Piez, J. Gross, The amino acid composition of some fish collagens: The relation between composition and structure, J. Biol. Chem., 235 (1960), 995-998.
[357] F. Flandin, C. Buffevant, D. Herbage, A differential scanning calorimetry analysis of the age-related changes in the thermal stability of rat skin collagen, Biochim. Biophys. Acta, 791 (1984), 205-211.
[358] L. O. Damink, P. Dijkstra, M. Van Luyn, P. Van Wachem, P. Nieuwenhuis, J. Feijen, Cross-linking of dermal sheep collagen using a water-soluble carbodiimide, Biomaterials, 17 (1996), 765-773.
[359] F. Lennox, Shrinkage of collagen, Biochim. Biophys. Acta, 3 (1949) 170-187.
[360] N. N. Fathima, M. P. Kumar, J. R. Rao, B. Nair, A DSC investigation on the changes in pore structure of skin during leather processing, Thermochim. Acta, 501 (2010), 98-102.
[361] A. E. Cronkite, The tensile strength of human tendons, The Anatomical Record, 64 (1936), 173-186.
[362] P. L. Blanton, N. L. Biggs, Ultimate tensile strength of fetal and adult human tendons, J. Biomech., 3 (1970), 181-184 & IN5 185-189.
[363] G. Kempson, Relationship between the tensile properties of articular cartilage from the human knee and age, Ann. Rheum. Dis., 41 (1982), 508-511.
[364] A. K. Williamson, A. C. Chen, K. Masuda, E. J. Thonar, R. L. Sah, Tensile mechanical properties of bovine articular cartilage: variations with growth and relationships to collagen network components, J. Orth. Res., 21 (2003), 872-880.
[365] W. Yang, V. R. Sherman, B. Gludovatz, E. Schaible, P. Stewart, R. O. Ritchie, M. A. Meyers, On the tear resistance of skin, Nat. Comm., 6 (2015), 1-10.
[366] F. H. Silver, J. W. Freeman, D. DeVore, Viscoelastic properties of human skin and processed dermis, Skin Res. Technol., 7 (2001), 18-23.

[367] G. P. Seehra, F.H. Silver, Viscoelastic properties of acid-and alkaline-treated human dermis: a correlation between total surface charge and elastic modulus, Skin Res. Technol., 12 (2006), 190-198.
[368] P. Fratzl, K. Misof, I. Zizak, G. Rapp, H. Amenitsch, S. Bernstorff, Fibrillar structure and mechanical properties of collagen, J. Struct. Biol., (1998), 119-122.
[369] J. Vincent, Structural Biomaterials, 3rd ed., Princeton University Press, New Jersey, USA, (2012).
[370] J. Diamant, A. Keller, E. Baer, M. Litt, R. Arridge, Collagen; ultrastructure and its relation to mechanical properties as a function of ageing, Proc. Royal Soc. B: Biological Sciences, 180 (1972), 293-315.
[371] A. Sharma, A. Licup, K. Jansen, R. Rens, M. Sheinman, G. Koenderink, F. MacKintosh, Strain-controlled criticality governs the nonlinear mechanics of fibre networks, Nat. Phys., (2016), 584-587.
[372] B. Lee, X. Zhou, K. Riching, K. W. Eliceiri, P. J. Keely, S. A. Guelcher, A. M. Weaver, Y. Jiang, A three-dimensional computational model of collagen network mechanics, PloS one, 9 (2014), e111896.
[373] A. J. Licup, S. Münster, A. Sharma, M. Sheinman, L. M. Jawerth, B. Fabry, D. A. Weitz, F. C. MacKintosh, Stress controls the mechanics of collagen networks, PNAS, 112 (2015), 9573-9578.
[374] K. Misof, G. Rapp, P. Fratzl, A new molecular model for collagen elasticity based on synchrotron X-ray scattering evidence, Biophys. J., 72 (1997), 1376-1381.
[375] A. L. Kwansa, R. De Vita, J. W. Freeman, Tensile mechanical properties of collagen type I and its enzymatic crosslinks, Biophys. Chem., 214 (2016), 1-10.
[376] B. Depalle, Z. Qin, S. J. Shefelbine, M. J. Buehler, Influence of cross-link structure, density and mechanical properties in the mesoscale deformation mechanisms of collagen fibrils, J. Mech. Behav. Biomed. Mater., 52 (2015), 1-13.
[377] P. Agache, C. Monneur, J. Leveque, J. De Rigal, Mechanical properties and young's modulus of human skin in vivo, Arch. Dermatol. Res., 269 (1980), 221-232.
[378] D. Bader, P. Bowker, Mechanical characteristics of skin and underlying tissues in vivo, Biomaterials, 4 (1983), 305-308.
[379] S. Motte, L.J. Kaufman, Strain stiffening in collagen I networks, Biopolymers, 99 (2013), 35-46.
[380] A. S. van Oosten, M. Vahabi, A. J. Licup, A. Sharma, P. A. Galie, F. C. MacKintosh, P. A. Janmey, Uncoupling shear and uniaxial elastic moduli of semiflexible biopolymer networks: compression-softening and stretch-stiffening, Scient. Rep., 6 (2016), 1-9.
[381] M. Spivak, Calculus, 3rd ed., Cambridge University Press, Cambridge, UK, (2006).
[382] F. H. Silver, D. L. Christiansen, P. B. Snowhill, Y. Chen, Transition from viscous to elastic-based dependency of mechanical properties of self-assembled type I collagen fibres, J. Appl. Polym. Sci., 79 (2001), 134-142.
[383] R. Sopakayang, R. De Vita, A. Kwansa, J. W. Freeman, Elastic and viscoelastic properties of a type I collagen fibre, J. Theor. Biol., 293 (2012), 197-205.
[384] S. A. Cohen, D. P. Michaud, Synthesis of a fluorescent derivatizing reagent, 6-aminoquinolyl-N-hydroxysuccinimidyl carbamate, and its application for the analysis

of hydrolysate amino acids via high-performance liquid chromatography, Anal. Biochem., 211 (1993), 279-287.
[385] C. Cooper, N. Packer, K. Williams, Amino Acid Analysis Protocols, Springer Science & Business Media, New York, USA, (2001).
[386] S. D. Choudhury, G. Norris, Improved Binary High Performance Liquid Chromatography for Amino Acid Analysis of Collagens, Proceedings of The First International Conference on Sensing Technology, Palmerston North, New Zealand, (2005), 332-337.
[387] S. Å. Gustavsson, J. Samskog, K. E. Markides, B. Långström, Studies of signal suppression in liquid chromatography–electrospray ionization mass spectrometry using volatile ion-pairing reagents, J. Chromatogr. A, 937 (2001), 41-47.
[388] F. Gosetti, E. Mazzucco, D. Zampieri, M.C. Gennaro, Signal suppression/enhancement in high-performance liquid chromatography tandem mass spectrometry, J. Chromatogr. A, 1217 (2010), 3929-3937.
[389] J. B. Fenn, M. Mann, C. K. Meng, S. F. Wong, C. M. Whitehouse, Electrospray ionization–principles and practice, Mass Spectrom. Rev., 9 (1990), 37-70.
[390] C. Salazar, J. M. Armenta, D. F. Cortés, V. Shulaev, Combination of an AccQ· Tag-ultra performance liquid chromatographic method with tandem mass spectrometry for the analysis of amino acids, Amino Acid Analysis: Methods and Protocols, (2012), 13-28.
[391] S. Hou, H. He, W. Zhang, H. Xie, X. Zhang, Determination of soil amino acids by high performance liquid chromatography-electro spray ionization-mass spectrometry derivatized with 6-aminoquinolyl-N-hydroxysuccinimidyl carbamate, Talanta, 80 (2009), 440-447.
[392] K. Iwaki, N. Nimura, Y. Hiraga, T. Kinoshita, K. Takeda, H. Ogura, Amino acid analysis by reversed-phase high-performance liquid chromatography: Automatic pre-column derivatization with activated carbamate reagent, J. Chromatogr. A, 407 (1987), 273-279.
[393] R. Naffa, G. Holmes, M. Ahn, D. Harding, G. Norris, Liquid Chromatography-Electrospray Ionization Mass Spectrometry for the Simultaneous Quantitation of Collagen and Elastin Crosslinks, J. Chromatogr. A, (2016), 60-67.
[394] R. Nueman, M. Logan, Determination of hydroxyproline content, J. Biol. Chem., 184 (1950), 299-304.
[395] R. E. Neuman, M. A. Logan, The determination of collagen and elastin in tissues, J. Biol. Chem., 186 (1950), 549-556.
[396] C. R. Kliment, J. M. Englert, L. P. Crum, T. D. Oury, A novel method for accurate collagen and biochemical assessment of pulmonary tissue utilizing one animal, International Journal of Clinical and Experimental Pathology, 4 (2011), 349-355.
[397] K. I. Kivirikko, R. Myllyla, T. Pihlajaniemi, Hydroxylation of proline and lysine residues in collagens and other animal and plant proteins, Post-translational modifications of proteins, (1992), 1-51.
[398] D. W. Hukins, Connective Tissue Matrix, Macmillan Press, CA, USA, (1990).

[399] P. Brown-Augsburger, T. Broekelmann, J. Rosenbloom, R. Mecham, Functional domains on elastin and microfibril-associated glycoprotein involved in elastic fibre assembly, Biochem. J, 318 (1996), 149-155.
[400] P. L. Brown, L. Mecham, C. Tisdale, R.P. Mecham, The cysteine residues in the carboxy terminal domain of tropoelastin form an intrachain disulfide bond that stabilizes a loop structure and positively charged pocket, Biochem. Biophys. Res. Commun., 186 (1992), 549-555.
[401] K. Piez, The separation of the diastereoisomers of isoleucine and hydroxylysine by ion exchange chromatography, J. Biol. Chem., 207 (1954), 77-80.
[402] D. V. Sommer, R. Larsen, Detection of COL III in parchment by amino acid analysis, Amino Acids, 48 (2016), 169-181.
[403] A. Serafini-Fracassini, J. M. Field, G. W. Rodger, M. Spina, Application of affinity chromatography to the purification of collagenase for the isolation of insoluble elastin, BBA-Protein Structure, 386 (1975), 80-86.
[404] H. Zahn, L. Zürn, DL-Hydroxylysin und DL-Allohydroxylysin und ihre Lactone, Chem. Ber., 91 (1958), 1359-1371.
[405] P. B. Hamilton, R. A. Anderson, Hydroxylysine: isolation from gelatin and resolution of its diastereoisomers by ion exchange chromatography, J. Biol. Chem., 213 (1955), 249-258.
[406] S. Kimura, Determination of the glycosylated hydroxylysines in several invertebrate collagens, The Journal of Biochemistry, 71 (1972), 367-370.
[407] A. G. Brownell, A. Veis, The intracellular location of the glycosylation of hydroxylysine of collagen, Biochem. Biophys. Res. Commun., 63 (1975), 371-377.
[408] A. Oikarinen, H. Anttinen, K. I. Kivirikko, Hydroxylation of lysine and glycosylation of hydroxylysine during collagen biosynthesis in isolated chick-embryo cartilage cells, Biochem. J, 156 (1976), 545-551.
[409] B. Witkop, The application of Hudson's lactone rule to γ- and δ-hydroxyamino acids and the question of the configuration of δ-hydroxy-l-lysine from collagen, Experientia, 12 (1956), 372-374.
[410] S. Nakornchai, P. Atsawasuwan, E. Kitamura, R. Surarit, M. Yamauchi, Partial biochemical characterisation of collagen in carious dentin of human primary teeth, Arch. Oral Biol., 49 (2004), 267-273.
[411] J. H. Bowes, R. H. Kenten, The effect of alkalis on collagen, Biochem. J, 43 (1948), 365-372.
[412] R. L. Edmonds, S. Deb Choudhury, R. G. Haverkamp, M. Birtles, T. F. Allsop, G. E. Norris, Using proteomics, immunohistology, and atomic force microscopy to characterize surface damage to lambskins observed after enzymatic dewooling, J. Agric. Food. Chem., 56 (2008), 7934-7941.
[413] S. Frazier, K. Roodhouse, D. Hourcade, L. Zhang, The quantification of glycosaminoglycans: a comparison of HPLC, carbazole, and alcian blue methods, Open glycoscience, 1 (2008), 31-39.
[414] I. Barbosa, S. Garcia, V. Barbier-Chassefière, J. P. Caruelle, I. Martelly, D. Papy-García, Improved and simple micro assay for sulfated glycosaminoglycans

quantification in biological extracts and its use in skin and muscle tissue studies, Glycobiology, 13 (2003), 647-653.
[415] R. W. Farndale, C. A. Sayers, A. J. Barrett, A direct spectrophotometric microassay for sulfated glycosaminoglycans in cartilage cultures, Connect. Tissue Res., 9 (1982), 247-248.
[416] T. Masuko, A. Minami, N. Iwasaki, T. Majima, S. Nishimura, Y. Lee, Carbohydrate analysis by a phenol-sulfuric acid method in microplate format, Anal. Biochem., 534 (2005), 69-72.
[417] J. Folch, M. Lees, G. Sloane-Stanley, A simple method for the isolation and purification of total lipids from animal tissues, J. Biol. Chem., 226 (1957) 497-509.
[418] J. C. Dittmer, M. A. Wells, Quantitative and Qualitative Analysis of Lipids and Lipid Components, in: J.M. Lowenstein (Ed.) Methods Enzymol., Elsevier, Amsterdam, The Netherlands, (1969), 482-530.
[419] B. Fuchs, R. Süß, K. Teuber, M. Eibisch, J. Schiller, Lipid analysis by thin-layer chromatography—A review of the current state, J. Chromatogr. A, 1218 (2011), 2754-2774.
[420] J. Wren, A. D. Szczepanowksa, Chromatography of lipids in presence of an antioxidant, 4-methyl-2, 6-di-tert.-butylphenol, J. Chromatogr. A, 14 (1964) 405-410.
[421] P. Thanikaivelan, J. R. Rao, B. U. Nair, T. Ramasami, Progress and recent trends in biotechnological methods for leather processing, Trends Biotechnol., 22 (2004), 181-188.
[422] M. Dubois, K. A. Gilles, J. K. Hamilton, P. Rebers, F. Smith, Colorimetric method for determination of sugars and related substances, Anal. Chem., 28 (1956), 350-356.
[423] A. A. Albalasmeh, A. A. Berhe, T. A. Ghezzehei, A new method for rapid determination of carbohydrate and total carbon concentrations using UV spectrophotometry, Carbohydr. Polym., 97 (2013), 253-261.
[424] P. Rao, T. N. Pattabiraman, Reevaluation of the phenol-sulfuric acid reaction for the estimation of hexoses and pentoses, Anal. Biochem., 181 (1989), 18-22.
[425] R.G. Spiro, Study of the Carbohydrates of Glycoproteins, Methods Enzymol., 28 (1972), 3-43.
[426] C. Van Gent, Separation and micro determination of lipids by thin-layer chromatography followed by densitometry, Fresenius' Zeitschrift für analytische Chemie, 236 (1968), 344-350.
[427] J. C. Touchstone, Thin-layer chromatographic procedures for lipid separation, J. Chromatogr. B: Biomed.Sci. App., 671 (1995), 169-195.
[428] H. K. Mangold, Thin-layer chromatography of lipids, Journal of the American Oil Chemists' Society, 41 (1964), 762-773.
[429] V. P. Skipski, M. Barclay, Thin-layer chromatography of lipids, Methods Enzymol., 14 (1969), 530-598.
[430] J. O'Kelly, H. Reich, S. Mills, The composition of the skin surface lipids of European cattle and buffalo steers, Compar. Biochem. Physiol. Part B: Compar. Biochem., 67 (1980), 217-220.
[431] R. W. Layer, The chemistry of imines, Chem. Rev., 63 (1963), 489-510.

[432] M. Ledvina, F. Bartoš, Determination of cross-links in elastin, J. Chromatogr. A, 31 (1967), 56-61.
[433] E. Stahl, Thin-layer chromato-graphy. A laboratory handbook, Springer-Verlag, Germany, (1962).
[434] D. P. Thornhill, Separation of amino acids on highly crosslinked polyacrylamide gel and some observations on the mechanism of adsorption, BBA - General Subjects, 279 (1972), 1-7.
[435] D. Thornhill, Separation of amino acids on highly crosslinked polyacrylamide gel and some observations on the mechanism of adsorption, Biochimica et Biophysica Acta (BBA)-General Subjects, 279 (1972), 1-7.
[436] D. Thornhill, Desmosines: A rapid single-column isolation procedure, Anal. Biochem., 46 (1972), 119-122.
[437] G. Reddy, R. Hobgood, J. Goldstein, NMR studies of pyrimidine, imidazole and their monomethyl derivatives, JACS, 84 (1962), 336-340.
[438] G. Wider, R. Baumann, K. Nagayama, R. R. Ernst, K. Wüthrich, Strong spin-spin coupling in the two-dimensional J-resolved 360-MHz 1H NMR spectra of the common amino acids, J. Magn. Reson., (1969), 42 (1981), 73-87.
[439] P. Allevi, M. Anastasia, Synthesis of all four possible stereoisomers of 5-hydroxylysine, Tetrahedron: Asymmetry, 11 (2000), 3151-3160.
[440] L. Guo, T. Liu, K. Chen, T. Song, P. G. Wang, W. Zhao, Facile synthesis of 5-hydroxy-L-lysine from D-galactose as a chiral-precursor, Org. Biomol. Chem., 12 (2014), 7310-7317.
[441] N. R. Davis, A. J. Bailey, The chemistry of the collagen cross-links. A convenient synthesis of the reduction products of several collagen cross-links and cross-link precursors, Biochem. J, 129 (1972), 91-96.
[442] M. L. Tanzer, G. Mechanic, P. M. Gallop, Isolation of hydroxylysinonorleucine and its lactone from reconstituted collagen fibrils, BBA-Protein Structure, 207 (1970), 548-552.
[443] R. Cribiù, P. Allevi, M. Anastasia, Reduced collagen cross links: the first synthesis of all the possible (2S,2'S)-stereoisomers of 5-hydroxylysinonorleucine and of 5,5'-dihydroxylysinonorleucine in enantiomerically pure form, Tetrahedron: Asymmetry, 16 (2005), 3059-3069.
[444] A. M. C. H. van den Nieuwendijk, J. C. J. Benningshof, V. Wegmann, R. A. Bank, J. M. te Koppele, J. Brussee, A. van der Gen, Synthesis of reduced collagen crosslinks, Biorg. Med. Chem. Lett., 9 (1999), 1673-1676.
[445] J. Keeler, Understanding NMR Spectroscopy, 2nd ed., John Wiley & Sons, New York, USA, (2011).
[446] S. P. Robins, A. J. Bailey, The chemistry of the collagen cross links. Characterization of the products of reduction of skin, tendon and bone with sodium cyanoborohydride, Biochem. J, 163 (1977), 339-346.
[447] T. L. Constantopoulos, G. S. Jackson, C. G. Enke, Effects of salt concentration on analyte response using electrospray ionization mass spectrometry, J. Am. Soc. Mass. Spectrom., 10 (1999), 625-634.

[448] J. Nawrocki, The silanol group and its role in liquid chromatography, J. Chromatogr. A, 779 (1997), 29-71.
[449] S. Ahuja, N. Jespersen, Modern Instrumental Analysis, 1st ed., Elsevier, Amsterdam, The Netherland, (2006).
[450] K. Blau, G. S. King, Handbook of Derivatives for Chromatography, Wiley, New York, USA, (1993).
[451] B. A. Bidlingmeyer, S. A. Cohen, T. L. Tarvin, Rapid analysis of amino acids using pre-column derivatization, J. Chromatogr. B: Biomed.Sci. App., 336 (1984), 93-104.
[452] C. van Wandelen, S. A. Cohen, Using quaternary high-performance liquid chromatography eluent systems for separating 6-aminoquinolyl-N-hydroxysuccinimidyl carbamate-derivatized amino acid mixtures, J. Chromatogr. A, 763 (1997), 11-22.
[453] J. J. Pesek, M. T. Matyska, Hydride-based silica stationary phases for HPLC: Fundamental properties and applications, J. Sep. Sci., 28 (2005), 1845-1854.
[454] J. J. Pesek, M. T. Matyska, S. M. Fischer, T. R. Sana, Analysis of hydrophilic metabolites by high-performance liquid chromatography–mass spectrometry using a silica hydride-based stationary phase, J. Chromatogr. A, 1204 (2008), 48-55.
[455] S. Banerjee, S. Mazumdar, Electrospray ionization mass spectrometry: a technique to access the information beyond the molecular weight of the analyte, International Journal of Analytical Chemistry, (2012), 1-40.
[456] A. T. Iavarone, J. C. Jurchen, E. R. Williams, Effects of solvent on the maximum charge state and charge state distribution of protein ions produced by electrospray ionization, J. Am. Soc. Mass. Spectrom., 11 (2000), 976-985.
[457] S. Sakura, D. Fujimoto, K. Sakamoto, A. Mizuno, K. Motegi, Photolysis of pyridinoline, a cross-linking amino acid of collagen, by ultraviolet light, Can. J. Biochem., 60 (1982), 525-529.
[458] B. Meddah, S. Kamel, C. Giroud, M. Brazier, Effects of ultraviolet light on free and peptide-bound pyridinoline and deoxypyridinoline cross-links. Protective effect of acid pH against photolytic degradation, J. Photochem. Photobiol. B: Biol., 54 (2000), 168-174.
[459] T. Housley, M. L. Tanzer, E. Henson, P. M. Gallop, Collagen crosslinking: isolation of hydroxyaldol-histidine, a naturally-occurring crosslink, Biochemical and Biophysical Research Communications, 67 (1975), 824-830.
[460] R. Fairweather, M. L. Tanzer, P. M. Gallop, Aldol-histidine, a new trifunctional collagen crosslink, Biochemical and biophysical research communications, 48 (1972), 1311-1315.
[461] P. Fratzl, Collagen: structure and mechanics, Springer, New York, USA, 2008.
[462] A. N. Annaidh, K. Bruyère, M. Destrade, M. D. Gilchrist, M. Otténio, Characterization of the anisotropic mechanical properties of excised human skin, J. Mech. Behav. Biomed. Mater., 5 (2012), 139-148.
[463] E. McNerny, B. Gong, M. D. Morris, D. H. Kohn, Bone fracture toughness and strength correlate with collagen cross-link maturity in a dose-controlled lathyrism mouse model, J. Bone Miner. Res., 30 (2015), 455-464.

[464] D. Pankova, Y. Chen, M. Terajima, M. J. Schliekelman, B. N. Baird, M. Fahrenholtz, L. Sun, B.J. Gill, T.J. Vadakkan, M. P. Kim, Cancer-associated Fibroblasts Induce a Collagen Cross-link Switch in Tumor Stroma, Mol. Cancer Res., (2015), 287-295.
[465] T. Starborg, N. Kalson, Y. Lu, A. Mironov, T. Cootes, D. Holmes, K. Kadler, Using transmission electron microscopy and 3View to determine collagen fibril size and three-dimensional organization, Nat. Prot., 8 (2013), 1433-1448.
[466] V. K. Yadavalli, D. V. Svintradze, R. M. Pidaparti, Nanoscale measurements of the assembly of collagen to fibrils, Int. J. Biol. Macromol., 46 (2010), 458-464.
[467] G. S. Kassab, M. S. Sacks, Structure-Based Mechanics of Tissues and Organs, Springer, New York, USA, (2016).
[468] M. Żak, P. Kuropka, M. Kobielarz, A. Dudek, K. Kaleta-Kuratewicz, S. Szotek, Determination of the mechanical properties of the skin of pig foetuses with respect to its structure, Acta of Bioengin. Biomech., 13 (2011), 37-43.
[469] A. J. van der Slot-Verhoeven, E. A. van Dura, J. Attema, B. Blauw, J. DeGroot, T.W.J. Huizinga, A.-M. Zuurmond, R.A. Bank, The type of collagen cross-link determines the reversibility of experimental skin fibrosis, Biochimica et Biophysica Acta (BBA) - Mol. Basis Dis., 1740 (2005), 60-67.
[470] S. Kalamajski, C. Liu, V. Tillgren, K. Rubin, Å. Oldberg, J. Rai, M. Weis, D.R. Eyre, Increased C-telopeptide cross-linking of tendon type I collagen in fibromodulin-deficient mice, J. Biol. Chem., 289 (2014), 18873-18879.
[471] A. L. Kwansa, R. De Vita, J. W. Freeman, Mechanical recruitment of N-and C-crosslinks in collagen type I, Matrix Biol., 34 (2014), 161-169.
[472] H. Oxlund, T. Andreassen, The roles of hyaluronic acid, collagen and elastin in the mechanical properties of connective tissues, J. Anat., 131 (1980), 611-620.
[473] V. Arumugam, M. Naresh, R. Sanjeevi, Effect of strain rate on the fracture behaviour of skin, J. Biosci., 19 (1994) 307-313.
[474] G. Jenkins, Molecular Mechanisms of Skin Ageing, Mechanisms of Ageing and Development, 123 (2002), 801-810.
[475] A. J. Bailey, Molecular mechanisms of ageing in connective tissues, Mech. Ageing Devel., 122 (2001), 735-755.
[476] A. J. Bailey, The stabilization of the intermolecular crosslinks of collagen with ageing, Gerontologia, 15 (1969), 65-76.
[477] S. J. Wilkinson, D. W. L. Hukins, Determination of collagen fibril structure and orientation in connective tissues by X-ray diffraction, Radiat. Phys. Chem., 56 (1999), 197-204.
[478] B. Vogel, H. Siebert, U. Hofmann, S. Frantz, Determination of collagen content within picrosirius red stained paraffin-embedded tissue sections using fluorescence microscopy, MethodsX, 2 (2015), 124-134.
[479] N. M. Kirby, S. T. Mudie, A. M. Hawley, D. J. Cookson, H. D. Mertens, N. Cowieson, V. Samardzic-Boban, A low-background-intensity focusing small-angle X-ray scattering undulator beamline, J. Appl. Crystallogr., 46 (2013), 1670-1680.
[480] A. Hammersley, FIT2D: An introduction and overview, European Synchrotron Radiation Facility Internal Report ESRF97HA02T, (1997).

[481] R. A. Berg, D. J. Prockop, The thermal transition of a non-hydroxylated form of collagen. Evidence for a role for hydroxyproline in stabilizing the triple-helix of collagen, Biochem. Biophys. Res. Commun., 52 (1973), 115-120.
[482] M. Cócera, G. Rodríguez, L. Rubio, L. Barbosa-Barros, N. Benseny-Cases, J. Cladera, M. Sabés, F. Fauth, A. de La Maza, O. López, Characterisation of skin states by non-crystalline diffraction, Soft Matter, 7 (2011), 8605-8611.
[483] A. Bigi, A. M. Fichera, N. Roveri, M. H. J. Koch, Structural modifications of air-dried tendon collagen on heating, Int. J. Biol. Macromol., 9 (1987), 176-180.
[484] C.R. Worthington, S.G. Tomlin, Low angle X-ray diffraction patterns of collagen, Nature, 175 (1955), 189-201.
[485] O. Antipova, J.P. Orgel, In situ D-periodic molecular structure of type II collagen, J. Biol. Chem., 285 (2010) 7087-7096.
[486] C. A. Maxwell, K. Smiechowski, J. Zarlok, A. Sionkowska, T. J. Wess, X-ray studies of a collagen material for leather production treated with chromium salt, JALCA, 101 (2006), 9-17.
[487] P. Fratzl, N. Fratzl-Zelman, K. Klaushofer, Collagen packing and mineralization. An X-ray scattering investigation of turkey leg tendon, Biophys. J., 64 (1993), 260-266.
[488] M. M. Basil-Jones, R. L. Edmonds, S. M. Cooper, R. G. Haverkamp, Collagen fibril orientation in ovine and bovine leather affects strength: A small angle X-ray scattering (SAXS) study, J. Agric. Food. Chem., 59 (2011), 9972-9979.
[489] C. H. Lee, W. Zhang, J. Liao, C.A. Carruthers, J. I. Sacks, M. S. Sacks, On the presence of affine fibril and fibre kinematics in the mitral valve anterior leaflet, Biophys. J., 108 (2015), 2074-2087.
[490] A. Tawara, H. H. Varner, J. G. Hollyfield, Proteoglycans in the mouse interphotoreceptor matrix. I. Histochemical studies using cuprolinic blue, Exp. Eye Res., 46 (1988), 689-704.
[491] T. H. Van Kuppevelt, T. L. Rutten, C. M. Kuyper, Ultrastructural localization of proteoglycans in tissue using cuprolinic blue according to the critical electrolyte concentration method: comparison with biochemical data from the literature, Histochem. J., 19 (1987), 520-526.
[492] J. E. Scott, Affinity, competition and specific interactions in the biochemistry and histochemistry of polyelectrolytes, Biochem. Soc. Trans, 1 (1973), 787-806.
[493] D. A. D. Parry, G. R. G. Barnes, A. S. Craig, A comparison of the size distribution of collagen fibrils in connective tissues as a function of age and a possible relation between fibril size distribution and mechanical properties, Proc. Royal Soc. B: Biological Sciences, 203 (1978), 305-321.
[494] A. S. Craig, E. F. Eikenberry, D. A. D. Parry, Ultrastructural organization of skin: classification on the basis of mechanical role, Connect. Tissue Res., 16 (1987), 213-223.
[495] M. Goldberg, M. Triller, F. Escaig, D. Genotelle-Septier, R. Weill, Detection sur coupes ultrafines de mucopolysaccharides acides par le bleu alcian dans des tissues dentaires inclus en Epon, J. Biol. Buccale, 4 (1976), 155-164.

[496] M. Goldberg, D. Genotelle-Septier, M. Molon-Noblot, R. Weill, Ultrastructural study of the proteoglycans in enamel from rat incisors during late enamel maturation, Arch. Oral Biol., 23 (1978), 1007-1011.
[497] J. R. Gordon, M. R. Bernfield, The basal lamina of the postnatal mammary epithelium contains glycosaminoglycans in a precise ultrastructural organization, Dev. Biol., 74 (1980), 118-135.
[498] Y. S. Kanwar, M. G. Farquhar, Presence of heparan sulfate in the glomerular basement membrane, PNAS, 76 (1979), 1303-1307.
[499] J. E. Scott, The molecular biology of histochemical staining by cationic phthalocyanin dyes: the design of replacements for Alcian Blue, J. Microsc., 119 (1980), 373-381.
[500] J. E. Scott, Histochemistry of Alcian blue, Histochemie, 32 (1972) 191-212.
[501] J. E. Scott, Alcian blue. Now you see it, now you don't, Eur. J. Oral Sci., 104 (1996), 2-9.
[502] K. Király, T. Lapveteläinen, J. Arokoski, K. Törrönen, L. Modis, I. Kiviranta, H. Helminen, Application of selected cationic dyes for the semiquantitative estimation of glycosaminoglycans in histological sections of articular cartilage by microspectrophotometry, Histochem. J., 28 (1996), 577-590.
[503] J. E. Scott, J. Dorling, Differential staining of acid glycosaminoglycans (mucopolysaccharides) by alcian blue in salt solutions, Histochemistry and Cell Biology, 5 (1965), 221-233.
[504] J. E. Scott, Proteoglycan histochemistry—a valuable tool for connective tissue biochemists, Collagen Rel. Res., 5 (1985), 541-575.
[505] M. Raspanti, A. Alessandrini, V. Ottani, A. Ruggeri, Direct visualization of collagen-bound proteoglycans by tapping-mode atomic force microscopy, J. Struct. Biol., 119 (1997), 118-122.
[506] M. Raspanti, M. Viola, A. Forlino, R. Tenni, C. Gruppi, M.E. Tira, Glycosaminoglycans show a specific periodic interaction with type I collagen fibrils, J. Struct. Biol., 164 (2008), 134-139.
[507] G. Fessel, J. G. Snedeker, Evidence against proteoglycan mediated collagen fibril load transmission and dynamic viscoelasticity in tendon, Matrix Biol., 28 (2009), 503-510.
[508] P. N. Lewis, C. Pinali, R. D. Young, K. M. Meek, A. J. Quantock, C. Knupp, Structural interactions between collagen and proteoglycans are elucidated by three-dimensional electron tomography of bovine cornea, Structure, 18 (2010), 239-245.
[509] S. A. Alanazi, T. Almubrad, A. I. AlIbrahim, A. A. Khan, S. Akhtar, Ultrastructure organization of collagen fibrils and proteoglycans of stingray and shark corneal stroma, J. Ophthalm., 2015, 1-11.
[510] J. E. Scott, M. Haigh, Identification of specific binding sites for keratan sulphate proteoglycans and chondroitin-dermatan sulphate proteoglycans on collagen fibrils in cornea by the use of cupromeronic blue in 'critical-electrolyte-concentration' techniques, Biochem. J, 253 (1988) 607-610.
[511] J. E. Scott, Proteoglycan-fibrillar collagen interactions, Biochem. J, 252 (1988) 313-232.

[512] J. E. Scott, M. Haigh, Proteoglycan-type I collagen fibril interactions in bone and non-calcifying connective tissues, Biosci. Rep., 5 (1985), 71-81.
[513] V. R. Sherman, W. Yang, M. A. Meyers, The materials science of collagen, J. Mech. Behav. Biomed. Mater., 52 (2015), 22-50.
[514] L. C. U. Junqueira, G. Bignolas, R. Brentani, Picrosirius staining plus polarization microscopy, a specific method for collagen detection in tissue sections, Histochem. J., 11 (1979), 447-455.
[515] F. Sweat, H. Puchtler, S.I. Rosenthal, Sirius red F3BA as a stain for connective tissue, Arch. Pathol., 78 (1964), 69-72.
[516] A. Changoor, N. Tran-Khanh, S. Methot, M. Garon, M. Hurtig, M. Shive, M. Buschmann, A polarized light microscopy method for accurate and reliable grading of collagen organization in cartilage repair, Osteo. & Cartil., 19 (2011), 126-135.
[517] T. C. Gasser, S. Gallinetti, X. Xing, C. Forsell, J. Swedenborg, J. Roy, Spatial orientation of collagen fibres in the abdominal aortic aneurysm's wall and its relation to wall mechanics, Acta Biomater., 8 (2012), 3091-3103.
[518] K. T. Weber, R. Pick, M. A. Silver, G. W. Moe, J. S. Janicki, I. H. Zucker, P. W. Armstrong, Fibrillar collagen and remodeling of dilated canine left ventricle, Circulation, 82 (1990), 1387-1401.
[519] J. H. Smith, P. B. Canham, J. Starkey, Orientation of collagen in the tunica adventitia of the human cerebral artery measured with polarized light and the universal stage, J. Ultrastruct. Res., 77 (1981), 133-145.
[520] R. J. Rizzo, W. J. McCarthy, S. N. Dixit, M. P. Lilly, V. P. Shively, W. R. Flinn, J. S. Yao, Collagen types and matrix protein content in human abdominal aortic aneurysms, J. Vasc. Surg., 10 (1989), 365-373.
[521] P. Canham, H. Finlay, J. Kiernan, G. Ferguson, Layered structure of saccular aneurysms assessed by collagen birefringence, Neurol. Res., 21 (1999), 618-626.
[522] C. Segnani, C. Ippolito, L. Antonioli, C. Pellegrini, C. Blandizzi, A. Dolfi, N. Bernardini, Histochemical detection of collagen fibres by sirius red/fast green is more sensitive than van gieson or sirius red alone in normal and inflamed rat colon, PloS one, 10 (2015), e0144630.
[523] C. R. Drifka, A. G. Loeffler, K. Mathewson, G. Mehta, A. Keikhosravi, Y. Liu, S. Lemancik, W. A. Ricke, S. M. Weber, W. J. Kao, Comparison of picrosirius red staining with second harmonic generation imaging for the quantification of clinically relevant collagen fibre features in histopathology samples, J. Histochem. & Cytochem., 64 (2016), 519-529.
[524] R. A. Carlton, Polarized Light Microscopy, Springer, New York, USA, 2011.
[525] W. C. McCrone, L. B. McCrone, J. G. Delly, Polarized Light Microscopy, 8th ed., Microscope Publications, DC, USA, (1978).
[526] M. Wolman, F. Kasten, Polarized light microscopy in the study of the molecular structure of collagen and reticulin, Histochem. & Cell Biol., 85 (1986), 41-49.
[527] D. P. Speer, L. Dahners, The collagenous architecture of articular cartilage: correlation of scanning electron microscopy and polarized light microscopy observations, Clin. Orthop. Relat. Res., 139 (1979), 267-275.

[528] M. Mantri, N. D. Loik, R. B. Hamed, T. D. Claridge, J. S. McCullagh, C. J. Schofield, The 2-Oxoglutarate-Dependent Oxygenase JMJD6 Catalyses Oxidation of Lysine Residues to give 5S-Hydroxylysine Residues, ChemBioChem, 12 (2011), 531-534.
[529] D. A. D. Parry, A. S. Craig, G. R. G. Barnes, Tendon and ligament from the horse: an ultrastructural study of collagen fibrils and elastic fibres as a function of age, Proceedings of the Royal Society of London B: Biological Sciences, 203 (1978), 293-303.
[530] S. Ono, M. Yamauchi, Collagen fibril diameter and its relation to cross-linking of collagen in the skin of patients with amyotrophic lateral sclerosis, J. Neurol. Sci., 119 (1993), 74-78.
[531] U. Sharma, L. Carrique, S. Vadon-Le Goff, N. Mariano, R. Georges, F. Delolme, P. Koivunen, J. Myllyharju, C. Moeli, N. Aghajari and D. J.S. Hulmes, Structural basis of homo-and heterotrimerization of collagen I. Nat. Comm., 8 (2017), 1-10.
[532] S. A. Jimenez and R. I. Bashey, Identification of collagen alpha1(I) trimer in embryonic chick tendons and calvaria. Biochem. Biophys. Res. Comm., 78, (1977), 1354-1361.